Statistical Prediction Methods for the In-Plane Shear Strength of Partially Grouted Masonry Walls

by

Karren Nadine Izquierdo Duque

A thesis submitted in partial fulfillment of the requirements for the degree of

Master of Science

in

STRUCTURAL ENGINEERING

Department of Civil and Environmental Engineering
University of Alberta

ABSTRACT

The behaviour of partially grouted masonry shear walls is complex due to their anisotropic nature and the nonlinear interactions between blocks, mortar, grouted cells, ungrouted cells and steel reinforcement. Currently available code- and research-based shear strength equations give highly variable results when predicting the in-plane shear strength of partially grouted masonry. It is crucial to develop a greater understanding in this area, as sudden shear failures of masonry walls can lead to catastrophic losses of human life and property.

This study presents the development of several new in-plane shear strength models for partially grouted masonry walls using stepwise regression and model trees. Stepwise regression allows the number of input variables to be reduced from a large pool of candidates to an appropriate subset for predicting the output variable. It does so by identifying the most significant input variables while eliminating interdependencies between variables that are included in the regression. Model trees split data into groups of similar data so that nonlinear functions can be represented using piecewise linear approximation. In this study, model trees used stepwise regressions as those linear approximations.

The models were generated using data compiled from 292 experimentally tested partially grouted masonry shear walls. The data was synthesized and scrutinized to minimize variation between studies and eliminate inconsistencies. The data was also used to test the performance of 17 existing code- and research-based shear strength equations.

Both the stepwise regressions and model trees were found to significantly outperform existing code- and research-based shear strength models. The stepwise regressions generally performed slightly better than the model trees, however it was shown that the potential of model trees is significant, and it was suggested that the benefits of model trees may be more apparent with a larger dataset. Five models, including 3 stepwise regression and 2 model trees, were selected as the proposed models. It was found that, of the variables studied, the most significant ones for estimating the shear strength of partially grouted masonry walls are the axial load, wall geometry, compressive strength of mortar, and area of interior vertical reinforcement.

DEDICATION

To Oscar:

Thank you for your support and encouragement.

And to the One who makes all things possible:

"O Lord, I have trusted in thee,

and I will trust in thee forever."

2 Nephi 4:34

ACKNOWLEDGEMENTS

I wish to thank my supervisor, Dr. Cruz-Noguez, for his guidance, assistance and for allowing me the freedom to learn and grow by experience. I also wish to thank Dr. Arash Mohsenijam for the time he took out of his schedule to meet with me many times and teach me about statistics. Assistance in understanding and interpreting the referenced works that were written in Spanish was provided by Alan Alonso-Rivers.

I wish to thank my mother, my husband, and my sisters, Amber and Brenda, for their assistance in proofreading this thesis. Despite it being an unfamiliar area of research for each of them, their suggestions have been immensely helpful in improving this work.

No one has been more supportive to me in the past two years than my husband Oscar. Thank you for cooking meals, cleaning, washing dishes and buying groceries countless times without me to let me write my thesis. Thank you for your unfeigned interest in my research and for always being willing to listen. Most of all, thank you for supporting and encouraging me in everything I do.

I owe much to my parents, Glen and Carole Hudson, for teaching me from a young age the value of hard work and study. I could not have been so successful in my academic pursuits if it were not for both of them taking the time to help me turn my weaknesses into strengths, from practicing for spelling tests with me to quizzing me on multiplication flash cards. The support you have given me from that age until now has been instrumental in helping me to achieve my goals.

Thank you to my sisters, Amber, Brenda, Linda and Jami, and their families for loving and supporting me. I consider myself blessed to belong to such a wonderful family. Thank you to my friends who have supported and encouraged me in this endeavor.

This research was funded by the Natural Sciences and Engineering Research Council of Canada, the Canada Masonry Design Centre, the Canadian Concrete Masonry Producers Association, and the Alberta Masonry Council.

TABLE OF CONTENTS

LIST OF TABLES

LIST OF FIGURES

LIST OF SYMBOLS AND ABBREVIATIONS

ANN Artificial Neural Network

A_{cell} Estimated area of a single cell of a block (mm^2). For 2-cell blocks:

$$A_{cell} = L_b t \frac{1 - v}{2}$$

A_{gross} Gross wall area (mm^2)

$$A_{gross} = Lt$$

A_h Total area of horizontal reinforcement (mm^2)

$$A_h = A_{hbb} + A_{hj}$$

$A_{h,m}$ Total cross-sectional area of horizontal reinforcement, modified to ignore bond beam reinforcement in the bottom course of the wall (mm^2)

$$A_h = A_{hbb,m} + A_{hj}$$

$A_{h,m2}$ Total cross-sectional area of horizontal reinforcement, modified to ignore bond beam reinforcement in the top course of the wall (mm^2)

$$A_h = A_{hbb,m2} + A_{hj}$$

A_{hbb} Total cross-sectional area of horizontal bond beam reinforcement (mm^2)

$A_{hbb,m}$ Total cross-sectional area of horizontal bond beam reinforcement, modified to ignore reinforcement in the bottom course of the wall (mm^2)

$A_{hbb,m2}$ Total cross-sectional area of horizontal bond beam reinforcement, modified to ignore reinforcement in the top course of the wall (mm^2)

$A_{hbb,bar}$ Cross-sectional area of a single horizontal reinforcing bar (mm^2)

A_{hj} Total cross-sectional area of horizontal joint reinforcement (mm^2)

$A_{hj,bar}$ Cross-sectional area of horizontal reinforcement in a single joint reinforcement ladder (mm^2)

A_{net} Net wall area (mm^2). For 2-cell blocks:

$$A_{net} = n_g * \frac{L_b}{2} t + \left(L - n_g * \frac{L_b}{2}\right)(2t_{fs})$$

A_v Total cross-sectional area of vertical reinforcement (mm^2)

$$A_v = A_{vf} + A_{vi}$$

A_{vf} Total cross-sectional area of flexural (outer vertical) reinforcement (mm^2)

$A_{vf,bar}$ Cross-sectional area of one flexural (outer vertical) reinforcement bar (mm^2)

A_{vi} Total cross-sectional area of interior vertical reinforcement (mm^2)

$A_{vi,bar}$ Cross-sectional area of a single interior vertical reinforcing bar (mm^2)

d Distance from compressive face of flexural member to the centroid of the longitudinal tensile reinforcement (mm)

FG Fully grouted

f_{block} Compressive strength of the masonry block, based on net area (MPa)

f_{grout} Compressive strength of the grout (MPa)

f_{mortar} Compressive strength of the mortar (MPa)

$f'_{m,eff}$ Effective prism strength, which is a weighted average of the grouted and ungrouted prism strengths (MPa)

f'_{mg} Grouted prism strength, based on a height-to-thickness ratio of 5:1 (MPa)

$f'_{mg,u}$ Uncorrected grouted prism strength (MPa)

f'_{mu} Ungrouted prism strength, based on a height-to-thickness ratio of 5:1 (MPa)

$f'_{mu,u}$ Uncorrected ungrouted prism strength (MPa)

f_{yhbb} Yield strength of horizontal bond beam reinforcement (MPa)

f_{yhj} Yield strength of horizontal joint reinforcement (MPa)

f_{yvf} Yield strength of vertical flexural reinforcement (MPa)

f_{yvi} Yield strength of interior vertical reinforcement (MPa)

GDF Generalized degrees of freedom

H Height of the masonry wall, not including courses which are loaded directly (mm)

H_b Actual height of the masonry block (mm)

H_{eff} Effective height of the lateral loading, taken as the distance between the bottom of the wall and the location of lateral load application for cantilever walls, or half of this distance for walls in double curvature (mm)

H_v Height of the lateral loading (mm)

k Correction factor to convert uncorrected prism strengths to a value based on a height-to-thickness ratio of 5:1

k_{ave} Correction factor to convert V_{max} to an estimated value of V_{ave} when V_{min} is unavailable (taken as 0.944)

k_{mono} Correction factor to convert the shear strength of a monotonically tested wall to that of an equivalent cyclically tested wall (taken as 0.814)

k_{rate} Correction factor to convert the shear strength of a dynamically tested wall to that of an equivalent statically tested wall (taken as 0.9)

L Length of the wall (mm)

L_b Actual length of the CMU (mm)

ME Mean error

MSE Mean squared error

MT Model tree

$\frac{M}{VL}$ Shear span depth ratio (unitless)

$$\frac{M}{VL} = \frac{H_{eff}}{L}$$

n_b Number of blocks. For 2-cell blocks:

$$n_b = \frac{n_g}{2}$$

n_g Number of grouted cells

n_t Total number of cells in the wall

OLS Ordinary least squares

PG	Partially grouted
P	The axial load applied at the point of ultimate shear strength (N or kN)
R^2	Coefficient of determination
RMSE	Root mean squared error
Std. dev.	Standard deviation
$s_{gh,ave}$	Average spacing between horizontal grouted courses (mm)
$s_{gh,max}$	Maximum spacing between horizontal grouted courses (mm)
$s_{gv,ave}$	Average spacing between vertical grouted cells (mm)
$s_{gv,max}$	Maximum spacing between vertical grouted cells (mm)
$s_{h,ave}$	Average spacing between horizontal reinforcing bars (mm)
$s_{h,max}$	Maximum spacing between horizontal reinforcing bars (mm)
$s_{v,ave}$	Average spacing between vertical reinforcing bars (mm)
$s_{v,max}$	Maximum spacing between vertical reinforcing bars (mm)
t	Wall thickness (mm)
t_{fs}	Face shell thickness (mm)
URM	Unreinforced masonry
VIF	Variance inflation factor
v	Ratio of net to gross area for a masonry block/prism (unitless)

V_{ave} Uncorrected experimental shear strength, taken as the average of V_{min} and V_{max} (kN)

V_{exp} Ultimate experimental shear strength (kN), which is the corrected version of V_{ave}:

$$V_{exp} = k_{ave}k_{mono}k_{rate} * V_{ave}$$

V_{min} Minimum peak experimental shear strength, taken as the smaller peak shear strength in either the push or pull direction (kN)

V_{max} Maximum peak experimental shear strength, taken as the larger peak shear strength in either the push or pull direction (kN)

V_n Nominal analytical shear strength (kN)

V_r Factored (design) analytical shear strength (kN)

ρ_{hbb} Bond beam reinforcement ratio

$$\rho_{hbb} = \frac{A_{hbb}}{Ht}$$

ρ_{hj} Joint reinforcement ratio

$$\rho_{hj} = \frac{A_{hj}}{Ht}$$

ρ_{vf} Flexural reinforcement ratio

$$\rho_{vf} = \frac{A_{vf}}{A_{gross}}$$

ρ_{vi} Interior vertical reinforcement ratio

$$\rho_{vi} = \frac{A_{vi}}{A_{gross}}$$

σ_{gross} Shear stress based on gross wall area (MPa)

$$\sigma_{gross} = \frac{P}{A_{gross}}$$

σ_{net} Shear stress based on net wall area (MPa)

$$\sigma_{net} = \frac{P}{A_{net}}$$

1 INTRODUCTION

1.1 Background

Reinforced masonry shear walls are commonly used in multi-storey masonry buildings to provide lateral stability against loads such as those caused by wind and earthquakes. Partially grouted (PG) masonry walls differ from fully grouted (FG) walls in that they are grouted only in locations where reinforcement bars are placed (either vertical reinforced columns or horizontal bond beams, or both). Due to the associated reductions in material and labour, PG walls offer an economic advantage over FG walls (Dhanasekar, 2011; Hassanli et al., 2014; Bolhassani et al., 2016a). However, recent studies have found that current design equations give highly variable results in terms of accuracy when predicting the in-plane shear strength of PG masonry (Dillon and Fonseca, 2017a; Hudson et al., 2019).

While FG walls subjected to shear behave similarly to reinforced concrete, the behaviour of PG walls under in-plane shear loads is not well understood (Haider, 2007; Dhanasekar, 2011). Many of the expressions used to predict the in-plane shear capacity were initially derived using data exclusively from FG masonry shear wall tests (Minaie et al., 2010; Dillon and Fonseca, 2017a). Several researchers have compiled datasets of PG walls to evaluate the performance of existing shear strength expressions. Their findings show that many of these expressions, when applied to PG walls, are unconservative on average (Haider, 2007; Minaie et al., 2010; Dhanasekar, 2011, Hassanli et al., 2014; Bolhassani et al., 2016b). Overpredictions of shear capacity may lead to incorrect prediction of failure modes (Minaie et al., 2010). Masonry failures occur often even under moderate lateral loading, causing significant loss of lives and property (Dhanasekar, 2011). To compensate for the high variability of shear strength predictions, most codes apply severe reduction factors, leading to estimated factors of safety ranging from 1.75 to 5.29 (Dickie and Lissel, 2009). For example, the CSA S304-14 (2014) design shear strength equation was found to be highly conservative by Oan (2013) and Dillon and Fonseca (2017a).

Researchers have noted that, unlike FG walls, PG shear walls behave similar to in-filled frames (Minaie et al., 2010; Bolhassani et al., 2016b). Variables which are commonly accepted as contributing to shear strength include wall geometry, level of axial load, ratio of net to gross area, and distribution of horizontal and vertical reinforcement (Matsumura, 1987; Fattal, 1993a; Haider, 2007). Numerous researchers have proposed equations to predict the in-plane shear strength of PG walls using regression analysis to determine the influence of these parameters (Matsumura, 1987; Fattal, 1993b; Oan, 2013; Hassanli et al., 2014; Dillon, 2015). A few researchers have attempted to use Artificial Neural Networks (ANNs) to achieve greater prediction accuracy (Aguilar et al., 2016; Hung, 2018). Still, international standards have vastly different methods for predicting the in-plane shear strength of masonry, showing a lack of consensus on the matter of analytical prediction (Dickie and Lissel, 2009).

To be practical as a design equation, a model must give accurate results while maintaining appropriate levels of complexity and transparency. So far, regression analysis has had limited success in predicting the in-plane shear strength of PG masonry walls. Although ANNs exhibit impressive accuracy in modeling nonlinearities inherent in PG shear wall behaviour, they are often overly complex and lack interpretability (Hung, 2018). Few researchers have made use of stepwise regression and none have attempted to use model trees to represent the behaviour of masonry shear walls, techniques which can produce accurate equations without sacrificing interpretability and simplicity. Dillon (2015) used stepwise regression to assist with selecting variables for his proposed equation, however he limited the potential variables that could be selected to a relatively small set, and he didn't use stepwise regression to build his final model directly.

Stepwise regression allows for many possible input variables to be considered simultaneously, and then a smaller subset of input variables is objectively selected to be in the model. Model trees split data into similar groups, accounting for nonlinearities in a simple and interpretable way. Combining the techniques of stepwise regression with model trees has been shown to be an effective solution for complex modeling problems, capable of achieving high prediction accuracies (Mohsenijam, 2019).

Due to the time and expense involved in testing masonry walls, no one study contains enough data to build a model to predict the in-plane shear strength of PG walls (Dillon and Fonseca, 2014a). As a result, it is necessary to compile a dataset using the results of multiple experimental studies. To ensure data from different studies are compatible with each other, data must be scrutinized, by determining which specimens to include or exclude, and synthesized to minimize variation between studies and estimate missing values.

1.2 Problem Statement

The in-plane shear behaviour of PG masonry walls is complex, and historical prediction methods have failed to adequately capture this behaviour. Current design equations used to predict the in-plane shear strength of PG masonry walls are unreliable and may lead to designs that are overly conservative or unsafe. To address the shortcomings of these equations, an improved understanding of PG wall behaviour and alternate methods of generating new prediction models are needed.

1.3 Objectives, Methods and Scope

The main objective of this study is to develop an improved model to predict the in-plane shear strength of PG masonry walls using stepwise regression. A broad set of raw variables is selected, which extends beyond those which have been considered in previous design expressions, so that parameters that influence shear strength can be identified. Competing definitions of variables are considered simultaneously to identify the best ones. The possibility of using model trees is also investigated, to see whether model trees combined with stepwise regression can produce a viable analysis model.

The methods used to achieve the objectives are as follows.

1. Prepare a dataset
    a. Assemble a database by compiling PG concrete block masonry walls exhibiting in-plane shear failure

   b. Data scrutinization is performed by creating and applying a set of selection/inclusion criteria to ensure experimental results are comparable while making use of the largest amount of data possible
   c. Rigorous data synthesization is performed to ensure consistency in the variables used
2. Evaluate the performance of existing code- and research-based equations with experimental results
   a. Discuss expressions from researchers and design codes
   b. Identify appropriate statistical performance indicators to evaluate and compare the performance of prediction equations
   c. Evaluate the performance of each expression using the experimental data and statistical performance indicators
3. Develop new models using stepwise regression and model trees
   a. Use as wide a range of input variables as possible to identify any important variables that have previously not been accounted for
   b. Use multiple definitions of individual variables to determine which ones are the best
   c. Refine dataset as needed to improve models
   d. Generate models of various levels of complexity for comparison purposes
   e. Compare all generated models and select a few optimum models based on accuracy, simplicity, and transparency
   f. Compare optimum (proposed) models with existing code- and research-based equations

The scope of this thesis is to develop a model to predict the in-plane shear strength of PG concrete block masonry walls, using stepwise regression and model trees. FG walls and unreinforced masonry (URM) walls are not considered in this study, nor are walls constructed from clay bricks. Walls with openings and double pier specimens are not considered. Only walls failing in diagonal

shear are considered; walls with failure dominated by flexure, sliding shear and crushing of the masonry compressive strut are out of the scope of this study.

1.4 Organization of Thesis

This thesis is composed of seven chapters:

- Chapter 1 introduces the research study as well as the objectives and scope.
- Chapter 2 discusses the literature review, including a review of failure mechanisms, the effects of various parameters on PG walls, and a review of existing expressions for predicting the shear strength of PG walls. It also explains stepwise regression and model trees.
- Chapter 3 introduces the experimental studies.
- Chapter 4 explains the dataset assembly, scrutinization and synthesization that were performed, explains how raw and transformed variables were selected and summarizes the distribution of specimen parameters.
- Chapter 5 presents the models generated in this study.
- Chapter 6 compares the generated models to select a few proposed models, and then compares those proposed models to existing expressions. Insights are made regarding the behaviour of PG walls.
- Chapter 7 gives the conclusions and recommendations based on Chapter 6.

2 LITERATURE REVIEW

2.1 Introduction

Masonry is a composite construction material capable of carrying compressive loads, however it has a relatively low capacity to carry tension and shear (Tomaževič, 2009). Reinforced concrete masonry walls are composed of several constituent materials: concrete blocks, also known as Concrete Masonry Units (CMUs), mortar, grout, and steel reinforcement. Mortar is typically placed in the horizontal (bed) joints and vertical (head) joints between blocks. In the case of Fully Grouted (FG) walls, all the vertical cells in a wall are filled with grout, whereas Partially Grouted (PG) walls are typically grouted only in the cells which contain vertical reinforcement. Unreinforced Masonry (URM) also exists and is characterized by an absence of grouting and steel reinforcement.

Horizontal reinforcement may be in the form of joint reinforcement or bond beam reinforcement. Joint reinforcement may be of ladder type or truss type and is placed between horizontal courses of masonry in the bed joints. Bond beam reinforcement typically consists of standard deformed steel bars, which are placed in grouted courses built with blocks that allow the placement of reinforcement. For PG walls, a barrier, such as a fine plastic net, is used to prevent the grout from falling into the courses below (Minaie et al., 2010). A typical PG masonry wall with vertical and horizontal reinforcement is illustrated in Figure 2.1.

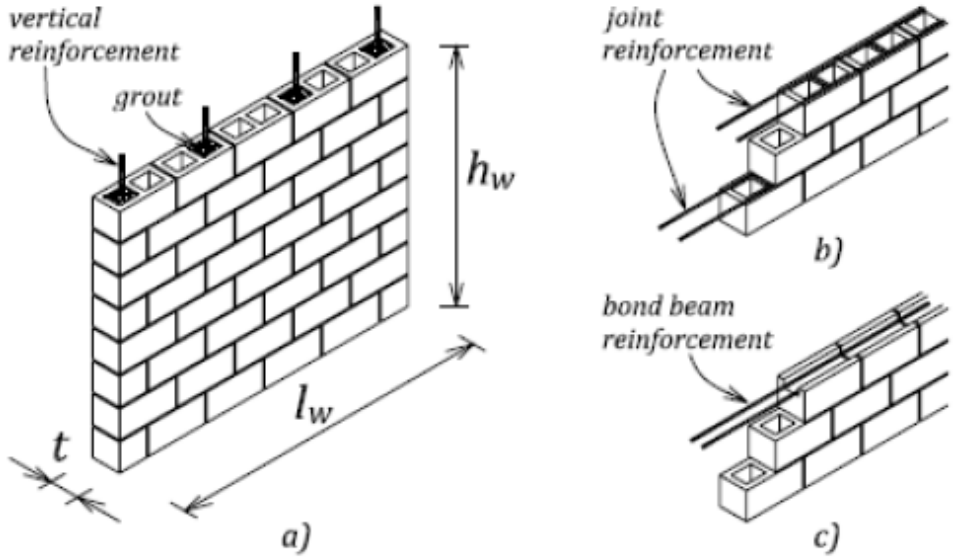

Figure 2.1 - Typical PG masonry wall showing: (a) vertical reinforcement, (b) joint reinforcement and (c) bond beam reinforcement (Anderson and Brzev, 2009)

Unlike other structural materials like concrete or steel that behave in an isotropic manner, masonry exhibits orthotropic behaviour due to the mortar joints acting as planes of weakness (Haider, 2007; Hamedzadeh, 2011). In ungrouted masonry prisms, both the deformation and strength of specimens are related to the bed joint orientation, while in grouted prisms, the effect of anisotropy is less pronounced due to the presence of grout, which acts as an isotropic material (Hamedzadeh, 2011). Due to the non-homogeneity and anisotropy of masonry, the behaviour is complex (Tomaževič, 2009).

The in-plane shear behaviour of masonry in general is not fully understood (Dhanasekar, 2011). In FG walls, shear is resisted largely through aggregate interlock in the grout, dowel action of vertical reinforcement and the tensile action of horizontal reinforcement, with no significant contribution from the mortar joints (Shing et al., 1990; Dhanasekar, 2011). For URM walls, shear is resisted largely through deformation in the mortar bed joints, and ultimate shear capacity is influenced by the mortar strength, the axial stress, and the aspect ratio (Haider, 2007; Dhanasekar, 2011). PG masonry walls, on the other hand, behave similarly to in-filled frames, and can be

thought of as a "mixed" system consisting of reinforced core elements and unreinforced masonry panels spanning between the cores (Minaie et al., 2010; Dhanasekar, 2011; Bolhassani et al., 2016b). While FG and URM walls can be designed safely using the provisions in most design standards, safe designs may not always be achieved for PG walls, and as a result further research is urgently needed to examine the in-plane behaviour of PG masonry walls (Dhanasekar, 2011).

The purpose of this literature review is to provide background information on PG masonry walls subject to lateral loading, explain the equations which are currently available to predict PG wall shear resistance and provide an overview of the statistical methods that were used in analysis.

2.2 Behaviour of Partially Grouted Shear Walls Subjected to In-Plane Lateral Loading

2.2.1 Failure Modes

The main failure modes for a masonry shear wall are flexure, sliding shear and diagonal shear (Figure 2.2). Often, masonry walls exhibit mixed modes of failure involving more than one of these modes (Dhanasekar, 2011; Oan, 2013). Walls failing in a combined flexure-shear mode exhibit higher lateral load resistance than those that fail due to flexure only (Haider, 2007). Compression failure is also possible.

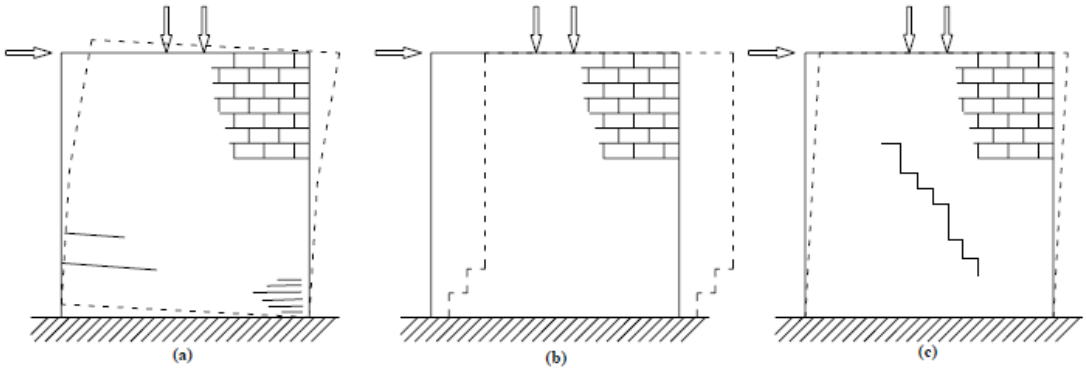

Figure 2.2 - Failure modes for masonry walls subjected to in-plane lateral loads: (a) flexural, (b) sliding, and (c) shear (Voon, 2007)

Both sliding shear failure and diagonal shear failure are brittle, meaning that the wall cannot maintain stability for long after the maximum lateral strength is reached (Rizaee, 2015). Brittle failures can be quite sudden, often leading to catastrophic loss of life and property, while ductile failures allow building occupants more time to escape. Flexural failures are more ductile, making them the preferred failure mode (Voon, 2007; Oan, 2013; Rizaee, 2015). To ensure that masonry walls are safe, walls are designed in a manner such that shear failure does not occur (Hamedzadeh, 2013).

2.2.1.1 Flexural Failure

Flexural failures tend to exhibit high ductility and energy dissipation, largely because this type of failure requires yielding of the reinforcement (Dillon, 2015; Rizaee, 2015). Flexural resistance can be estimated with reasonable accuracy using simple flexural theory (Hamedzadeh, 2013).

Flexural failure is characterized by horizontal bed joint cracking in the bottom courses, yielding of the vertical reinforcement at the tension heel, overturning of the wall, and buckling of the vertical reinforcement and crushing of the masonry at the compression toe (Hamedzadeh, 2013; Dillon, 2015; Rizaee, 2015; Hung, 2018). For walls with large amounts of vertical reinforcement, the reinforcement may yield only slightly or not at all prior to crushing of the masonry at the toe (Dillon, 2015). On the other hand, walls with small amounts of vertical reinforcement will experience extensive plastic yielding of the reinforcement before toe crushing begins (Dillon, 2015). Flexural failure occurs most often in relatively slender walls, with aspect ratios greater than 1.5 (Haider, 2007; Rizaee, 2015). They are more likely to occur in walls with insufficient vertical reinforcement that are subjected to low axial stresses (Oan, 2013).

2.2.1.2 Sliding Failure

Sliding shear failure occurs when the lateral load exceeds the friction between the mortar and the masonry units and the dowel action of the vertical reinforcement (Hamedzadeh, 2013; Rizaee, 2015). Axial load also contributes by increasing the friction between the mortar and the units (Hamedzadeh, 2013). This type of failure is characterized by sliding of the wall along bed joints (Hung, 2018). Sliding shear failure is not common in reinforced masonry, as typical axial loads

and amounts of vertical reinforcement, along with adequate mortar quality, are able to prevent sliding failure (Oan, 2013; Rizaee, 2015). In URM walls, however, seismic events may cause this type of failure at the top levels of masonry buildings, due to low axial stresses (Tomaževič, 2009). Sliding failure may also become significant in situations where there is a low friction coefficient, such as when friction breakers or waterproof membranes are used or when the wall is positioned on a smooth finished slab (Voon, 2007).

2.2.1.3 Diagonal Shear Failure

Diagonal shear failure, also known as diagonal tension shear failure or simply shear failure, occurs when the principal tensile stress exceeds the tensile strength of the masonry units or mortar joints (Hamedzadeh, 2013). This type of failure occurs in walls with relatively high axial loading, particularly in the case of squat walls (Oan, 2013; Rizaee, 2015).

Diagonal shear failure is characterised by the formation of a diagonal crack along the shear wall, which spreads from the centre of the wall (Voon, 2007; Hamedzadeh, 2013; Dillon, 2015). This crack may follow a stepped pattern through the head and bed joints, a diagonal path passing through the masonry units, or a combination of the two (Figure 2.3). The cracking pattern depends on the strength of the masonry units and the mortar, as well as the level of axial load (Tomaževič, 2009; Oan, 2013; Rizaee, 2015). High axial stresses increase the chances that the crack will pass through the units (Hamedzadeh, 2013).

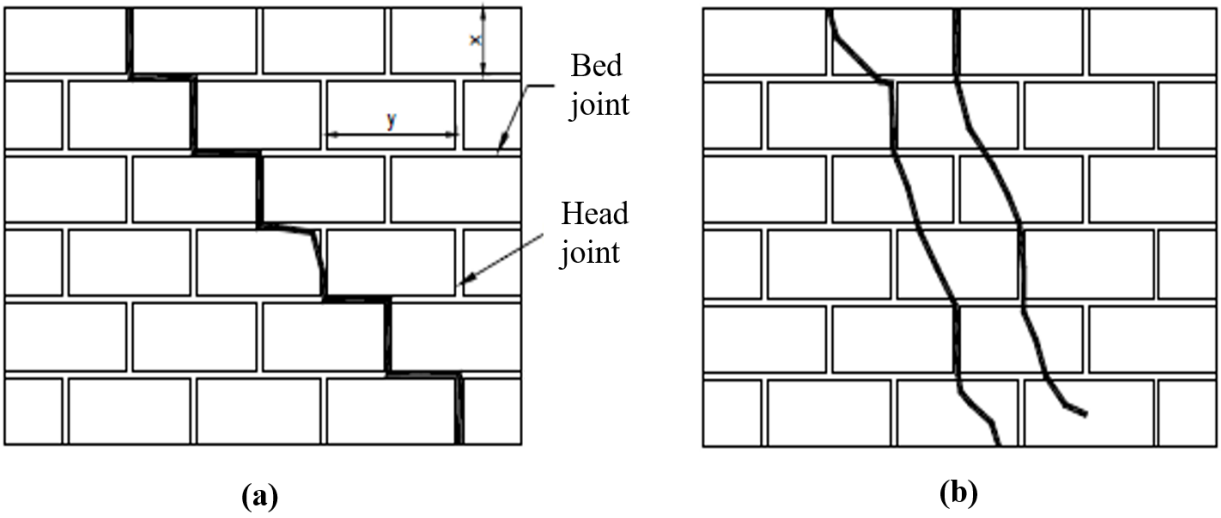

Figure 2.3 - Diagonal shear cracks: (a) in stepped formation and (b) passing through units and joints (adapted from Voon, 2007)

The reinforcement is not engaged until cracking initiates, after which point the wall strength is provided by the horizontal and vertical reinforcement and by aggregate interlock (Shing et al., 1990; Dillon, 2015). Distributed vertical reinforcement keeps the cracks from opening, allowing for additional shear stress transfer through crack friction beyond the initial cracking load (Dillon, 2015). Similarly, the axial load also contributes to post-cracking shear strength by increasing aggregate-interlock force (Ghanem et al., 1992; Dillon, 2015).

Diagonal shear failure can be either brittle or ductile. With adequate reinforcement, distributed throughout the wall and properly anchored, it is possible to increase wall ductility (Hamedzadeh, 2013; Dillon, 2015; Rizaee, 2015). The stresses are redistributed across the wall and the horizontal reinforcement resists the lateral load in the cracked zone, preventing the initial crack from further widening (Hamedzadeh, 2013). Instead, new cracks form throughout the wall and localized crushing of the masonry at severely cracked portions of the wall leads to a complete loss of strength (Voon, 2007; Hamedzadeh, 2013; Dillon, 2015; Rizaee, 2015). However, if the reinforcement is not well distributed or axial loads are high, the failure will be brittle (Dillon, 2015). This type of failure is characterized by one major diagonal crack (or, in the case of reverse-cyclic loading, a

major X-shaped diagonal crack pair) and sudden crushing of the masonry between adjacent horizontal reinforcement (Voon, 2007; Dillon, 2015, Rizaee, 2015). Both types of diagonal shear failure are illustrated in Figure 2.4.

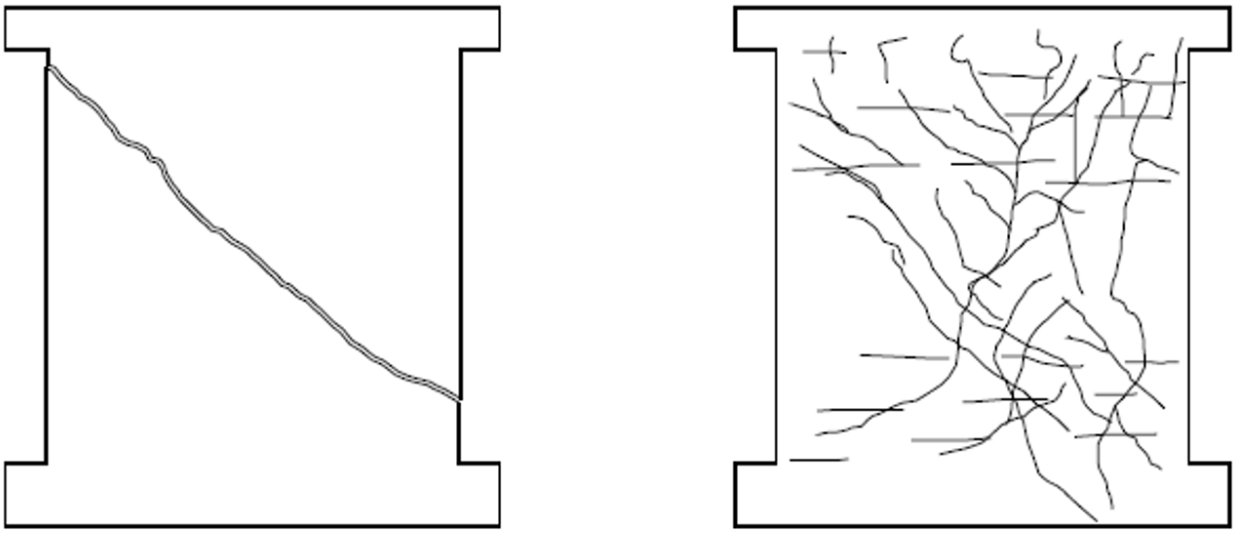

Figure 2.4 - Cracking patterns associated with diagonal shear failure: (a) brittle failure and (b) ductile failure (adapted from Voon, 2007)

2.2.1.4 Masonry Compressive Strut Shear Failure

Compressive failure, though rare in masonry walls, occurs under axial loads that are high enough to exceed the compressive strength of the masonry units (Oan, 2013). Shear walls that are heavily reinforced with horizontal steel are also susceptible to this type of failure (Hung, 2018). It is characterized by the formation of vertical cracks parallel to the compressive strut (Oan, 2013).

2.2.2 Effects of Wall Properties on Behaviour

Although failure modes are agreed upon, international standards have very different methods for predicting the in-plane shear strength of masonry (Dickie and Lissel, 2009). Existing code- and research-based models differ in terms of parameter choice and overall form, showing a lack of

consensus on shear resisting mechanisms (Dillon, 2015). Wall properties that are generally considered to contribute to shear strength include masonry compressive strength, axial load, aspect ratio and horizontal reinforcement. Some researchers have found that vertical reinforcement also contributes to the shear strength of masonry, while others have found the opposite. Details of how all these variables are theorized to affect shear strength are discussed in the following sections.

2.2.2.1 Effect of Masonry Compressive Strength

Matsumura (1987) suggested that shear strength of masonry walls increases approximately in proportion to the square root of the masonry compressive strength. This relationship appears in many of the available shear strength expressions for PG walls, and is often assumed to be empirical (Dillon, 2015). However, Hassanli et al. (2014) have suggested that masonry tensile strength is represented by the square root of the masonry compressive strength. Compared with strut-and-tie modeling, Dillon (2015) found that the square root relationship has the tendency to over-predict the masonry strength component for very low and high values of f'_m. However, these extreme strength values are uncharacteristic for masonry, particularly in the case of low compressive strength values. Researchers have noted that increasing the value of f'_m causes some shear strength equations to produce increasingly unconservative predictions (Hassanli et al., 2014; Bolhassani et al., 2016b). This finding suggests that, for the typical range of compressive masonry strength, the effect is overestimated in the provisions of these codes (Hassanli et al., 2014). For walls with high masonry compressive strength, cracks in mortar layers usually govern the failure, so it may be appropriate to limit the contribution from f'_m (Hassanli et al., 2014).

It has been suggested that until initial cracking, all of the shear load is carried by the masonry, after which point the shear carried by the masonry across the crack is reduced (Anderson and Priestley, 1992). Shing et al. (1990) suggested that the residual strength of masonry depends on the amount of vertical steel as well as the applied axial stress, as both enhance aggregate-interlock forces by resisting crack opening. As a result, the shear strength equation proposed by Shing et al. (1990) combines the vertical reinforcement ratio and the axial stress with the compressive strength of masonry.

2.2.2.2 Effect of Axial Load

Many researchers have concluded that axial load increases the ultimate shear resistance (Meli and Salgado, 1969; Matsumura, 1987; Okamoto et al., 1987; Haach, 2009; Voon and Ingham, 2006; Oan, 2013). Ramírez et al. (2016) found that this effect is more pronounced in squat walls. Increasing axial load increases the shear capacity by preventing the principal stresses from reaching the tensile damage limit (Hamedzadeh, 2013). Larger lateral force is required to overcome the compressive field produced by the larger axial load, which delays initial cracking (Voon, 2007). After cracking, shear is resisted in part by aggregate-interlock forces, which are increased by axial stresses that minimize crack openings (Shing et al., 1990).

Fattal (1993a) found that within the limits of 0 to 1.8 MPa, ultimate strength increases linearly with increasing axial stress. The strut-and-tie model developed by Dillon (2015) predicts that the relationship between axial load and shear capacity is non-linear, particularly as the strength of the masonry decreases. Hassanli et al. (2014) used univariate regression analysis and multivariate regression analysis to assess the performance of the Canadian, American, Australian and New Zealander shear strength equations on PG wall data. While univariate regression analysis indicated that the expressions did not have significant bias towards the level of axial stress, multivariate regression analysis showed that all four expressions underestimate the effect of axial stress. This contradiction reveals that the effect of axial stress cannot be completely isolated as it is inter-related with other parameters (Hassanli et al., 2014).

Increasing axial load decreases wall ductility, characterized by a decrease in lateral deformations and dissipation of energy (Voon and Ingham, 2006; Haach, 2009). High levels of axial stress reduce the yielding of vertical reinforcing bars, leading to more severe diagonal cracking and brittle failures (Hung, 2018). The axial load also affects failure mode, as noted earlier. Walls with low axial loading have a greater tendency to fail in flexure, and as axial load is increased the failure mode transitions to a combined flexure-shear mode, then to shear-dominated behaviour (Dillon, 2015). If the axial load exceeds a certain threshold, the failure mode will change to compression (Page, 1989; Hamedzadeh, 2013).

2.2.2.3 Effect of Wall Aspect Ratio / Shear Span Ratio

Many researchers have found that decreasing the height-to-length aspect ratio of masonry walls leads to an increase in shear strength (Matsumura, 1988; Fattal, 1993a; Voon and Ingham, 2006; Hamedzadeh, 2013, Ramírez et al., 2016). In other words, the more squat the wall is, the higher the shear strength will be. Walls having a greater aspect ratio have a more vertically inclined compressive strut, which carries less force and hence leads to a lower shear capacity (Hassanli et al., 2014). Shear stress based on net wall area, on the other hand, has been observed to increase with increasing aspect ratio (Schultz, 1996; Schultz et al., 1998).

Most studies of shear strength have focused on aspect ratios of 1 or less (Hung, 2018). This is in part because in slender walls failure is dominated by flexure (Haider, 2007). Maleki et al. (2009) found that walls having an aspect ratio of 1 or less experienced a shear dominated failure, while a wall with an aspect ratio of 1.5 exhibited mixed shear-flexure failure. Ramírez et al. (2016) also found that energy dissipation capacity was higher for walls with lower aspect ratios.

Dillon and Fonseca (2017b) stated that the consensus amongst researchers is that shear strength has a better correlation with the shear span ratio than to aspect ratio. Many shear strength expressions reflect this by including the shear span ratio instead of the aspect ratio, expressed as M/VL or a variation. Unlike the aspect ratio, the shear span ratio accounts for the increase in stiffness provided by double curvature as opposed to cantilever boundary conditions. The shear span ratio accounts for both the aspect ratio and the boundary conditions simultaneously, as illustrated by Figure 2.5.

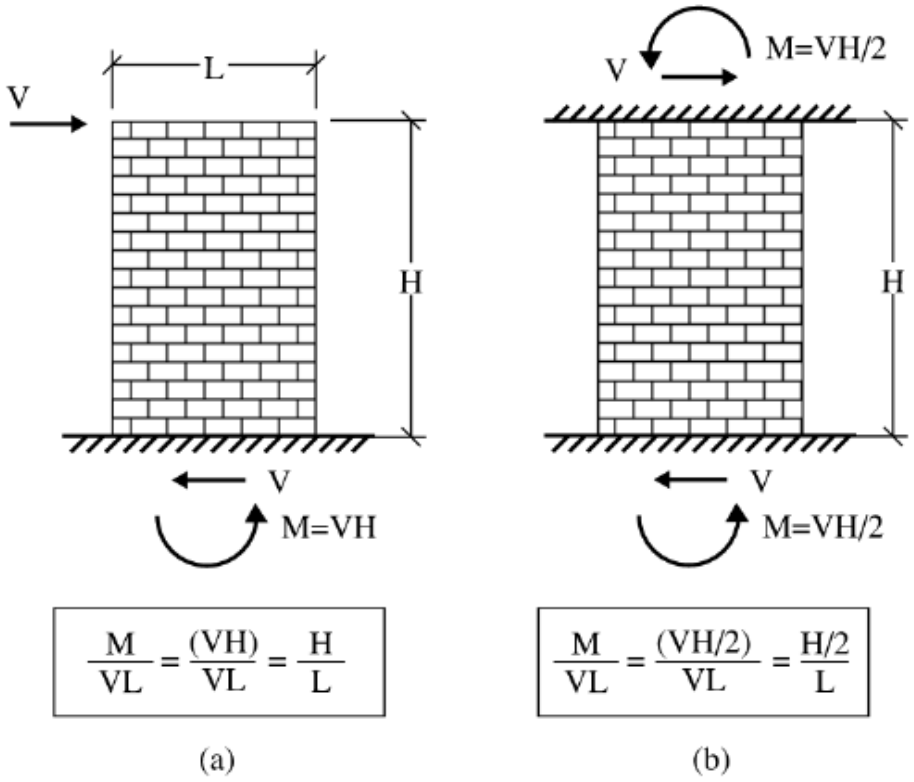

Figure 2.5 - Shear span ratio for (a) cantilever boundary conditions and (b) double curvature boundary conditions (Hung, 2018)

Dillon (2015) observed during the development of his proposed shear strength equation that a better fit to the experimental data was achieved when the inverse of the shear span ratio was used.

2.2.2.4 Effect of Horizontal Reinforcement

While it is widely accepted that horizontal reinforcement contributes to shear strength (Matsumura, 1987, Tomaževič and Lutman, 1988; Voon and Ingham, 2006), the increase in shear strength is not proportional to the amount of reinforcement added (Yancey and Scribner, 1989). Researchers have reported that horizontal reinforcement ratios above 0.2% provide a negligible increase in shear strength (Fattal, 1993b; Elmapruk, 2010; Nolph and ElGawady, 2012). Hassanli et al. (2014) provided a possible explanation for this phenomenon: in highly reinforced walls, the steel does not yield, and shear strength is governed by the formation of large cracks through which the force

cannot pass. As a result, increasing the amount of reinforcement past a certain threshold does not increase the shear strength. Many shear strength expressions, including the CSA S304-14 equation, the Blondet et al. and Anderson and Priestley models, the TCCMaR equation and the AS 3700 (Australian code) equation, overestimate the influence of horizontal reinforcement (Hassanli et al., 2014; Dillon, 2015).

Horizontal reinforcement does not contribute to shear strength until after cracking has initiated (Shing et al., 1990; Oan, 2013). This is illustrated by the finding of Fattal (1993a) that the cracking strength of PG masonry is not significantly affected by increasing the horizontal reinforcement ratio in the range of 0 to 0.34%. Prior to diagonal cracking, the shear load is resisted mainly by the masonry (Anderson and Priestley, 1992). Dillon (2015) hypothesized that, rather than being involved directly in resisting shear loads, the horizontal reinforcement works similarly to vertical reinforcement by keeping diagonal cracks closed. This enables the transfer of stresses through truss action and aggregate friction, and since diagonal cracks typically form at a 45° angle, horizontal and vertical reinforcement are presumed to be equally effective in restricting cracking (Dillon, 2015).

Due to the finer aggregates (compared with concrete), it is expected that the shear capacity of masonry decreases with smaller crack openings, meaning the horizontal reinforcement likely has not begun yielding when the wall reaches its maximum shear capacity (Hung, 2018). Janaraj and Dhanasekar (2016) studied the influence of increasing horizontal reinforcement in a bond beam at mid-height of a masonry wall modeled using FEM and found that the maximum tensile stress in the reinforcement was only 30% of the yield strength. They considered the contribution of horizontal reinforcement to the in-plane shear strength to be negligible (Janaraj and Dhanasekar, 2016).

Hoque (2013) studied PG masonry walls using different types of horizontal reinforcement anchorage, noting that there was no significant effect on the shear strength, presumably because the bars did not yield. Rizaee (2015) performed a similar study and, using strain gauges at various locations on the horizontal reinforcement, found that reinforcement in PG walls can reach yield

and is more likely to do so when 180° hooks are provided, as opposed to other types of anchorage. The majority of the walls were reinforced with bond beams in the top and middle courses, and the measured strains in the bars in the top course were significantly lower, with none of the selected locations on the top bars yielding. There was still no significant difference in the performance of the walls, and it was concluded that the effect of bar size on the performance of the walls is more pronounced than the end anchorage (Rizaee, 2015).

Researchers have reported that walls with increased horizontal reinforcement exhibit improved post-cracking ductility and energy-dissipation capability (Tomaževič and Lutman, 1988; Shing et al., 1989). It has also been found that increasing the amount of horizontal reinforcement can change the failure mode to flexure (Thurston and Hutchison, 1982; Shing et al., 1990).

Some researchers have reported that horizontal reinforcement results in greater benefits for slender walls (Schultz, 1998; Ramírez et al., 2016). Using strut-and-tie theory, Hassanli et al. (2014) explained this phenomenon by stating that as a wall becomes more slender, the shear load transfer mechanism shifts from a direct strut (path 1 in Figure 2.6) to a truss action through horizontal reinforcement (path 2).

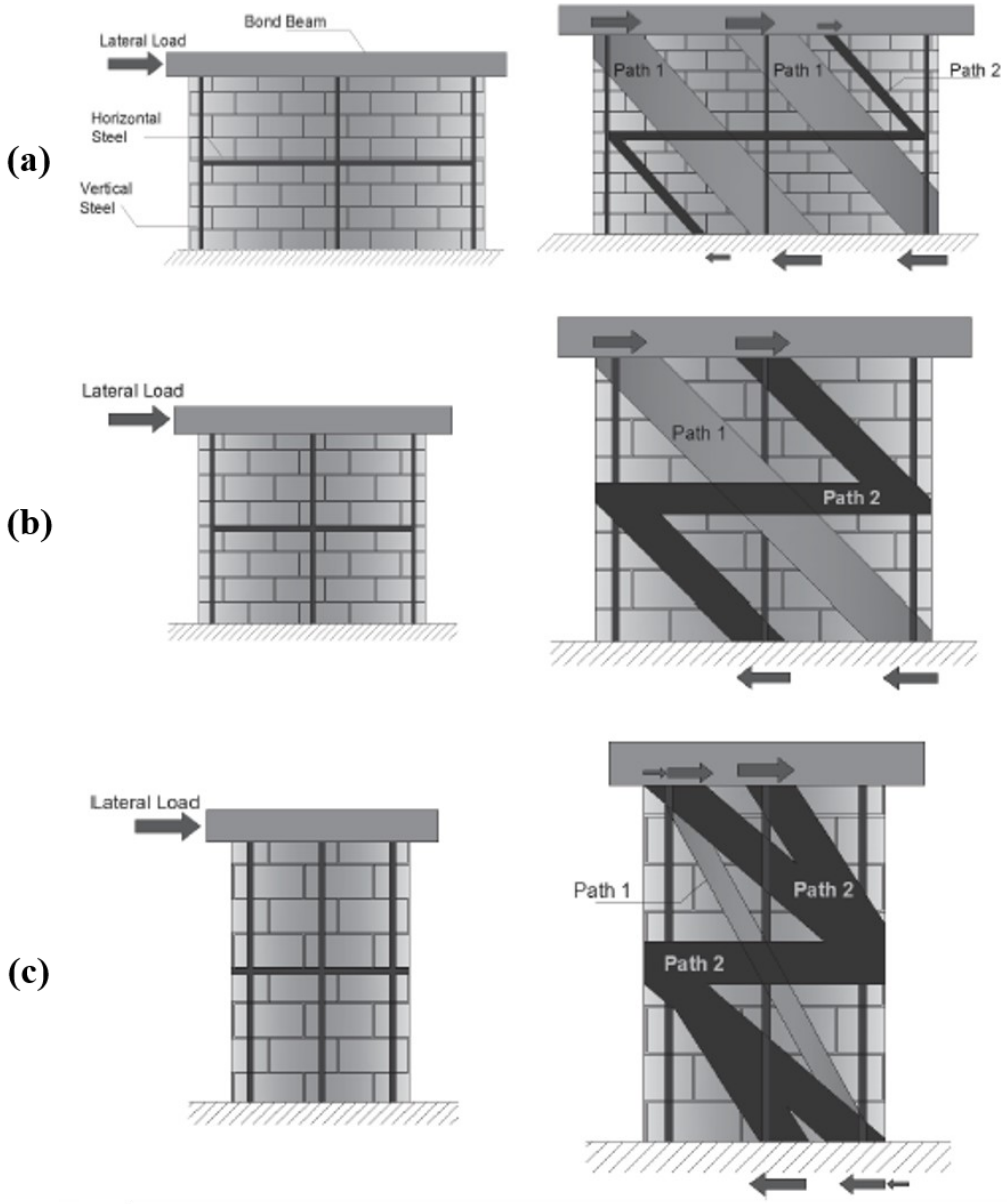

Figure 2.6 - Strut-and-tie models for (a) squat, (b) square, and (c) slender PG masonry walls (adapted from Hassanli et al., 2014)

Oan (2013) found no significant effect on the shear strength of PG masonry walls with joint reinforcement, however the walls tested by Oan were all squat walls (H/L=0.63). In fact, using larger diameter joint reinforcement resulted in lower shear strengths, which was attributed to the

reduced bond between the mortar and masonry units due to the relatively high diameter of reinforcement in the joint (Oan, 2013).

Current design equations do not differentiate between bond beam and joint reinforcement, however researchers have studied the differences between these two types of reinforcement. Fattal (1993a) and Yancey and Scribner (1989) observed that the contribution of joint reinforcement to shear capacity and deflection were comparable to that of bond beam reinforcement. Schultz et al. (1998) found that vertical cracks between the grouted vertical cells and the adjacent ungrouted masonry dominated walls with bond beams, while walls with joint reinforcement exhibited more inclined cracking. They surmised that the joint reinforcement bridged the vertical cracks and prevented interruption of stress flow (Schultz et al., 1998). Baenziger and Porter (2011) found that walls with distributed joint reinforcement had comparable or better shear capacity, better crack control, and better ductility than walls with concentrated bond beam reinforcement. Hoque (2013) found that cracking in walls with bond beams was more distributed and deformation was smaller compared to walls with joint reinforcement, which exhibited X-pattern cracking. These findings are significant, because the use of joint reinforcement in place of bond beams allows for substantial construction cost savings (Fattal, 1993a).

Oan (2013) investigated two different methods of joint reinforcement placement: embedded and dry. The embedded method involves placing mortar on the masonry unit face shells, embedding the joint reinforcement in the mortar, then covering the reinforcement in mortar. The dry placement method, which is typically used in industry to save time, consists of placing joint reinforcement directly on the dry face shell, followed by the mortar (Oan, 2013). It was concluded that the method of joint reinforcement placement did not affect the shear strength significantly (Oan, 2013).

2.2.2.5 Effect of Vertical Reinforcement

Vertical reinforcement is frequently used to increase the flexural resistance of masonry walls. Since the tensile stresses are greatest at the end of the wall, the exterior vertical reinforcement is most effective in resisting flexural moment force (Dillon, 2015). The interior vertical reinforcement is not as effective in flexure due to a smaller moment arm and reduced level of strain

compared to the exterior reinforcement (Dillon, 2015). While the effect of vertical reinforcement on flexural strength of masonry is well known, the effect on shear strength is not agreed upon. This is reflected in contradicting findings by different researchers, and by the absence of a vertical reinforcement term in many existing code- and research-based shear strength expressions.

Chen et al. (1978) found that increasing vertical reinforcement from two No. 5 bars to two No. 8 bars had no noticeable effect on the shear behaviour of FG walls. It should be noted, however, that the vertical reinforcement was located in the exterior cells of the walls; no interior vertical reinforcement was used. Oan (2013) found that vertically reinforced walls showed no change in the shear strength or ductility of PG walls, as compared with vertically unreinforced walls. However, they pointed out that normally the vertical steel would be embedded in a concrete base beam, causing the bars to bend at their bases under lateral loading, and thus contributing to the resistance of the wall through dowel action (Oan, 2013). The vertical bars in the walls tested by Oan were not embedded in this manner.

Anderson and Priestley (1992) assembled a dataset of 65 FG walls to fit an equation to the data and found that the contribution of the vertical reinforcement was insignificant. The Technical Coordinating Committee on Masonry Research (TCCMaR) investigated whether to include a contribution of vertical reinforcement in the shear strength equation they developed, and found that the equation did not perform as well when a vertical reinforcement parameter was included (NEHRP, 1997a). Both the CSA and TMS shear strength equations for masonry are based off the TCCMaR equation, and consequently neither includes a vertical reinforcement term (Dillon and Fonseca, 2017b).

Dillon and Fonseca (2017b) pointed out flaws in the methodology used by Anderson and Priestley and the TCCMaR in developing their models, and reanalyzed both models using the same data from the original studies. They concluded that in the case of the Anderson and Priestley dataset, the vertical reinforcement did not contribute to the overall wall shear strength (Dillon and Fonseca, 2017b). However, in the case of the TCCMaR study, there was a statistically significant contribution from the vertical reinforcement (Dillon and Fonseca, 2017b).

Scrivener (1967) found that vertical and horizontal reinforcement are equally effective in providing crack control and increased shear strength. Shing et al. (1990) also found that the vertical reinforcement has an influence on the shear strength, which they explained by saying that it helps to resist crack opening, thereby enhancing aggregate-interlock forces. Ghanem et al. (1992) found that distributed vertical reinforcement increases shear strength, while concentrating the vertical steel at the ends increases the flexural strength of the wall with little increase in shear strength. Hassanli et al. (2014) compiled a database of experimental results from 89 PG walls and found that shear strength equations in current design codes overestimate the shear strength of PG walls as vertical reinforcement spacing increases. Dillon (2015) explained that vertical reinforcement contributes to shear strength through confining crack openings and dowel action (Figure 2.7). He suggested that the finding of Ghanem et al. (1992) that only interior vertical reinforcement is effective in increasing shear capacity is because the exterior vertical reinforcement is principally engaged in resisting the overturning moment of the wall (Dillon, 2015). Ba Rahim et al. (2019) studied the effect of interior vertical reinforcement on the shear strength of PG masonry walls using FEM and concluded that it does contribute to the shear strength.

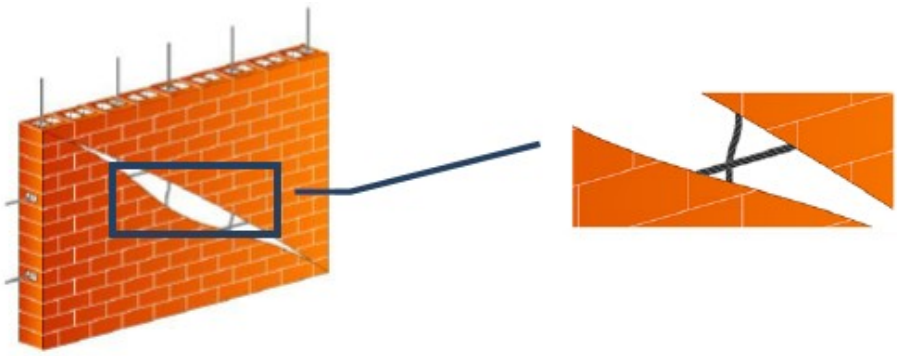

Figure 2.7 - Illustration of dowel action of vertical reinforcement (Hassanli and ElGawady, 2013)

Matsumura (1987) included a contribution from the exterior vertical (flexural) reinforcement in his equation. Shing et al. (1990) included a term to account for vertical reinforcement in their equation. The same term was subsequently adopted in the NZS 4230:2004 (2004) and Voon and Ingham (2007) equations. Dillon (2015) and Hung (2018) also included vertical reinforcement

terms in their shear strength models. Hassanli et al. (2014) affirmed that the vertical reinforcement spacing plays a significant role in the shear strength of PG walls, and this effect should be accounted for in design expressions.

The spacing of vertical reinforcement may be more critical than the amount (Hassanli et al., 2014). Elmapruk (2010) found that decreasing the spacing between vertical cells greatly improved shear strength. Similarly, Nolph and ElGawady (2012) found that increasing the spacing between vertical grouted cells caused a decrease in shear strength. However, Maleki et al. (2009) used three different spacings of horizontal and vertical reinforcement in PG walls and observed that the overall response of the walls was not sensitive to the reinforcement spacing. They also found that widely spaced reinforcement improved wall ductility (Maleki, 2008).

The effect of vertical reinforcement spacing in PG walls can be explained using strut-and-tie theory. In walls with widely spaced vertical reinforcement, the shear force cannot be transferred along the wall using intermediate reinforcement in the same way as closely spaced reinforcement (Figure 2.8). Instead, vertical cracks form due to tension forces that are not being carried by reinforcement, and the wall shear capacity is reduced compared to code predictions (Hassanli et al., 2014).

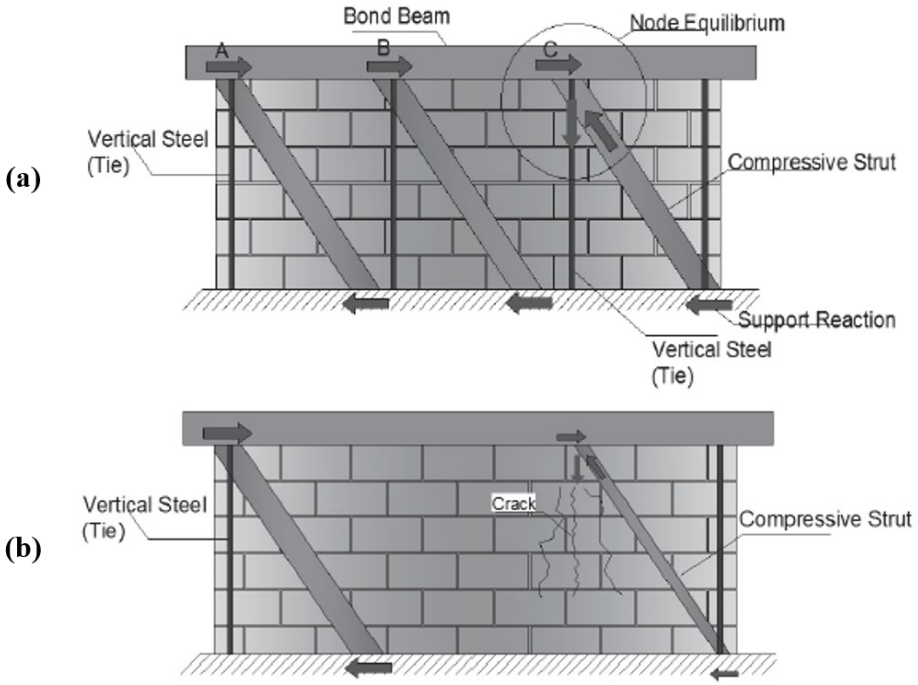

Figure 2.8 - Effect of vertical reinforcement spacing in PG walls (a) with closely spaced reinforcement, and (b) with widely spaced reinforcement (adapted from Hassanli et al., 2014)

While the size of vertical reinforcement has a negligible impact on construction costs, the cost of grouting can be high (Fattal, 1993a). Therefore, from an economic standpoint, it may not always be practical to decrease the spacing between vertically reinforced cells to achieve higher shear strengths.

Similar to horizontal reinforcement, the ability of vertical reinforcement to increase PG wall shear strength is likely limited. Scrivener (1967) noted that shear strength increased as the quantity of horizontal and vertical reinforcement increased from zero up to approximately 0.3% of the gross cross-sectional wall area. Further increase of reinforcing percentage did little to increase the shear strength. This can be explained through strut-and-tie theory: when vertical reinforcement spacing is reduced beyond a certain point, the number and width of compressive struts cannot be increased and the shear strength does not improve (Hassanli et al., 2014). This is illustrated in Figure 2.9.

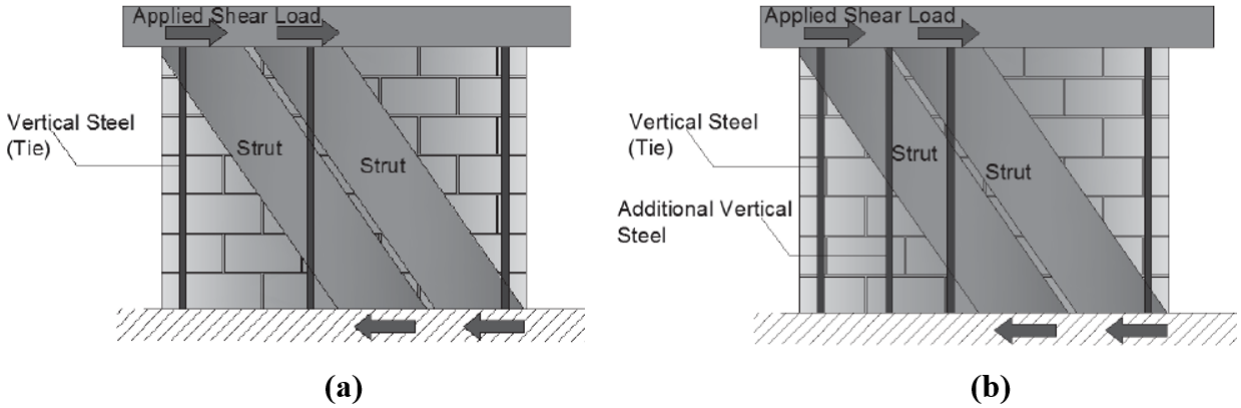

Figure 2.9 - Effect of vertical reinforcement spacing of PG walls with (a) normally spaced reinforcement, and (b) very closely spaced reinforcement (adapted from Hassanli et al., 2014)

The strut-and-tie model in Figure 2.9 is based on the assumption that the shear strength is controlled by the capacity of the masonry strut, such that increasing the amount or size of ties cannot increase the shear strength (Hung, 2018).

2.2.2.6 Effects of Other Wall Properties

Mortar is responsible for the uniform distribution of stresses, correction of irregularities of blocks and accommodation of deformations due to thermal expansion and shrinkage (Haach, 2009). In FG masonry, cracks pass through the blocks more than the joints (Hassanli et al., 2014). Shing et al. (1990) referred to this fact as reason to believe that mortar joints had little influence on the shear strength of the FG walls they tested. In PG walls, however, the mortar typically plays the role of weak layers that are vulnerable to cracking (Hassanli et al., 2014). For walls with high masonry compressive strength, cracks in mortar layers usually control the failure, meaning that the contribution of f'_m may be less in PG walls than it is in FG walls (Hassanli et al., 2014).

Hoque (2013) stated that the material properties of the mortar that influence the structural performance of masonry are compressive strength, bond strength and elasticity, workability, and water retention, with the compressive strength of mortar being less important than the other

properties. The workability of mortar is of particular importance because it directly influences the workmanship, which can influence the mechanical properties of masonry considerably (Haach, 2009). Oan (2013) attributed lower shear strengths to reduced bond between mortar and masonry units due to increased joint reinforcement diameter. Tomaževič and Lutman (1988) noted that masonry units and mortar must be of adequate quality, and reinforcement bond and anchorage conditions must be sufficient for the reinforcement to be effective.

Woodward and Rankin (1985) tested 17 URM walls and found that the effect of block and mortar strength on shear strength was very small at low axial stress (0.69 MPa). At high axial stress (2.76 MPa) the effect of increasing material strength became significant and led to increased shear strength (Woodward and Rankin, 1985). They noted that there is an interaction between the block and mortar strengths, such that wall behaviour may not be adequately predicted by considering the two independently.

Haach et al. (2007) found that bond pattern had no effect on the behaviour of PG masonry walls.

2.3 Existing Expressions Predicting In-plane Shear Strength of PG Masonry Walls

The following section gives an overview of existing code- and research-based expressions for predicting the in-plane shear strength of PG masonry walls. The equations listed in this section will be used as a benchmark to assess the performance of the models generated in the present study. By no means is this an exhaustive list of existing code- and research-based shear strength expressions, but it seeks to provide some history of the development of some of the existing code- and research-based equations, with a focus on equations used in North America. Some of the equations were developed exclusively for PG walls, while others were developed based on a combination of PG and FG wall data, and some were developed based solely on FG wall data. The full details of how each equation was derived are not provided, but additional information can be found in the original studies. Dillon (2015) also provides helpful commentary and insights on many of the equations presented herein.

Note that some of the variable symbols have been changed to maintain consistency in this study. Where imperial units were used in the original equations, they have been converted to metric units. Strength reducing factors have been omitted to allow for investigation of the unfactored shear resistance.

2.3.1 Matsumura (1987)

Matsumura (1987) developed a shear strength model based on the results of his experimental study of 80 masonry walls, 57 of which were concrete masonry walls while the remaining 23 were brick masonry walls. Of the 57 concrete masonry walls, 28 were PG walls. Matsumura's tested walls were all reinforced with flexural reinforcement. Where horizontal reinforcement was present, it was in the form of bond beams. More information about this experimental study is provided in Chapter 3.

Matsumura built his equation in a piecewise manner by examining the influence of each parameter individually, adding them to the equation one by one (Dillon, 2015). The equation expresses shear strength as a sum of contributions from masonry, steel reinforcement and the applied axial force, as given in Equation (2.1).

$$V_n = 0.875td\left\{\left[k_u k_p\left(\frac{0.76}{\frac{H}{d}+0.7}+0.012\right)\sqrt{f'_{mu,gr}}\right]+\left(0.18\gamma\delta\sqrt{\rho_h f_{yh} f'_{mu,gr}}\right)+0.2\sigma_{gr}\right\} \quad (2.1)$$

where k_u = 1.0 for FG walls, 0.8 for PG brick masonry walls, 0.64 for PG concrete masonry walls

k_p = $1.16\left(\rho_{vf}\right)^{0.3}$

ρ_{vf} = ratio of outermost vertical reinforcement steel

$= \frac{A_{vf}}{td} \times 100$

A_{vf} = cross-sectional area of vertical reinforcing bar(s) in one side (mm^2)

d = effective wall length, taken as the distance from the extreme compression fibre to the centroid of the flexural tension reinforcement

$f'_{mu,gr}$ = ungrouted prism strength, based on gross area (MPa)

γ = factor that accounts for the type of reinforcement used to confine grout; 1.0 for hoop-type reinforcement in FG masonry, 0.8 for a single reinforcing bar with semi-circular hooks at the ends in FG masonry, and 0.6 for PG masonry, regardless of reinforcement type (Matsumura, 1988)

δ = factor that accounts for the effect of boundary conditions; 1.0 for double curvature and 0.6 for single curvature

ρ_h = horizontal reinforcement ratio

$= \frac{A_{h,bar}}{ts_h}$

$A_{h,bar}$ = area of a single horizontal bar (mm^2)

s_h = spacing of horizontal bars (mm)

σ_{gr} = axial stress applied to the wall, based on gross area (MPa)

Fattal (1993b) pointed out that this equation cannot predict the strength of unreinforced walls, because it makes no provision for the effect of the compressive strength of masonry on shear capacity in the absence of reinforcement. It also produces overly conservative strength estimates for walls in which only horizontal reinforcement is used (Fattal et al., 1993b).

2.3.2 AIJ (1987)

The Architectural Institute of Japan developed a shear strength equation for masonry walls, which appears in Okamoto et al. (1987). Information available on this equation in English is limited, so the derivation process is unknown. The equation is provided here as Equation (2.2).

$$V_n = \left[0.053 \rho_{vf}^{0.23} \frac{f'_m + 17.65}{\frac{M}{VL} + 0.12} + 0.1\sigma_{net} + 0.8456\sqrt{\rho_h f_{yh}} \right] \frac{t_e d}{tL} A_{net} \qquad (2.2)$$

where ρ_{vf} = flexural reinforcement ratio

$= \frac{A_{vf,bar}}{t_e d}$

$\frac{M}{VL}$ = shear span ratio

$= 1 \leq \frac{M}{VL} \leq 3$

σ_{net} = net axial stress (MPa)

ρ_h = shear (horizontal) reinforcement ratio

$= \frac{A_{h,bar}}{s_h t}$

f_{yh} = yield strength of shear reinforcement

t_e = "equivalent width of wall" (mm)

t = wall thickness ("width") (mm)

d = effective wall length (mm)

L = wall length (mm)

Okamoto et al. (1987) provided the AIJ equation in terms of stress, so all the terms have been multiplied by A_{net} to get the equivalent shear strength. Okamoto et al. (1987) also did not specify whether the axial stress referred to should be calculated based on gross or net area, however this multiplication by A_{net} means that Equation (2.2) essentially uses axial load, P, instead of axial stress. Note that some coefficients were adjusted to convert the equation from units of kg/cm^2 to MPa. Reinforcement ratios were converted from percentages to unitless values.

2.3.3 UBC (1988)

The Uniform Building Code (UBC) uses an empirically derived formula to predict the in-plane shear strength of masonry walls. The nominal shear strength is calculated by adding the contributions of the masonry and the horizontal reinforcement (Equation (2.3)).

$$V_n = 0.083 C_d A_{net} \sqrt{f'_m} + A_{net} \rho_h f_{yh} \tag{2.3}$$

where C_d = masonry shear strength coefficient, which is obtained from Equation (2.4)

A_{net} = net area of masonry section (mm^2)

f'_m = compressive strength of masonry at 28 days (MPa)

ρ_h = ratio of shear (horizontal) reinforcement to the area

f_{yh} = yield strength of reinforcement (MPa)

$$C_d = \begin{cases} 2.4 & \text{for } \dfrac{M}{Vd} \leq 0.25 \\ 2.8 - 1.6\left(\dfrac{M}{Vd}\right) & \text{for } 0.25 < \dfrac{M}{Vd} < 1.0 \\ 1.2 & \text{for } \dfrac{M}{Vd} \geq 1.0 \end{cases} \tag{2.4}$$

where d = distance from extreme compression fiber to centroid of tension reinforcement (mm)

In the 1988 version of the UBC, the following upper limit was provided, with interpolation allowed for intermediate values:

$$V_n \leq \begin{cases} 0.50 A_e \sqrt{f'_m} & \text{for } \dfrac{M}{Vd} \leq 0.25 \\ 0.33 A_e \sqrt{f'_m} & \text{for } \dfrac{M}{Vd} \geq 1.00 \end{cases} \tag{2.5}$$

where A_e = effective area of masonry (mm^2), taken as the lesser of the minimum bedded area or the minimum cross-sectional area

Unlike most other design equations, the UBC equation does not account for the effects of axial load on shear strength. It also does not apply a reduction to the contribution of horizontal reinforcement.

This equation has since been superseded by UBC (1997) and by the International Building Code (IBC) in 2000.

2.3.4 Blondet et al. (1989)

Blondet et al. (1989) developed two models for predicting the in-plane shear strength of masonry walls built with CMUs. The models were developed on experimental data from tests done at UC Berkeley, consisting only of FG walls (Dillon and Fonseca, 2017b). The first model, referred to by Blondet et al. (1989) as "Method A", is given as Equation (2.6).

$$V_n = \begin{cases} \left(5.0 - 2.5 \dfrac{M}{Vd}\right) \sqrt{f'_m} A_{net} & \text{if } \rho_h < 0.2\% \\ \left(6.0 - 3.0 \dfrac{M}{Vd}\right) \sqrt{f'_m} A_{net} & \text{if } \rho_h \geq 0.2\% \end{cases} \tag{2.6}$$

where $\frac{M}{Vd}$ = "aspect ratio of the wall"

≤ 1

f'_m = masonry compressive strength (psi)

ρ_h = horizontal reinforcement ratio

The second model, "Method B", was developed based on the assumption that the ultimate shear strength is equal to the sum of contributions from the masonry and the horizontal reinforcement. The masonry shear strength was assumed to be equal to the cracking shear strength, while the horizontal reinforcement was assumed to be 50% effective, as it was thought that only the horizontal shear in the centre of the wall was effective in resisting shear. Method B is given here as Equation (2.7).

$$V_n = \left[\sqrt{v_{cr0}^2 + \frac{v_{cr0}\sigma}{1.5}} + 0.5\rho_h f_{yh}\right] A_{net} \quad (2.7)$$

where v_{cr0} = average shear cracking strength of the masonry at zero axial load

= $\left(3.5 + 1.75\frac{M}{Vd}\right)\sqrt{f'_m}$

σ = average axial stress (psi)

f_{yh} = yield strength of horizontal reinforcement (psi)

The TCCMaR model was based off of Method 2 (Equation (2.7)) as well as the Anderson and Priestley (1992) model. Hence, Equation (2.7) is referred to as the Blondet model. It should be noted that both models developed by Blondet et al. (1989) use imperial units.

2.3.5 Shing et al. (1990)

Shing et al. (1990) tested 22 FG masonry walls and, based on the results, proposed a new shear strength equation (Equation (2.8)).

$$V_n = \left(0.166 + 0.0217\rho_v f_{yv}\right)A_{net}\sqrt{f'_m} + 0.0217P\sqrt{f'_m} + \left(\frac{L - 2d'}{s_h} - 1\right)A_{h,bar}f_{yh} \quad (2.8)$$

where ρ_v = the ratio of vertical steel

$= \frac{A_{vt}}{Lt}$

A_{vt} = total area of vertical steel (mm^2)

L = wall length (mm)

t = wall thickness (mm)

A_{net} = net horizontal cross-sectional area (mm^2)

f'_m = compressive strength of masonry at the age of 28 days (MPa)

P = axial load (N)

d' = the distance from the extreme vertical steel to the edge of the wall (taken as 4"=101.6 mm for 16" long blocks)

s_h = spacing of the horizontal reinforcement (mm)

$A_{h,bar}$ = area of a horizontal reinforcing bar (mm^2)

Shing et al. (1990) suggested that a 45° crack would not permit adequate development lengths for horizontal reinforcement in the top and bottom courses to develop tensile resistance. Because the equation was developed purely based on FG wall data, A_{net} used by Shing et al. (1990) would have been no different from the gross area of the walls. Schultz (1994) suggested that in this equation, the product of the vertical reinforcement ratio and the wall area should be equal to the total area of vertical steel. However, Shing et al. (1990) clearly defined the area to be multiplied by the vertical reinforcement ratio as the "net horizontal area."

2.3.6 Anderson and Priestley (1992)

Anderson and Priestley (1992) took data from three studies, two of which tested FG walls exclusively (Sveinsson et al., 1985; Shing et al., 1990) while the other study tested both PG and

FG walls (Matsumura, 1987). Although Anderson and Priestley did not clearly identify which of the Matsumura walls were included in their database, other researchers have indicated that they only used FG wall data to develop their equation (Dillon and Fonseca, 2017b). Anderson and Priestley started with an assumed shear strength equation form consisting of contributions from the masonry, axial load, vertical reinforcement, and horizontal reinforcement. The assumed equation form is given by Equation (2.9).

$$V_n = b_1 * k_1 k_2 \sqrt{f'_m} Lt + b_2 * P + b_3 * A_v f_{yv} + b_4 * A_{h,bar} f_{yh} \frac{d}{s_h} \quad (2.9)$$

where k_1 = the aspect ratio coefficient

k_2 = the ductility coefficient

f'_m = masonry compressive strength (MPa)

L = wall length (mm)

t = wall thickness (mm)

P = axial load (N)

A_v = area of vertical steel in the middle third of the wall (mm^2)

f_{yv} = yield strength of the vertical reinforcement (MPa)

$A_{h,bar}$ = area of horizontal steel (mm^2) at a spacing of s_h (mm)

f_{yh} = yield strength of the horizontal reinforcement (MPa)

d = distance from the compression face to the extreme tension bar (mm)

They then determined the coefficients b_1, b_2, b_3 and b_4 by fitting the equation to the compiled test data, using an iterative trial-and-error approach (Dillon and Fonseca, 2017b). There was not sufficient data to determine the coefficients k_1 and k_2, so they were removed from the final model.

For walls built using concrete blocks, Anderson and Priestley (1992) found the best fit to be expressed as given in Equation (2.10).

$$V_n = 0.24\sqrt{f'_m}Lt + 0.25P + 0.5A_{h,bar}f_{yh}\frac{d}{s_h} \tag{2.10}$$

Anderson and Priestley (1992) noted that, unexpectedly, the vertical reinforcement had a coefficient of 0 in the best-fit model. Dillon and Fonseca (2017b) reanalyzed the model using multivariate regression and new data and still found the contribution of the vertical reinforcement parameter to be insignificant. However, in other models reanalyzed by Dillon and Fonseca (2017b), the contribution of the vertical reinforcement was significant, which suggests that the form of the equation affects the significance of variable contributions.

2.3.7 Fattal (1993)

Fattal (1993b) complied data from 72 PG masonry shear walls. Of those walls, 51 were tested by Matsumura (1987), 11 were tested by Chen et al. (1987), and the remaining 10 were tested by Yancey and Scribner (1989). PG walls built with concrete blocks and clay bricks were both included in the dataset. Fattal (1993b) altered the equation by Matsumura (1987) to improve it, using the compiled data to compare the performance of the two equations. The equation proposed by Fattal (1993b) is given by Equation (2.11).

$$V_n = \left[k_o k_u \left(\frac{0.5}{\frac{H}{L} + 0.8} + 0.18 \right) \sqrt{f'_m f_{yv}} \rho_v^{0.7} + 0.011 k_o \gamma \delta f_{yh} \rho_h^{0.31} + 0.012 k_o f'_m + 0.2\sigma_{gross} \right] Lt \tag{2.11}$$

where k_o = a reduction factor for PG masonry

= 0.8 for PG walls, 1.0 for FG walls

k_u = 1.0 for FG walls, 0.8 for PG brick masonry walls, 0.64 for PG concrete masonry walls

H = height of wall (mm)

L = length of wall (mm)

f'_m = compressive strength of masonry prism (MPa)

f_{yv} = yield strength of the vertical reinforcement (MPa)

ρ_v = total vertical reinforcement ratio

$= \frac{A_v}{Lt}$

t = thickness of wall (mm)

γ = coefficient accounting for the type of masonry and amount of grout; 1.0 for FG masonry and brick masonry, 0.6 for PG concrete masonry

δ = coefficient to account for the effect of boundary conditions; 1.0 for walls with inflection point at mid-height (double curvature), 0.6 for cantilever walls

f_{yh} = yield strength of the horizontal reinforcement (MPa)

ρ_h = horizontal reinforcement ratio

$= \frac{A_h}{s_h t}$

σ_{gross} = "nominal" axial stress on wall, based on gross wall area (MPa)

Based on the data from the 72 PG walls, the strength values predicted by Equation (2.11) varied from 41% to 146% of measured strength values, with 68% falling within the ±20% range (Fattal, 1993b). This was an improvement over the Matsumura (1987) equation, which had strength

predictions varying from 23% to 180% of measured values, with only 46% falling within the ±20% range (Fattal, 1993b).

2.3.8 TCCMaR (1997)

The masonry shear strength equation found in the 1997 edition of the National Earthquake Hazards Reduction Program (NEHRP) recommended provisions was developed by the Technical Coordinating Committee on Masonry Research (TCCMaR). The 1997 NEHRP Provisions commentary states that the TCCMaR equation is a combination of the Blondet et al. (1989) and Anderson and Priestley (1992) equations (NEHRP, 1997a). For the masonry component, the Blondet form was used, as previous research had concluded that the M/VL ratio should be included in this term (NEHRP, 1997a). Since there was little difference in the values used to account for the vertical load contribution, it was decided to use the more simplified form of Anderson and Priestley. The shear strength equation developed by TCCMaR is provided in section 11.7.3 of NEHRP (1997b) and here as Equation (2.12).

$$V_n = 0.083\left[4.0 - 1.75\left(\frac{M}{VL}\right)\right]A_{net}\sqrt{f'_m} + 0.5A_{h,bar}f_{yh}\frac{L}{s_h} + 0.25P \tag{2.12}$$

where V_n is limited by

$$V_n \leq \begin{cases} 0.5A_{net}\sqrt{f'_m} & \text{for } \dfrac{M}{VL} \leq 0.25 \\ \left(0.56 - 0.22\dfrac{M}{VL}\right)A_{net}\sqrt{f'_m} & \text{for } 0.25 < \dfrac{M}{VL} < 1.0 \\ 0.33A_{net}\sqrt{f'_m} & \text{for } \dfrac{M}{VL} \geq 1.00 \end{cases} \tag{2.13}$$

and $\frac{M}{VL}$ = shear span depth ratio, which need not be taken greater than 1

A_{net} = net cross-sectional area of the masonry (mm^2)

f'_m = specified compressive strength of the masonry (MPa)

$A_{h,bar}$ = area of (horizontal) shear reinforcement (mm^2)

f_{yh} = yield strength of shear reinforcement (MPa)

L = length of member in direction of shear force (mm)

s_h = spacing of shear reinforcement (mm)

P = axial load on the masonry section due to unfactored design loads (N)

In Equation (2.12), the coefficient of 1.75 appears to have been taken directly from the Blondet et al. equation, while the coefficient of 0.25 was taken directly from the Anderson and Priestley equation (NEHRP, 1997a; Dillon and Fonseca, 2017b). The coefficient of 0.5 was the same for both studies. With three of the four coefficients assigned, the value of the remaining coefficient (4.0) seems to have been derived from the data (Dillon and Fonseca, 2017b). This method of assigning coefficient values was criticized by Dillon and Fonseca (2017b), who pointed out that because the form of the TCCMaR differed from those of the previous models, new coefficients should have been derived. Using values other than those determined through least squares regression introduces additional modeling error into the predictions made by the model (Dillon and Fonseca, 2017b).

The issue of whether to include the contribution of vertical reinforcement was investigated by the TCCMaR, using two different forms of a vertical steel parameter and an assumed coefficient of 0.25 (NEHRP, 1997a). They found that their equation did not perform as well when either vertical reinforcement parameter was included as compared to when no vertical reinforcement parameter was included (NEHRP, 1997a). This methodology was not suitable for determining whether to include the parameters; an analysis of variance to determine the statistical significance of the vertical reinforcement terms would have been more appropriate (Dillon and Fonseca, 2017b). Dillon and Fonseca (2017b) reanalyzed the TCCMaR model using the same data and found the vertical reinforcement contribution to be statistically significant at the $\alpha = 0.10$ level.

2.3.9 NTC-2004

NTC-2004 is the standard for design and construction in Mexico City, and is used in most regions of Mexico (Alcocer et al., 2003). The shear strength equation for reinforced masonry is found in section 6.4 of NTC-2004. The nominal shear strength according to NTC-2004 (2004) is calculated using Equation (2.14).

$$V_n = 0.5v_m^* A_{gross} + 0.3P + \eta\rho_h f_{yh} A_{gross} \quad (2.14)$$

where the first two terms are limited as shown in Equation (2.15).

$$0.5v_m^* A_{gross} + 0.3P \leq 1.5v_m^* A_{gross} \quad (2.15)$$

and v_m^* = design diagonal shear resistance (MPa), obtained through diagonal compression tests of wallettes (2.8.2.1 of NTC-2004), or using the following equation:

$$= \begin{cases} 0.35 \leq 0.25\sqrt{f_m'^*} & \text{if } f_{mortar} \geq 12.5 \\ 0.25 \leq 0.25\sqrt{f_m'^*} & \text{if } f_{mortar} \leq 12.5 \end{cases}$$

$f_m'^*$ = design compressive strength of masonry (MPa), see 2.8.1.1 of NTC-2004

$$= \frac{f'_{m,MX}}{1+2.5c_m}$$

$f'_{m,MX}$ = average ungrouted compressive strength of masonry prisms (MPa), based on gross area and a height-to-thickness ratio of 4 to 1 (correction factors for different height-to-thickness ratios are provided in Table 2.5 of NTC-2004; the correction factor for a height-to-thickness of 5 to 1 is 1.05)

c_m = coefficient of variation of the compressive resistance of masonry prisms, which shall not be taken as less than 0.15 (taken as 0.15 in the present study)

A_{gross} = gross cross-sectional area of the wall (mm^2)

P = vertical load, taken as positive in compression (N)

ρ_h = horizontal reinforcement ratio; joint ladder reinforcement is not considered to be effective under seismic loads

= $\frac{A_{h,bar}}{s_h t}$

$A_{h,bar}$ = area of horizontal steel (mm^2) placed at a spacing of s_h (mm)

t = wall thickness (mm)

f_{yh} = specified yield stress of horizontal reinforcement (MPa)

$\leq$ 600 MPa

η = efficiency factor for horizontal reinforcement, given by Equation (2.16)

$$\eta = \begin{cases} 0.6 & \text{if } \rho_h f_{yh} \leq 0.6 \\ 0.2 & \text{if } \rho_h f_{yh} \geq 0.9 \end{cases} \quad (2.16)$$

In Equation (2.16), linear interpolation is allowed for values of $\rho_h f_{yh}$ between 0.6 and 0.9.

NTC-2004 has since been superseded by the 2017 version of the code. The shear strength equation is identical in both versions, except that the calculation of η is more complex in the 2017 version. Although bond beam reinforcement is not used in masonry construction in Mexico, it will be included in calculations of ρ_h to evaluate the performance of Equation (2.14).

2.3.10 NZS 4230:2004

The New Zealand code equation for in-plane shear strength of masonry walls is found in section 10.3.2.2 of NZS 4230:2004. It was formulated largely based on research by Voon and Ingham (2002). The equation is given here as Equation (2.17):

$$V_n = \left[0.2\sqrt{f'_m}(C_1 + C_2) + \frac{0.8 A_{h,bar} f_y}{t_{eff} s_h}\right] t_{eff} d + 0.9 P_f \tan\alpha \quad (2.17)$$

An upper limit is included to avoid critical shear failures (Equation (2.18)).

$$V_n \leq 0.45\sqrt{f'_m}t_{eff}d \tag{2.18}$$

A limit on the contribution of the axial stress term is also included, to prevent excessive dependence on this term in relatively squat masonry (Equation (2.19)).

$$0.9P_f \tan\alpha \leq 0.1f'_m t_{eff} d \tag{2.19}$$

where f'_m = specified compressive strength of masonry (MPa), which may be determined by testing prisms with a minimum of 3 courses, based on gross area and normally at 28 days

C_1 = coefficient to account for the dowel action of vertical steel when longitudinal steel in excess of the minimum value of 0.07% is used (Equation (2.20))

C_2 = coefficient to account for the shear span ratio (Equation (2.21))

P_f = design axial load in compression (N) at given eccentricity, limited to prevent brittle shear failure

$\leq 0.1f'_m A_{gross}$

t_{eff} = effective web width (mm); equal to wall thickness for FG walls

= $2t_{fs}$ for PG walls

t_{fs} = face shell thickness (mm)

d = distance from extreme compression fibre to centroid of longitudinal tension reinforcement (mm)

= $0.8L$ for walls

L = wall length (mm)

α = angle between lines of axial load action and resulting reaction (Figure 2.10)

$A_{h,bar}$ = area of shear (horizontal) reinforcement within a distance s_h (mm^2)

f_y = lower characteristic yield strength of reinforcement (MPa); the value of yield strength below which not more than 5% of production tests in each size falls

s_h = spacing of horizontal reinforcement in vertical direction (mm)

The coefficient C_1 is calculated as follows:

$$C_1 = 33\rho_v \frac{f_y}{300} \text{ for } \rho_v \geq 0.07\% \tag{2.20}$$

where ρ_v = the vertical reinforcement ratio

$= \frac{A_v}{t_{eff} d}$

A_v = total vertical reinforcement area

The coefficient C_2 is calculated as follows:

$$C_2 = \begin{cases} 1.5 & \text{if } \frac{M}{VL} < 0.25 \\ 0.42\left[4 - 1.75\frac{M}{VL}\right] & \text{if } 0.25 \leq \frac{M}{VL} \leq 1 \\ 1 & \text{if } \frac{M}{VL} > 1 \end{cases} \tag{2.21}$$

The following figure is provided to explain the definition of α.

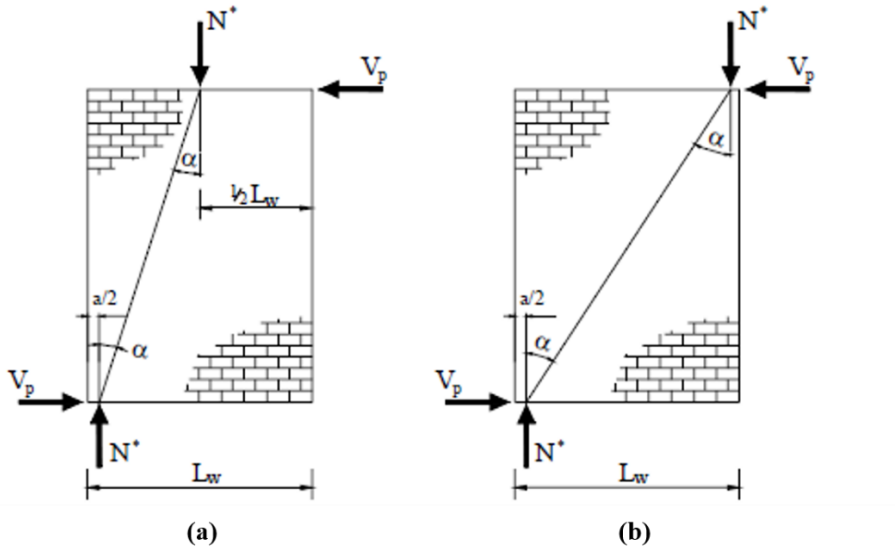

Figure 2.10 - Contribution of axial force to masonry shear strength for (a) single curvature and (b) double curvature (adapted from Voon, 2007)

In Figure 2.10, "a" denotes the depth of equivalent rectangular stress block, measured in mm.

2.3.11 Eurocode 6 (2005)

The European code equation for in-plane shear strength of masonry walls is given in section 6.7.2 of EN 1996-1-1 (2005), also known as Eurocode 6. For masonry walls in which the perpend (head) joints do not satisfy the requirements of section 8.1.5(3) so as to be considered as filled, the shear strength is predicted by Equation (2.22):

$$V_n = 0.5 f_{vko} tL + 0.4P + 0.9 A_h f_{yh} \leq 2.0 tL \tag{2.22}$$

which is limited by

$$0.5 f_{vko} + \frac{0.4P}{tL} \leq 0.045 f_b \text{ or } f_{vlt} \tag{2.23}$$

where f_{vko} = is the characteristic initial shear strength of masonry under zero compressive stress (MPa), to be determined from tests in accordance with EN 1052-3 or EN 1052-4, or from the values given in Table 3.4 of EN 1996-1-1 (2005)

= 0.20 for general purpose mortar and standard CMUs

t = wall thickness (mm)

L = wall length (mm)

P = the design compressive load perpendicular to the shear, using the appropriate load combination

A_h = total area of horizontal shear reinforcement

f_{yh} = design strength of the reinforcement

f_b = the normalized compressive strength of the masonry units, which is either given by the manufacturer or obtained by converting the compressive strength using EN 772-1, Annex A

f_{vlt} = a limit to be found in the National Annex of a given country, if it is to be used

Notably, the initial shear strength of masonry value (0.20) given in Table 3.4 of EN 1996-1-1 (2005) is an arbitrarily low value. As a result, Eurocode 6 predicts overly conservative values of shear strength (El-Dakhakhni et al. 2013). In addition, Eurocode 6 does not distinguish between FG and PG walls, likely because the use of PG masonry is uncommon in Europe (Oan, 2013).

2.3.12 Voon and Ingham (2007)

Voon and Ingham (2007) proposed an equation that echoed the form of the TCCMaR (1997) equation, while adding a term proposed by Shing et al. (1990) to account for the contribution of vertical reinforcement, and taking ideas from Priestley et al. (1994). The equation developed by Voon and Ingham (2007) is given here as Equation (2.24).

$$V_n = k\left(0.022\rho_v f_{yv} + 0.083\left[4 - 1.75\frac{M}{VL}\right]\right)\sqrt{f'_m}td + 0.9P_f \tan\alpha + A_{h,bar} f_{yh}\frac{d_{eff}}{s_h} \quad (2.24)$$

The lowest of the upper limits used by the TCCMaR (Equation (2.25)) was adopted by Voon and Ingham (2007) to ensure that their equation would be as conservative as the TCCMaR equation.

$$V_n \leq 0.33\sqrt{f'_m}A_{net} \tag{2.25}$$

where k = ductility reduction factor (Figure 2.11)

ρ_v = vertical reinforcement ratio

f_{yv} = yield strength of vertical reinforcing steel (MPa)

$\frac{M}{VL}$ = shear span ratio

$$0.25 \leq \frac{M}{VL} \leq 1.0$$

f'_m = masonry compressive strength (MPa)

t = wall width (mm)

d = distance from extreme compression fibre to the centroid of longitudinal tension reinforcement, or 0.8L for walls (mm)

P_f = factored axial compressive load (kN)

α = angle formed between centres of load application and reaction (Figure 2.10)

$A_{h,bar}$ = area of a single horizontal reinforcement bar (mm^2)

f_{yh} = yield strength of horizontal reinforcing steel (MPa)

d_{eff} = effective depth of section (mm)

$= L - 2d' - l_{dh}$

d' = distance between wall edge and outermost vertical reinforcement (mm)

$= L - d$

l_{dh} = development length of shear reinforcement (mm)

$= 20d_b$ for reinforcement with a yield strength of 300 MPa; $35d_b$ for reinforcement with a yield strength of 500 MPa

s_h = spacing of horizontal reinforcement (mm)

A_{net} = net cross-sectional area (mm^2)

The value of k is determined using the relationship shown in Figure 2.11.

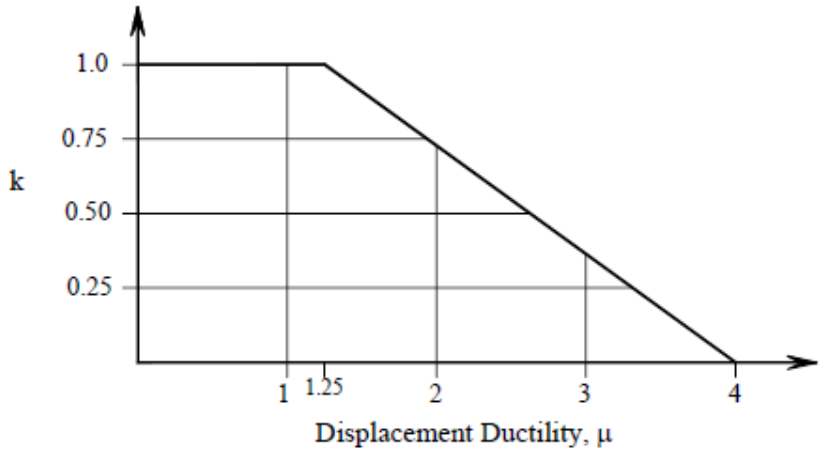

Figure 2.11 - Relationship between ductility and masonry shear resisting mechanism (Voon, 2007)

2.3.13 CSA S304-14 (2014)

The Canadian code equation for in-plane shear strength of masonry walls is given in section 10.10.2.1 of CSA S304-14 (2014), and here as Equation (2.26):

$$V_n = \left(0.16\left(2 - \frac{M_f}{V_f d_v}\right)\sqrt{f'_m}td_v + 0.25P\right)\gamma_g + 0.6A_{h,bar}f_{yh}\frac{d_v}{s_h} \leq 0.4\sqrt{f'_m}td_v\gamma_g \quad (2.26)$$

where $\frac{M_f}{V_f d_v}$ = shear span to depth ratio (unitless), taken as not more than 1 and not less than 0.25 for the concurrent factored moment, M_f, and factored shear, V_f, at the section under consideration

$$0.25 \leq \frac{M_f}{V_f d_v} \leq 1$$

f'_m = compressive strength of masonry normal to the bed joint at 28 days (MPa)

t = wall thickness (mm)

d_v = effective depth (mm), which need not be taken as less than 0.8 times L

P = axial compressive load on the section under consideration (N)

γ_g = factor to account for partial grouting; 1.0 for FG masonry

= $\frac{A_{net}}{Lt} \leq 0.5$ otherwise

$A_{h,bar}$ = cross-sectional area of horizontal reinforcement (mm^2)

f_{yh} = yield strength of horizontal reinforcement (MPa)

s_h = spacing of horizontal reinforcement (mm)

$\leq \begin{cases} 2400 \text{ mm} \\ 0.5L \end{cases}$ for bond beams

$\leq$ 600 mm for joint reinforcement

For squat walls with $H/L < 1$, the upper limit may be increased as provided in section 10.10.2.2 (Equation (2.27)).

$$V_n \leq 0.4\sqrt{f'_m} t d_v \gamma_g [2 - H/L] \qquad (2.27)$$

where H = height of the wall (mm)

L = length of the wall (mm)

and $0.5 \leq \frac{H}{L} \leq 1$

The CSA equation was developed based on the TCCMaR equation, meaning that all the errors present in the TCCMaR equation have been carried over to this equation (Dillon and Fonseca, 2017b).

2.3.14 Dillon (2015)

Dillon (2015) assembled a dataset of 172 FG and 181 PG masonry walls built using either CMUs or clay bricks. He considered several potentially influential parameters that combined measured variables, some of which were from other existing code- and research-based models while others were created "using logic and the theory of mechanics" (Dillon, 2015). Various forms of each parameter were included, which varied in terms of which variables were included as well as which variable definitions were used. In total, 48 potential parameters were considered in 5 categories: masonry, axial load, interior vertical reinforcement, bond beam reinforcement, and joint reinforcement.

Stepwise regression was used to narrow the pool of candidate parameters to a smaller set, and then various models were assembled using one parameter from each category. Model coefficients were selected using least squares regression. An optimum model was selected on the basis of model performance and simplicity, however the ability of the model to describe the nominal shear strength equally well for both grouting types was prioritized over how well the model fit the data. Two slightly different versions of the same equation were created, one of which was fitted to FG wall data while the other was fitted to PG wall data. The version for PG walls is given by Equation (2.28).

$$V_n = 0.083\left(1.1 + 0.9\frac{Vs_{gv,ave}}{M}\right)A_{nv}\sqrt{f'_m} + 0.15P + 0.12\left[\frac{A_{vi,bar}f_{yvi}}{s_{vi}}L + \left(\frac{A_{hbb,bar}f_{yhbb}}{s_{hbb}} + \frac{A_{hj,bar}f_{yhj}}{s_{hj}}\right)H\right] \quad (2.28)$$

where $\frac{V}{M}$ = ratio of ultimate shear demand to ultimate moment demand (mm^{-1})

$s_{gv,ave}$ = average spacing between vertically grouted cells (mm)

A_{nv} = net shear area of wall (mm^2), which is defined as the sum of the areas of the face shells, the grouted cores, and webs adjacent to the grouted cores

f'_m = compressive strength of the masonry

P = applied vertical axial load

$A_{vi,bar}$ = area of confinement (interior vertical) reinforcement (mm^2)

f_{yvi} = tensile strength of confinement reinforcement (MPa)

s_{vi} = average spacing of confinement reinforcement (mm)

$A_{hbb,bar}$ = area of bond beam reinforcement (mm^2)

f_{yhbb} = tensile strength of bond beam reinforcement (MPa)

s_{hbb} = average spacing of bond beam reinforcement (mm)

$A_{hj,bar}$ = area of joint reinforcement (mm^2)

f_{yhj} = tensile strength of joint reinforcement (MPa)

s_{hj} = spacing of joint reinforcement (mm)

H = geometric height of the wall (mm)

This model includes contributions from three types of reinforcement: interior vertical reinforcement, bond beam reinforcement and joint reinforcement. It was assumed that the coefficients for all three reinforcement types should be the same (Dillon, 2015).

The shear strength is limited by Equation (2.29):

$$V_n \leq \frac{0.8f'_m a t_{eff} \frac{L-a}{2} + A_f f_y \left(d - \frac{a}{2}\right)}{\frac{M_u}{V_u}} \tag{2.29}$$

where t_{eff} = the shear thickness of the wall, taken as t for FG walls and taken as the total face shell thickness for PG walls

a = the length of the compression block, as determined using Equation (2.30)

$$a = \frac{\left(A_f f_y + P + \frac{A_c f_{yc}}{s_c} L\right)}{0.8f'_m t_{eff}} \tag{2.30}$$

Dillon's model showed minor improvement over other existing code- and research-based equations, possibly due to the inclusion of a term accounting for vertical reinforcement (Hung, 2018). Dillon (2015) also developed strut-and-tie models for 116 FG and PG walls, 10 of which contained openings, and found that these models outperformed his proposed equation, particularly in the case of PG walls.

Although the analysis done by Dillon (2015) made use of stepwise regression, it failed to take advantage of the full capabilities of this technique because stepwise regression was not used to generate the final models. The main advantage of stepwise regression is its ability to identify an appropriate subset of input parameters for predicting the output variable. By subjectively deciding which parameters to include, Dillon neglected the possibility that a simpler form of the shear strength equation may be able to achieve the same or almost the same level of accuracy. He also did not explore all of the possible variables which may contribute to shear strength. The amount

of data which is now available, and the power of stepwise regression make for an ideal opportunity to explore new possibilities, including those which have been previously ignored by researchers.

2.3.15 Bolhassani et al. (2016)

Bolhassani et al. (2016b) developed a shear strength model for PG walls based on modified infilled-frame mechanism (Equation (2.31)).

$$V_n = (n_g - 1)\left[t * t_{eff}\sqrt{f'_{mu}}\cos\theta + \mu P_{infill} + \frac{4M_p}{H}\right] \quad (2.31)$$

where n_g = is the number of vertical grouted cells

≥ 2

t = unit thickness (mm)

t_{eff} = effective wall thickness (mm); equal to the unit thickness in FG masonry, otherwise it is equal to the thickness of face shells

f'_{mu} = ungrouted masonry compressive strength (MPa)

θ = angle of inclination of the compressive strut

μ = coefficient of friction (taken as 0.25 by Bolhassani et al. (2016b))

P_{infill} = axial load in the infill panel (kN)

$$= \frac{PA_{infill}}{(n_g-1)(A_{infill}+1.5A_{vgc})} + \frac{t*t_{eff}\sqrt{f'_{mu}}\sin\theta}{n_g-1}$$

P = axial load (kN)

A_{infill} = area of a single infill panel (mm^2), or the length of the wall between grouted cells, including half of the interior cell length, multiplied by the wall thickness

A_{vgc} = area of a single vertical grouted cell, including vertical steel (mm^2)

$= A_{gc} + A_s \left(\frac{E_{steel}}{E_{grout}} - 1\right)$

A_{gc} = area of a single grouted cell minus the area of steel, including face shells, outer web, and half of the inner web (mm^2)

A_s = area of vertical steel in a single grouted cell (mm^2)

E_{steel} = modulus of elasticity of steel (MPa)

E_{grout} = modulus of elasticity of "concrete" (MPa)

M_p = plastic moment (N*mm)

H = wall height (mm)

This equation is described as being best applicable to walls with vertical and horizontal grout spacing over 1.2 m, whereas the shear strength of walls with smaller grout spacing can be estimated well enough using the TMS equation (Bolhassani et al., 2016b).

2.3.16 TMS 402/602-16 (2016)

The American code equation for in-plane shear strength of masonry walls is given in section 9.3.4.1.2 of TMS402/602-16 (2016), and here as Equation (2.32):

$$V_n = \left\{ \left[0.083\sqrt{f'_m} \left(4.0 - 1.75 \frac{M}{VL} \right) + 0.5 \left(\frac{A_{h,bar} f_{yh} L}{A_{nv} s_h} \right) \right] A_{net} + 0.25P \right\} \gamma_{g,US} \qquad (2.32)$$

The shear strength is limited by Equation (2.33).

$$V_n \leq \begin{cases} 0.5\gamma_{g,US}A_{net}\sqrt{f'_m} & \text{for } \dfrac{M}{VL} \leq 0.25 \\ \left(0.56 - 0.22\dfrac{M}{VL}\right)\gamma_{g,US}A_{net}\sqrt{f'_m} & \text{for } 0.25 < \dfrac{M}{VL} < 1.0 \\ 0.33\gamma_{g,US}A_{net}\sqrt{f'_m} & \text{for } \dfrac{M}{VL} \geq 1.00 \end{cases} \quad (2.33)$$

and $\frac{M}{VL}$ = maximum moment at the section under consideration divided by the shear force times length, which shall be taken as a positive number and need not be taken greater than 1.0

f'_m = specified compressive strength of masonry (MPa)

$\gamma_{g,US}$ = 0.75 for PG walls, 1.0 otherwise

P = axial load, considered positive for compressive axial loads (N)

L = actual depth of a member in direction of shear considered (mm)

$A_{h,bar}$ = cross-sectional area of (horizontal) shear reinforcement (mm^2)

f_{yh} = allowable tensile or compressive stress in reinforcement (MPa)

A_{nv} = net shear area (mm^2); for members without flanges, net shear area is equal to the net cross-sectional area

s_h = spacing of horizontal reinforcement (mm)

A_{net} = net cross-sectional area of a member (mm^2)

Like the CSA equation, the TMS equation was developed from the TCCMaR equation, and all the associated errors have been carried over to it (Dillon and Fonseca, 2017b). Because PG walls can produce lower shear strengths than those predicted by the TCCMaR equation, the grouting factor was added to compensate for this effect until more accurate methods can be developed (TMS 402/602-16, 2016).

2.3.17 Hung (2018)

Hung (2018) compiled a database of 292 PG masonry walls built with CMUs. Data synthesization and scrutinization were then performed, resulting in several smaller datasets that included different numbers of specimens based on various combinations of inclusion criteria. From these datasets, several Artificial Neural Networks (ANNs) were generated and one was selected based on criteria of accuracy and representativeness of the data used to train the model. The selected ANN used 7 input parameters and 5 hidden layers, and showed major improvement in accuracy over that of conventional code equations, with a reported R^2 value of 0.850 (Hung, 2018). The selected ANN, identified by Hung as F-7-5-1, is given by Equations (2.34) to (2.37).

$$v_{n,gross} = \frac{(y_{min} - y_{max})(y_{norm} - 1)}{-2} + y_{max} \tag{2.34}$$

$$y_{norm} = [LW] \cdot \tanh(b_1 + [IW]\{X_{norm}\}) + b_2 \tag{2.35}$$

$$X_{\text{norm}} = \begin{bmatrix} x_{1,norm} \\ x_{2,norm} \\ x_{3,norm} \\ x_{4,norm} \\ x_{5,norm} \\ x_{6,norm} \\ x_{7,norm} \end{bmatrix} \tag{2.36}$$

$$x_{i,norm} = \frac{(-2)(x_i - x_{i,max})}{x_{i,min} - x_{i,max}} + 1 \tag{2.37}$$

where $v_{n,gross}$ = estimated gross shear stress (MPa)

= $\frac{V_n}{Lt}$

V_n = nominal shear strength (kN)

L = wall length (mm)

t = wall thickness (mm)

$$IW = \begin{bmatrix} -0.6183 & -0.6835 & 1.6011 & -0.3643 & 1.1593 & -0.0237 & 0.0430 \\ 1.3134 & 1.2532 & -2.1502 & -1.6223 & -0.0682 & -1.3960 & -1.7227 \\ 0.0637 & -1.3889 & -2.4748 & -0.9587 & -1.2993 & -0.8316 & 1.8284 \\ 0.0070 & -0.9053 & 1.0992 & -0.9918 & 1.9170 & 1.0863 & 1.9599 \\ 0.0206 & -0.6339 & 0.4812 & -0.4361 & 0.8425 & -1.2191 & 1.0364 \end{bmatrix}$$

$$LW = [0.8144 \quad -0.3618 \quad 0.3675 \quad 0.8712 \quad -0.8893]$$

$$b_1 = \begin{bmatrix} 1.5154 \\ 1.7618 \\ -0.4254 \\ -0.0269 \\ -1.3641 \end{bmatrix}$$

$$b_2 = -0.6123$$

The definition of each of the input variables, x_1 through x_7, as well as the corresponding minimum and maximum values, is given in Table 2.1. The minimum and maximum values of the output are also provided in Table 2.1.

Table 2.1 - Input/output minimum and maximum values for linear normalization (adapted from Hung, 2018)

Input Variable ($\boldsymbol{x_i}$)		Minimum ($\boldsymbol{x_{i,min}}$)	Maximum ($\boldsymbol{x_{i,max}}$)
x_1	A (m^2)	0.66	19.43
x_2	M/VL (unitless)	0.250	2.295
x_3	A_{net}/A_{gross} (unitless)	0.405	0.808
x_4	$f'_{m,eff}$ (MPa)	4.25	22.29
x_5	$\rho_v f_{yv}$ (MPa)	0	4.842
x_6	$\rho_h f_{yh}$ (MPa)	0	1.290
x_7	σ_{gross} (MPa)	0	1.724
Output Variable ($\boldsymbol{y}$)		Minimum ($\boldsymbol{y_{min}}$)	Maximum ($\boldsymbol{y_{max}}$)
y	$v_{max,gross}$ (MPa)	0.232	1.081

where A = wall area

= $H * L$

H = wall height (mm)

L = wall length (mm)

$\frac{M}{VL}$ = shear span ratio

$\frac{A_{net}}{A_{gross}}$ = ratio of net to gross cross-sectional wall area

A_{gross} = gross cross-sectional wall area (mm^2)

= $L * t$

t = wall thickness (mm)

$f'_{m,eff}$ = effective masonry strength (MPa); weighted average of ungrouted and grouted prism strengths using the standard aspect ratio of 5:1

$\rho_v f_{yv}$ = $\frac{A_{vi}f_{yvi}+A_{vf}f_{yvf}}{0.8Lt}$

A_{vi} = total area of interior vertical reinforcement (mm^2)

f_{yvi} = yield strength of interior vertical reinforcement (MPa)

A_{vf} = total area of flexural (outer vertical) reinforcement (mm^2)

f_{yvf} = yield strength of flexural reinforcement (MPa)

$\rho_h f_{yh}$ = $\frac{A_{hbb}f_{yhbb}+A_{hj}f_{yhj}}{Ht}$

A_{hbb} = total area of horizontal bond beam reinforcement (mm^2)

f_{yhbb} = yield strength of bond beam reinforcement (MPa)

A_{hj} = total area of horizontal joint reinforcement (mm^2)

f_{yhj} = yield strength of joint reinforcement (MPa)

σ_{gross} = gross applied axial stress (MPa)

$= \frac{P}{A_{gross}}$

P = applied compressive axial stress (N)

Section 4.7.4 of Hung (2018) provides a sample calculation that illustrates how this ANN can be used to predict the shear strength of a PG wall.

2.3.18 Summary of Design Expressions

Table 2.2 - Summary of existing code- and research-based shear strength equations for PG masonry walls

Code / Author	Shear Strength Contribution			
	Masonry (V_m)	**Axial Stress** (V_p)	**Horizontal Steel** (V_{sh})	**Vertical Steel** (V_{sv})
Matsumura (1987)	$0.875td\left[k_u k_p\left(\frac{0.76}{\frac{H}{d}+0.7}+0.012\right)\sqrt{f'_{mu,gr}}\right]$	$0.175td\cdot\sigma_{gr}$	$0.1575td\cdot\gamma\delta\sqrt{\rho_h f_{yh} f'_{mu,gr}}$	included in V_m
AIJ (1987)	$0.053\rho_{vf}^{0.23}\frac{f'_m+17.65}{\frac{M}{VL}+0.12}\cdot\frac{t_e d}{tL}A_{net}$	$0.1\sigma_{net}\frac{t_e d}{tL}A_{net}$	$0.8456\sqrt{\rho_h f_{yh}}\frac{t_e d}{tL}A_{net}$	included in V_m
UBC (1988)	$0.083C_d A_{net}\sqrt{f'_m}$	-	$A_{net}\rho_h f_{yh}$	-
Blondet et al. (1989)	$\sqrt{v_{cr0}^2+\frac{v_{cr0}\sigma}{1.5}}A_{net}$		$0.5\rho_h f_{yh}A_{net}$	-
Shing et al. (1990)	$(0.166A_{net}+0.0217P)\sqrt{f'_m}$		$\left(\frac{L-2d'}{s_h}-1\right)A_{h,bar}f_{yh}$	$(0.0217\rho_v f_{yv})A_{net}\sqrt{f'_m}$
Anderson and Priestley (1992)	$0.24\sqrt{f'_m}Lt$	$0.25P$	$0.5A_{h,bar}f_{yh}\frac{d}{s_h}$	-
Fattal (1993)	$0.512\left[\left(\frac{0.5}{\left(\frac{H}{L}\right)+0.8}\right)+0.18\right]\sqrt{f'_m f_{yv}}(\rho_v)^{0.7}Lt + 0.0096f'_m$	$0.20P$	$0.00528\delta f_{yh}(\rho_h)^{0.31}$	included in V_m

Code / Author	Shear Strength Contribution			
	Masonry (V_m)	**Axial Stress** (V_p)	**Horizontal Steel** (V_{sh})	**Vertical Steel** (V_{sv})
TCCMaR (1997)	$0.083\left[4.0-1.75\left(\frac{M}{VL}\right)\right]A_{net}\sqrt{f'_m}$	$0.25P$	$0.5A_{h,bar}f_{yh}\frac{L}{s_h}$	-
NTC-2004	$0.5v^*_m A_{gross}$	$0.3P$	$\eta\rho_h f_{yh}A_{gross}$	-
NZS 4230:2004	$C_2\cdot 0.2\sqrt{f'_m}t_{eff}d$	$0.9P_f\tan\alpha$	$0.8\frac{A_{h,bar}f_y}{s_h}d$	$C_1\cdot 0.2\sqrt{f'_m}t_{eff}d$
Eurocode 6 (2005)	$0.5f_{vko}tL$	$0.4P$	$0.9A_h f_{yh}$	-
Voon and Ingham (2007)	$k\left(0.083\left[4-1.75\frac{M}{VL}\right]\right)\sqrt{f'_m}td$	$0.9P_f\tan\alpha$	$A_{h,bar}f_{yh}\frac{d_{eff}}{s_h}$	$k\left(0.022\rho_v f_{yv}\right)\sqrt{f'_m}td$
CSA S304-14 (2014)	$0.16\left(2-\frac{M_f}{V_f d_v}\right)\sqrt{f'_m}td_v\gamma_g$	$0.25P\gamma_g$	$0.6A_{h,bar}f_{yh}\frac{d_v}{s_h}$	-
Dillon (2015)	$0.083\left(1.1+0.9\frac{Vs_{gv,ave}}{M}\right)A_{nv}\sqrt{f'_m}$	$0.15P$	$0.12\left(\frac{A_{hbb,bar}f_{yhbb}}{s_{hbb}}+\frac{A_{hj,bar}f_{yhj}}{s_{hj}}\right)H$	$0.12\frac{A_{vi,bar}f_{yvi}}{s_{vi}}L$
Bolhassani et al. (2016)	$(n_g-1)\left(t\cdot t_{eff}\sqrt{f'_{mu}}\cos\theta+\frac{4M_p}{H}\right)$	$(n_g-1)\mu P_{infill}$	-	-
TMS 402/602-16 (2016)	$0.083\left(4.0-1.75\frac{M}{VL}\right)\sqrt{f'_m}A_{net}\gamma_{g,\mathrm{US}}$	$0.25P\gamma_{g,\mathrm{US}}$	$0.5\left(\frac{A_{h,bar}f_{yh}L}{A_{nv}s_h}\right)A_{net}\gamma_{g,US}$	-
Hung (2018)	$A, \frac{M}{VL}, \frac{A_{net}}{A_{gross}}$ and $f'_{m,eff}$	σ_{gross}	$\rho_h f_{yh}$	$\rho_v f_{yv}$

2.4 Statistical Methods

Yu et al. (2006) stated that the ultimate goal of model selection is to choose the model which will perform the best on future testing data, meaning that the goal is to achieve a good generalization. To reach this goal in the context of predicting the in-plane shear strength of PG masonry walls, a methodology was used which had not been previously employed to solve this problem. Using stepwise variable selection and model trees, this study aims to generate several new shear strength models which are accurate and precise, yet simple enough to be used in design by practicing engineers. The performance of the generated equations will then be compared to existing code- and research-based models using statistical parameters.

2.4.1 Stepwise Variable Selection

The main challenge of developing a prediction model is selecting an appropriate input variable set (Mohsenijam and Lu, 2016). Without enough input variables, the model will be unable to capture the patterns in the data (Yu et al., 2006). On the other hand, increasing the number of inputs beyond a certain point will not only increase the model complexity, it will increase prediction error and worsen the model performance (Gardner et al., 2016). When too many variables are used, the model begins to fit itself to the noise in the training data, in addition to fitting itself to the underlying patterns of the data (Yu et al., 2006).

Variable selection methods allow the number of input variables to be reduced to an appropriate subset for predicting the output (Mohsenijam and Lu, 2016). Stepwise regression is one such method. It identifies significant input variables while eliminating multicollinearity (interdependencies) between variables, or cases where an input variable does not need to be included in the model because it could be explained by other input variables (Leung et al., 2001; Mohsenijam and Lu, 2016). Figure 2.12 illustrates how stepwise regression reduces potential input variables to an appropriate subset while eliminating multicollinearities.

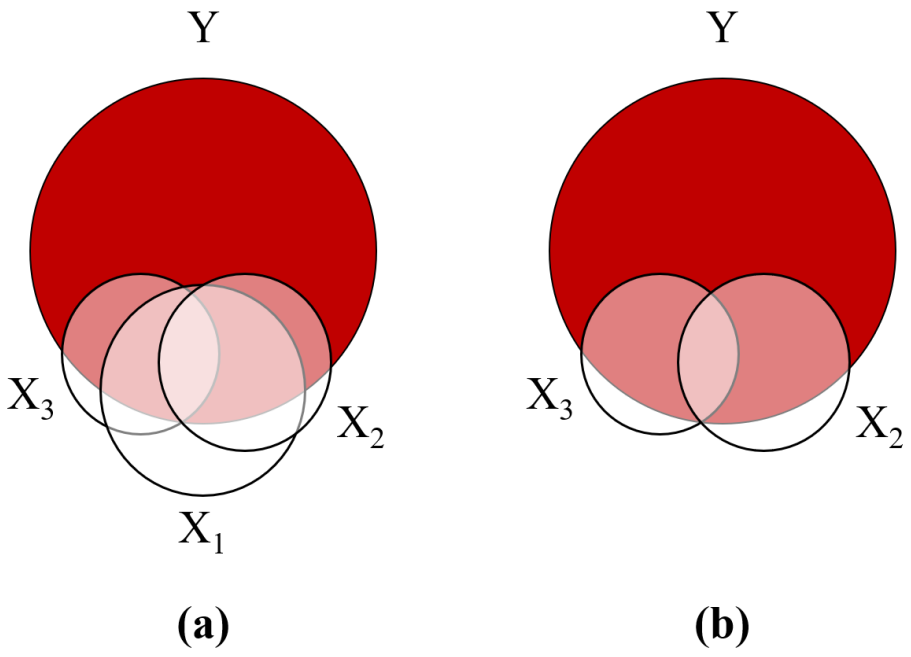

Figure 2.12 - Contrasting (a) multicollinearity between X_1, X_2 and X_3 and (b) almost no multicollinearity

In Figure 2.12 (a), all three of the input variables X_1 and X_2 and X_3 explain a significant portion of the output variable Y, however multicollinearities exist between the input variables because they are highly correlated to each other. Figure 2.12 (b) shows what happens if the variable X_1 is removed: the multicollinearities are eliminated, and only a small amount of the combined explanatory power of the variables is lost. This is what stepwise regression is designed to achieve.

Mohsenijam and Lu (2016) provide the following explanation of the stepwise regression procedure. In the first step, the variables are separated into two sets: a selected set, and an ignored set, with all the variables beginning in the ignored set while the selected set is left null. Next, correlation coefficients are determined to measure the association between each of the ignored variables and the output variable. The ignored variable with the highest correlation is moved from the ignored set to the selected set. This selected set is then used to formulate the regression model. To assess the significance of the variables in the resulting regression model, a partial F-test is performed. If a variable is not significant, meaning that its p-value is higher than a predetermined

exclusion value (for example 0.05), it is removed from the regression model and returns to the ignored set. In a particular iteration, if the ignored variable with the highest correlation does not satisfy the required level of significance (the inclusion threshold), it is not added to the selected set, and the stepwise procedure ends (Mohsenijam and Lu, 2016).

Stepwise regression offers important advantages over traditional regression methods. Unlike the methods used to develop existing empirical research-based shear strength equations, stepwise regression does not require the form of the equation to be assumed by the researcher. This eliminates much of the guesswork involved in the empirical equation derivation process. The ease of testing different combinations of input variables also eliminates constraints on how many variables can be investigated in analysis (Dillon, 2015).

One weakness of the automated stepwise regression procedure is the inability to eliminate certain terms from consideration for logical reasons when another term has already been selected (Dillon, 2015). This limitation can be overcome by manually removing terms when it is not logical to include them or by adjusting the inclusion and exclusion p-value thresholds. Preference is given to the latter method, as the manual removal of one term may change the optimum set that would be selected based on variable p-values. In other words, removing one term manually might increase the p-value of a variable in the ignored set, or decrease the p-value of a variable in the selected set, such that the remaining variables in the selected set are not what would have been chosen using stepwise regression.

2.4.2 Model Trees

Model Trees (MT) are an extension of Regressions Trees. The latter use a tree structure with constant values at the end of each branch, while in place of a constant value on each leaf, MTs have regression models (Frank et al., 1998). MTs split data so that similar samples are clustered together and can be approximated by the same multiple linear regression (Mohsenijam, 2019). In other words, MTs find local linearities in the data, allowing them to represent an unknown, nonlinear function using piecewise linear approximation (Quinlan, 1992; Frank et al., 1998). This is illustrated by Figure 2.13.

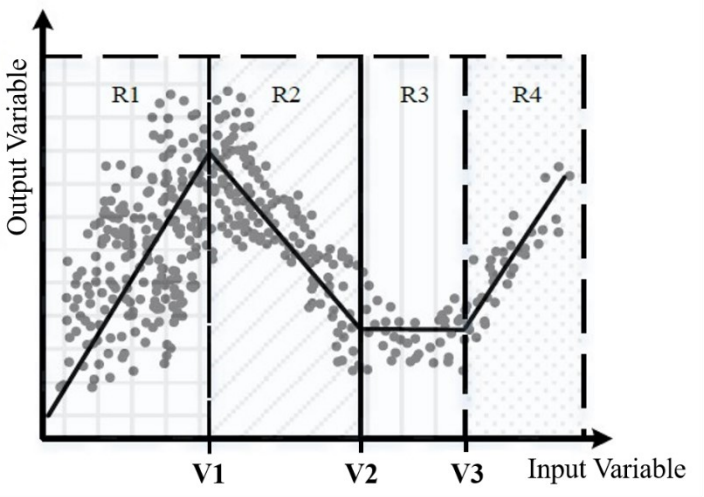

Figure 2.13 - Model tree representation of a non-linear data trend (adapted from Mohsenijam, 2019)

Although the one-dimensional case depicted in Figure 2.13 is rare, as most predictive models include more than one input variable, it serves as a good illustration of how a MT uses piecewise linear functions to represent a nonlinear trend in data. Figure 2.14 shows the corresponding model tree structure.

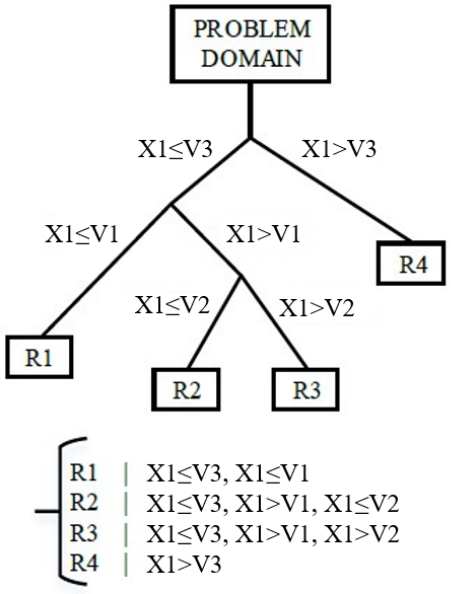

Figure 2.14 - Model tree structure example (adapted from Mohsenijam, 2019)

MTs can produce models with higher accuracy than commonly applied multiple linear regression methods, and they can provide more insightful models than those produced by ANNs (Quinlan, 1992; Frank et al., 1998; Mohsenijam, 2019).

Model trees were first developed by Quinlan (1992), who used a methodology called M5. Wang and Witten (1996) then improved upon this method, developing the M5' methodology. Mohsenijam (2019) used this M5' methodology to define rules for clustering samples, while implementing stepwise regression using Ordinary Least Squares (OLS) method at the resulting leaves to eliminate redundant input variables and calculate equation coefficients. The combination of MTs and stepwise regression was then validated on a large building information model dataset from the structural steel fabrication industry. The resulting MT was well aligned with industry knowledge and outperformed a linear regression, a stepwise regression, and an ANN in terms of predictive accuracy (Mohsenijam, 2019). A similar methodology is used to generate MTs in the present study, and is described in detail in Chapter 5.

2.4.3 Model Comparison

Estimation error consists of three components: bias, variance, and noise (Yu et al., 2006). Bias can be defined as the learning error for the algorithm of choice (Mohsenijam, 2019). A model with high bias oversimplifies the problem being studied (Mohsenijam, 2019). Variance is the sensitivity of the model to the training data and represents the model's prediction performance on new cases (Mohsenijam, 2019). Noise in data originates from measurement tools, data collection errors and human errors (Mohsenijam, 2019). Noise is unavoidable and difficult to reduce but is generally small. Thus, the estimation error is roughly equal to the sum of the squared bias and variance (Yu et al., 2006).

The concepts of bias and variance can be illustrated using a dart board (Figure 2.15). Low bias (accuracy) is achieved when the points hit the true value on average, while low variance (precision) is achieved when the points are relatively close together.

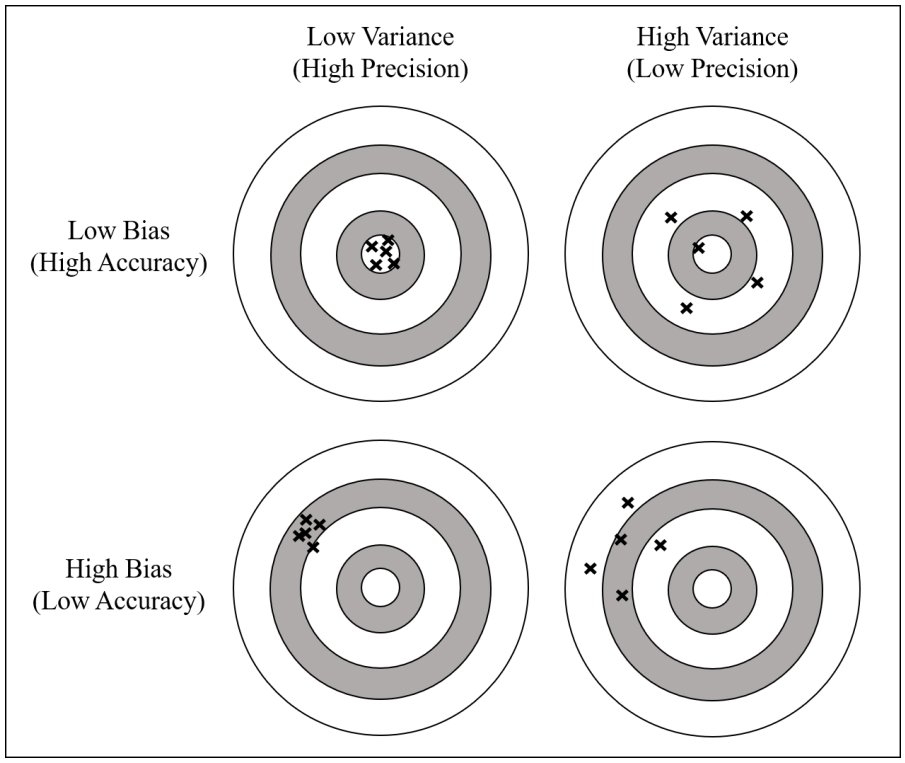

Figure 2.15 - Visualization of variance vs. complexity

As model complexity increases, bias decreases, and variance increases (Geman et al., 1992; Yu et al., 2006). An oversimplified model cannot capture the underlying patterns in the data no matter how much data is available, leading to underfitting, or high bias (Yu et al., 2006). Such a model would perform poorly both on training and testing data. On the other hand, if a model is overly complex, it memorizes some of the noise in the data as well as the underlying patterns, resulting in overfitting, or high variance (Yu et al., 2006). A complex model can fit a range of data patterns, not because it is the true model, but because it is flexible enough to absorb random error in the data (Myung and Pitt, 1997; Myung, 2000). It succeeds in fitting the observed data very well despite having large errors for each parameter, because the errors cancel each other out in order to fit the observed data (Myung, 2000). Such a model may fit the training data very well, but it will perform poorly on testing data, indicating a weak generalization (Myung, 2000; Yu et al., 2006). This is illustrated in Figure 2.16.

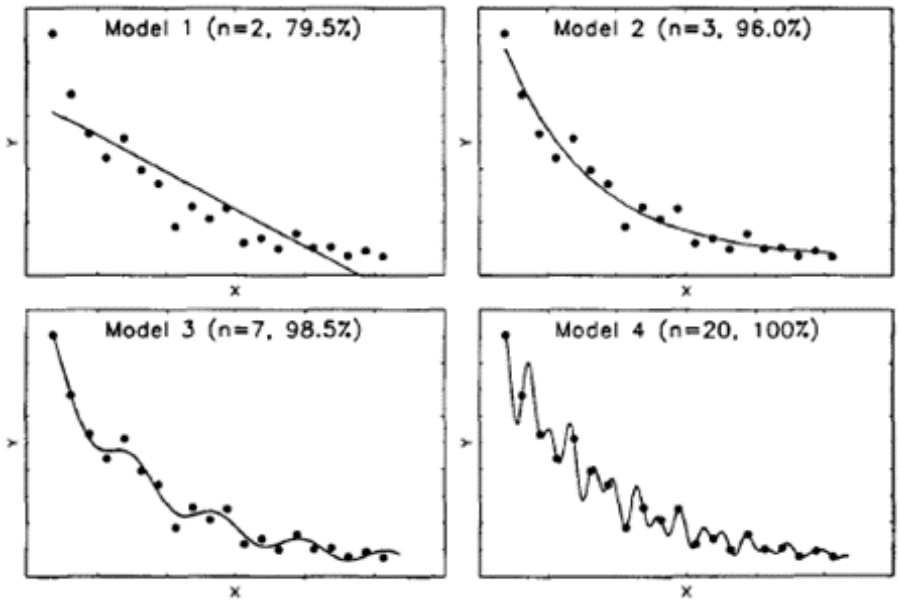

Figure 2.16 - Effect of model complexity on the model's ability to fit data, where *n* is the number of parameters used in each model. Percentage of variance accounted for by each model is shown in parentheses (Myung and Pitt, 1997)

In Figure 2.16, Model 1 underfits to the data, meaning that it is overly simple and is not able to capture the patterns in the data as well as Model 2. Model 3 has four more parameters than Model 2, significantly increasing the level of complexity and the flexibility of the model, however it only provides a 2.5% improvement in fit to the data. Model 4 contains 20 parameters, the same number as the data points, and even "tells us more than the data do" (Myung and Pitt, 1997). A complex model will fit an observed data set better than a simple model, even if the latter generated the data (Myung, 2000). This illustrates the danger of overfitting: although Model 4 fits the data perfectly, it fits only one data set and will generalize poorly to new data, as will Model 3 (Myung and Pitt, 1997).

As demonstrated by this example, there is a trade-off between bias, variance, and complexity through which the optimal complexity that minimizes the total error can be found (Yu et al., 2006). This trade-off is illustrated in Figure 2.17.

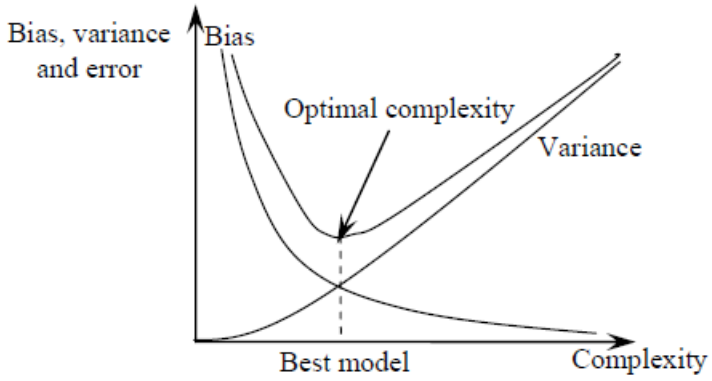

Figure 2.17 - Trade-off between bias, variance and complexity (Yu et al., 2006)

There is an inverse relationship between complexity and generalizability; simple models generalize better to new data sets than do complex models (Myung, 2000). This is one reason why, when choosing between two or more models having equal total error, the simplest model should be selected. In addition, acceptance of a model for inclusion in a design standard to be used frequently by practicing engineers is prerequisite on the model being simple (Dillon, 2015). Thus, a more complex model should only be favored if it decreases the total error enough to justify the additional complexity (Myung and Pitt, 1997).

2.4.4 Performance Indicators

Several different statistical indicators were considered as possible performance indicators to compare existing code- and research-based shear strength expressions with the ones generated in this study. Mohsenijam (2019) and Dillon (2015) both used the Akaike Information Criteria (AIC) and Bayesian Information Criteria (BIC) in model selection. However, models can only be compared using these metrics when they have been fitted to the same data set (Burnham and Anderson, 1998). In the current study, different datasets were used to develop various models, ruling out the possibility of using AIC and BIC.

Various performance indicators have been used by researchers in developing shear strength models for masonry. Fattal (1993b) provided minimum and maximum values of V_n/V_{exp}. as well as the

percentage falling within the range of 0.8-1.2 range. to compare the performance of the Fattal equation with that of the Matsumura equation. NEHRP (1997a) used mean, standard deviation, and variance of V_{exp}/V_n to compare the TCCMaR equation with other existing code- and research-based expressions. Minaie et al. (2010) used minimum, maximum, average, and standard deviation of V_{exp}/V_n as performance indicators to compare existing shear strength expressions with a modified version of the MSJC (2008) equation (a previous version of the TMS 402/602-16 equation). They also provided the percentage of specimens with V_{exp}/V_n<1, to quantify the percentage of unconservative predictions, and the percentage of specimens with $V_{exp}/\phi V_n$<1, to quantify potentially unsafe predictions. Hassanli et al. (2014) used minimum, maximum, average, standard deviation, and variation of V_{exp}/V_n to compare existing code-based equations with a proposed modified version of the MSJC (2011) equation. They also provided a percentage of over-predicted (unconservative) specimens. Dillon (2015) compared existing code- and research-based models with his generated model using RMSE, R^2, and mean and standard deviation of residuals. Aigular et al. (2016) used MSE, R^2, as well as average, standard deviation, and 5th percentile of V_{exp}/V_n as performance indicators to compare existing code-based expressions with their generated ANNs. Bolhassani et al. (2016b) created a histogram of V_{exp}/V_n values and plotted V_{exp}/V_n against various equation variables to evaluate the TMS (2016) equation. Hung (2018) used MSE, as well as average, standard deviation, and fifth percentile of V_{exp}/V_n to evaluate his ANN compared to previously developed code- and research-based shear strength equations.

The use of V_{exp}/V_n measures is widespread in masonry literature, as is the use of RMSE or MSE, and R^2. The V_{exp}/V_n measures have the advantage of being relatively easy to understand. R^2 is also a commonly used statistic that is familiar to many people, however it has several limitations that make it inadequate to use on its own. These performance indicators will be used to evaluate the new models and to compare them with existing code- and research-based shear strength expressions, and are explained in the following sections.

2.4.4.1 R^2 and Adjusted R^2

The coefficient of determination (R^2) is commonly used in statistics to evaluate the fit of prediction models. R^2 measures the degree of association along the "best" line relating the two variables, but when one variable is predicting the other, what is really important is the degree of association along the line of identity (Sheiner and Beal, 1981). Hence, R^2 can often be misleading and give overly optimistic results if it is used as the sole performance indicator. It also depends heavily on the number of observations, giving higher values when there is a higher number of observations. R^2 can be calculated using Equation (2.38).

$$R^2 = \left[\frac{N\sum \hat{y}_i y_i - \sum \hat{y}_i \sum y_i}{\sqrt{N\sum \hat{y}_i^2 - (\sum \hat{y}_i)^2}\sqrt{N\sum y_i^2 - (\sum y_i)^2}}\right]^2 \tag{2.38}$$

where N = number of samples in dataset

y_i = experimental (observed) output

$\hat{y}_i$ = analytical (fitted) output

R^2 is also lacking in the fact that it does not account for the complexity of a given model. Adjusted R^2 is a modified version of R^2 that penalizes models with higher numbers of parameters. Thus, it offers a small improvement over R^2. Adjusted R^2 can be calculated using Equation (2.39).

$$Adj\ R^2 = 1 - \left[\frac{(1-R^2)(N-1)}{N-p-2}\right] \tag{2.39}$$

where N = the number of observations (data points)

p = the number of parameters in the model, including the constant

2.4.4.2 Root Mean Squared Error (RMSE)

Both the Mean Squared Error (MSE) and the Root Mean Squared Error (RMSE) are measures of variance, meaning that they indicate the level of precision of the prediction model (Sheiner and Beal, 1981). RMSE is the square root of the MSE, and has the same units as the model output variable. It can be calculated using Equation (2.40).

$$RMSE = \sqrt{\sum_{i=1}^{N} \frac{(y_i - \hat{y}_i)^2}{N}} \tag{2.40}$$

where y_i = experimental (observed) output

$\hat{y}_i$ = analytical (fitted) output

N = number of samples in dataset

As is apparent from Equation (2.40), RMSE will always give a positive value. As this value is a measure of error, the closer it is to zero, the lower the error.

2.4.4.3 ME

Mean prediction error (ME) is a measure of bias, meaning that it indicates the level of accuracy of the prediction model. ME can be calculated using Equation (2.41).

$$\text{ME} = \sum_{i=1}^{N} \frac{y_i - \hat{y}_i}{N} \tag{2.41}$$

where y_i = experimental (observed) output

$\hat{y}_i$ = analytical (fitted) output

N = number of samples in dataset

Unlike RMSE, ME may be negative or positive, indicating whether there is a systematic component of the prediction error; a biased model will produce predictions that are typically either too high or too low (Sheiner and Beal, 1981). A negative value of ME indicates that the fitted values tend to overestimate the observed values, while a positive value of ME indicates that the fitted values tend to underestimate the observed values.

2.4.4.4 V_{exp}/V_n performance indicators

V_{exp}/V_n is the ratio between the experimental shear strength (the value obtained during testing) and the analytical shear strength (the value predicted by a given equation). A value of V_{exp}/V_n of one indicates the ideal situation, where the equation predicts shear strength perfectly. A value of V_{exp}/V_n greater than one indicates that the equation underpredicts the shear strength, while a value less than one indicates that the equation overpredicts the shear strength.

The average V_{exp}/V_n value helps to identify whether there is equation bias. If the average value of V_{exp}/V_n is greater than one, the equation underpredicts the shear strength on average (conservative predictions). If the average value of V_{exp}/V_n is less than one, the equation overpredicts the shear strength on average (unconservative predictions).

Minimum and maximum values of V_{exp}/V_n help to establish the range of variation of the prediction model. In general, if the range is high, the standard deviation will also be high because the data points are more spread out.

The standard deviation is a measure of the extent of dispersion of V_{exp}/V_n from its mean. A low standard deviation is desirable, as it indicates a smaller spread of data around the mean and higher model precision. Combined with an average V_{exp}/V_n value close to 1, which indicates high model accuracy, a low standard deviation of V_{exp}/V_n is evidence that the predictive model is performing well. The sample standard deviation formula is used, as given in Equation (2.42).

$$\sigma = \sqrt{\frac{\Sigma\left(\frac{V_{exp}}{V_n} - \frac{\overline{V_{exp}}}{V_n}\right)^2}{N-1}} \tag{2.42}$$

where σ = standard deviation of V_{exp}/V_n

$\frac{\overline{V_{exp}}}{V_n}$ = average value of V_{exp}/V_n

N = number of samples in dataset

The fifth percentile of V_{exp}/V_n represents the value of V_{exp}/V_n exceeded by 95% of the specimens in the dataset (Hung, 2018). The higher the fifth percentile of V_{exp}/V_n is, the more conservative the prediction model is.

Most design codes apply reduction factors when calculating the strength of structural materials, adding a greater degree of conservatism to reduce the probability of failure. The percentage of reduced shear strength estimates that are smaller than (or greater than) the experimental shear strength serves as an estimate of how often the design equation would produce conservative (or unconservative) predictions.

2.4.5 Complexity Metrics

Complexity has been defined as the flexibility inherent in a model that enables it to fit diverse patterns of data (Myung and Pitt, 1997). Often complexity is measured simply as the number of parameters, or "degrees of freedom", in a given model (Yu et al., 2006). However, this simplistic measurement ignores an often-neglected dimension of model complexity: the functional form, or the way in which parameters are combined in the model equation (Myung and Pitt, 1997).

Because the functional form is crucial in determining the model complexity in the present study, a method for quantifying complexity that accounts for model form and can be easily implemented is needed. Generalized Degrees of Freedom (GDF) was originally proposed by Ye (1998) and can

be used as a measure of model complexity for models of various forms (Hauenstein et al., 2018). GDF can be calculated as shown in Equation (2.43).

$$\text{GDF} = \frac{\sum_{i=1}^{N} \text{Cov}(y_i, \hat{y}_i)}{\text{Var}(e)} \tag{2.43}$$

where N = the number of observations

$\text{Cov}(\hat{y}_i, y_i)$ = covariance of the fitted values with respect to the observed values

$= \frac{\sum_{i=1}^{N}(y_i - \bar{y}) * (\hat{y}_i - \bar{\hat{y}})}{N-1}$

y_i = the i[th] observed value

$\bar{y}$ = the average observed value

$\hat{y}_i$ = the i[th] fitted value

$\bar{\hat{y}}$ = the average fitted value

$\text{Var}(e)$ = variance of the error

$= \frac{\sum_{i=1}^{N}(e_i - \bar{e})^2}{N-1}$

e_i = the error of the i[th] specimen

$= y_i - \hat{y}_i$

$\bar{e}$ = the mean error

2.4.6 Model Verification

The validity of a model formulated using Ordinary Least Squares (OLS) must be verified by checking the assumptions listed below (Mohsenijam, 2019).

1. There variance of the error is constant (homoscedasticity)

2. There is no perfect linear dependence between input variables (no collinearity)
3. The errors follow a normal distribution (normality of the error term)
4. The errors are serially independent (no autocorrelation)

Autocorrelation is the dependence of errors between serial observations over time (Mohsenijam et al., 2016). Because time is not an important variable in the present study, the serial dependence check does not apply and will not be performed. The other three assumptions are explained in the following sections and were used to verify the proposed models (Chapter 6).

2.4.6.1 Heteroscedasticity

The first assumption is violated when the variance of the error terms differs across observations (Mohsenijam, 2019). This violation is termed heteroscedasticity and can be visually inspected using residual plots.

Residuals are the difference between the experimental (observed) valued and the corresponding analytical (fitted by the model) value, given by Equation (2.44).

$$e_i = y_i - \hat{y}_i \tag{2.44}$$

where y_i = experimental (observed) output

$\hat{y}_i$ = analytical (fitted) output

When plotted against the fitted values, residuals exhibiting homoscedasticity (satisfactory variance of the error) can be contained in a horizontal band, as illustrated in Figure 2.18(a) (Montgomery et al., 2012). Figure 2.18(b) illustrates an example of heteroscedasticity in which the model is accurate when predicting low values but becomes highly inconsistent when predicting higher values.

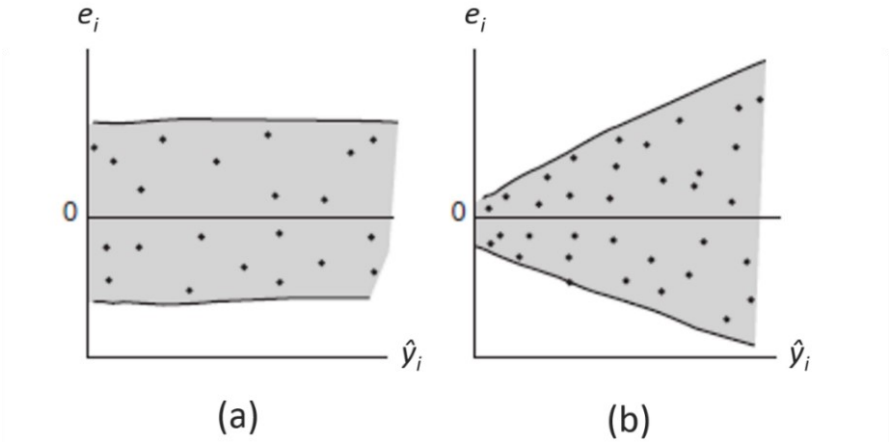

Figure 2.18 - Residual plots showing: (a) homoscedasticity and (b) heteroscedasticity (adapted from Montgomery et al., 2012)

The proposed models will be checked for heteroscedasticity through visual inspection of the residual plots.

2.4.6.2 Multicollinearity

The variance inflation factor (VIF) is one of the most widely used rules for diagnosing the presence of multicollinearity (Yoo et al., 2014). The VIF of each input variable, X_i, in a model is determined by forming an OLS regression with X_i as the dependent variable, while all other variables are considered as input variables (Mohsenijam, 2019). The OLS regression has the form shown in Equation (2.45).

$$X_i = \alpha_0 + \alpha_1 X_1 + \alpha_2 X_2 + \cdots + \alpha_k X_k + e \tag{2.45}$$

The R^2 value of the regression is determined, and then VIF is calculated using Equation (2.46).

$$VIF_i = \frac{1}{1 - R_i^2} \tag{2.46}$$

where VIF_i = VIF of the i^{th} input variable, X_i

R_i^2 = coefficient of determination for the OLS regression with X_i as the dependent variable (Equation (2.38))

As the degree of multicollinearity increases, VIF becomes larger; it is generally accepted that a VIF value greater than 10 may be harmful (Yoo et al., 2014).

2.4.6.3 Normality of the error term

The normality of the error terms can be checked using the Anderson-Darling test (D'Agostino and Stephens, 1986), as shown in Equation (2.47).

$$A^2 = -N - \sum_{i=1}^{N} \frac{2i-1}{N} [\ln F(e_i) + \ln(1 - F(e_{N+1-i}))] \quad (2.47)$$

where A^2 = the Anderson-Darling statistic

N = the sample size

F = cumulative distribution of the errors

e_i = regression error of the i^{th} observation

Full details of the test procedure can be found in D'Agostino & Stephens (1986).

3 EXPERIMENTAL DATA FROM THE LITERATURE

3.1 Introduction

To develop a new expression for predicting the in-plane shear strength of PG masonry walls through statistical analysis, an extensive amount of data is needed. Due to constraints of time and expense, no single experimental study of PG walls contains sufficient data to build or validate such a model (Dillon and Fonseca, 2014a; Hung, 2018). As a result, models generated using statistical analysis require data compiled from multiple experimental studies.

Several researchers have taken similar approaches. Oan (2013) and Hassanli et al. (2014) compiled experimental datasets to evaluate the performance of existing code- and research-based design equations in predicting the in-plane shear strength of PG masonry walls. Aguilar (2013) and Dillon (2015) conducted analyses by compiling datasets of FG and PG walls made of concrete blocks and clay bricks. In the case of Aguilar (2013), the objective was to obtain an ANN for each of the four distinct masonry types. Dillon (2015) used automated and stepwise regression techniques to generate a unified prediction model for both FG and PG walls. Hung (2018) compiled a dataset of PG walls built with concrete blocks, which he used to develop an ANN to predict the in-plane shear strength of PG masonry walls.

Once compiled, the data can then be synthesized and scrutinized to make them compatible with each other. This was an important step in the studies by Dillon (2015) and Hung (2018), which will be treated in Chapter 4. This chapter will introduce the experimental studies from which the data was compiled for analysis in the present study. The studies are presented in chronological order.

3.2 Experimental Studies Compiled

Because FG walls and walls made of clay bricks are outside the scope of this study, only studies that tested PG walls made of concrete blocks were included in the database compilation. The selected studies were chosen because they focused on the shear behaviour of masonry walls.

Data were collected from published works such as theses, conference papers and journal papers. In some cases, multiple works published on the same study contained conflicting data. In these cases, the most consistent value was used wherever possible, otherwise values from a journal paper or conference paper were prioritized over those from the thesis, due to the high levels of scrutiny these papers undergo. Where variables of interest were not reported by a researcher, assumptions were made for the missing values. These assumptions are described in detail in Appendix A.

3.2.1 Scrivener (1967)

Total Number of PG Walls in Study: 11			USA
Loading Type:	Monotonic	$f'_{m,eff}$	15.1 - 19.4 MPa
Loading Rate:	Quasi-Static	A_{net}/A_{gross}	0.36 - 0.62
Boundary Conditions:	Cantilever	Net Axial Stress	1.09 - 2.51 MPa
Scale:	1	Gross Axial Stress	0.39 - 1.55 MPa
Panel Height:	2438 mm	Flexural reinf., ρ_{vf}	0 - 0.19 %
Length:	2438 mm	Interior Vertical reinf., ρ_{vi}	0 - 0.17 %
Thickness:	143 mm	Joint reinf., ρ_{hj}	0 %
H/L:	1	Bond Beam reinf., ρ_{hbb}	0 - 0.23 %

Scrivener tested 12 masonry walls, of which 11 were partially grouted while 1 was unreinforced. The variables that were studied were horizontal and vertical reinforcement ratios and placement of vertical reinforcement. The test setup used is illustrated in Figure 3.1.

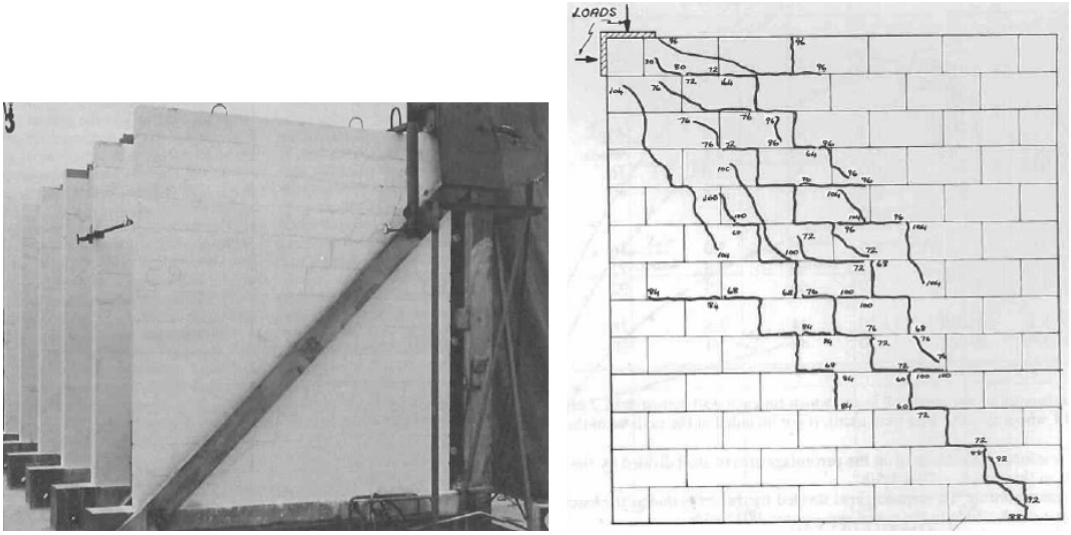

Figure 3.1 - Test setup used by Scrivener (1967)

Prior to applying each increment of lateral load, a vertical load sufficient to balance the overturning moment of the lateral load was applied (Scrivener, 1967). For analysis purposes in the present study, the axial load was taken as the axial load that was applied at the point of ultimate shear stress, which was estimated as described in Appendix A.

Scrivener (1967) concluded that vertical and horizontal reinforcement are equally effective in resisting cracking and increasing shear strength. Above a combined (horizontal and vertical) reinforcement ratio of 0.3% (based on gross area of the wall, taken as wall height multiplied by thickness), adding reinforcement increased shear strength only marginally. Evenly distributing vertical reinforcement delayed the onset of severe cracking compared to walls with vertical reinforcement concentrated in the jambs (Scrivener, 1967).

One of the walls tested by Scrivener (wall D4) was reportedly too strong to fail in shear using the given test setup. As a result, this wall failed in a predominantly flexural mode (Scrivener, 1967).

3.2.2 Meli et al. (1968)

Total Number of PG Walls in Study: 10			Mexico
Loading Type:	Reverse Cyclic	$f'_{m,eff}$	9.2 - 10.6 MPa
Loading Rate:	Quasi-Static	A_{net}/A_{gross}	0.54 - 0.62
Boundary Conditions:	Cantilever	Net Axial Stress	0 - 0.66 MPa
Scale:	1	Gross Axial Stress	0 - 0.41 MPa
Panel Height:	2650 mm	Flexural reinf., ρ_{vf}	0.11 - 0.21 %
Length:	3200 mm	Interior Vertical reinf., ρ_{vi}	0.01 - 0.04 %
Thickness:	150 mm	Joint reinf., ρ_{hj}	0 - 0.01 %
H/L:	0.83	Bond Beam reinf., ρ_{hbb}	0 %

Meli et al. (1968) tested 18 PG walls in total, 8 of which were subjected to diagonal compression tests while the remaining 10 walls were tested as cantilever walls subject to lateral loading. The variables of interest were the amount of interior vertical reinforcement and the applied axial load. Two of the walls had closed stirrups placed at 80 mm spacing to enclose the vertical jamb reinforcement. The cantilever test setup is illustrated in Figure 3.2.

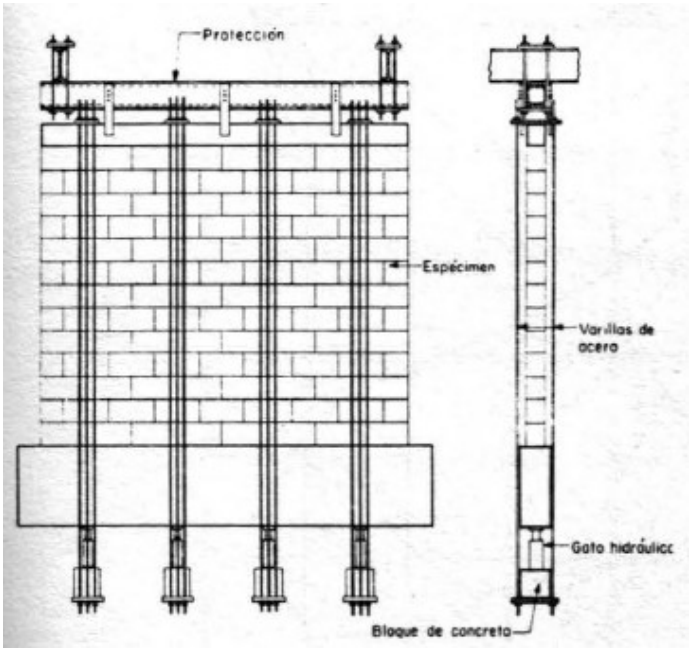

Figure 3.2 - Test setup used by Meli et al. (1968)

Meli et al. (1968) found that increasing axial load reduced the deterioration of the walls. The presence of stirrups confining jamb reinforcement also improved wall behaviour in terms of deterioration.

3.2.3 Meli and Salgado (1969)

Total Number of PG Walls in Study: 10			Mexico
Loading Type:	Monotonic	$f'_{m,eff}$	Unknown
Loading Rate:	Quasi-Static	A_{net}/A_{gross}	0.47 - 0.60
Boundary Conditions:	Cantilever	Net Axial Stress	0 - 2.1 MPa
Scale:	1	Gross Axial Stress	0 - 0.98 MPa
Panel Height:	2000 mm	Flexural reinf., ρ_{vf}	0.05 - 0.27 %
Length:	2000 mm	Interior Vertical reinf., ρ_{vi}	0 - 0.08 %
Thickness:	150 mm	Joint reinf., ρ_{hj}	0 %
H/L:	1	Bond Beam reinf., ρ_{hbb}	0 %

Meli and Salgado (1969) tested 46 masonry walls, 19 of which were monotonically tested PG walls built with hollow concrete blocks. Of those 19 walls, several failed predominantly in flexure while a few others experienced local failures, leaving 10 walls that failed in shear. The studied

variables were the effect of axial load and the quantity of interior vertical reinforcement. The setup used is illustrated by Figure 3.3.

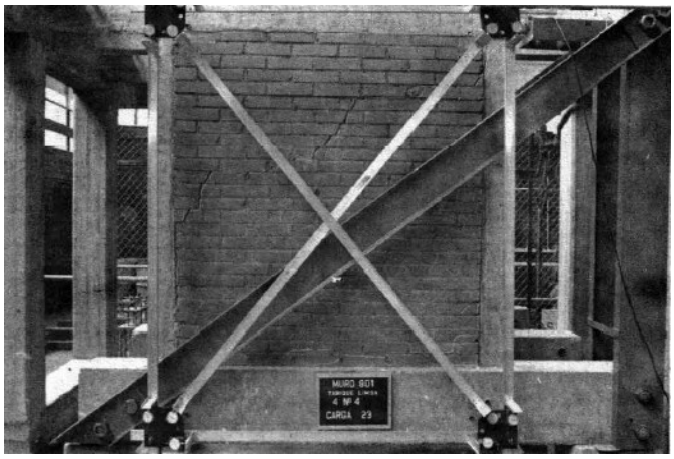

Figure 3.3 - Test setup used by Meli and Salgado (1969)

Meli and Salgado (1969) noted that if the quantity of vertical reinforcement in jambs was high, the failure mode was diagonal shear. They also observed that shear strength increased as axial load increased. For values up to 20% of the compressive strength of the wall, the shear resistance increased by an increment of half of the applied axial load (Meli and Salgado, 1969).

Meli and Salgado (1969) stated that blocks from two different fabricators were used to build the walls, however no value of compressive strength of either type of block was provided. Average ungrouted prism strengths were provided, however no grouted prism strengths were reported.

3.2.4 Mayes et al. (1976)

Total Number of PG Walls in Study: 2			USA
Loading Type:	Reverse Cyclic	$f'_{m,eff}$	16.7 MPa
Loading Rate:	Varied	A_{net}/A_{gross}	0.72
Boundary Conditions:	Double Curvature	Net Axial Stress	2.41 MPa
Scale:	1	Gross Axial Stress	1.72 MPa
Panel Height:	1626 mm	Flexural reinf., ρ_{vf}	0.49 %
Length:	813 mm	Interior Vertical reinf., ρ_{vi}	0 %
Thickness:	143 mm	Joint reinf., ρ_{hj}	0 %
H/L:	1.17	Bond Beam reinf., ρ_{hbb}	None

Mayes et al. (1976) tested 17 double pier masonry walls, 2 of which were PG while the rest were FG walls. The walls were constructed in identical pairs (except for one FG wall which was unique) with one of each pair being tested dynamically while the other was tested under pseudo-static conditions. The test setup used is illustrated in Figure 3.4.

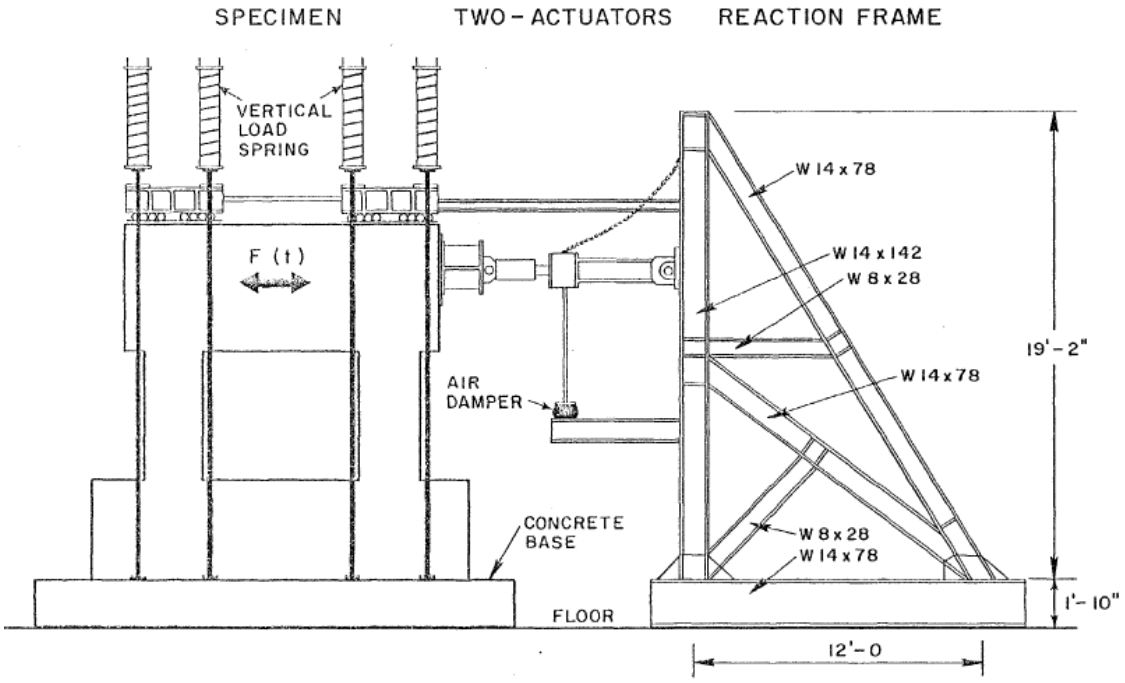

Figure 3.4 - Test setup used by Mayes et al. (1976)

Mayes et al. (1976) observed that piers failing in shear had higher ultimate strengths when tested dynamically as compared to the equivalent statically tested walls. They noted that the net ultimate shear strength of the PG masonry piers was similar to that of the equivalent FG walls (Mayes et al., 1976).

3.2.5 Chen et al. (1978)

Total Number of PG Walls in Study: 3			USA
Loading Type:	Reverse Cyclic	$f'_{m,eff}$:	13.0 - 14.8 MPa
Loading Rate:	Dynamic	A_{net}/A_{gross}:	0.43 - 0.61
Boundary Conditions:	Double Curvature	Net Axial Stress:	0.90 - 1.87 MPa
Scale:	1	Gross Axial Stress:	0.55 - 0.79 MPa
Panel Height:	1422 mm	Flexural reinf., ρ_{vf}:	0 - 0.43 %
Length:	1219 mm	Interior Vertical reinf., ρ_{vi}:	0 %
Thickness:	194 mm	Joint reinf., ρ_{hj}:	0 %
H/L:	1.17	Bond Beam reinf., ρ_{hbb}:	0 - 0.15 %

Chen et al. (1978) tested a total of 31 masonry shear walls built from either hollow concrete blocks, hollow clay bricks or solid clay bricks. Of the 11 walls built with hollow concrete blocks, 3 were PG while 1 was unreinforced and the remaining 7 were FG walls. In addition to investigating these 3 types of masonry and the effect of grouting, the study explored the effects of varying amounts of vertical and horizontal reinforcement. The test setup is illustrated in Figure 3.5.

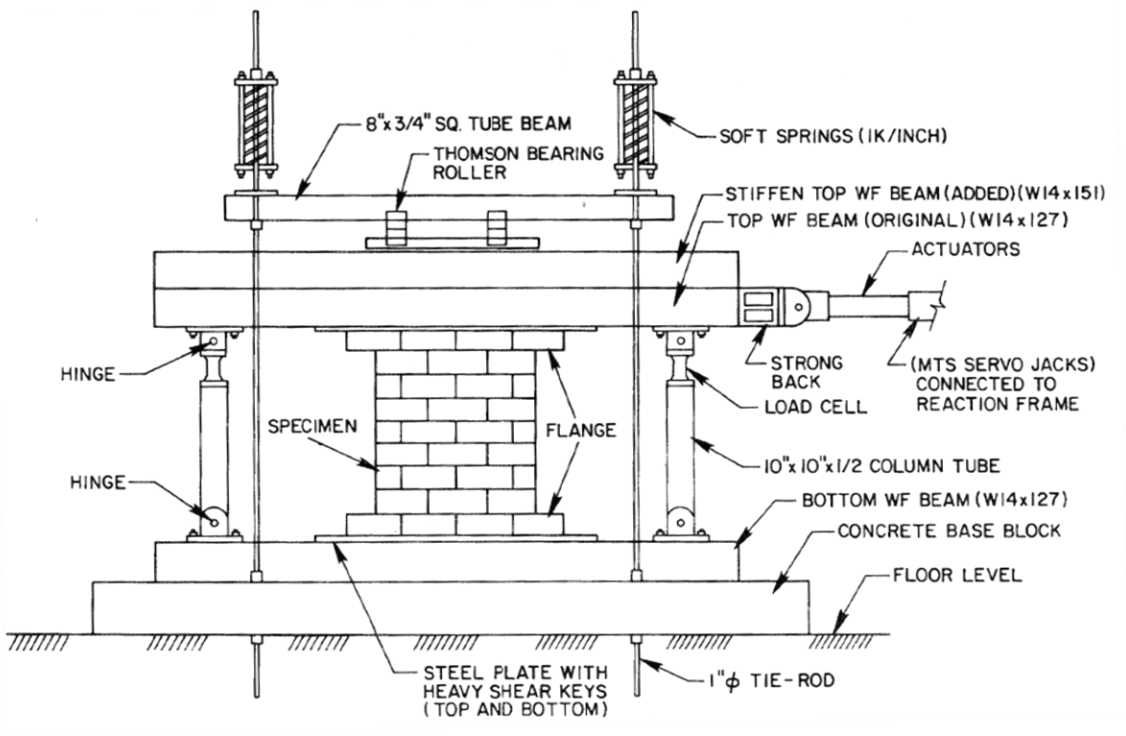

Figure 3.5 - Test setup used by Chen et al. (1978)

Chen et al. (1978) observed that, for walls built with concrete blocks, net ultimate shear stress was about 22% higher for PG walls than for the FG equivalent walls. Chen et al. (1978) also observed that increasing the area of vertical steel made no significant difference in the ultimate shear strength of the different wall types tested, concluding that this was because the shear strength of masonry walls is not influenced by the vertical steel. However, it should be noted that Chen et al. (1978) only used flexural vertical reinforcement in their tests; they did not include interior vertical reinforcement in any of the tested walls. Walls with horizontal reinforcement had equal or greater strength than corresponding walls with no horizontal reinforcement (Chen et al., 1978).

3.2.6 Thurston and Hutchison (1982)

Total Number of PG Walls in Study: 3			New Zealand
Loading Type:	Reverse Cyclic	$f'_{m,eff}$:	Unknown
Loading Rate:	Quasi-Static	A_{net}/A_{gross}:	0.71
Boundary Conditions:	Double Curvature	Net Axial Stress:	0 MPa
Scale:	1	Gross Axial Stress:	0 MPa
Panel Height:	2400 mm	Flexural reinf., ρ_{vf}:	0.07 - 0.18 %
Length:	1600 mm	Interior Vertical reinf., ρ_{vi}:	0.07 - 0.09 %
Thickness:	140 mm	Joint reinf., ρ_{hj}:	0 %
H/L:	1.5	Bond Beam reinf., ρ_{hbb}:	0 - 0.13 %

Thurston and Hutchison (1982) tested 8 masonry walls, 3 of which were PG while the rest were FG walls. One of the FG walls was tested, then repaired using epoxy grout injection and tested again 6 days later. The study was designed to investigate the effects of axial load, extent of grouting, and size and distribution of reinforcement, as well as the effectiveness of repair by epoxy grout injection. No axial loads were applied to the PG specimens, however. The test setup is illustrated in Figure 3.6.

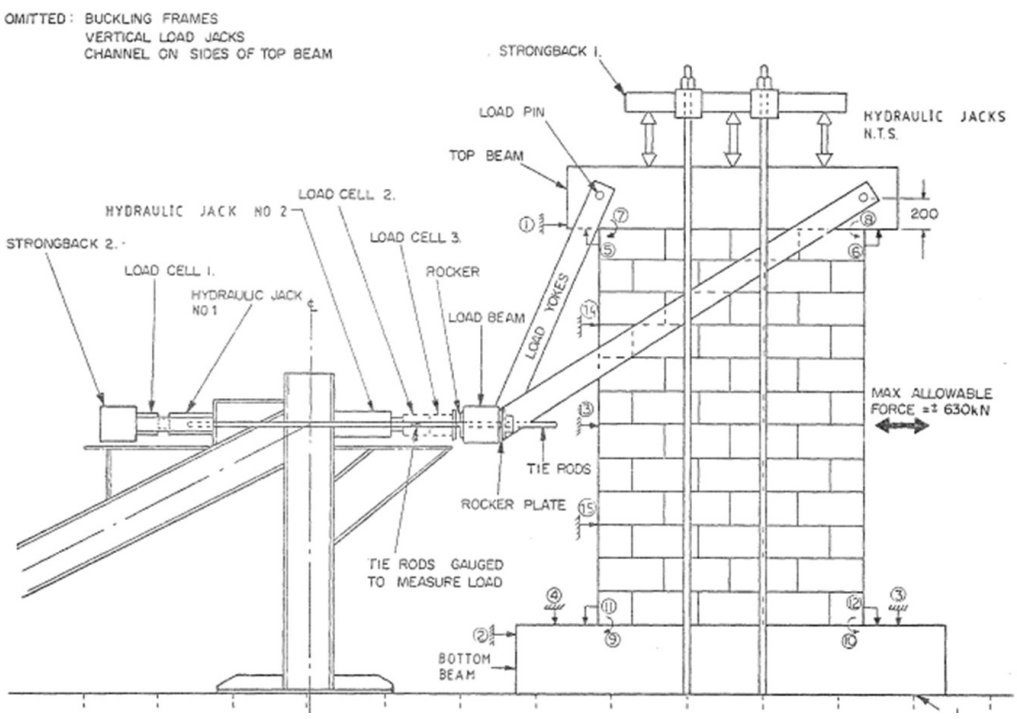

Figure 3.6 - Test setup used by Thurston and Hutchison (1982)

Thurston and Hutchison (1982) concluded that PG walls exhibit similar ductility to that of FG walls, however they have significantly reduced strength and stiffness compared to FG walls. It was observed that closely spaced small diameter reinforcement leads to better inelastic performance than similar quantities of reinforcement in the form of larger bars at greater spacings (Thurston and Hutchison (1982).

The mortar compressive strength was given as a range of over 10 MPa, however no specific values of f_{mortar} were given. Ungrouted prism strength was also not reported.

3.2.7 Matsumura (1987)

Total Number of PG Walls in Study: 29			Japan
Loading Type:	Reverse Cyclic	$f'_{m,eff}$:	Unknown
Loading Rate:	Quasi-Static	A_{net}/A_{gross}:	0.61 - 0.64
Boundary Conditions:	Double Curvature	Net Axial Stress:	0 - 2.35 MPa
Scale:	1	Gross Axial Stress:	0 - 1.47 MPa
Panel Height:	1800 mm	Flexural reinf., ρ_{vf}:	0.28 - 1.12 %
Length:	920 - 1970 mm	Interior Vertical reinf., ρ_{vi}:	0.05 - 0.10 %
Thickness:	150 mm	Joint reinf., ρ_{hj}:	0 %
H/L:	0.91 - 1.96	Bond Beam reinf., ρ_{hbb}:	0 - 0.30 %

Matsumura tested 55 masonry walls. Of those 55 walls, there were 31 PG walls built with concrete blocks, which all failed in shear except for 2 walls which failed in flexure. Matsumura also tested 25 specimens laid horizontally in a "beam type" loading configuration, as supplementary tests. Variables of interest were vertical and horizontal reinforcement ratios, shear span ratio, axial stress, material strengths and type of grouting. The test setup for the regular loading configuration is illustrated in Figure 3.7.

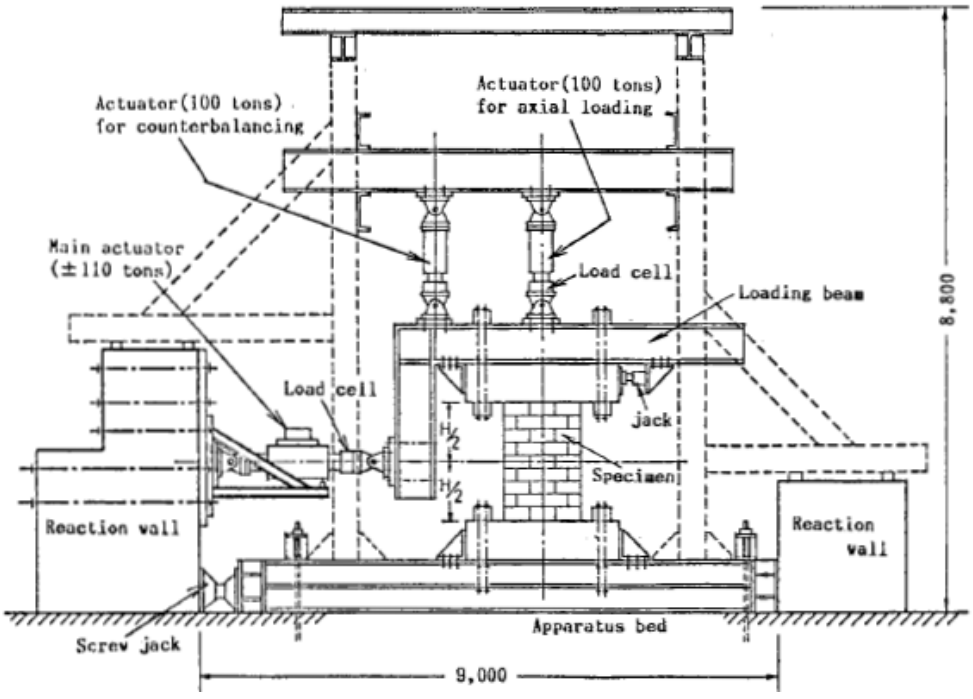

Figure 3.7 - Test setup used by Matsumura (1987)

Matsumura (1987) concluded that shear stress is approximately proportional to the square root of masonry prism strength ($\sqrt{f'_{m,u}}$). Shear stress increased as axial stress increased, and as the horizontal reinforcement ratio increased, while increasing shear span ratio caused a decrease in shear stress. Matsumura also formulated an equation to predict the in-plane shear strength of masonry walls based on his experimental study, as described in Section 2.3.1.

Although Matsumura did provide diagrams for 4 FG walls detailing the configuration of horizontal and vertical reinforcement, no such diagrams were provided for any of the PG walls. The ratio of flexural reinforcement and ratio of horizontal reinforcement was provided for each wall, but the ratio of interior vertical reinforcement was not reported, so this information must be assumed (Appendix A). In addition, the concrete blocks used in the study contained 3 void cells (Figure 3.8), as opposed to the 2-celled blocks which are typical in North American masonry.

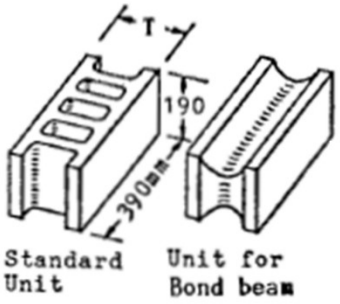

Figure 3.8 - Concrete blocks used by Matsumura (1987) for PG walls

Large ranges were provided for the compressive strength of blocks and compressive strength of mortar, but no specific values of f_{block} or f_{mortar} were reported. Ungrouted prism strength values were provided for each wall, but no grouted prism strength values were provided.

3.2.8 Tomaževič and Lutman (1988)

Total Number of PG Walls in Study: 10			Yugoslavia
Loading Type:	Reverse Cyclic	$f'_{m,eff}$:	8.0 - 9.5 MPa
Loading Rate:	Quasi-Static	A_{net}/A_{gross}:	0.60
Boundary Conditions:	Cantilever	Net Axial Stress:	1.65 MPa
Scale:	0.5	Gross Axial Stress:	0.98 MPa
Panel Height:	760 - 1405 mm	Flexural reinf., ρ_{vf}:	0.26 - 0.52 %
Length:	610 mm	Interior Vertical reinf., ρ_{vi}:	0 %
Thickness:	100 mm	Joint reinf., ρ_{hj}:	0 - 0.45 %
H/L:	1.25 - 2.30	Bond Beam reinf., ρ_{hbb}:	0 %

Tomaževič and Lutman (1988) tested a total of 16 PG masonry walls. Half of the walls were 760 mm in height while the other half were 1405 mm in height. In both the short walls group and the tall walls group, the same 4 horizontal reinforcement ratios (0, 0.12, 0.22 and 0.45%) and the same 2 vertical reinforcement ratios (0.26 and 0.52%) were used. Tomaževič and Lutman (1988) noted that for the taller walls which had horizontal reinforcement, the shear resistance of the walls improved such that they failed in flexure. This accounts for 6 of the tested walls, leaving 10 walls that failed in shear. The test setup was not illustrated in detail, however the configuration used was provided (Figure 3.9).

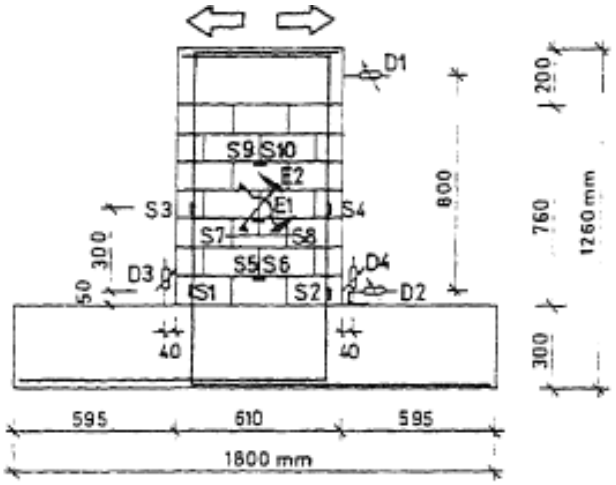

Figure 3.9 - Test configuration used by Tomaževič and Lutman (1988)

Tomaževič and Lutman (1988) concluded that vertical and horizontal reinforcement improved the seismic behaviour of the walls. Horizontal reinforcement improved shear capacity and ductility, causing vertical reinforcement to yield in some walls and changing the failure mode from shear to flexure. Tomaževič and Lutman (1988) also observed that the horizontal joint reinforcement acted in tension after wall cracking was initiated, however the horizontal reinforcement did not yield. This was attributed to the loss of bond between mortar and reinforcement, as well as crushing of concrete masonry blocks not allowing full development of the tension capacity of the horizontal reinforcement. The effectiveness of the horizontal reinforcement ranged from 41-66% at the ultimate shear load, and from 61-83% at the maximum displacement (failure load). Tomaževič and Lutman (1988) noted that masonry units and mortar must be of adequate quality, and reinforcement bond and anchorage conditions must be sufficient for the reinforcement to be fully activated.

3.2.9 Johal and Anderson (1988)

Total Number of PG Walls in Study: 16			USA
Loading Type:	Reverse Cyclic	$f'_{m,eff}$:	9.2 - 11.0 MPa
Loading Rate:	Quasi-Static	A_{net}/A_{gross}:	0.66
Boundary Conditions:	Double Curvature	Net Axial Stress:	0 MPa
Scale:	1	Gross Axial Stress:	0 MPa
Panel Height:	813 mm	Flexural reinf., ρ_{vf}:	0.25 %
Length:	813 mm	Interior Vertical reinf., ρ_{vi}:	0 %
Thickness:	194 mm	Joint reinf., ρ_{hj}:	0 %
H/L:	1	Bond Beam reinf., ρ_{hbb}:	0 %

Johal and Anderson (1988) tested 32 PG masonry walls, 16 of which were constructed using concrete block while the rest were constructed with hollow clay block. The study investigated the use of Type M and S mortars of two categories: masonry cement and Portland cement lime. Specimens were minimally reinforced and partially grouted so that the shear strength would be influenced primarily by the mortar (Johal and Anderson, 1988). The test setup is illustrated in Figure 3.10.

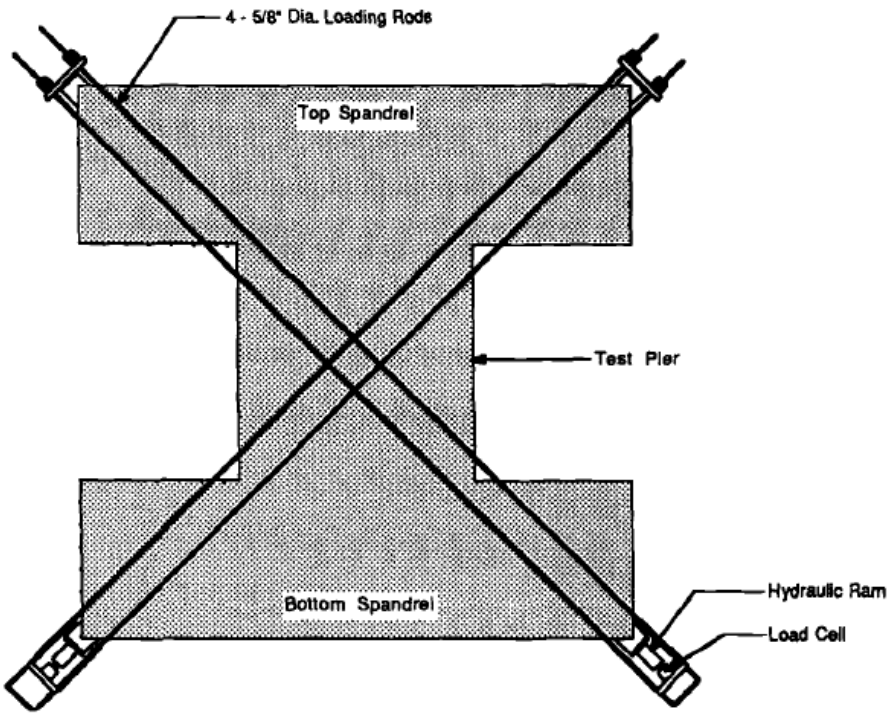

Figure 3.10 - Test setup used by Johal and Anderson (1988)

Johal and Anderson (1988) found that the shear strength of masonry walls constructed with masonry cement-based mortars were similar to those of masonry walls constructed using Portland cement-based mortars. They recommended the elimination of restrictions on the used of masonry cement from the Uniform Building Code. They also noted that shear strength was not influenced significantly by the use of Type M or Type S mortar.

3.2.10 Yancey and Scribner (1989)

Total Number of PG Walls in Study: 9			USA
Loading Type:	Reverse Cyclic	$f'_{m,eff}$:	Unknown
Loading Rate:	Quasi-Static	A_{net}/A_{gross}:	0.54
Boundary Conditions:	Double Curvature	Net Axial Stress:	1.38 MPa
Scale:	1	Gross Axial Stress:	0.74 MPa
Panel Height:	1422 mm	Flexural reinf., ρ_{vf}:	0 %
Length:	1219 mm	Interior Vertical reinf., ρ_{vi}:	0 %
Thickness:	194 mm	Joint reinf., ρ_{hj}:	0 - 0.01 %
H/L:	1.17	Bond Beam reinf., ρ_{hbb}:	0 - 0.03 %

Yancey and Scribner tested a total of 13 walls, 3 of which failed in flexure. Of the 10 walls failing in shear, 1 was unreinforced while the remaining 9 were PG walls. The objective of the study was to determine the effect of varying the amount and distribution of horizontal reinforcement. Two specimens were reinforced with joint reinforcement, five specimens were reinforced with bond beams and the remaining two specimens had both joint and bond beam reinforcement. The test setup is illustrated in Figure 3.11.

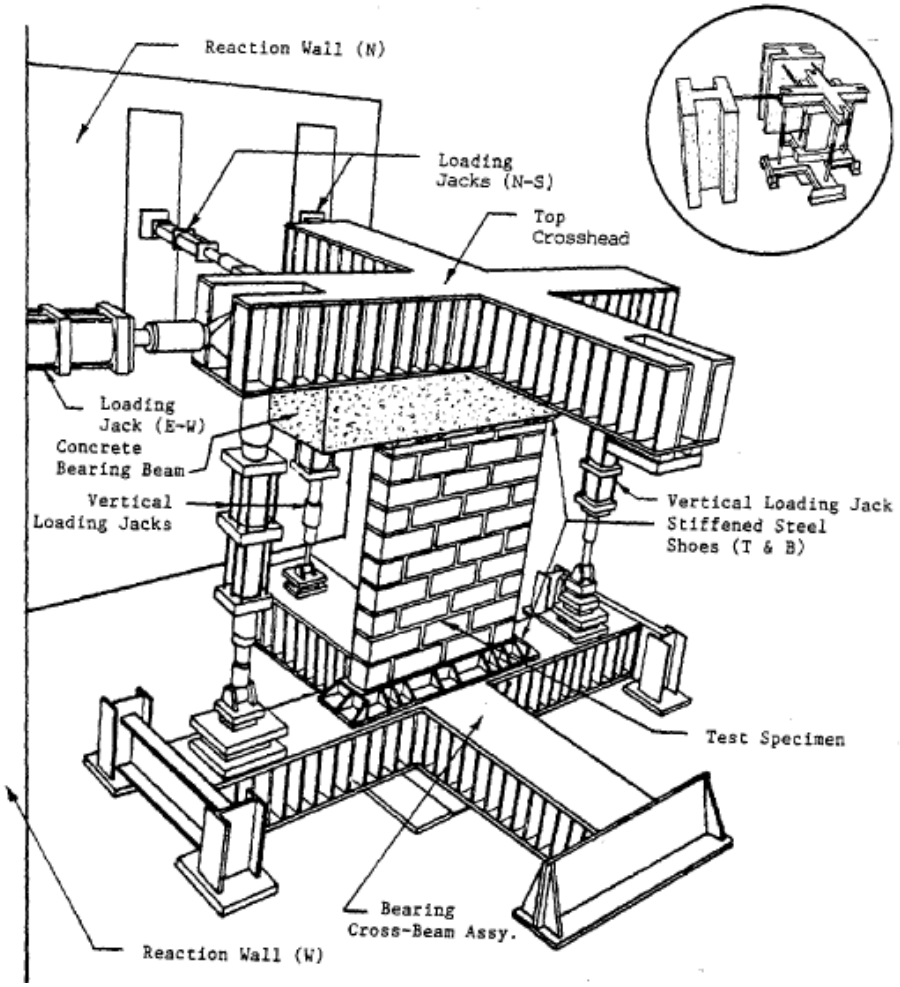

Figure 3.11 - Test setup used by Yancey and Scribner (1989)

Yancey and Scribner (1989) concluded that increasing horizontal reinforcement increases shear strength, however not proportionally to the amount of reinforcement added. They observed that

bed joint reinforcement placed in alternating courses was as effective in increasing shear strength as bed joint reinforcement placed in each course (Yancey and Scribner, 1989).

Neither the compressive strength of mortar, nor grouted and ungrouted prism strengths were reported.

3.2.11 Ghanem et al. (1992, 1993)

Total Number of PG Walls in Study: 4			USA
Loading Type:	Monotonic	$f'_{m,eff}$:	14.9 - 15.1 MPa
Loading Rate:	Quasi-Static	A_{net}/A_{gross}:	0.45 - 0.49
Boundary Conditions:	Cantilever	Net Axial Stress:	1.39 - 2.79 MPa
Scale:	0.33	Gross Axial Stress:	0.69 - 1.38 MPa
Panel Height:	920 mm	Flexural reinf., ρ_{vf}:	0.08 - 0.12 %
Length:	939 mm	Interior Vertical reinf., ρ_{vi}:	0 - 0.04 %
Thickness:	48 mm	Joint reinf., ρ_{hj}:	0 %
H/L:	0.98	Bond Beam reinf., ρ_{hbb}:	0.12 - 0.13 %

Ghanem et al. tested a total of 14 PG masonry walls to study axial compression, block strength, lateral load and the amount and distribution of vertical and horizontal steel. Two papers were published from the study, each of them presenting 3 of the specimens from the full study (Ghanem et al., 1992; Ghanem et al., 1993). Of the 6 specimens in these two papers, 4 failed in shear while the remaining 2 failed in flexure. The test setup is illustrated in Figure 3.12.

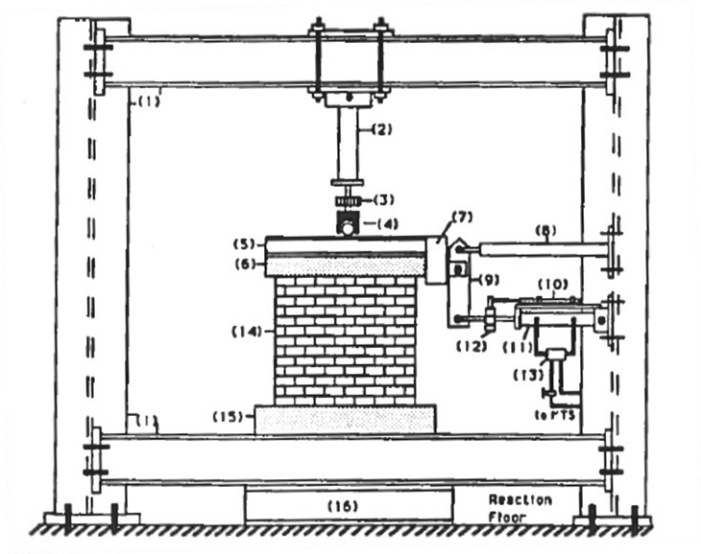

Figure 3.12 - Test setup used by Ghanem et al. (1992)

Ghanem et al. (1992) concluded that the distribution of horizontal and vertical reinforcement controlled the failure mode of the walls. When reinforcement was distributed throughout the wall, the shear strength increased, while concentrating vertical steel at the wall ends increased the flexural strength with little increase in shear strength. Distributing the horizontal steel also improved wall ductility (Ghanem et al., 1992). On the other hand, increasing axial stress decreased wall ductility and changed the failure mode from flexure to shear (Ghanem et al., 1993). The onset of diagonal cracking was delayed by increasing axial stress (Ghanem et al., 1993).

3.2.12 Tomaževič et al. (1996)

Total Number of PG Walls in Study: 32			Slovenia
Loading Type:	Varied	$f'_{m,eff}$:	Unknown
Loading Rate:	Varied	A_{net}/A_{gross}:	0.69
Boundary Conditions:	Cantilever	Net Axial Stress:	2.84 MPa
Scale:	0.5	Gross Axial Stress:	1.97 MPa
Panel Height:	760 mm	Flexural reinf., ρ_{vf}:	0.26 %
Length:	610 mm	Interior Vertical reinf., ρ_{vi}:	0 %
Thickness:	100 mm	Joint reinf., ρ_{hj}:	0.07 %
H/L:	1.25	Bond Beam reinf., ρ_{hbb}:	0 %

Tomaževič et al. (1996) tested 32 concrete masonry walls, consisting of 16 pairs of identical walls. Only the average results, including shear strength, was reported for each pair of walls. To investigate the influence of different loading conditions, the loading type was varied. Eight walls each were tested under monotonic, reverse cyclic, phased-sequential and simulated seismic loading. In each group of 8 walls, 4 were tested statically, while 4 were tested dynamically. Two vertical load levels were used: 60 kN and 120 kN. The four displacement time histories used to drive the actuator are illustrated in Figure 3.13.

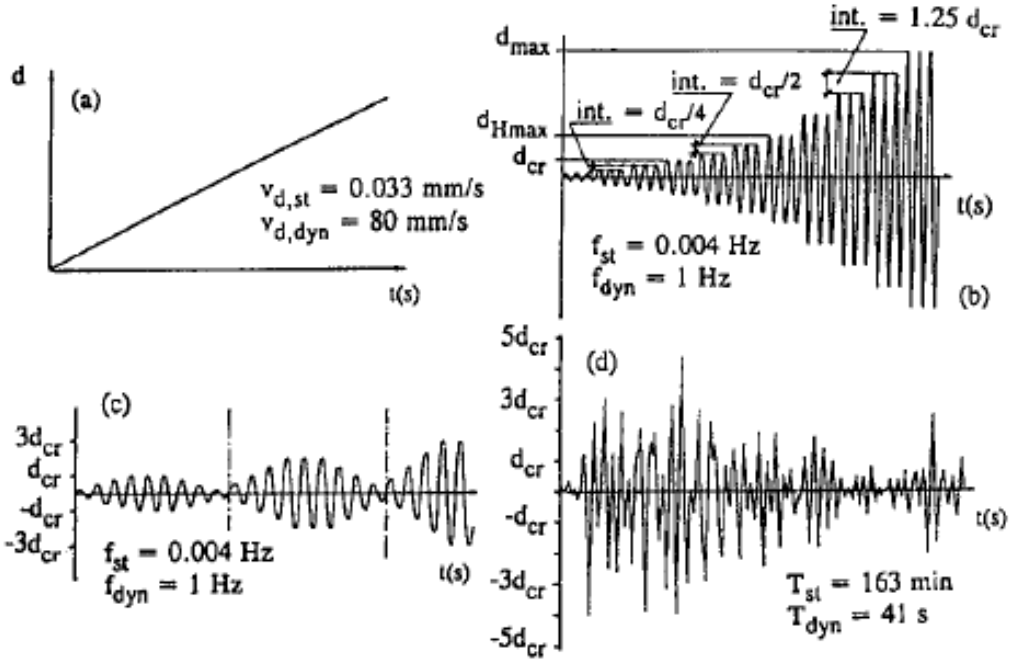

Figure 3.13 - Displacement time histories used: (a) monotonic, (b) reverse cyclic, (c) phased-sequential & (d) simulated earthquake (Tomaževič et al., 1996)

The researchers concluded that loading type and rate had a significant impact on the observed strength and stiffness degradation of the walls (Tomaževič et al., 1996). They recommended that the cyclic character of seismic loads should be simulated, noting that the reverse cyclic and phased-sequential loading procedures used in the study were adequate for this purpose (Tomaževič et al., 1996). They also suggested that test results should be modified when dynamic loading is applied, to account for the increase in observed shear strength (Tomaževič et al., 1996).

Tomaževič et al. (1996) noted that "predominant flexural behavior" was observed, however the ultimate behavior of the walls was more brittle at the higher axial load level. For this reason, only the 6 wall pairs exhibiting brittle failure are considered to have failed in shear. The strength properties of constituent materials and grouted prism strength were not reported.

3.2.13 Schultz (1996)

Total Number of PG Walls in Study: 6			USA
Loading Type:	Phased-Sequential	$f'_{m,eff}$:	13.9 - 14.0 MPa
Loading Rate:	Quasi-Static	A_{net}/A_{gross}:	0.44 - 0.53
Boundary Conditions:	Double Curvature	Net Axial Stress:	0.90 - 1.10 MPa
Scale:	1	Gross Axial Stress:	0.45 - 0.48 MPa
Panel Height:	1422 mm	Flexural reinf., ρ_{vf}:	0.20 - 0.41 %
Length:	1422 - 2845 mm	Interior Vertical reinf., ρ_{vi}:	0 %
Thickness:	195 mm	Joint reinf., ρ_{hj}:	0 %
H/L:	0.5 - 1	Bond Beam reinf., ρ_{hbb}:	0.05 - 0.12 %

Schultz (1996) tested 6 PG masonry walls to determine the influence of horizontal reinforcement ratio and height-to-length ratio on shear strength and wall behaviour. The walls each had 2#6 (19 mm) bars in the exterior vertical cells, while horizontal reinforcement consisted of a bond beam at mid-height. The bond beam reinforcement was either 2#3 (9.5 mm) bars or 1#4 (13 mm) bar and 1#5 (16 mm) bar for reinforcement ratios of 0.051% and 0.119%, respectively. The test setup used in this study is illustrated in Figure 3.14.

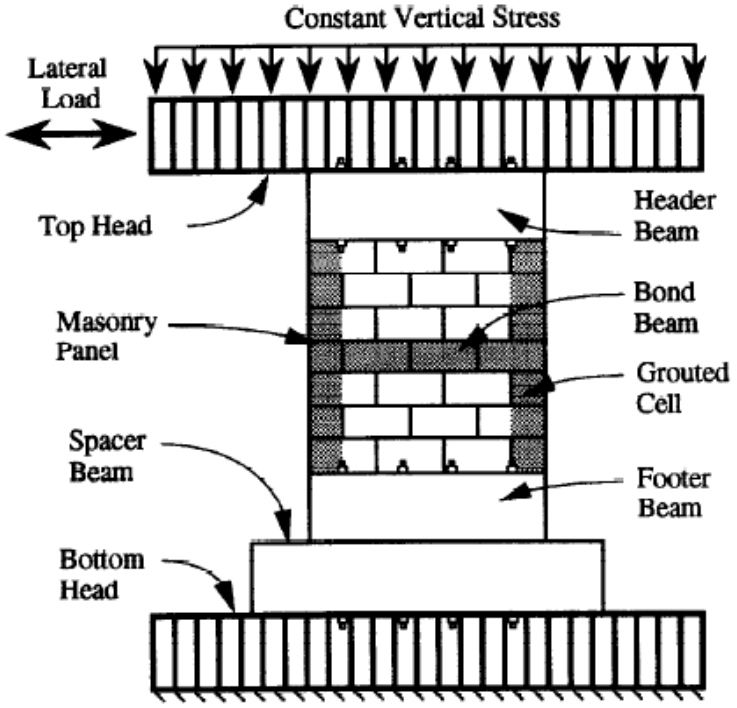

Figure 3.14 - Test setup used by Schultz (1996)

Walls with increasing height-to-length ratio showed a decrease in shear strength, however Schultz (1996) found that increasing height-to-length ratio increased ultimate shear stress (based on net wall area). Increasing the horizontal reinforcement ratio caused a modest increase in ultimate shear stress. One of the walls did not follow either of these trends, however, and was considered to be "out of character" for the series of shear wall tests (Schultz, 1996).

3.2.14 Schultz et al. (1998)

Total Number of PG Walls in Study: 6			USA
Loading Type:	Phased-Sequential	$f'_{m,eff}$:	12.0 - 12.2 MPa
Loading Rate:	Quasi-Static	A_{net}/A_{gross}:	0.44 - 0.53
Boundary Conditions:	Double Curvature	Net Axial Stress:	0.89 - 1.10 MPa
Scale:	1	Gross Axial Stress:	0.47 - 0.48 MPa
Panel Height:	1422 mm	Flexural reinf., ρ_{vf}:	0.20 - 0.41 %
Length:	1422 - 2845 mm	Interior Vertical reinf., ρ_{vi}:	0 %
Thickness:	195 mm	Joint reinf., ρ_{hj}:	0.06 - 0.11 %
H/L:	0.5 - 1	Bond Beam reinf., ρ_{hbb}:	0 %

Like the Schultz (1996) study, the Schultz et al. (1998) study tested 6 PG masonry walls to determine the influence of horizontal reinforcement ratio and height-to-length ratio on shear strength and wall behaviour. This time, joint reinforcement was used, to investigate the effect of horizontal reinforcement type. The walls each had 2#6 (19 mm) bars in the exterior vertical cells, while horizontal reinforcement consisted of a ladder joint reinforcement at every course. Joint reinforcement was either 9-gauge (3.76 mm) or 5-gauge (5.26 mm) ladder reinforcement for reinforcement ratios of 0.056% and 0.110%, respectively. Vertical loads were maintained only approximately constant (Schultz et al., 1998). The test setup used in this study is illustrated in Figure 3.15.

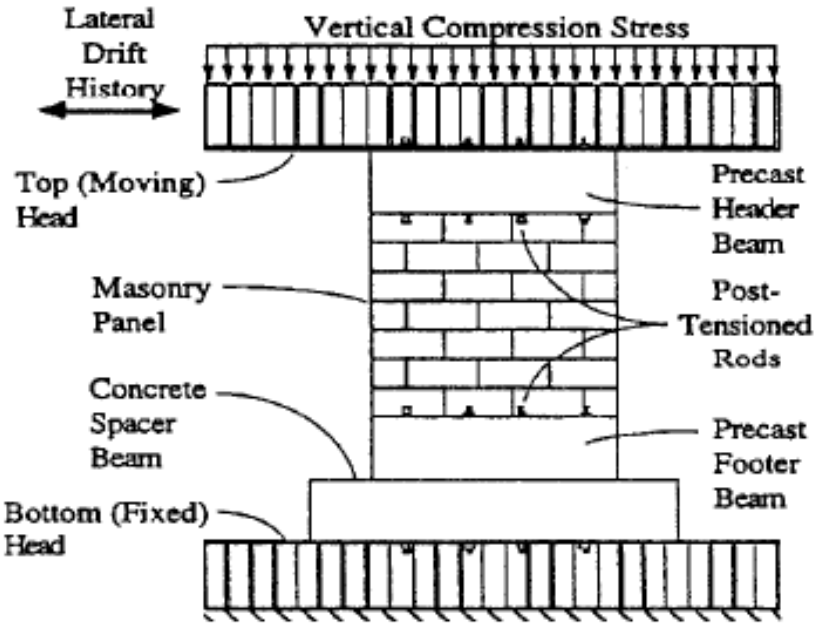

Figure 3.15 - Test setup used by Schultz et al. (1998)

Again, it was found that increasing height-to-length ratio (increasing wall slenderness) increased ultimate shear stress (Schultz et al., 1998). Increasing the horizontal reinforcement ratio caused a modest increase in ultimate shear stress. Unlike the Schultz (1996) study, the ladder-reinforced walls were not dominated by vertical cracks adjacent to the grouted jamb cells (Schultz et al.,

1998). Schultz et al. (1998) theorized that the bed joint reinforcement served to bridge the vertical cracks and prevent interruption of stress transfer throughout the wall.

3.2.15 Voon and Ingham (2006), Voon (2007)

Total Number of PG Walls in Study: 2			New Zealand
Loading Type:	Reverse Cyclic	$f'_{m,eff}$:	Unknown
Loading Rate:	Quasi-Static	A_{net}/A_{gross}:	0.74
Boundary Conditions:	Cantilever	Net Axial Stress:	0 MPa
Scale:	1	Gross Axial Stress:	0 MPa
Panel Height:	1800 mm	Flexural reinf., ρ_{vf}:	0.25 %
Length:	1800 mm	Interior Vertical reinf., ρ_{vi}:	0.12 - 0.37 %
Thickness:	140 mm	Joint reinf., ρ_{hj}:	0 %
H/L:	1	Bond Beam reinf., ρ_{hbb}:	0 %

Voon and Ingham (2006) tested 10 masonry walls, 2 of which were partially grouted while the rest were fully grouted. The two PG walls were reinforced vertically only, one with 5-D20 bars at 400 mm and the other with 3-D20 bars at 800 mm. The test setup used in this study is illustrated in Figure 3.16.

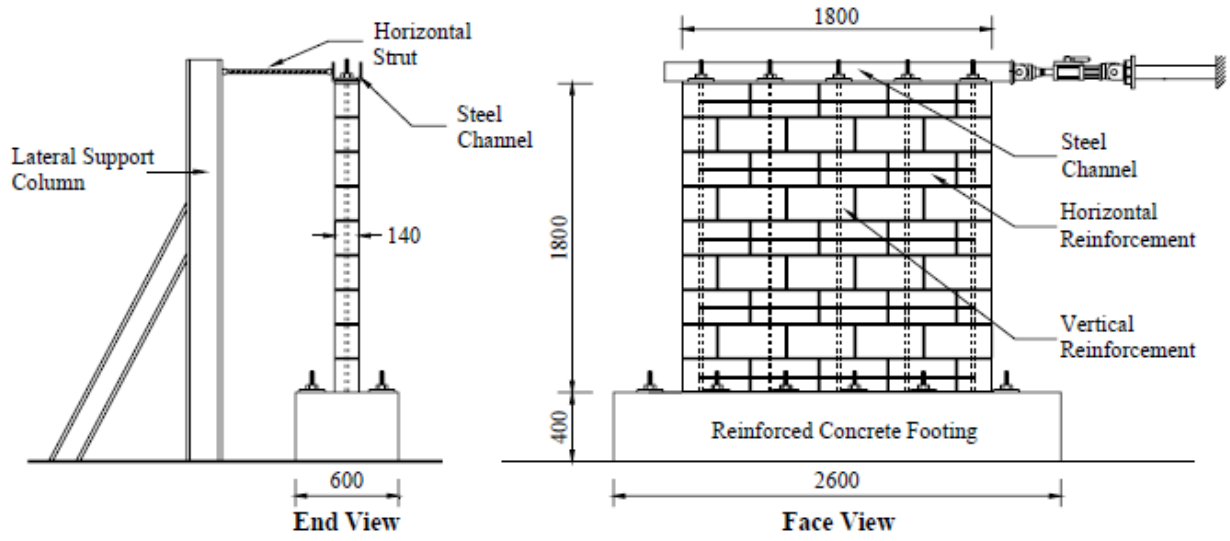

Figure 3.16 - Test setup used by Voon (2007)

Voon and Ingham (2006) observed that the PG walls had significantly lower shear strength than the FG walls, however their net shear strengths were comparable. The PG wall with smaller

vertical reinforcement spacings had significantly higher shear strength than the one with only 3 vertical bars (Voon and Ingham, 2006).

No information about compressive strengths of constituent materials or prisms was reported, except for the grouted prism strength.

3.2.16 Haach et al. (2007, 2010)

Total Number of PG Walls in Study: 4			Portugal
Loading Type:	Reverse Cyclic	$f'_{m,eff}$:	7.71 - 9.94 MPa
Loading Rate:	Quasi-Static	A_{net}/A_{gross}:	0.37
Boundary Conditions:	Cantilever	Net Axial Stress:	1.37 - 3.42 MPa
Scale:	0.5	Gross Axial Stress:	0.5 - 1.25 MPa
Panel Height:	808 mm	Flexural reinf., ρ_{vf}:	0.07 %
Length:	1200 mm	Interior Vertical reinf., ρ_{vi}:	0.03 %
Thickness:	100 mm	Joint reinf., ρ_{hj}:	0.09 %
H/L:	0.67	Bond Beam reinf., ρ_{hbb}:	0 %

Haach et al. (2007) tested 5 masonry walls, 4 of which were partially grouted while the remaining wall was unreinforced. The objective of the study was to investigate the effect of axial load and bond pattern (stacked and running bond). Truss reinforcement was used in both the horizontal and vertical directions, and 3-cell concrete masonry blocks were used (Figure 3.17).

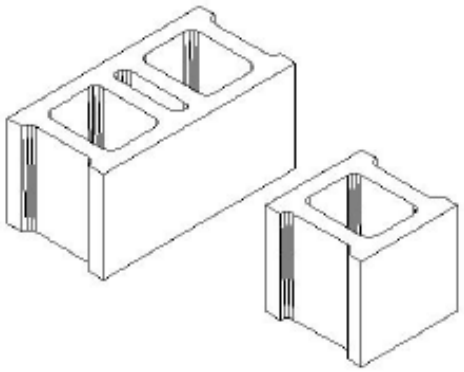

Figure 3.17 - Three-cell blocks used by Haach et al. (2007)

The mortar was also used as grout, which was used to fill the central cell of the block, where vertical reinforcement was placed. The test setup is illustrated in Figure 3.18.

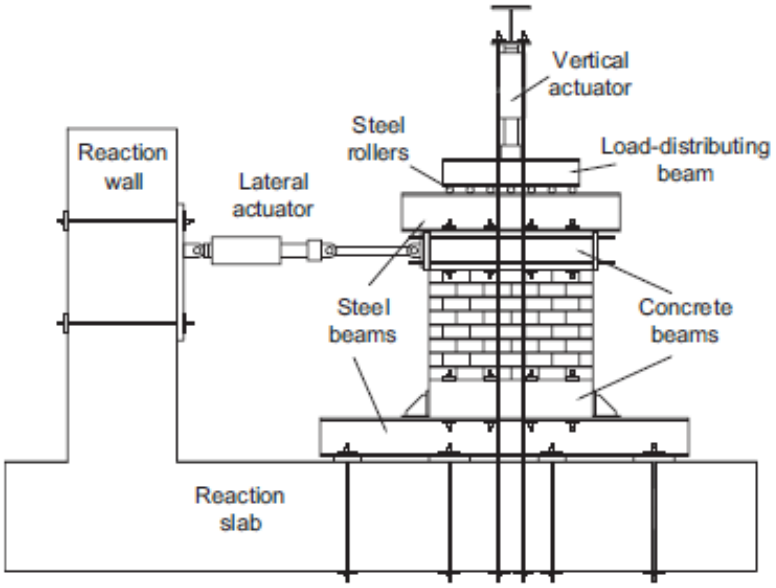

Figure 3.18 - Test setup used by Haach et al. (2010)

Haach et al. (2007) found that the bond pattern made no difference in the behaviour or ultimate shear capacity of the walls. Increased axial stresses led to an increase in shear strength, however it also led to more brittle failures. Haach et al. (2007) attributed the lower axial stiffness of one wall to the fact that the mortar used in this wall had a lower compressive strength. They noted, however, that the lower strength of mortar seemed to have no influence on the lateral behaviour of the wall (Haach et al., 2007).

3.2.17 Maleki (2008), Maleki et al. (2009)

Total Number of PG Walls in Study: 5			Canada
Loading Type:	Reverse Cyclic	$f'_{m,eff}$:	19.0 - 19.9 MPa
Loading Rate:	Quasi-Static	A_{net}/A_{gross}:	0.41 - 0.48
Boundary Conditions:	Cantilever	Net Axial Stress:	1.55 - 1.80 MPa
Scale:	0.47	Gross Axial Stress:	0.74 MPa
Panel Height:	945 - 2655 mm	Flexural reinf., ρ_{vf}:	0.09 - 0.16 %
Length:	1800 mm	Interior Vertical reinf., ρ_{vi}:	0 - 0.09 %
Thickness:	90 mm	Joint reinf., ρ_{hj}:	0 %
H/L:	0.53 - 1.48	Bond Beam reinf., ρ_{hbb}:	0.04 - 0.05%

Maleki et al. (2009) tested 5 PG masonry walls to investigate the performance of PG walls with larger bar spacing than allowed in the seismic requirements of CSA S304.1-04. Three different reinforcement spacings and three different aspect ratios were used, while horizontal reinforcement ratio and total vertical reinforcement ratio remained approximately equal for all the walls. The test setup is illustrated in Figure 3.19.

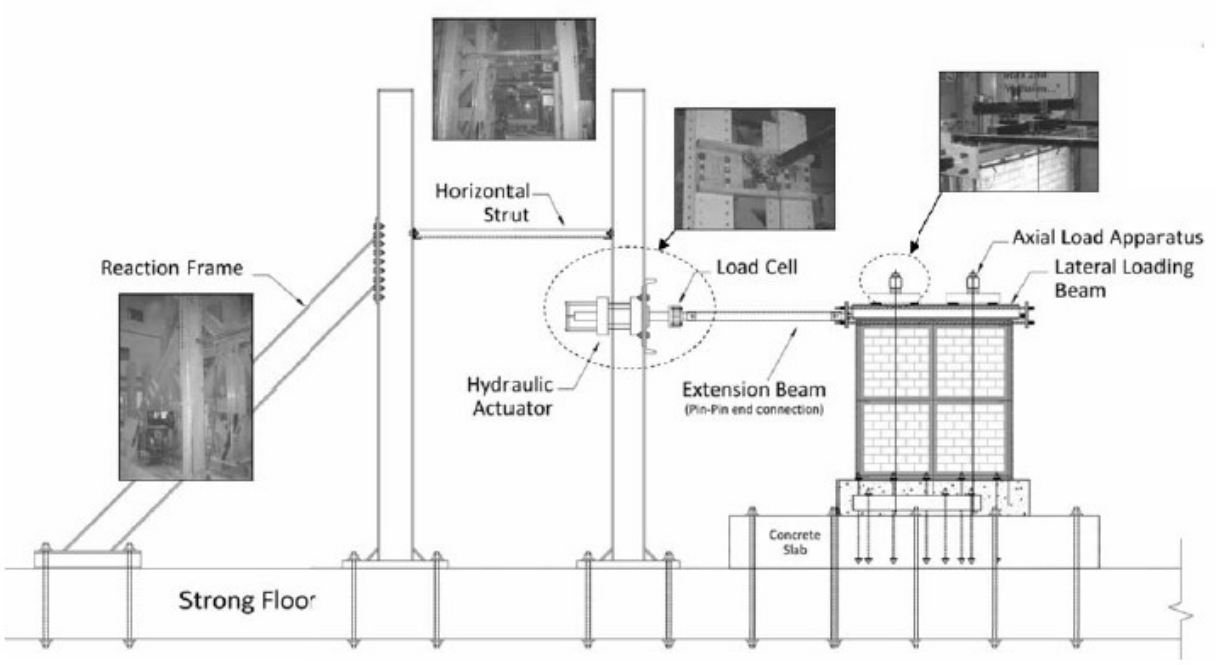

Figure 3.19 - Test setup used by Maleki et al. (2009)

It was observed that PG masonry shear walls with widely spaced reinforcement provide relatively ductile behaviour (Maleki, 2008). The overall response of the walls was not sensitive to the reinforcement spacing, however it was sensitive to the aspect ratio. The four walls with aspect ratios equal to or less than 1.0 failed primarily in shear, indicated by the lack of vertical bar yielding before the peak load was reached. The fifth wall, which had an aspect ratio of 1.5, was characterized as having a mixed shear-flexure failure mode, with yielding of vertical reinforcement and diagonal cracking both observed (Maleki et al., 2009). Maleki et al. (2009) concluded that the

Canadian masonry design standard underestimates the energy dissipation ability of masonry walls in general.

3.2.18 Elmapruk (2010)

Total Number of PG Walls in Study: 6			USA
Loading Type:	Reverse Cyclic	$f'_{m,eff}$:	15.5 - 16.3 MPa
Loading Rate:	Quasi-Static	A_{net}/A_{gross}:	0.48 - 0.58
Boundary Conditions:	Double Curvature	Net Axial Stress:	0.16 - 0.20 MPa
Scale:	1	Gross Axial Stress:	0.10 MPa
Panel Height:	1422 mm	Flexural reinf., ρ_{vf}:	0.22 %
Length:	2642 mm	Interior Vertical reinf., ρ_{vi}:	0.11 - 0.12 %
Thickness:	194 mm	Joint reinf., ρ_{hj}:	0 %
H/L:	0.54	Bond Beam reinf., ρ_{hbb}:	0.07 - 0.15 %

Elmapruk (2010) tested 6 PG masonry walls with varying horizontal reinforcement ratios and vertical reinforcement spacing. Vertical reinforcement spacings of 24, 32 and 48 inches were used. Horizontal reinforcement ratios were varied by using either 1#5, 1#6 or 2#5 bars (for ρ_{hbb} values of 0.73%, 0.10% or 0.15 %, respectively) in the bond beam at mid-height of the wall. The test setup is illustrated in Figure 3.20.

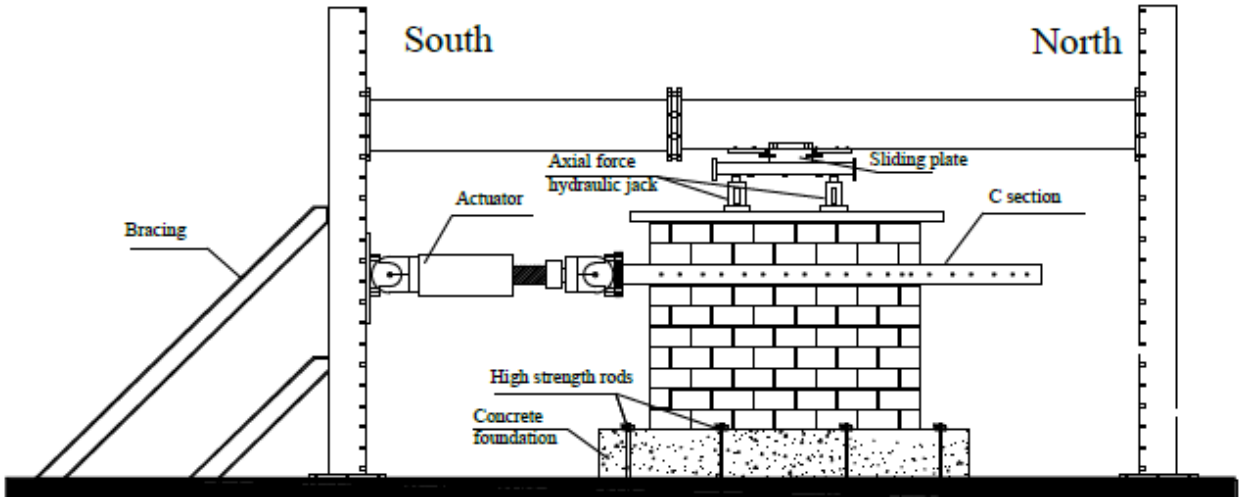

Figure 3.20 - Test setup used by Elmapruk (2010)

Elmapruk (2010) found that decreasing the spacing between vertically grouted, reinforced cells greatly improved the shear strength of the walls. It was also noted that there seems to be a threshold

horizontal reinforcement ratio above which increasing the amount of reinforcement does not improve the shear strength of the walls. Elmapruk (2010) also found that the MSJC (2008) equation for PG masonry shear walls was highly unconservative, overestimating the shear strength of the tested walls by as much as 91%.

Several inconsistencies in the descriptions of tested walls provided by Elmapruk (2010) were discovered and are discussed in detail in Appendix A.

3.2.19 Minaie (2009), Minaie et al. (2010)

Total Number of PG Walls in Study: 4			USA
Loading Type:	Reverse Cyclic	$f'_{m,eff}$:	7.2 - 9.4 MPa
Loading Rate:	Quasi-Static	A_{net}/A_{gross}:	0.47
Boundary Conditions:	Varied	Net Axial Stress:	0 - 0.7 MPa
Scale:	1	Gross Axial Stress:	0 - 0.33 MPa
Panel Height:	2438 mm	Flexural reinf., ρ_{vf}:	0.08 %
Length:	3861 mm	Interior Vertical reinf., ρ_{vi}:	0.08 %
Thickness:	194 mm	Joint reinf., ρ_{hj}:	0 %
H/L:	0.63	Bond Beam reinf., ρ_{hbb}:	0.12 %

Minaie et al. (2010) tested 4 PG walls with identical geometric properties and the same reinforcement pattern, with the objective of assessing the accuracy of the MSJC (2008) shear strength and seismic design provisions for PG masonry walls. Test variables consisted of mortar type (masonry cement or Portland cement lime), axial stress level (0 or 0.7 MPa) and boundary conditions (double curvature or cantilever). The test setup used in this study is illustrated in Figure 3.21.

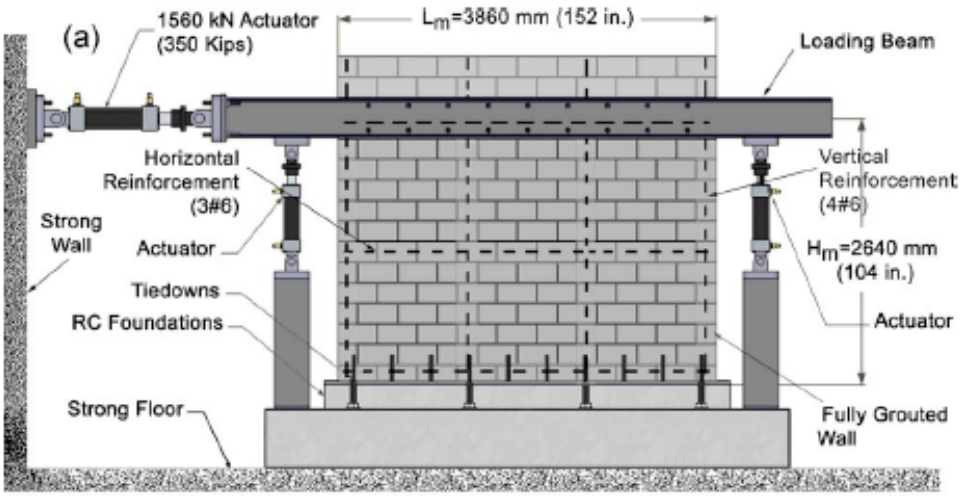

Figure 3.21 - Test setup used by Minaie et al. (2010)

Minaie et al. (2010) found that the tested PG walls behaved similarly to in-filled frames. They concluded that the MSJC shear strength expression is unconservative for PG masonry, possibly because it was derived empirically, based exclusively on FG shear wall test data (Minaie et al., 2010).

3.2.20 Baenziger and Porter (2011)

Total Number of PG Walls in Study: 8			USA
Loading Type:	Reverse Cyclic	$f'_{m,eff}$:	13.9 - 19.8 MPa
Loading Rate:	Quasi-Static	A_{net}/A_{gross}:	0.56 - 0.65
Boundary Conditions:	Cantilever	Net Axial Stress:	0 MPa
Scale:	1	Gross Axial Stress:	0 MPa
Panel Height:	2438 mm	Flexural reinf., ρ_{vf}:	0.14 - 0.25 %
Length:	2845 - 4267 mm	Interior Vertical reinf., ρ_{vi}:	0.05 - 0.06 %
Thickness:	194 mm	Joint reinf., ρ_{hj}:	0 - 0.18 %
H/L:	0.57 - 0.86	Bond Beam reinf., ρ_{hbb}:	0.05 - 0.11 %

Baenziger and Porter (2011) tested 10 walls, 8 of which were PG while 2 were FG. The primary objective of the study was to compare walls constructed using conventional bond beam reinforcement with walls constructed using joint reinforcement. All walls were reinforced horizontally with top and bottom bond beams and either joint reinforcement in each bed joint

(single ladder style or double seismic style joint) or a bond beam at mid-height. The test setup is illustrated in Figure 3.22.

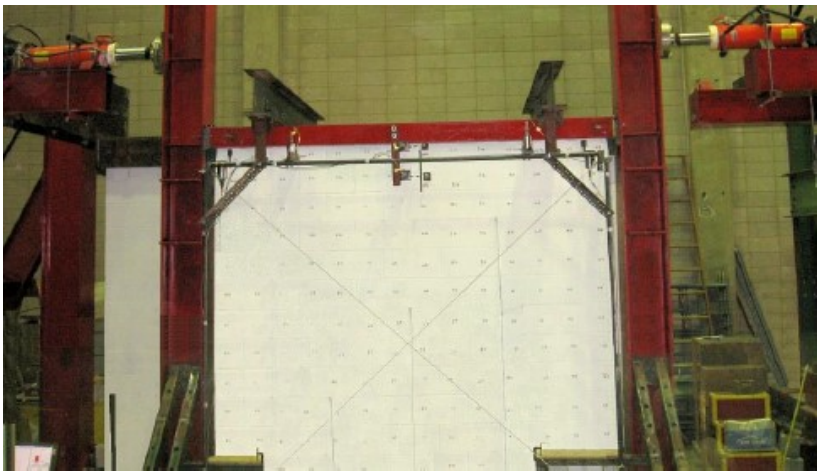

Figure 3.22 - Test setup used by Baenziger and Porter (2011)

Baenziger and Porter (2011) concluded that joint reinforcement can provide the required capacity and ductility to serve as primary shear reinforcement in PG walls. In fact, the walls with evenly distributed joint reinforcement provided better crack control than the walls with reinforcement concentrated in bond beams (Baenziger and Porter, 2011).

3.2.21 Nolph (2010), Nolph and ElGawady (2012)

Total Number of PG Walls in Study: 5			USA
Loading Type:	Reverse Cyclic	$f'_{m,eff}$:	11.6 - 12.8 MPa
Loading Rate:	Quasi-Static	A_{net}/A_{gross}:	0.48 - 0.58
Boundary Conditions:	Cantilever	Net Axial Stress:	0.17 - 0.20
Scale:	1	Gross Axial Stress:	0.10
Panel Height:	2235 mm	Flexural reinf., ρ_{vf}:	0.22 - 0.30 %
Length:	2631 mm	Interior Vertical reinf., ρ_{vi}:	0.15 - 0.24 %
Thickness:	194 mm	Joint reinf., ρ_{hj}:	0 %
H/L:	0.85	Bond Beam reinf., ρ_{hbb}:	0.05 - 0.09 %

Nolph and ElGawady (2012) tested 5 PG walls to quantify the effects of horizontal reinforcement ratio and spacing between vertical grouted cells. The horizontal reinforcement ratio was varied by using either 1#5, 1#6, or 2#5 bars in the bond beam at mid-height, for ρ_{hbb} values of 0.05%, 0.07%

and 0.09%, respectively. Vertical reinforcement spacings of 1219 mm, 813 mm or 610 mm were used. The test setup used is illustrated in Figure 3.23.

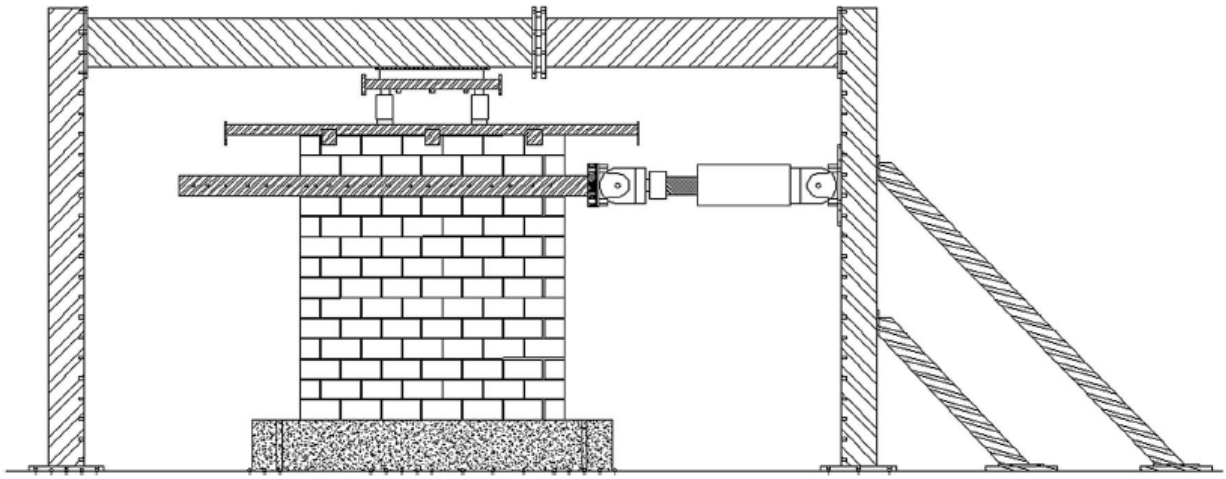

Figure 3.23 - Test setup used by Nolph and ElGawady (2012)

Like Elmapruk (2010), Nolph and ElGawady (2012) concluded that there appears to be a maximum horizontal reinforcement ratio above which no additional shear capacity is achieved. Based on their study, this threshold value is estimated to be 0.1% for specimens with vertical grouted cells spaced at 1219 mm. It was also observed that the MSJC shear equation overestimated the strength of the 3 walls with 1219 mm spacing between vertical grouted cells, particularly as horizontal reinforcement increased (Nolph and ElGawady, 2012).

3.2.22 Oan (2013)

Total Number of PG Walls in Study: 51			Canada
Loading Type:	Monotonic	$f'_{m,eff}$:	12.5 - 19.1 MPa
Loading Rate:	Quasi-Static	A_{net}/A_{gross}:	0.68
Boundary Conditions:	Cantilever	Net Axial Stress:	2.02 - 4.08 MPa
Scale:	1	Gross Axial Stress:	1.37 - 2.76 MPa
Panel Height:	1000 mm	Flexural reinf., ρ_{vf}:	0 - 0.13 %
Length:	1600 mm	Interior Vertical reinf., ρ_{vi}:	0 - 0.13 %
Thickness:	190 mm	Joint reinf., ρ_{hj}:	0 - 0.10 %
H/L:	0.63	Bond Beam reinf., ρ_{hbb}:	0 %

Oan tested 22 sets of 3 identical walls, of which 5 sets (15 walls) were ungrouted, for a total of 51 PG walls. The parameters studied were net axial stress level (2, 3 or 4 MPa), type of reinforcement (none, vertical reinforcement, horizontal reinforcement or both), amount of horizontal reinforcement (either 3.7 mm or 4.9 mm ladder reinforcement) and method of laying joint reinforcement (dry or embedded). For the dry placement method, joint reinforcement was placed directly on the dry face shell of the mortar, followed by the mortar. For the embedded method, the mortar was first placed on the face shell of the masonry, then the joint reinforcement was embedded in the mortar, followed by another layer of mortar. The test setup used in this study, which was based on the ESECMaSE guidelines, is illustrated in Figure 3.24.

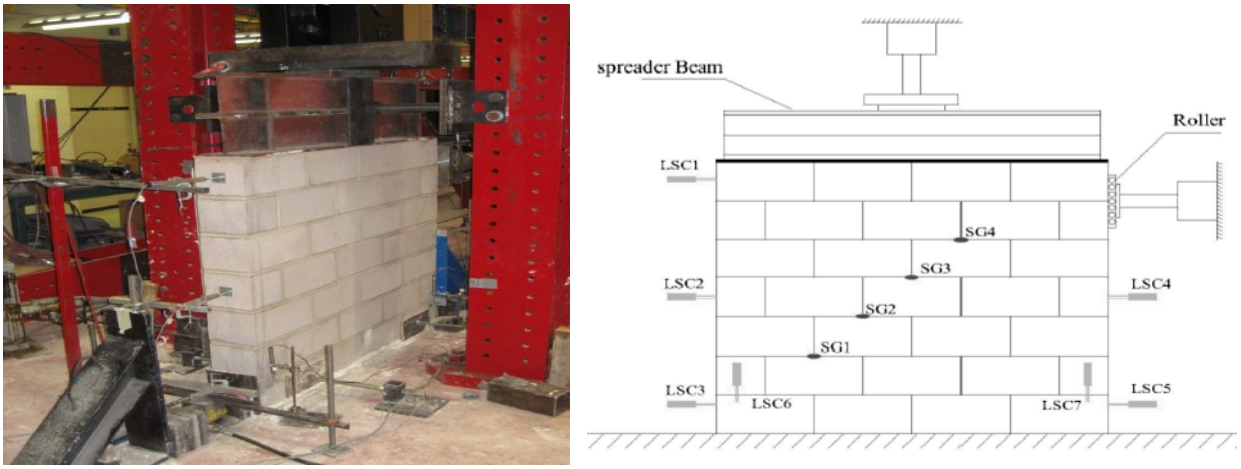

Figure 3.24 - Test setup used by Oan (2013)

Oan (2013) observed that increasing the axial stress led to significant increases in shear resistance of the walls. Although the joint reinforcement improved wall ductility, it was not found to increase shear strength. In fact, the findings of Oan (2013) suggest that the larger diameter joint reinforcement (4.9 mm diameter) decreased the shear strength of the walls tested at 2 MPa axial load level, due to reduced bond between the mortar and the masonry units. Vertical reinforcement had no effect on shear strength or ductility of the walls, however it should be noted that the vertical bars were not embedded in a concrete base beam as is typical of most masonry wall tests. In such cases, as the wall deforms laterally the vertical bars bend at their base, allowing them to contribute

to the resistance of the wall (Oan, 2013). The method of joint reinforcement placement showed no statistically significant difference in resulting values of shear strength (Oan, 2013).

The use of replicates of each wall was deemed essential for obtaining reliable results, because significant differences in results of duplicate walls were observed (Oan, 2013). It was also found that the Canadian code was very conservative in predicting the shear strength of the walls.

3.2.23 Hoque (2013)

Total Number of PG Walls in Study: 18			Canada
Loading Type:	Varied	$f'_{m,eff}$:	16.6 MPa
Loading Rate:	Quasi-Static	A_{net}/A_{gross}:	0.58
Boundary Conditions:	Double Curvature	Net Axial Stress:	2.05 - 2.17 MPa
Scale:	1	Gross Axial Stress:	1.20 - 1.26 MPa
Panel Height:	1800 mm	Flexural reinf., ρ_{vf}:	0.12 %
Length:	1800 mm	Interior Vertical reinf., ρ_{vi}:	0.06 %
Thickness:	190 mm	Joint reinf., ρ_{hj}:	0 - 0.03 %
H/L:	1.0	Bond Beam reinf., ρ_{hbb}:	0 - 0.12 %

Hoque (2013) tested 8 sets of PG walls: 6 sets of 2 identical walls, and 2 sets of 3 identical walls, for a total of 18 walls. The variables of interest were bond beam location and anchorage conditions (straight ends, 180° hooks, 90° hooks or circular discs welded to the bar ends), presence of dowels at the top and bottom of the walls, and differences in loading protocol (monotonic or reverse cyclic lateral load and variable or constant axial load). The test setup, which was based on the ESECMaSE (2005) guidelines, is illustrated in Figure 3.25.

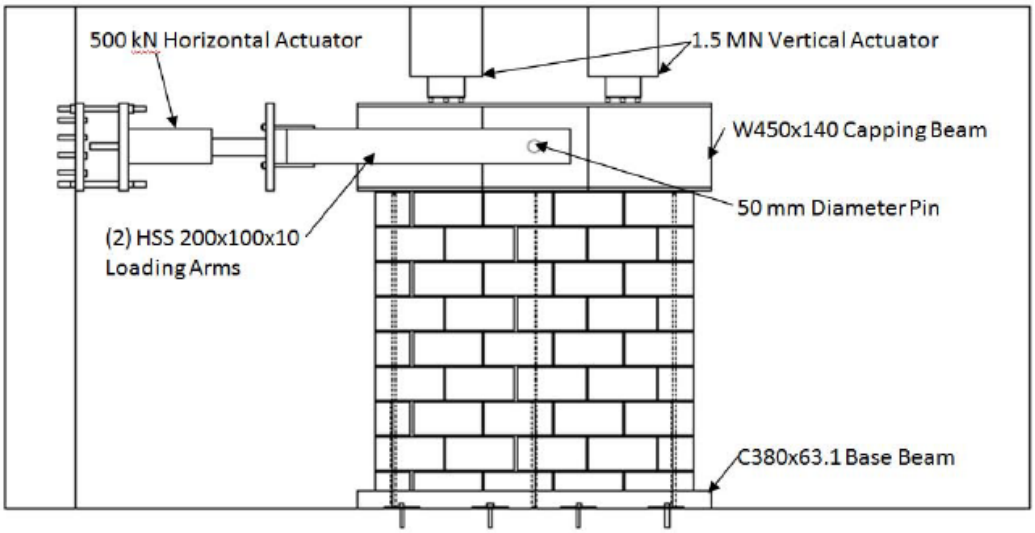

Figure 3.25 - Test setup used by Hoque (2013)

All of the walls except for the fifth set were constructed with dowels welded to the steel base beam. The two walls belonging to the fifth set had no mechanical connection to the base beam. The sixth set was provided with additional dowels at the top, which were welded to a steel plate connected to the capping beam. All the walls, except for two belonging to the eighth set, were subjected to reverse cyclic lateral loading. The eighth set of walls was monotonically loaded in the lateral direction. To maintain zero moment at wall mid-height, the axial load applied by each of the two vertical actuators varied throughout the tests (Hoque, 2013), except for one set of walls. The two walls belonging to the seventh set had constant vertical load applied by both vertical actuators throughout the test.

Hoque (2013) found that there was no significant difference in shear strength due to changes in bond beam anchorage and suggested that this might be due to insufficient stress in the bar. Using smaller reinforcement was suggested as a way of achieving sufficient stress to exceed the bond strength between the grout and reinforcement (Hoque, 2013). The lack of dowels in some walls, and additional dowels at the top of other walls, also resulted in no significant changes in wall behaviour or strength (Hoque, 2013). It was observed that the monotonically loaded walls had shear strength values about 7% higher than equivalent cyclically loaded walls (Hoque, 2013).

Hoque (2013) noted that there was a significant decrease in shear strength for the seventh set of walls, which had constant vertical loading. This was attributed to the fact that, for the wall sets with variable axial load, the vertical load in a given actuator sometimes reached very high values. For analysis purposes in the present study, the axial load was taken as the total axial load that was applied at the point of ultimate shear stress. This value was estimated as described in Appendix A.

3.2.24 Hamedzadeh (2013)

Total Number of PG Walls in Study: 21			Canada
Loading Type:	Monotonic	$f'_{m,eff}$:	7.0 - 7.2 MPa
Loading Rate:	Quasi-Static	A_{net}/A_{gross}:	0.43 - 0.50
Boundary Conditions:	Double Curvature	Net Axial Stress:	0.96 - 3.23 MPa
Scale:	0.48	Gross Axial Stress:	0.48 - 0.96 MPa
Panel Height:	760 - 1235 mm	Flexural reinf., ρ_{vf}:	0.09 - 0.26 %
Length:	853 - 2372 mm	Interior Vertical reinf., ρ_{vi}:	0 - 0.09 %
Thickness:	90.7 mm	Joint reinf., ρ_{hj}:	0 %
H/L:	0.32 - 1.0	Bond Beam reinf., ρ_{hbb}:	0 - 0.15 %

Hamedzadeh (2013) tested 8 sets of PG walls: 3 sets of 2 identical walls, and 5 sets of 3 identical walls, for a total of 21 walls. Variables of interest were initial axial stress, aspect ratio, interface between specimen and the steel loading beam (mortar or fiberboard) and method of lateral load application (point load or uniformly distributed load). The test setup, which was based on the ESECMaSE (2005) guidelines, is illustrated in Figure 3.26.

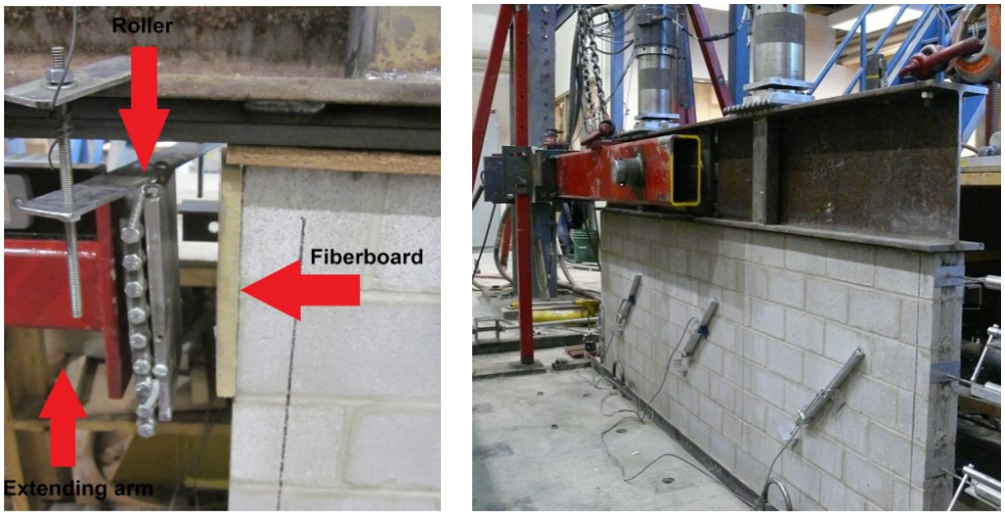

Figure 3.26 - Test setup used by Hamedzadeh: (a) first four walls, (b) remaining walls (adapted from Hamedzadeh, 2013)

For the first four walls, lateral load was applied directly to the wall (Figure 3.26 (a)). Either mortar or fiberboard was used as the interface between the steel capping beam and the wall, such that the only difference between the two wall sets was the distribution of the axial load over the wall due to the different interface materials. For the remaining 17 walls, lateral load was applied through a pin connection located at middle height of the steel capping beam (Figure 3.26 (b)), with mortar as the interface material.

Hamedzadeh (2013) observed that the different initial axial stresses did not influence the shear capacity of the walls. This is because the axial load varied throughout the tests, with peak axial loads being similar between different walls. The specified initial stress was applied to each wall, and then axial actuators were placed in displacement control, such that axial stress increased in proportion to shear stress throughout the tests. Hamedzadeh (2013) noted that because the axial load varied throughout the tests, the axial load corresponding to the ultimate shear stress was used for the purpose of evaluating design equations. In the same way, axial loads corresponding to ultimate shear stresses are used in the present study for analysis purposes, and were determined as

explained in Appendix A. The data acquisition system malfunctioned during testing of the first wall, so a design value of axial load was not available for this wall (Hamedzadeh, 2013).

Hamedzadeh also observed that shear capacity greatly increased as aspect ratio decreased. The differences in interface materials and lateral load application did not affect wall shear strengths significantly (Hamedzadeh, 2013).

3.2.25 Rizaee (2015)

Total Number of PG Walls in Study: 14			Canada
Loading Type:	Reverse Cyclic	$f'_{m,eff}$:	11.6 - 17.4 MPa
Loading Rate:	Quasi-Static	A_{net}/A_{gross}:	0.59
Boundary Conditions:	Double Curvature	Net Axial Stress:	2.02 - 2.39 MPa
Scale:	1	Gross Axial Stress:	1.20 - 1.42 MPa
Panel Height:	1800 mm	Flexural reinf., ρ_{vf}:	0.12 %
Length:	1800 mm	Interior Vertical reinf., ρ_{vi}:	0.06 %
Thickness:	190 mm	Joint reinf., ρ_{hj}:	0 %
H/L:	1.0	Bond Beam reinf., ρ_{hbb}:	0.03 - 0.12 %

Rizaee (2015) tested 7 sets of 2 identical PG walls, for a total of 14 walls. Variables of interest were bond beam reinforcement size (one 15M or 10M bar each bond beam), bond beam location and bond beam anchorage type (straight ends, 180° hooks, 90° hooks or circular discs welded to the bar ends). The test setup, which was based on the ESECMaSE (2005) guidelines, was the same test setup used by Hoque (2013), and is illustrated by Figure 3.27.

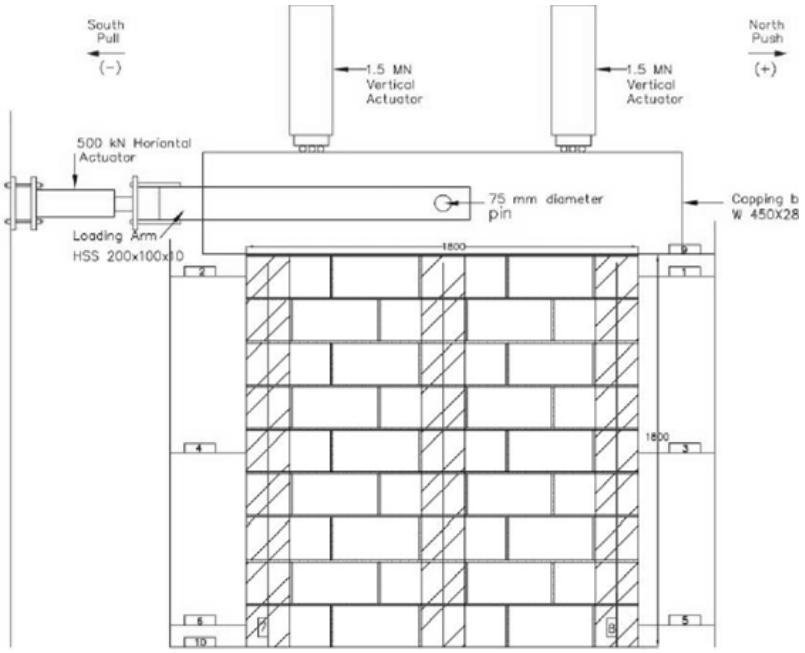

Figure 3.27 - Test setup used by Rizaee (2015)

As was done in the study by Hoque (2013), to maintain zero moment at wall mid-height, the axial load applied by each of the two vertical actuators varied throughout the tests (Rizaee, 2015). For analysis purposes in the present study, the axial load was taken as the total axial load that was applied at the point of ultimate shear stress. This value was estimated as described in Appendix A.

Rizaee (2015) concluded that the increasing bond beam bar size improves the performance of walls, in terms of strength, stiffness and energy dissipation, more than adjusting end anchorage. Reducing the bond beam bar size did not increase the effectiveness of anchorage or the amount of yielding of the rebar at critical locations (Rizaee, 2015). Changing the location of bond beams to lower in the wall improved energy dissipation and ductility, possibly because this moved more of the reinforcement to the cracked zone of the wall (Rizaee, 2015). There was not any significant difference in the performance of the various anchorage types, however reinforcement was more likely to reach yield with 180° hooks than with 90° hooks or with circular discs welded to the ends.

3.2.26 Ramírez et al. (2016)

Total Number of PG Walls in Study: 10			Chile
Loading Type:	Reverse Cyclic	$f'_{m,eff}$:	7.1 - 7.5 MPa
Loading Rate:	Quasi-Static	A_{net}/A_{gross}:	0.71 - 0.81
Boundary Conditions:	Cantilever	Net Axial Stress:	0 - 0.79 MPa
Scale:	1	Gross Axial Stress:	0 - 0.56 MPa
Panel Height:	1000 - 1800 mm	Flexural reinf., ρ_{vf}:	0.11 - 0.55 %
Length:	990 - 2590 mm	Interior Vertical reinf., ρ_{vi}:	0.06 %
Thickness:	140 mm	Joint reinf., ρ_{hj}:	0.04 - 0.10 %
H/L:	0.39 - 1.82	Bond Beam reinf., ρ_{hbb}:	0 %

Ramírez et al. (2016) tested 10 PG masonry walls to study the effect of aspect ratio, horizontal reinforcement ratio and axial stress on the behaviour of PG shear walls. Three aspect ratios were used, and ladder joint reinforcement was placed either at each course or every second course. Eight of the walls were subjected to a net axial compression of 0.79 MPa, while the other 2 walls had no axial load applied. The test setup is illustrated in Figure 3.28.

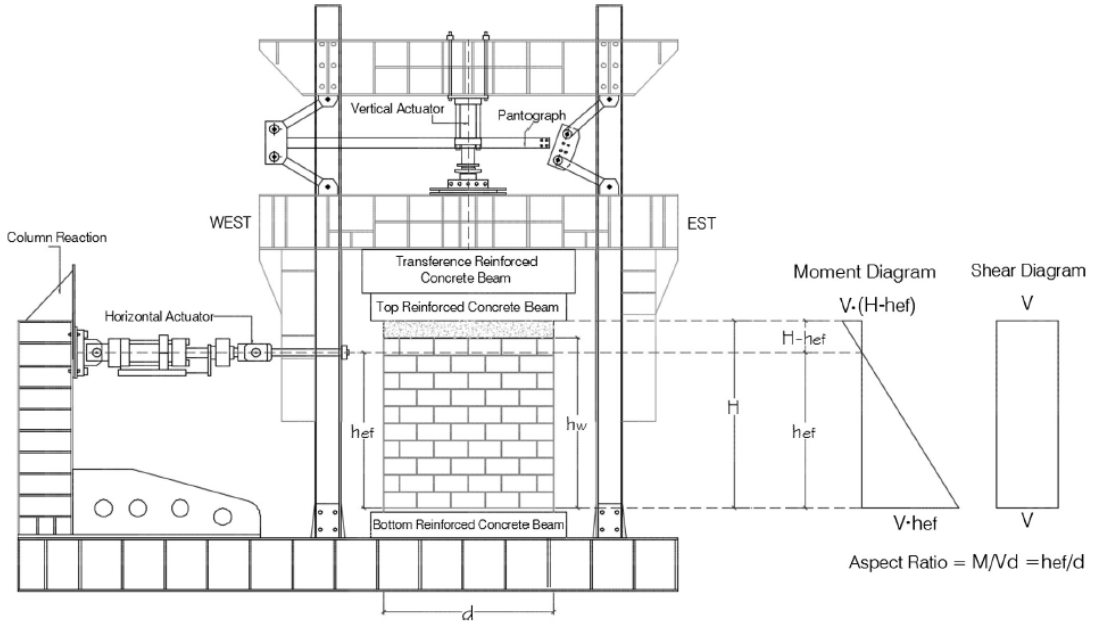

Figure 3.28 - Test setup used by Ramírez et al. (2016)

Ramírez et al. (2016) observed that shear strength (expressed in this study as net shear stress divided by the square root of compressive strength of the masonry prism) decreased as aspect ratio

increased, with only two exceptions. Aspect ratio was also found to be the predominant influence on stiffness degradation, with shorter walls experiencing greater stiffness degradation than slender walls (Ramírez et al., 2016). Shear strength increased as the horizontal reinforcement ratio increased, more so for moderately slender and slender walls than for squat walls. Shear strength also increased as axial compression increased, particularly for the squat walls (Ramírez et al., 2016).

4 DATASET ASSEMBLY

4.1 Introduction

Following data compilation, the assembled database was synthesized and scrutinized to minimize variation between studies, approximate missing values and eliminate inconsistencies. Similar data synthesization and scrutinization steps were performed by Dillon (2015) and Hung (2018) prior to analysis to improve database consistency.

In the following section, data synthesization will be defined and explained in the context of the current study. Then, data scrutinization will be defined and explained. The variables and datasets used in the present study will be described and the distribution of variables will be presented.

4.2 Data Synthesization

Data synthesization is defined as converting data to minimize variation between studies and estimating missing information (Hung, 2018). This step was necessary due to differences in the testing methodologies used by various researchers. Some of these differences include reported shear strength, loading pattern, loading rate and scaling. Many studies omitted information regarding material properties, and this information had to be estimated where possible. These variations and omissions were addressed through the correction factors developed by Dillon (2015), as well as estimation techniques, which are explained in the following section.

4.2.1 Reported Shear Strength

Some researchers reported peak shear strength values in both directions (push and pull), while others only reported the average peak shear strength. Others provided only the maximum shear strength (the highest in either the push or pull direction).

Wall strength may differ significantly between the push and pull directions due to imperfections in wall construction and lack of exact symmetry. Taking the shear strength as the maximum value of the two directions is unconservative, while using the minimum may be overly conservative. For

this reason, the average of shear strength in both directions is considered the best representation of the behaviour of a given wall.

Because the models developed in the present study were designed to predict the average peak shear strength, those studies which reported only the maximum shear strength required a correction factor to compensate for the exclusion of the peak strength in the weaker direction. Using data from 176 specimens, Dillon (2015) proposed a correction factor to reduce the shear strength in cases where only the maximum shear strength was provided. The correction factor chosen by Dillon (2015) was 0.94. The histogram generated by Dillon (2015) to obtain this correction factor is provided as Figure 4.1.

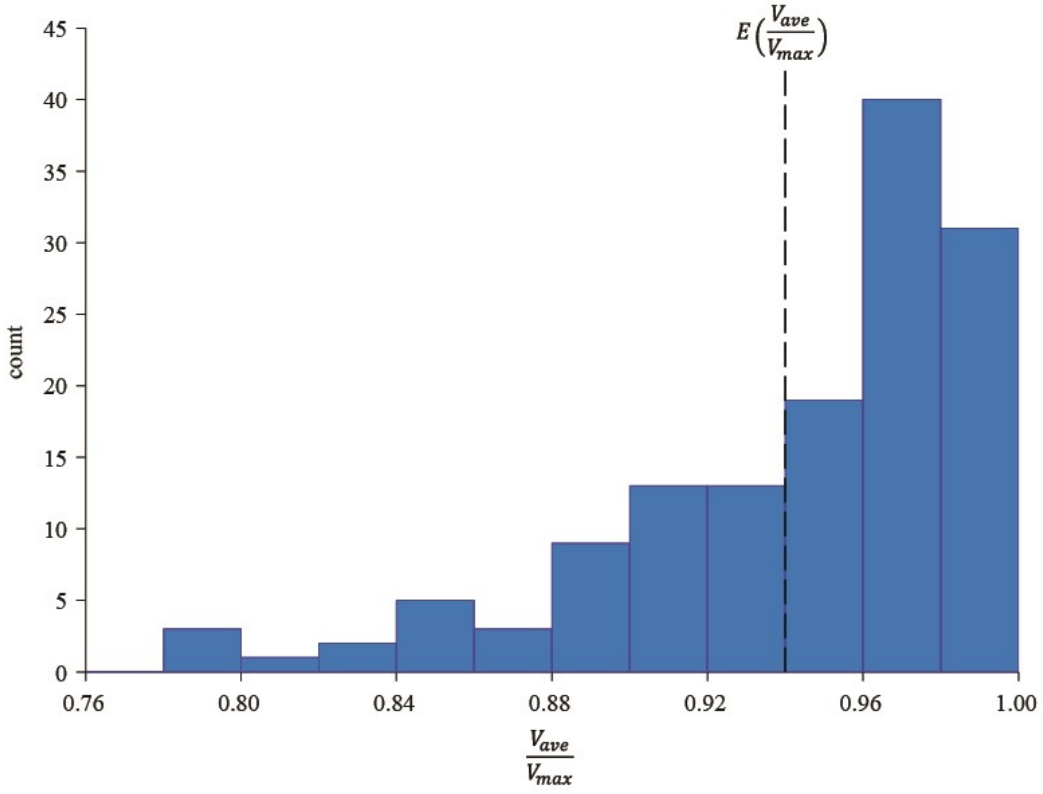

Figure 4.1 - Histogram of average to ultimate strength ratios (adapted from Dillon, 2015)

It should be noted that Dillon (2015) used data from both partially grouted and fully grouted masonry walls, made with CMUs and with clay bricks. It is unknown how much of the data used to obtain this correction factor was data from PG masonry walls built using CMUs.

4.2.2 Loading Pattern

The walls in the database were tested using various loading patterns: monotonic, reverse cyclic, sequential-phase displacement and simulated seismic. Tomaževič et al. (1996) noted that monotonically tested walls have higher shear strengths and larger ultimate displacements than their cyclically tested counterparts, due to less severe strength and stiffness degradation. When comparing shear strengths between walls tested using different cyclic loading patterns (reverse cyclic, sequential-phased displacement or simulated seismic), there is no significant difference (Dillon and Fonseca, 2014b).

Tomaževič et al. (1996) tested 32 equally sized and reinforced, half-scale PG masonry walls using both monotonic and periodic loading patterns, of which 8 were tested monotonically. Although a few other studies have used both monotonic and cyclic loading patterns, these studies did not duplicate design variables between monotonically and cyclically tested walls (Dillon, 2015). As a result, they could not be used to determine a correction factor for monotonically tested specimens.

Using the data from Tomaževič et al. (1996), Dillon (2015) determined that the mean ratio of cyclic-to-monotonic strength was 0.81, with a 95% confidence interval bounded below by 0.72 and above by 0.91. Dillon (2015) noted that the monotonically tested specimens appeared to fail predominantly in flexure. However, if this led to Dillon's value being farther from the true value for a correction factor, it would most likely be higher than the true value (Dillon, 2015). This is because the predominantly flexural failure indicates that the shear strengths of the monotonically tested specimens were higher than the loads at which they failed. Thus, if the true shear strengths of the monotonically tested walls could be obtained accurately, they would be higher than the reported strength values. To correct the true shear strengths to those of equivalent cyclically tested walls, the correction factor would need to be lower.

Hoque (2013) also tested two monotonically loaded walls and compared them with equivalent cyclically loaded walls that had been tested by Dickie & Lissel (2010). It was noted that the strength of the monotonically loaded walls was about 7% higher than the cyclically loaded ones (Hoque, 2013).

Although this is an issue that clearly requires future research, the correction factor of 0.81 represents the best estimate for the relationship between monotonic and cyclic specimens currently available (Dillon, 2015). The correction factor is applied to monotonically loaded specimens to transform the shear strength to that of a cyclically tested wall.

4.2.3 Loading Rate

Dynamic loading produces a greater shear capacity than that obtained through static loading due to strain-rate effects in the masonry materials and the steel reinforcement (Tomaževič et al., 1996). A small number of the specimens were tested dynamically and required a correction factor to convert the associated shear strength values to those of equivalent statically tested walls.

Dillon (2015) compared data of twelve pairs of specimens from three different studies (Williams, 1971; Mayes et al. 1976; Tomaževič et al, 1996) in which the influence of the loading rate was investigated. As a result of this analysis, Dillon (2015) proposed a correction factor of 0.9 for dynamically tested specimens.

4.2.4 Block Geometry

Detailed information on the geometry of CMUs, such as the actual length of blocks and thickness of face shells, was assumed where not provided by researchers. If clues were given by the researcher, such as providing enough information on their method of calculating $\boldsymbol{A_{net}}$ to allow for back-calculation of face shell thickness, then this information was used. Where no clues were given, it was assumed that the researcher used standard CMUs according to the country of testing. Details of these assumptions are provided in Table 4.1.

Table 4.1 - Assumed block dimensions according to country of experimental study

Country	Block thickness (mm)	Block height, actual (mm)	Block length, actual (mm)	Face shell thickness (mm)
Canada	190	190	390	32*
USA	193.7	193.7	396.9	31.8
	142.9	193.7	396.9	25.4
Mexico	150	200*	390	25.4
Japan	150	190	390	30.0

*these assumed values were not used in the database as other information was available

The values in Table 4.1 were obtained from specifications or product catalogues from the respective countries (Boehmers, 2005; National Concrete Masonry Association, 2012; Angelus Block Co., Inc., n.d.; JR. Blocks, n.d.; Hoei Company Ltd., n.d.). In two cases (Matsumura, 1987; Baenziger and Porter, 2011), an initial assumption was made for the face shell thickness of blocks, which was then adjusted to achieve better agreement between provided and estimated values of A_{net}. The adjusted values of t_{fs} for these two studies were 35.0 mm and 38.1 mm, respectively.

4.2.5 Compressive Strength of Blocks

A few researchers (Scrivener, 1967; Chen et al., 1978; Haach et al., 2007) provided the compressive strength of the masonry blocks based on gross block area. In these cases, the net compressive strength of masonry blocks was estimated using Equation (4.1).

$$f_{block} = \frac{P_{block}}{A_{block,n}} = \frac{f_{block,gr} * A_{block,gr}}{v * A_{block,gr}} = \frac{f_{block,gr}}{v} \tag{4.1}$$

where f_{block} = average compressive strength of the masonry block (MPa), based on net block area

P_{block} = axial load applied to the block (N)

$A_{block,n}$ = net area of masonry block (mm^2)

$f_{block,gr}$ = compressive strength of the masonry block (MPa), based on gross block area

$A_{block,gr}$ = gross area of masonry block (mm^2)

v = ratio of net to gross area of masonry block

In cases where the researchers did not indicate whether the compressive strength of the masonry blocks was based on net or gross area, it was assumed to be based on net area.

4.2.6 Prism Strength Estimation

Reporting of the compressive strength of masonry materials is often inconsistent in PG masonry wall studies. Some researchers only report the compressive strength of ungrouted prisms, others only provide the compressive strength of grouted prisms and some provide both. If sufficient information on the constituent materials strengths (compressive strength of concrete blocks, mortar, and grout) is provided, both the grouted and ungrouted prism compressive strengths can be estimated using the equations proposed by Dillon (2015).

As Dillon (2015) points out, the estimation of prism strength is likely to introduce measurement error into the analysis due to the high variability of masonry prisms strengths. However, masonry prism tests typically exhibit high variability, with a coefficient of variation of 10 percent considered to be acceptable (Blume and Proulx, 1968, as cited in Dillon, 2015; CSA S304-14, 2014). This variability can be attributed in large part to defects introduced during the assembly and handling of the prisms. Because constituent material tests typically have less variability than prism tests, Dillon (2015) suggested that the measurement error introduced by estimating f'_m values is likely to be smaller than the variation that would exist in measured prism tests.

Based on a statistical analysis of over 500 prism tests, Dillon (2015) developed two linear models to predict masonry prism strengths for ungrouted and grouted prisms. The model for predicting the prism strength for ungrouted masonry prisms is given by Equation (4.2).

$$f'_{mu} = v^{0.636} f_{block}^{0.688} f_{mortar}^{0.317} \tag{4.2}$$

The model for predicting prism strength of grouted masonry prisms is given by Equation (4.3).

$$f'_{mg} = t^{-0.221}(1-v)^{0.0818} f_{block}^{-0.425} (f_{mortar} + f_{block})^{1.01} \left(f_{grout} + f_{block}\right)^{0.312} \quad (4.3)$$

where f'_{mu} = ungrouted prism strength (MPa)

f'_{mg} = grouted prism strength (MPa)

v = ratio of net to gross area, which is taken as reported by the researcher or by dividing gross prism strength by net prism strength

f_{block} = compressive strength of concrete block (MPa)

f_{mortar} = compressive strength of mortar (MPa)

t = thickness of the prism in the smallest dimension (mm)

f_{grout} = compressive strength of the grout (MPa)

4.2.7 Prism Geometry

There is significant variability in the number of blocks in prisms used by researchers to determine f'_m, despite the fact that prism strength decreases with increasing aspect ratio (Boult, 1979). Hamid et al. (1978) tested 146 concrete block masonry prisms and concluded that two-block high prisms do not accurately represent f'_m (as cited in Dillon, 2015). For two-course prisms, the lateral confinement effect due to the end plates artificially enhances the compressive strength (Dillon, 2015). This effect is minimized in taller prisms as the plate confinement is localized at the ends of the specimen. Accidental eccentricity is another probable source of variation on prism strength, becoming more pronounced as the height of the prism increases (Dillon, 2015). Boult (1979) observed that the decrease in compressive strength became negligible for prism heights between five and twelve courses.

To obtain equivalent values of f'_m, it is important to account for differences in height-to-thickness ratios of prisms. Research has shown that the standardized prism aspect ratio of five best represents

the compressive strength of masonry in the field (Hegemier et al., 1978, as cited in Dillon, 2015). This is also the standard aspect ratio used in CSA S304-14 (2014) Annex D.

Dillon (2015) compared correction factors from four standards: ASTM C1314 (2014), CSA S304.1-04 (2004), BS 5628-2 (2000) and AS 4700 (2011). The latter three standards use the standard aspect ratio of five and Dillon (2015) converted the correction factors in ASTM to the equivalent values assuming the standard aspect ratio of five. He then determined a function which correlated well with the mean of the four sets of correction factors. The function is given by Equation (4.4).

$$k = 1 - 0.058\left(5 - \frac{h}{t}\right)^{1.07} \tag{4.4}$$

where k = the correction factor to account for the h/t ratio of the prism

h = height of the masonry prism (mm)

t = thickness of the masonry prism (mm)

Equivalent values of prism strength with the aspect ratio of five are obtained by multiplying the uncorrected value of f'_{mu} or f'_{mg} by k.

4.2.8 Scaling

Due to limitations related to space, cost, and capacity of loading devices, it is not always practical to test full-scale specimens (Hamedzadeh, 2013). One solution to these problems is to build a reduced-scale model of the desired full-scale prototype. Out of the 292 PG masonry walls compiled for the present study, 50 were small-scale walls. Scales used were either one-half or one-third.

Scaled modeling of structures consists of reducing the dimensions of a specimen proportionally by the same scale (Hamedzadeh, 2013). Other quantities such as force, time and frequency must also be scaled down. Depending on the type of model sought, material properties such as modulus of elasticity, stiffness and density should also be scaled down (Hamedzadeh, 2013).

There are two main approaches that can be used to relate the model and prototype properties. The first approach is complete model similarity, in which special model materials are manufactured such that their properties are the scaled versions of prototype material properties (Tomaževič and Velechovsky, 1992). The second approach is simple model similarity, in which prototype materials are used for the construction of the reduced-scale models (Tomaževič and Velechovsky, 1992). Because of the difficulty associated with scaling the material properties, most experimental studies use a simple model approach (Hamedzadeh, 2013). Tomaževič and Velechovsky (1992) pointed out that when prototype materials are used compensations are usually needed to meet the requirements of similar mass distribution and similar working stress level (the ratio between the axial stress and the compressive strength of the masonry). The scale factors for model similarity in both the cases of complete and simple models are given in Table 4.2.

Table 4.2 - Scaling factors for complete and simple reduced-scale models (Tomaževič and Velechovsky, 1992)

Quantity	General equation	Complete model	Simple model
Length (L)	$S_L = L_P/L_M$	S_L	S_L
Strain (ε)	$S_\varepsilon = \varepsilon_P/\varepsilon_M$	1	1
Strength (f)	$S_f = f_P/f_M$	S_L	1
Stress (σ)	$S_\sigma = f_P/f_M$	S_L	1
Young's modulus (E)	$S_E = S_\sigma/S_\varepsilon$	S_L	1
Sp. weight (Γ)	$S_\Gamma = \Gamma_P/\Gamma_M$	1	1
Force (F)	$S_F = S_L^2 S_f$	S_L^3	S_L^2
Time (t)	$S_t = S_L\sqrt{S_\Gamma S_\varepsilon/S_f}$	$\sqrt{S_L}$	S_L
Frequency (Ω)	$S_\Omega = 1/S_t$	$1/\sqrt{S_L}$	$1/S_L$
Displacement (d)	$S_d = S_L S_\varepsilon$	S_L	S_L
Velocity (v)	$S_v = S_\varepsilon\sqrt{S_f/S_\Gamma}$	$\sqrt{S_L}$	1
Acceleration (a)	$S_a = S_f/S_L S_\Gamma$	1	$1/S_L$

One of the problems with reduced-scale models is the commonly observed size effect: specimens of smaller size generally exhibit higher strength and a greater scatter of data compared with their prototype counterparts (Maleki, 2008). Although size effects are not fully understood, it is

important to take them into consideration, otherwise unconservative estimates of prototype behaviour may be made (Long, 2006). Additionally, reducing the physical dimensions of the model changes the effects of many parameters, such as bond between reinforcement and mortar or grout and adhesion between mortar and masonry units, on the overall behaviour of the structure (Tomaževič and Velechovsky, 1992; Long, 2006). This limits the reduction of size of masonry models; Tomaževič and Velechovsky (1992) suggested limiting the scale to one-fifth in order to achieve reliable models built using prototype materials. In general, reduced-scale models exhibit fewer cracks than do prototype structures, in part because the tensile strength of concrete as a percentage of the compressive strength is higher in model concrete (Long, 2006).

On the other hand, Janaraj and Dhanasekar (2016) pointed out that reduced-scale masonry walls can accommodate a greater number of bed joints than full-scale specimens, and failure modes are better represented in specimens with more bed joints. Thus, reduced-scale specimens may provide better representations of real-world masonry wall failure modes. Reduced-scale testing also allows for post-peak behaviour of the walls to be captured, which is not possible to the same degree with full-scale walls due to stability concerns (Long, 2006).

4.2.8.1 Case Study: Long (2006)

Although no studies comparing the shear behaviour of reduced-scale PG walls with full-scale prototypes could be located, a study comparing the shear strength of reduced-scale FG walls with their full-scale counterparts does exist. Long (2006) tested two half-scale FG masonry walls (47.4% scale walls) that were designed to exhibit shear-dominated failure at McMaster University. She then compared the results with those from full-scale prototypes that had been tested previously at the same university (El-Dakhakhni et al., 2013).

During testing of both the reduced-scale walls and the prototype walls there were issues with incomplete filling of cells with grout, due to the use of a coarse grout. The reduced-scale walls had slightly different material properties and reinforcement ratios from the prototype walls. The blocks used in the reduced-scale walls were also geometrically simpler than the full-scale blocks. The wall properties are given in Table 4.3.

Table 4.3 - Model and prototype properties (adapted from Long, 2006)

Wall		f'_m (MPa)	Length (mm)	Height (mm)	A_v (mm^2)	ρ_v (%)	Spacing (mm)	ρ_h (%)	σ (MPa)
1	Model	18.3	950	950	71	0.83	380	0.08	1
	Prototype	15.4	2000	2000	300	0.79	800	0.08	1
2	Model	18.3	1430	950	100	1.17	380	0.08	0
	Prototype	15.4	3000	2000	500	1.32	800	0.08	0

Despite the differences between the model and prototype walls, both model walls showed good agreement with the prototype walls in terms of shear strength. Based on the length scale factor of 0.474, the scale factor for a point load is $S_F = S_L^2 = 0.474^2 = 0.225$ (Long, 2006). This scale factor was used to scale up the shear strength of the model walls and compare them to the prototype walls, as shown in Table 4.4.

Table 4.4 - Shear strength of model and prototype walls (adapted from Long, 2006)

Wall	Shear Strength (kN)			Percentage Error (%)
	Model (unscaled)	Model (scaled)	Prototype	
1	114.7	509.8	408.4	+ 24.8
2	204.0	906.7	828.9	+ 9.4

Long (2006) also tested two reduced-scale walls designed to fail in flexure and compared them with equivalent full-scale walls that had previously been tested by Shedid (2006). Long (2006) observed that there was better similarity between reduced-scale model and prototype walls designed to fail in flexure than there was between the model and prototype walls that were designed to fail in shear. This was attributed to size effects related to cracking that were more significant in the walls failing in shear due to diagonal cracking.

4.2.8.2 Treatment of Scaling

From the limited amount of literature that is currently available on the topic, it is clear that further research is needed to investigate the reliability of reduced-scale PG masonry walls to predict the in-plane shear strength of their full-scale counterparts. It is recommended that a correction factor similar to the ones proposed by Dillon (2015), as discussed in 4.2.1, 4.2.2, 4.2.3, 4.2.6 and 4.2.7,

should be developed through statistical analysis to account for size effects. However, the findings of Long (2006) suggest that reduced-scale masonry walls can be used to predict the shear strength of prototype walls with reasonable accuracy. In addition, the number of scaled walls in the datasets used for analysis in the present study is low compared to the number of full-scale walls in these datasets (19-20% reduced-scale walls).

None of the studies using scaled specimens from which data has been collected attempted to achieve complete models, therefore the simple model scaling factors in Table 4.2 are used to scale wall properties in the analysis datasets. Geometric properties, such as wall height, length, and thickness, are scaled by a factor of S_L. Areas and forces, such as reinforcement areas, axial load, and shear load, are scaled by a factor of S_L^2. Material strengths, such as yield strength of reinforcement and compressive strength of blocks, mortar, and grout, are scaled by a factor of 1. Unitless variables, such as reinforcement ratios, and measures of stress, such as axial stress and shear stress, are scaled by a factor of 1.

4.2.9 Varying Axial Load

Although most researchers used constant axial load in their testing, a few used variable axial loading schemes (Scrivener, 1967; Hoque, 2013; Hamedzadeh, 2013; Rizaee, 2015). This was done primarily to maintain zero moment at the centre (or another location) of the wall. In the latter three studies, this was done to achieve double curvature (fixed-fixed) boundary conditions.

For these studies, the ultimate axial load (occurring concurrently with the ultimate shear strength) was estimated and used in the compiled database. Details of how the ultimate axial load was calculated for these studies can be found in Appendix A.

4.3 Data Scrutinization

Following data synthesization, scrutinization was performed. Data scrutinization is defined as using a set of selection criteria to determine which specimens should be included in analysis and which ones should be excluded (Hung, 2018). The variation present in the database that could not

be mitigated through synthesization was removed through scrutinization. Where missing variables were needed in analysis and could not be synthesized, these specimens were also removed.

4.3.1 Failure Mode

The experimental studies from which data was retrieved were primarily focused on the shear behaviour of masonry walls, however some of the tested walls failed in flexure. In most cases, walls failing in flexure were not included in the initial database of 292 walls. However, one of the walls tested by Scrivener (1967), which was included in the initial database, was reported to have failed in a predominantly flexural mode. This wall was removed from the final datasets.

One of the walls tested by Meli et al. (1969) that was included in the initial dataset was reported to have experienced a local failure. Additionally, one of the walls tested by Rizaee (2015) failed like an unreinforced masonry wall due to technical problems that arose during testing. Consequently, both walls were removed from the final datasets.

4.3.2 Wall Type

The present study focuses on the shear strength of single pier, PG walls. Of the 292 walls in the initial database, 17 were unreinforced (Scrivener, 1967; Chen et al., 1978; Oan, 2013). Because URM walls are out of the scope of this study, these walls were excluded from the final datasets. There were also 2 double pier walls tested by Mayes et al. (1976). Because double pier specimens are out of the scope of this study, these two walls were also removed.

4.3.3 Block Type

Two of the studies (Matsumura, 1987; Haach et al., 2007) used 3-cell blocks instead of the 2-cell blocks that are common in North American masonry. Although efforts were made to synthesize the data from these studies with the rest of the data, it was decided to exclude both studies from the final datasets. The blocks used by Haach et al. (2007) posed a particular challenge for synthesization, as the middle cells were smaller than the outer cells (Figure 3.17), making it impractical to use transformations involving the ratio of grouted to ungrouted cells. The same

transformations would have been relatively straightforward for the Matsumura (1987) specimens, however this study failed to report some of the variables under investigation in the present study.

4.3.4 Completeness of Reported Data

The data acquisition system used by Hamedzadeh (2013) malfunctioned during the testing of one wall, leading to faulty results of axial loads. Because there was no way to determine the correct value of axial load for this wall, it was removed from the final datasets.

Six of the studies (Meli et al., 1969; Thurston & Hutchison, 1982; Matsumura, 1987; Yancey & Scribner, 1989; Tomaževič et al., 1996; Voon & Ingham, 2006) did not report enough information for values of both f'_{mg} and f'_{mu} to be determined. As a result, the 60 walls from these studies were excluded from Datasets VA and VC (see Section 4.5 for more information on the data included in each of these datasets).

Several studies (Ghanem et al., 1992; Ghanem et al., 1993; Schultz, 1996; Elmapruk, 2010; Baenziger and Porter, 2011; Nolph and ElGawady, 2012) failed to report enough information for one or more of f_{block}, f_{mortar} and v to be determined. The 29 walls from these studies were excluded from Dataset VA.

4.4 Dataset Assembly

According to Dillon (2015), the first step of building and testing potential regression models is to determine which parameters to use in constructing the models. This step is not as important in common statistical analyses because they frequently use the experimental parameters directly in the model building process. However, empirical modeling in engineering is different because the parameters that influence the predicted value are often combinations of multiple variables (Dillon, 2015). Additionally, consistency is needed among all the parameters in the equation in order to relate them to some physical mechanism (Dillon, 2015).

The following section will explain the definitions used in the present study for variables that are often given distinct definitions by different researchers. Then the complete lists of variables used in analysis will be presented and explained.

4.4.1 Variable Definitions

4.4.1.1 Height of Masonry & Lateral Loading

Although many researchers applied lateral load to a capping beam made of concrete or steel, others applied lateral loading directly to one or two courses of the masonry wall. In such cases, the height of the wall was defined in this study as the height of the masonry panel, not including the laterally loaded course and any courses above it.

For purposes of calculating effective height accounting for boundary conditions, such as to calculate the shear span depth ratio as required in the CSA equation, the height from the base of the wall to the point of lateral load application was used. In the case of a concrete or steel capping beam, the height of the lateral load would be taken as half of the height of the capping beam added to the height of the wall. In cases where the lateral load was applied to one or two courses of masonry, the height of the lateral load was taken to the middle of the loaded course or courses. The effective height was then obtained as shown in Equation (4.5).

$$H_{eff} = \begin{cases} H_V & \text{for single curvature} \\ \frac{1}{2} H_V & \text{for double curvature} \end{cases} \tag{4.5}$$

where H_{eff} = effective height of the wall (mm)

H_V = height of the point of lateral load (mm)

For the reasoning behind this equation, refer to Section 2.2.2.3.

4.4.1.2 Modified Bond Beam Reinforcement

Many of the tested walls in the database included a bond beam in the top course, the bottom course or both. However, there is uncertainty regarding whether reinforcement located at the top or bottom

of the wall is effective in resisting shear. Dillon (2015) stated that the horizontal bars in the top and bottom quarters of the wall do not contribute to resisting the lateral load because of insufficient anchorage. This is reflected in the shear strength models developed by Blondet et al. (1989) and Shing et al. (1990), who hypothesized that only the reinforcement in the middle half of the wall contributes to shear strength.

To evaluate this theory, three versions of the total bond beam reinforcement term are included in the analysis: one with no modification, one that is modified to neglect bond beam reinforcement in the top course, and one that is modified to neglect bond beam reinforcement in the bottom course. The number of walls in the database with bottom course bond beam reinforcement was not large enough to justify applying the two modifications simultaneously.

4.4.1.3 Vertical Reinforcement

As discussed in Section 2.2.2.5, many existing code- and research-based shear strength expressions do not include any contribution from the vertical reinforcement, however several researchers have found that vertical reinforcement contributes to shear strength (Scrivener, 1967; Shing et al., 1990; Ghanem et al., 1992; Hassanli et al., 2014; Dillon, 2015; Ba Rahim et al., 2019). Some have suggested that only the interior vertical reinforcement is effective in increasing shear capacity (Ghanem et al., 1992; Dillon, 2015).

In order to study the influence of both the flexural (jamb) and interior vertical reinforcement, these two types of reinforcement were treated separately in the current study. In most of the experimental studies, flexural reinforcement was only included in the outermost cells of the tested walls, however a few walls had flexural reinforcement in two outer cells (Meli et al., 1968; Meli and Salgado, 1969, Baenziger and Porter, 2011). In this study, any vertical reinforcement located within 15% of the wall length away from the wall edge is considered as flexural reinforcement. In these cases, the spacing between the flexural bars is neglected when calculating the average spacing of vertical reinforcement.

4.4.1.4 Yield Strength

Because the yield strength of steel reinforcement often differed between the four types of reinforcement used (interior vertical, flexural, bond beam and joint reinforcement), four different yield strength variables were used for each specimen (f_{yvi}, f_{yvf}, f_{yhbb} and f_{yhj}, respectively). Only one of the experimental studies reported varying yield strengths within the same category of steel (Scrivener, 1967). In this case, there were two different yield strengths reported for the flexural steel category of the same wall, so a weighted average was used as f_{yvf}. This was done by multiplying the reinforcement ratio of each bar by the corresponding yield strength and then dividing this value by the total reinforcement ratio.

4.4.1.5 Reinforcement Ratios and Spacings

The literature presents different methods of calculating the reinforcement ratio. The two main methods are done either based on total reinforcement area and gross wall area or based on a single bar and the spacing of reinforcement. However, equal spacing of bond beam reinforcement is not always possible because it must be spaced at intervals that area multiple of the masonry unit height (Dillon, 2015). Vertical reinforcement is not always spaced evenly either. Thus, either average or maximum spacing values could feasibly be used in the calculation of reinforcement ratios. Average spacings provide a good representation of the total reinforcement present, while maximum spacings offer a "weakest link" approach, where the least reinforced portion of the wall is thought to govern the behaviour.

In the present study, both approaches to considering reinforcement were utilized in the analysis by including total reinforcement terms as well as single-bar terms for each of the vertical interior, bond beam and joint reinforcements. No differentiation was made between joint and bond beam reinforcement spacings, because Dataset VA did not include any specimens containing both types of horizontal reinforcement and Dataset VC only included 5 such specimens. For the single-bar terms, both the average spacings and maximum spacings were used prior to implementation of the stepwise variable selection procedure. In the case of joint reinforcement there was no difference between the average and maximum spacings for any of the specimens, so only the average

horizontal spacing was used. Spacings were calculated neglecting the space between the outermost bars and the edge of the wall when these were in the top/bottom course or outermost vertical cells. For further details on the terms included in analysis, see Sections 4.4.2 and 4.4.3.

When reinforcement ratios are used in the present study without decomposing them in terms of steel areas and wall geometries or reinforcement spacing, the values are overall reinforcement ratios. In other words, they represent total reinforcement areas divided by the gross horizontal or vertical area of the wall.

4.4.1.6 Net Area of Masonry Wall, A_{net}

Researchers use various methods to calculate the net area of their walls and few of them explain how they perform this calculation. To ensure consistency, it was decided to calculate the net area of all walls in the database using the same method (Equation (4.6)).

$$A_{net} = n_g * \frac{L_b}{2} t + \left(L - n_g * \frac{L_b}{2}\right)(2t_{fs}) \tag{4.6}$$

where A_{net} = net area of masonry wall (mm^2)

n_g = number of grouted cells in wall

L_b = actual length of concrete block (mm)

t = wall thickness (mm)

L = wall length (mm)

t_{fs} = face shell thickness (mm)

This method of calculating A_{net} is derived assuming that mortar bedding was placed only on the face shells and webs adjacent to grouted cells. This is the type of bedding that is used by most researchers.

Where the researchers provided values of A_{net}, these were compared with the values calculated using Equation (4.6) to ensure agreement between the provided and estimated values. All the calculated values of A_{net} were found to be within 15% of the values provided by the researchers.

Two of the studies (Matsumura, 1987; Haach et al., 2007) used 3-cell masonry blocks, meaning that A_{net} could not be calculated using Equation (4.6). For these walls, A_{net} was calculated as explained in Appendix A.

4.4.1.7 Effective Prism Strength

Because prisms can be either grouted or ungrouted, for PG walls it is useful to convert the compressive strength of both prism types to a weighted value based on the portion of grouted and ungrouted area in the wall. This weighted average of f'_{mg} and f'_{mu} is termed effective prism strength, or $f'_{m,eff}$, and can be calculated using Equation (4.7).

$$f'_{m,eff} = \frac{n_g \frac{L_b}{2} f'_{mg} + \left(L - n_g \frac{L_b}{2}\right) f'_{mu}}{L} \tag{4.7}$$

where n_g = number of grouted cells in wall

L_b = actual length (as opposed to nominal length) of concrete block (mm)

f'_{mg} = grouted prism compressive strength (MPa), based on a prism h/t ratio of 5

f'_{mu} = ungrouted prism compressive strength (MPa), based on a prism h/t ratio of 5

L = total length of masonry wall (mm)

4.4.2 Raw Variables

Prior to commencing the data analysis, it was necessary to identify the raw variables in the database. A raw variable can be measured directly, without any mathematical operations or transformations being applied. The purpose of this step is to identify a basic set of inputs that may influence the shear strength of PG masonry walls.

Based on the available data, a total of 34 raw variables were selected (Table 4.5).

Table 4.5 - Raw variables

Variable	Units	Definition
H	mm	Wall height
H_{eff}	mm	Effective wall height, dependent on support conditions
L	mm	Wall length, in direction of applied shear force
t	mm	Wall thickness
H_b	mm	Actual height of CMU blocks
L_b	mm	Actual length of CMU blocks
t_{fs}	mm	Face shell thickness of CMU blocks
n_g	-	Number of grouted cells
n_t	-	Total number of grouted and ungrouted cells
d	mm	Distance from extreme compression fibre to the centroid of tension reinforcement, taken as L minus ¼ of the nominal block length
f_{block}	MPa	Compressive strength of CMU blocks
f_{mortar}	MPa	Compressive strength of mortar
f_{grout}	MPa	Compressive strength of grout
f'_{mg}	MPa	Compressive strength of grouted masonry prism* with $h/t = 5$
f'_{mu}	MPa	Compressive strength of ungrouted masonry prism* with $h/t = 5$
A_{vi}	mm^2	Total area of interior vertical reinforcement
A_{vf}	mm^2	Total area of flexural (outer vertical) reinforcement
$A_{vi,bar}$	mm^2	Area of one interior vertical reinforcement bar
$A_{vf,bar}$	mm^2	Area of flexural (outer vertical) reinforcement in one jamb
f_{yvi}	MPa	Yield strength of interior vertical reinforcement
f_{yvf}	MPa	Yield strength of flexural (outer vertical) reinforcement
$s_{v,max}$	mm	Maximum spacing of interior vertical reinforcement

Variable	Units	Definition
$s_{v,ave}$	mm	Average spacing of interior vertical reinforcement
A_{hbb}	mm^2	Total area of bond beam reinforcement
$A_{hbb,m}$	mm^2	Modified† total area of bond beam reinforcement
$A_{hbb,m2}$	mm^2	Modified‡ total area of bond beam reinforcement
A_{hj}	mm^2	Total area of joint reinforcement
$A_{hbb,bar}$	mm^2	Area of one bond beam reinforcement bar
$A_{hj,bar}$	mm^2	Area of one joint reinforcement ladder
f_{yhbb}	MPa	Yield strength of bond beam reinforcement
f_{yhj}	MPa	Yield strength of joint reinforcement
$s_{h,max}$	mm	Maximum spacing of horizontal reinforcement
$s_{h,ave}$	mm	Average spacing of horizontal reinforcement
P	kN	Axial compressive load

*corrected as outlined in Section 4.2.6
†modified to neglect the area of bond beam steel located in the bottom course of the walls (4.4.1.2)
‡modified to neglect the area of bond beam steel located in the top course of the walls (4.4.1.2)

The raw variables defined in Table 4.5 are referred to as Group R in analysis.

It should be noted that the variables shown in Table 4.5 do not represent an exhaustive list of all the raw variables that could possibly be used to describe the behaviour of PG masonry shear walls. These are simply the variables that are relatively easy to measure and are generally reported by researchers. Other unaccounted for variables may also influence the shear strength of PG masonry walls, such as humidity and temperature. Although it is not possible to account for all the variables that may influence shear strength, the widest range of raw variables available has been selected.

4.4.3 Transformed Variables

A transformation is any mathematical operation that is applied to a raw variable, such as squaring or multiplying with another raw variable. A simple multiple linear regression may not be able to adequately capture the behaviour of PG masonry walls without any transformations applied to the

variables. Including transformations in a dataset allows for non-linearities to be considered in the analysis and potentially included in the generated models. Transformations are also needed to achieve consistent units within a generated equation.

Two groups of transformed data were used in analysis: a group of transformations with consistent units of kN, and a group that includes all the raw and transformed variables, regardless of units. The first group is referred to as Group T, because it consists mainly of transformed variables; Group T contains 38 transformations and 1 raw variable, P. The second variable group is referred to as Group RT, because it includes both raw variables and transformed variables.

The axial load is included in Group T because it is the only raw variable in Table 4.5 that has units of kN, and the axial load has been found by many researchers to contribute to shear strength (Meli and Salgado, 1969; Matsumura, 1987; Okamoto et al., 1987; Haach, 2009; Voon and Ingham, 2006; Oan, 2013). Transformations with consistent units are desirable in a shear strength model because they relate the contribution of individual raw variables to a mechanical process (Dillon, 2015). Many of the raw variables, such as the yield strengths of the various types of reinforcement, have little meaning unless they are combined with other variables, such as the corresponding area of steel. Using consistent units also makes it easier to compare the relative contribution of equation terms, increasing equation interpretability.

It should be noted that the transformed variables in Group T that involve a square root technically do not have units of kN. It is common in existing code- and research-based shear strength equations for a term including the square root of masonry compressive strength to appear, leading to this inconsistency in units. This inconsistency exists because it has been observed that the shear strength of masonry walls increases approximately in proportion to the square root of the masonry compressive strength (Matsumura, 1987). The inclusion of equivalent transformed variables that use either the masonry compressive strength (or, similarly, the compressive strength of mortar) or the square root of this variable allows both possible transformations to be considered as candidates. The more significant term can then be chosen through stepwise variable selection.

The parameters included in Group T are shown in Table 4.6.

Table 4.6 - Transformations belonging to Group T

Block strength	$f_{block}(L_b t)v * n_b$, $f_{block}(L_b t)v$
Mortar strength	$f_{mortar}t_{fs}L$, $f_{mortar}t_{fs}L_b$, $f_{mortar}t_{fs}H_b$
Mortar tensile strength	$\sqrt{f_{mortar}}t_{fs}L$, $\sqrt{\frac{f_{mortar}}{f_{block}}}f'_{m,eff}A_{net}$
Grout strength	$f_{grout}A_{cell} * n_g$, $f_{grout}A_{cell}$
Ungrouted prism strength	$f'_{mu}(t_{fs}L)\left(1-\frac{n_g}{n_t}\right)$, $f'_{mu}(t_{fs}*1m)\left(1-\frac{n_g}{n_t}\right)$
Grouted prism strength	$f'_{mg}A_{gross}\left(\frac{n_g}{n_t}\right)$, $f'_{mg}(1m*t)\left(\frac{n_g}{n_t}\right)$
Effective prism strength	$f'_{m,eff}A_{gross}$, $f'_{m,eff}A_{net}$
Flexural reinforcement	$A_{vf}f_{yvf}$
	$A_{vf}f_{yvf}$ & $\rho_{vf} \leq 0.02\%$, $A_{vf}f_{yvf} + A_{vi}f_{yvi}$ & $\rho_{vf} + \rho_{vi} \leq 0.02\%$
Interior vertical reinforcement	$A_{vi}f_{yvi}$, $\frac{A_{vi,bar}f_{yvi}L}{s_{v,ave}}$, $\frac{A_{vi,bar}f_{yvi}L}{s_{v,max}}$, $\frac{A_{vi,bar}f_{yvi}H}{s_{v,max}}$
Joint reinforcement	$A_{hj}f_{yhj}$, $\frac{A_{hj,bar}f_{yhj}L}{s_{h,ave}}$
Bond beam reinforcement	$A_{hbb}f_{yhbb}$, $A_{hbb,m}f_{yhbb}$, $A_{hbb,m2}f_{yhbb}$
	$\frac{A_{hbb,bar}f_{yhbb}L}{s_{h,ave}}$, $\frac{A_{hbb,bar}f_{yhbb}L}{s_{h,max}}$
Axial load	P , $P * \frac{A_{net}}{A_{gross}}$
Shear span depth ratio	$\frac{M}{VL}A_{gross}f'_{m,eff}$, $\frac{M}{VL}A_{net}f'_{m,eff}$, $\frac{M}{VL}A_{gross}\sqrt{f'_{m,eff}}$, $\frac{M}{VL}A_{net}\sqrt{f'_{m,eff}}$
Inverse of shear span depth ratio	$\frac{VL}{M}A_{gross}f'_{m,eff}$, $\frac{VL}{M}A_{net}f'_{m,eff}$, $\frac{VL}{M}A_{gross}\sqrt{f'_{m,eff}}$, $\frac{VL}{M}A_{net}\sqrt{f'_{m,eff}}$

The transformed variables that appear in Table 4.6 are defined as follows.

A_{cell} = estimated area of a single cell of a block (mm^2)

= $L_b t \frac{1-v}{2}$

A_{gross} = gross wall area (mm^2)

= Lt

A_{net} = net wall area (mm^2), which is calculated according to Equation (4.6)

$f'_{m,eff}$ = effective prism strength (MPa), which is calculated according to Equation (4.7)

ρ_{vf} = flexural reinforcement ratio

= $\frac{A_{vf}}{Lt}$

ρ_{vi} = interior vertical reinforcement ratio

= $\frac{A_{vi}}{Lt}$

$\frac{M}{VL}$ = The shear span depth ratio

= $\frac{H_{eff}}{L}$

n_b = The number of blocks. For 2-cell blocks:

= $\frac{n_g}{2}$

v = The ratio of net to gross area for a masonry block/prism

= $\frac{f'_{mg}}{f'_{mu}}$

The other variables that make up the parameters shown in Table 4.6 are the raw variables that were defined in Table 4.5**.**

The transformations in Table 4.6 are a combination of parameters designed to imitate terms from existing code- and research-based equations (Chapter 2) and new parameters that attempt to account for the potential influence of variables which have been excluded from previous equations, such as f_{block}, f_{mortar} and f_{grout}.

The findings of previous researchers (Section 2.2.2) have also been incorporated into the transformations included in Table 4.6. The creation of new horizontal reinforcement variables that do not account for reinforcing above the level of 0.2% was explored, to employ the observation that horizontal reinforcement ratios above this level provide a negligible increase in shear strength. However, it was found that only 1 specimen had bond beam reinforcement in excess of 0.2% and only 4 specimens had joint reinforcement in excess of 0.2% for both Dataset VA and Dataset VC. The number of specimens with flexural reinforcement and total vertical reinforcement above 0.2% was much higher, at 71 and 95 for Dataset VC and 51 and 73 for Dataset VA, respectively. For this reason, reinforcement variables transformations that do not account for flexural reinforcement and total vertical reinforcement above 0.2% were included in Group T.

Hassanli et al. (2014) noted that in PG walls mortar usually plays the role of weak layers vulnerable to cracking. They suggested that one way to account for this effect is to incorporate a compressive strength reduction factor, defined as the tensile strength of mortar divided by the tensile strength of the concrete block. Following this suggestion, two transformations were included which attempt to approximate the tensile strength of mortar by taking the square root of f_{mortar}. One of these transformations includes a division by the square root of f_{block}.

Dillon (2015) observed during the development of his proposed equation that the model provided a better fit to the experimental data when the inverse of the shear span ratio was used instead of simply using the shear span ratio directly. Based on this observation, four terms were included in Group T which used the inverse of the shear span ratio in place of the shear span ratio.

Group RT includes the raw variables shown in Table 4.5 and the transformed variables shown in Table 4.6. There are also 17 additional transformed variables that are included in Group RT, which are listed in Table 4.7.

Table 4.7 - Additional transformations included in Group RT

Grouted area	A_{net} , $\frac{A_{net}}{A_{gross}}$, A_{cell}
Shear span ratio	$\frac{M}{VL}$, $\frac{VL}{M}$
Masonry prism properties	v , $f'_{m,eff}$
Vertical reinforcement	ρ_{vi} , ρ_{vf} , $\rho_{vi} + \rho_{vf}$
Horizontal reinforcement	ρ_{hbb} , $\rho_{hbb,m}$, ρ_{hj} , $\rho_{hbb} + \rho_{hj}$
Other transformations*	σ_{net} , σ_{gross} , $\frac{n_g}{n_t}$

*These transformations were added to Group RT during model tree generation, and hence were not considered in the stepwise regression analysis. Additionally, n_g/n_t was not included in Group RT prior to splitting the data for MT generation, hence this transformation was not considered as a possible splitting candidate.

The transformed variables that appear in Table 4.7 that have not been defined previously are as follows.

ρ_{hbb} = bond beam reinforcement ratio

$= \frac{A_{hbb}}{Ht}$

$\rho_{hbb,m}$ = bond beam reinforcement ratio, modified to neglect bond beam reinforcement in the bottom course of walls

$= \frac{A_{hbb,mod}}{Ht}$

ρ_{hj} = joint reinforcement ratio

$= \frac{A_{hj}}{Ht}$

The additional transformations listed in Table 4.7 were added to the database primarily to facilitate calculations of the transformations from Group T. As such, they are not intended to provide an exhaustive list of possible transformations, nor were they selected based on presumptions

regarding the contributions to the shear strength of PG masonry walls that they may make. Rather, they were included in analysis to demonstrate which variables are deemed the most important in predicting shear strength of PG masonry walls through the stepwise variable selection procedure. Including these additional transformations also has the potential to allow for comparisons between models including different types of variables.

Group RT is a combination of the variables from Table 4.5, Table 4.6 and Table 4.7. As noted above, 3 of the additional transformations from Table 4.7 were added after the stepwise regression analysis had been completed. The variable P is included in both Table 4.5 and Table 4.6, so this variable should not be counted twice when adding up the number of variables included in Group RT. In total, this group had 86 variables for the stepwise regression analysis, 88 variables for the splitting of MTs, and 89 variables for the stepwise model analysis of MT branches.

4.5 Summary of Datasets

Two main datasets were used in analysis: Dataset VA and Dataset VC. The former includes all the variables considered in analysis, while the latter only includes conventional variables. Depending on which variable groups are included, 3 subsets of both datasets can be formed.

Data group VA-R contains all 34 of the raw variables listed in Table 4.5, including variables that are not found in any of the existing code- and research-based shear strength equations, namely f_{block}, f_{mortar} and f_{grout}. These variables may not always be readily available to a designer. Data group VA-T includes all of the transformations from Group T (Table 4.6) and Data group VA-RT includes all of the raw and transformed variables from Group RT (Table 4.5, Table 4.6 and Table 4.7). Because the VA data groups all include some form of the variables f_{block}, f_{mortar} and f_{grout}, these data groups only contain wall specimens for which all of those variables were reported (a total of 176 walls).

Data group VC-R only contains the 31 conventional raw variables that are commonly found in existing code- and research-based shear strength equations. It does not include the variables f_{block}, f_{mortar} and f_{grout}. Data groups VC-T and VC-RT exclude all of the transformations that involve

the variables f_{block}, f_{mortar}, f_{grout}, v and A_{cell}. Because they exclude those variables, the VC data groups can include more wall specimens than the VA data groups, for a total of 205 walls.

Table 4.8 summarizes the differences and similarities between the six data groups used in analysis.

Table 4.8 - Differences between PG wall data groups

	All variables included	Conventional variables only
Raw variables only	VA-R	VC-R
Transformations with consistent units*	VA-T	VC-T
Raw and transformed variables	VA-RT	VC-RT

*Includes one raw variable, P

In addition to the main datasets described here, expanded versions of both Dataset VA and Dataset VC were created over the course of analysis, which included more variables than the ones listed in this chapter. The expanded datasets are described in detail in Chapter 5.

Table 4.9 summarizes the number of specimens from each study that are included in Datasets VA and VC. The individual walls included in each dataset, and which ones were used for training and testing, are identified in Appendix B.

Table 4.9 - Summary of PG wall datasets composition

Source	Dataset		
	Complete	VA	VC
Scrivener (1967)	12	10	10
Meli et al. (1968)	10	10	10
Meli et al. (1969)	11	0	0
Mayes et al. (1967)	2	0	0
Chen et al. (1978)	4	3	3
Thurston and Hutchison (1982)	3	0	0
Matsumura (1987)	29	0	0
Tomaževič and Lutman (1988)	10	10	10
Johal and Anderson (1988)	16	16	16
Yancey and Scribner (1989)	10	0	0
Ghanem et al. (1992)	2	0	2
Ghanem et al. (1993)	2	0	2
Tomaževič et al. (1996)	6	0	0
Schultz (1996)	6	0	6
Shultz et al. (1998)	6	6	6
Voon and Ingham (2006)	2	0	0
Haach et al. (2007)	4	0	0
Maleki et al. (2009)	5	5	5
Elmapruk (2010)	6	0	6
Minaie et al. (2010)	4	4	4
Baenziger and Porter (2011)	8	0	8
Nolph and ElGawady (2012)	5	0	5
Oan (2013)	66	51	51
Hoque (2013)	18	18	18
Hamedzadeh (2013)	21	20	20
Rizaee (2015)	14	13	13
Ramírez et al. (2016)	10	10	10
Total number of specimens in dataset	292	176	205

4.6 Distribution of Variables

The distribution of specimen variables is presented here to identify the range of data studied, and to provide insights as to what gaps exist within the literature and within the datasets used for analysis.

Application of the models generated in this study to new data is contingent on the new data falling within the range of data used to develop these models. Using the models on new data that falls outside this data range would be extrapolation, resulting in greater uncertainty as to the accuracy of the model predictions. Table 4.10 gives the acceptable range into which new data should fall for the generated models to make valid predictions. This table provides minimum, maximum, average, and standard deviations of selected variables for both Dataset VA and Dataset VC. Additionally, the table provides unscaled maximum values that were calculated neglecting any specimens from the datasets that were tested as small-scale walls. This is done to give an accurate representation of the true maximum and average values obtained for properties such as height and length, without any scaling.

Table 4.10 - Minimum, maximum, average and standard deviation of wall properties of Datasets VA and VC

	Dataset VA					Dataset VC				
	Min	**Max**	**Unscaled Max**	**Average**	**Standard Deviation**	**Min**	**Max**	**Unscaled Max**	**Average**	**Standard Deviation**
H (mm)	813	5649	2650	1633	737	813	5649	2650	1689	725
H_{eff} (mm)	711	5690	2750	1445	744	711	5690	2750	1509	779
L (mm)	813	4973	3861	2082	1068	813	4973	4267	2178	1045
H/L	0.320	2.30	1.82	0.850	0.308	0.320	2.30	1.82	0.836	0.295
t (mm)	140	200	195	183	18.1	140	200	195	184	18.0
H_b (mm)	190	200	197	192	2.67	190	200	197	192	2.59
L_b (mm)	390	400	397	392	3.38	390	400	397	393	3.51
t_{fs} (mm)	25.4	41.3	41.3	34.2	3.81	25.4	41.3	41.3	34.0	3.86
n_g	0	7	7	3.37	1.20	0	8	8	3.43	1.30
n_t	4	25	19	10.3	5.37	4	25	21	10.6	5.25
A_{net} (mm^2)	103276	434898	348487	214493	77806	103276	511652	511652	222950	82948
A_{net}/A_{gross}	0.356	0.810	0.810	0.601	0.0902	0.356	0.810	0.810	0.590	0.0909
f_{block} (MPa)	6.36	35.7	35.7	19.7	6.02	6.36	35.7	35.7	19.6	5.87
f_{mortar} (MPa)	4.30	25.8	25.8	12.0	6.78	4.30	25.8	25.8	12.3	6.62
f_{grout} (MPa)	7.00	47.5	47.5	23.1	7.70	7.00	47.5	47.5	24.2	7.85
ν	0.495	0.640	0.640	0.531	0.045	0.495	0.640	0.640	0.531	0.044
f'_{mg} (MPa)	6.38	14.5	14.5	9.12	2.05	6.38	19.9	19.9	10.1	3.31
f'_{mu} (MPa)	6.44	20.8	20.4	13.9	4.75	6.44	20.8	20.4	13.9	4.49
$f'_{m,eff}$ (MPa)	6.97	19.9	19.4	12.0	3.53	6.97	19.9	19.8	12.4	3.48
P (kN)	0	1405	839	406	291	0	1405	839	364	293
σ_{gross} (MPa)	0	2.76	2.76	1.11	0.78	0	2.76	2.76	0.987	0.792
σ_{net} (MPa)	0	4.08	4.08	1.82	1.15	0	4.08	4.08	1.64	1.18
A_{vi} (mm^2)	0	879	594	177	219	0	1200	1200	208	250
$A_{vi,bar}$ (mm^2)*	71	453	284	214	115	71.0	453	387	214	111
ρ_{vi}	0	0.00170	0.00170	0.000410	0.000458	0	0.00235	0.00235	0.000456	0.000502

	Dataset VA					Dataset VC				
	Min	**Max**	**Unscaled Max**	**Average**	**Standard Deviation**	**Min**	**Max**	**Unscaled Max**	**Average**	**Standard Deviation**
A_{vf} (mm^2)	0	1257	1136	500	350	0	1548	1548	582	401
$A_{vf,bar}$ (mm^2)*	127	584	568	277	122	127	697	697	302	142
ρ_{vf}	0	0.00549	0.00549	0.00150	0.00125	0	0.00549	0.00549	0.00160	0.00122
f_{yvi} (MPa)*	245	503	480	428	76.4	245	503	480	431	69.1
f_{yvf} (MPa)*	245	565	488	433	72.7	245	565	488	433	66.5
$s_{v,max}$ (mm)*	396	3638	2642	1078	619	396	3638	2642	1122	609.9
$s_{v,ave}$ (mm)*	396	3638	2642	1049	637	396	3638	2642	1079	629.6
A_{hbb} (mm^2)	0	792	792	123	195	0	792	792	150	198
$A_{hbb,m}$ (mm^2)	0	792	792	114	182	0	792	792	128	178
$A_{hbb,m2}$ (mm^2)	0	792	792	59.4	139	0	792	792	91.3	156
$A_{hbb,bar}$ (mm^2)*	87.8	440	396	257	136	71.0	440	400	248	121
ρ_{hbb}	0	0.00227	0.00227	0.000327	0.000531	0	0.00227	0.00227	0.000401	0.000538
A_{hj} (mm^2)	0	1357	304	78.5	173	0	1357	855	82.0	185
$A_{hj,bar}$ (mm^2)*	9.82	226	43.5	35.5	37.1	9.82	226	71.3	36.4	36.3
ρ_{hj}	0	0.00446	0.00110	0.000324	0.000618	0	0.00446	0.00181	0.000309	0.000606
f_{ybb} (MPa)*	290	744	456	454	99.2	290	744	456	449	81.2
f_{yj} (MPa)*	245	610	610	494	115	245	610	610	502	115
$s_{h,max}$ (mm)*	200	3638	1321	743	695	200	3638	1321	767	663
$s_{h,ave}$ (mm)*	200	3638	1219	723	690	200	3638	1219	750	659
V_{exp} (kN)	78.0	667	383	240	108	78.0	667	431	242	104

*Zero values ignored in calculating minimum, average and standard deviation values

To further illustrate the distribution of the main specimen variables and the data gaps that are present, Figures 4.2 through 4.7 are provided.

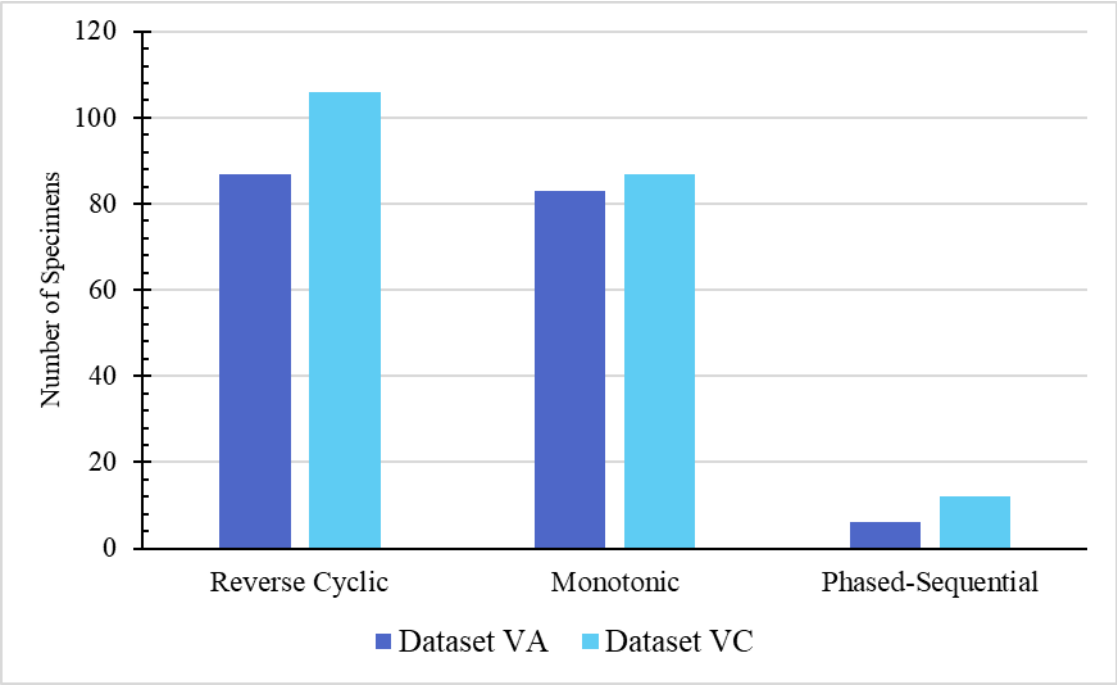

Figure 4.2 - Distribution of loading types

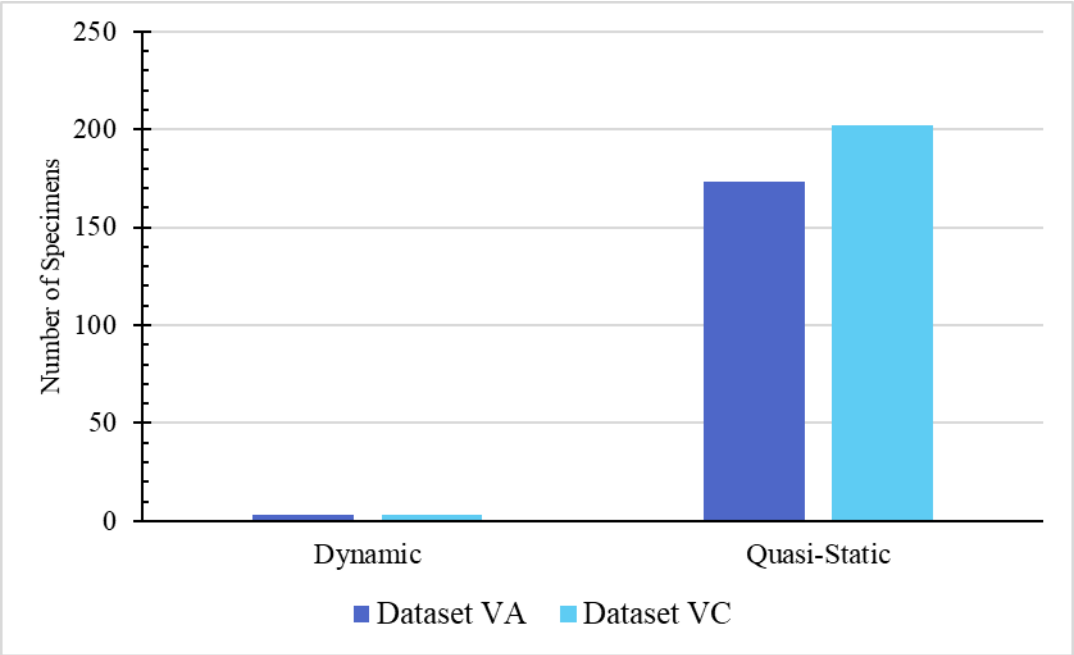

Figure 4.3 - Distribution of loading rate

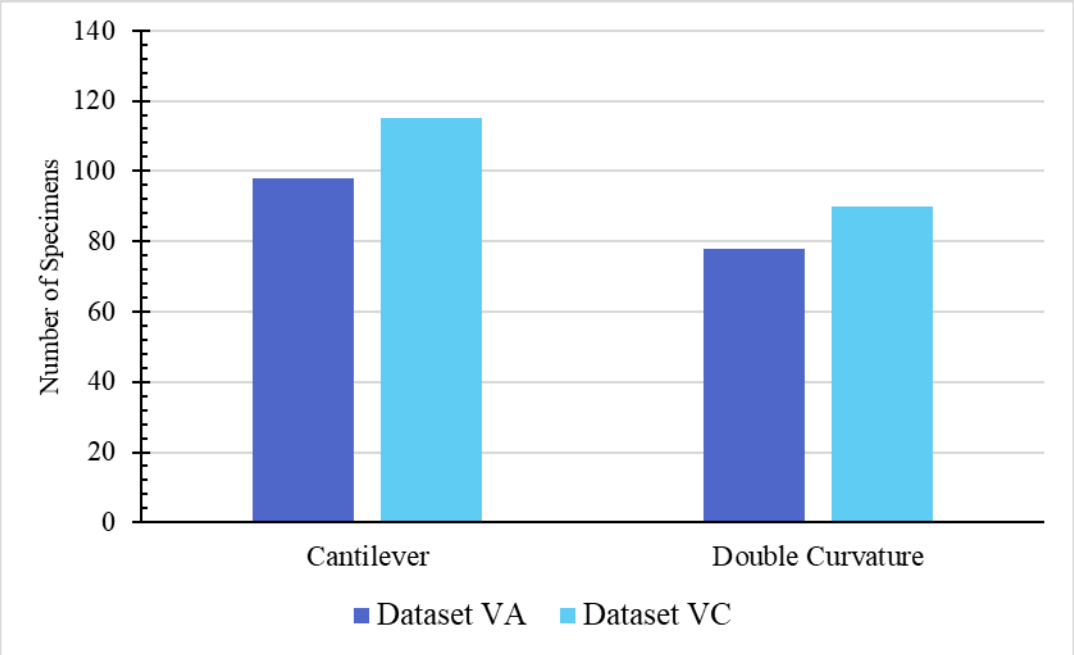

Figure 4.4 - Distribution of support type

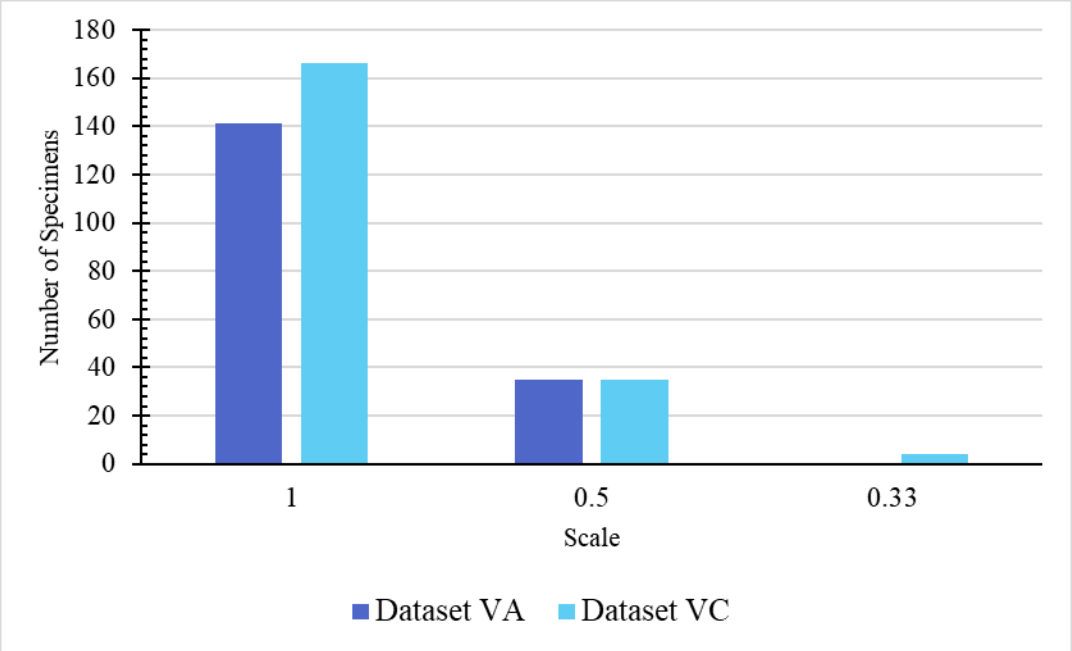

Figure 4.5 - Distribution of scale

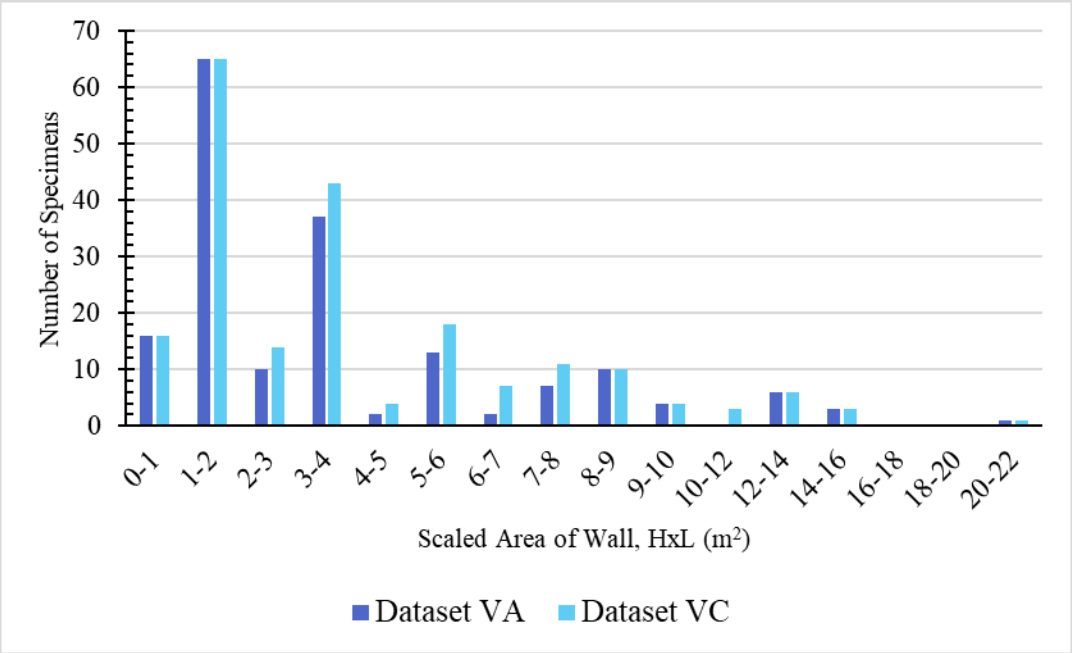

Figure 4.6 - Distribution of scaled wall area

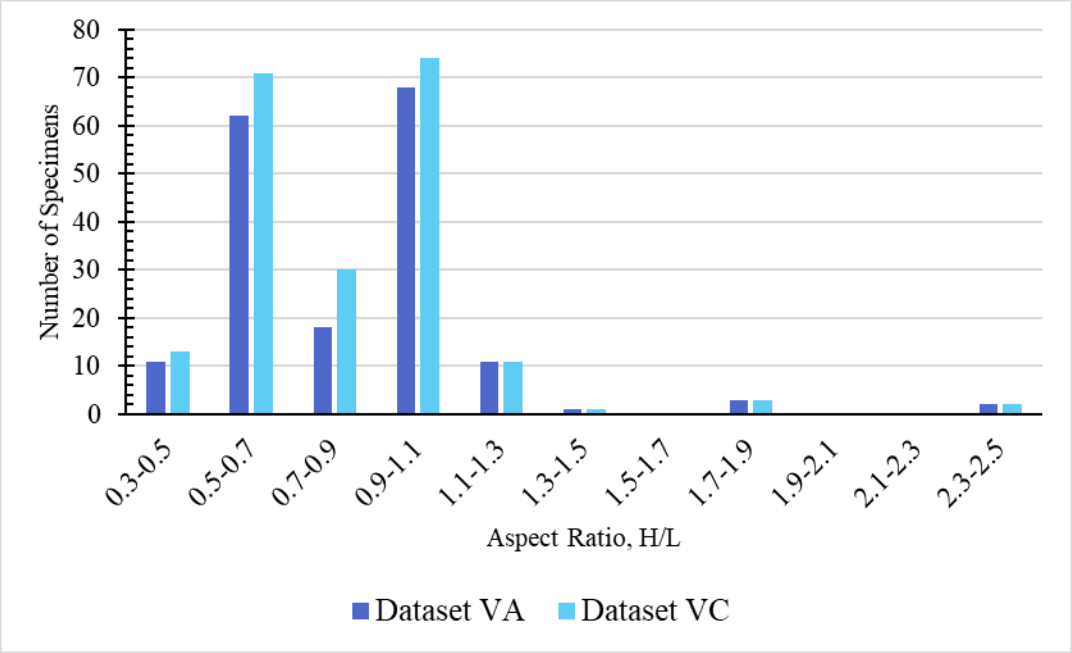

Figure 4.7 - Distribution of aspect ratio

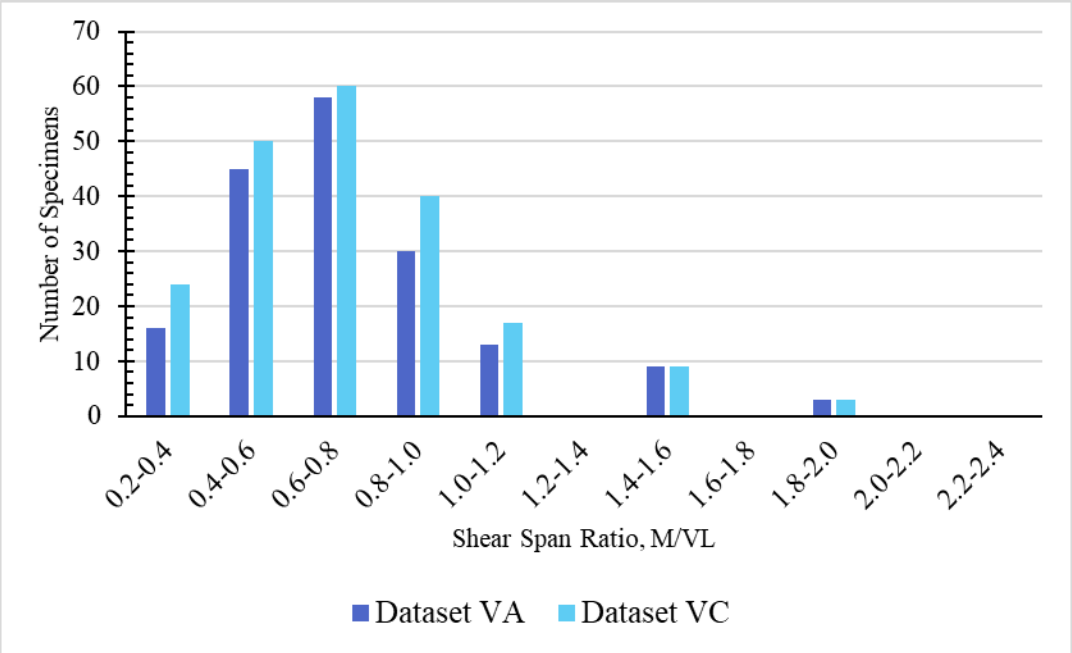

Figure 4.8 - Distribution of shear span ratio

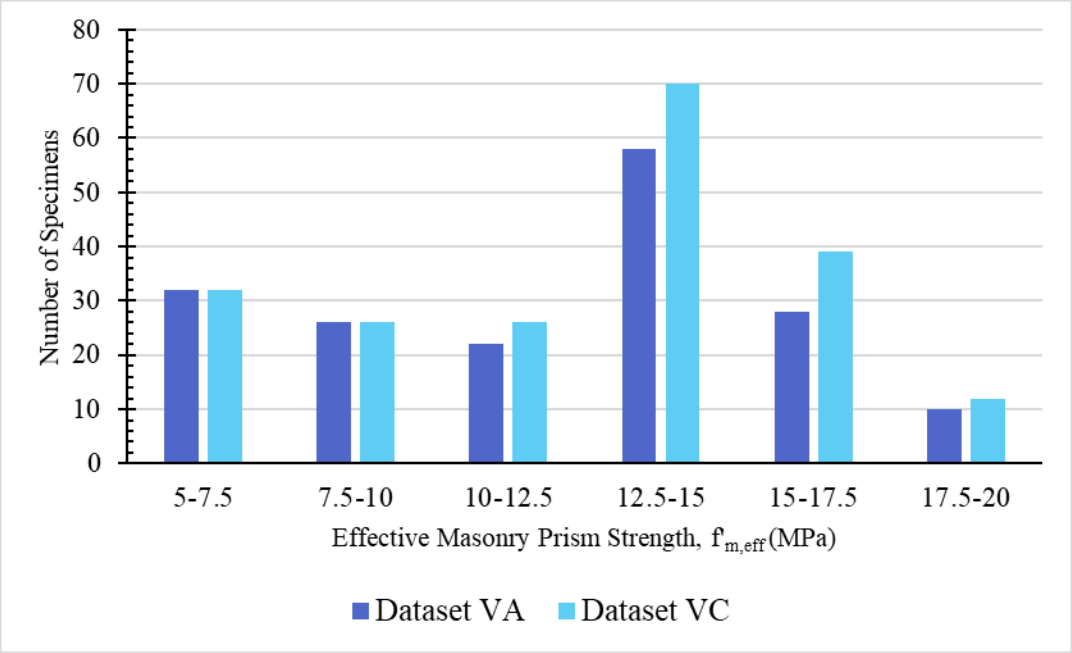

Figure 4.9 - Distribution of effective masonry prism strength

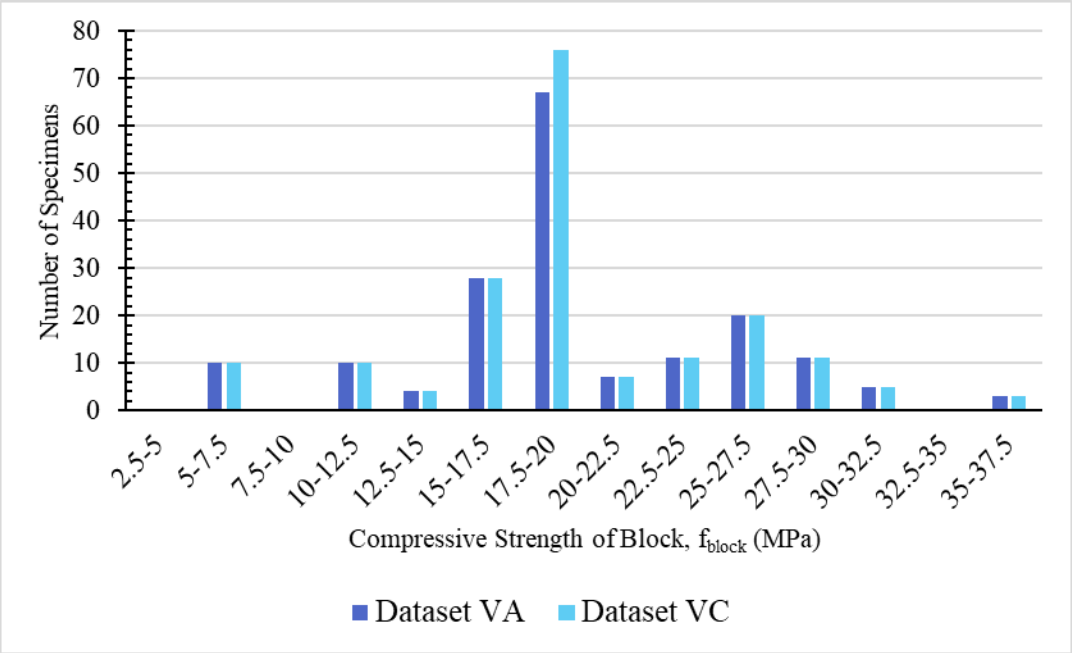

Figure 4.10 - Distribution of compressive block strength

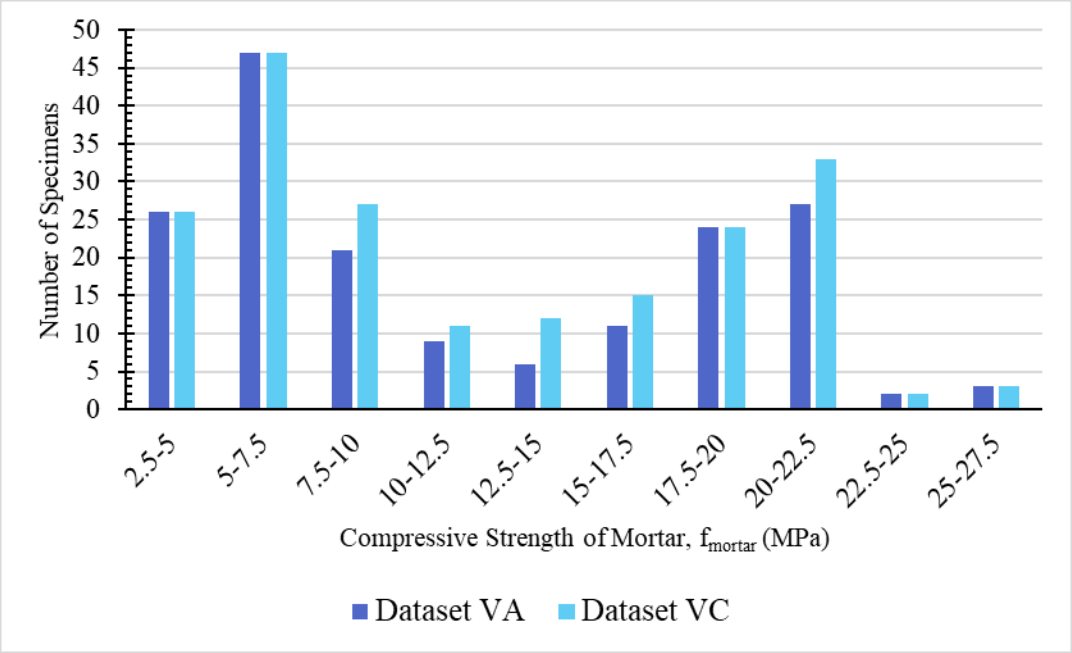

Figure 4.11 - Distribution of compressive strength of mortar

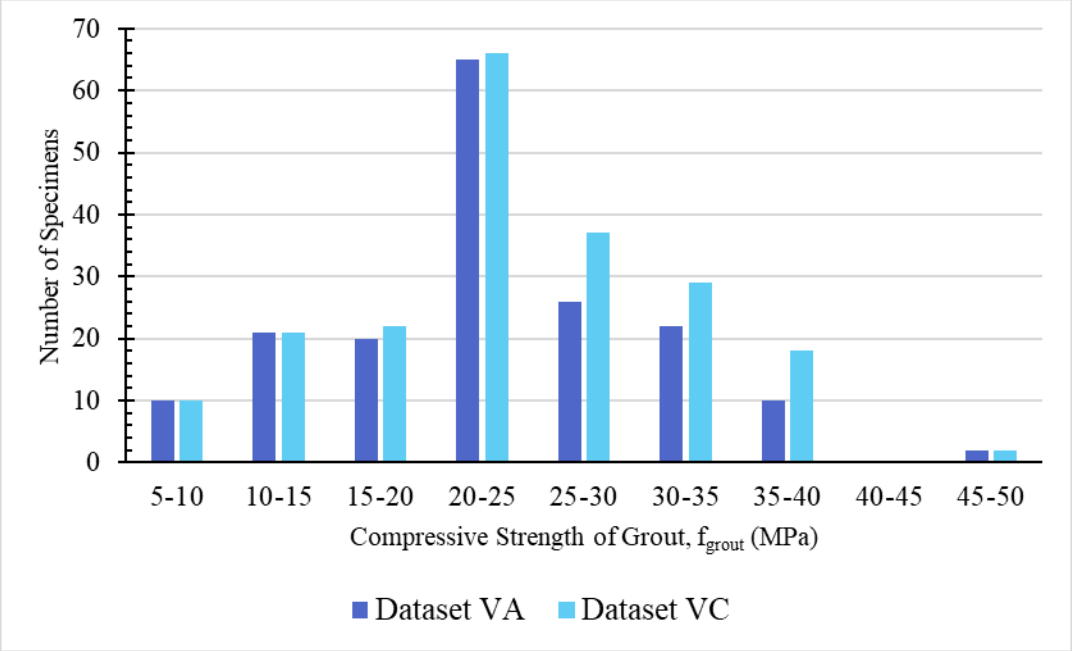

Figure 4.12 - Distribution of compressive strength of grout

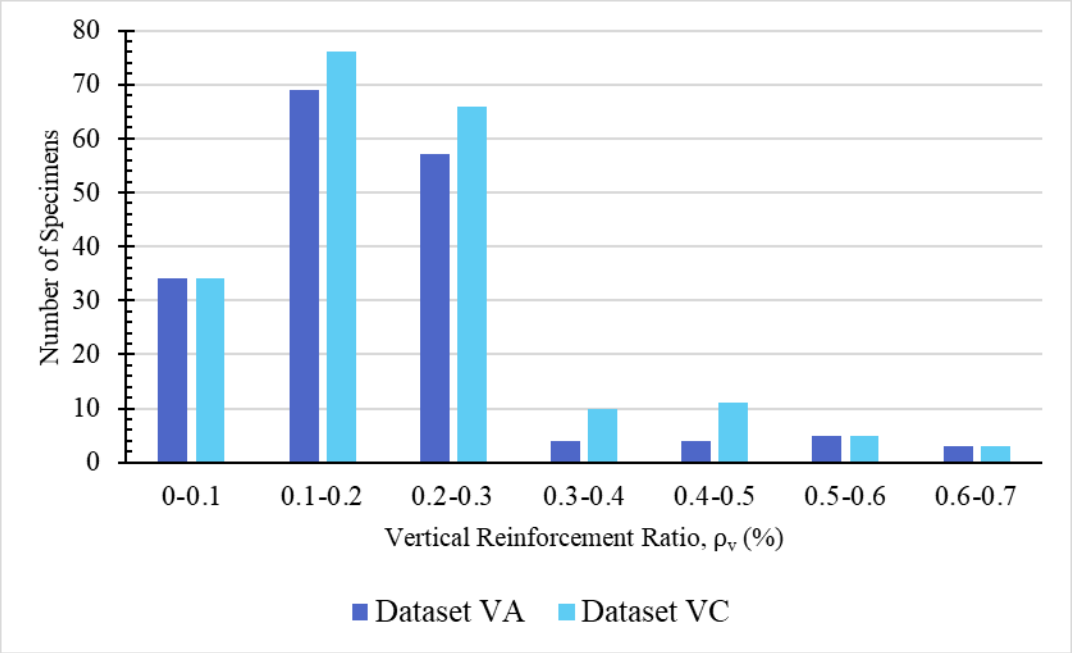

Figure 4.13 - Distribution of vertical reinforcement ratio (based on wall length)

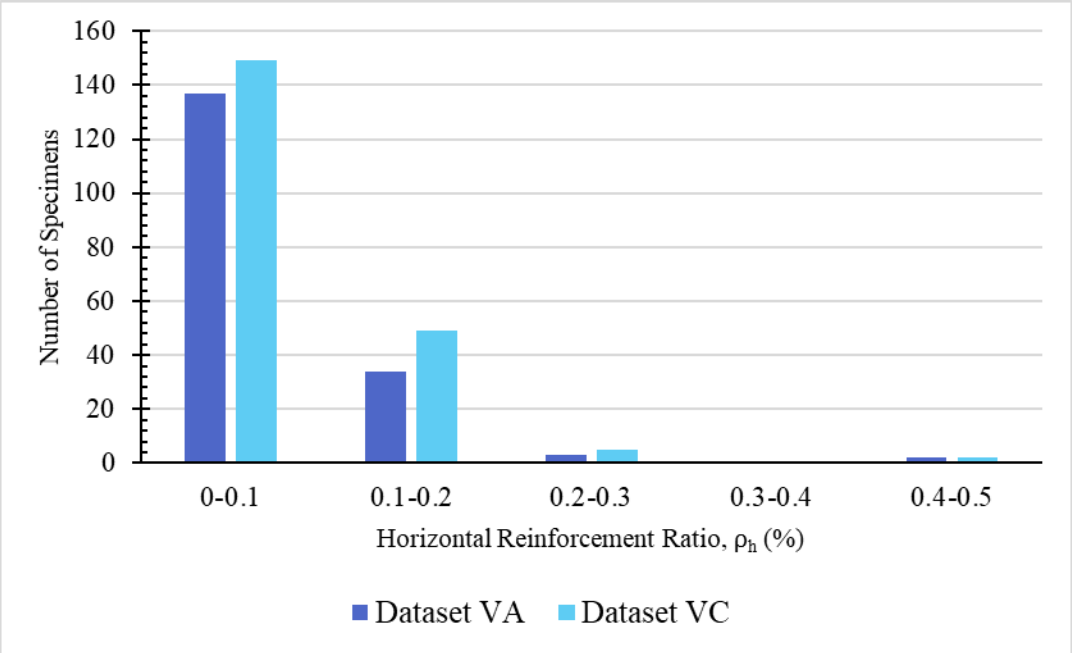

Figure 4.14 - Distribution of horizontal reinforcement ratio (based on wall height)

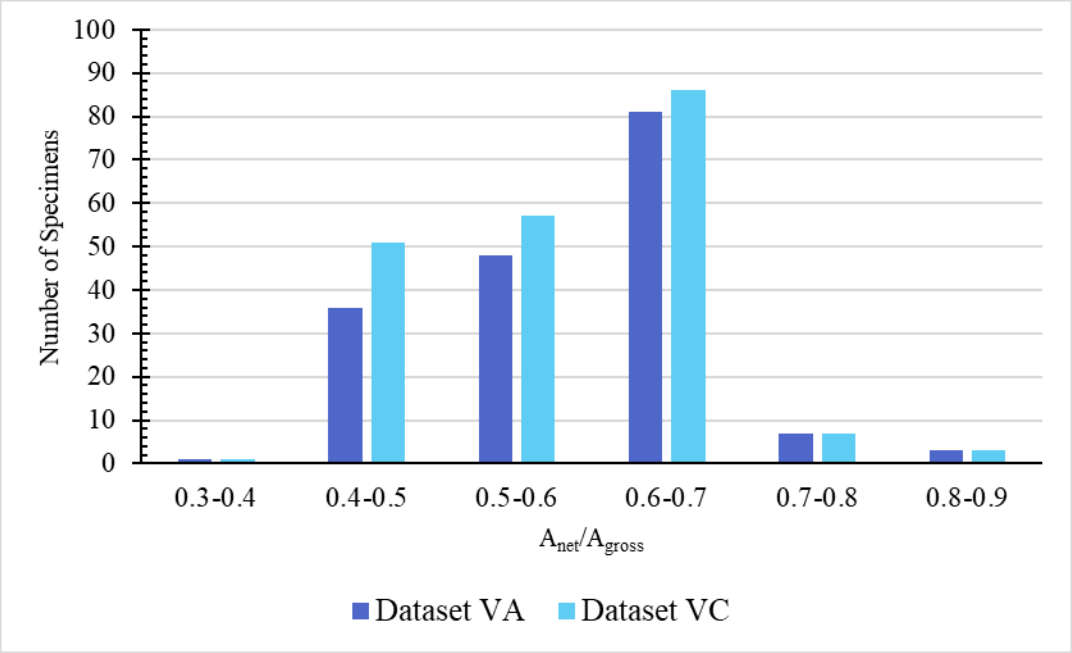

Figure 4.15 - Distribution of net to gross wall area

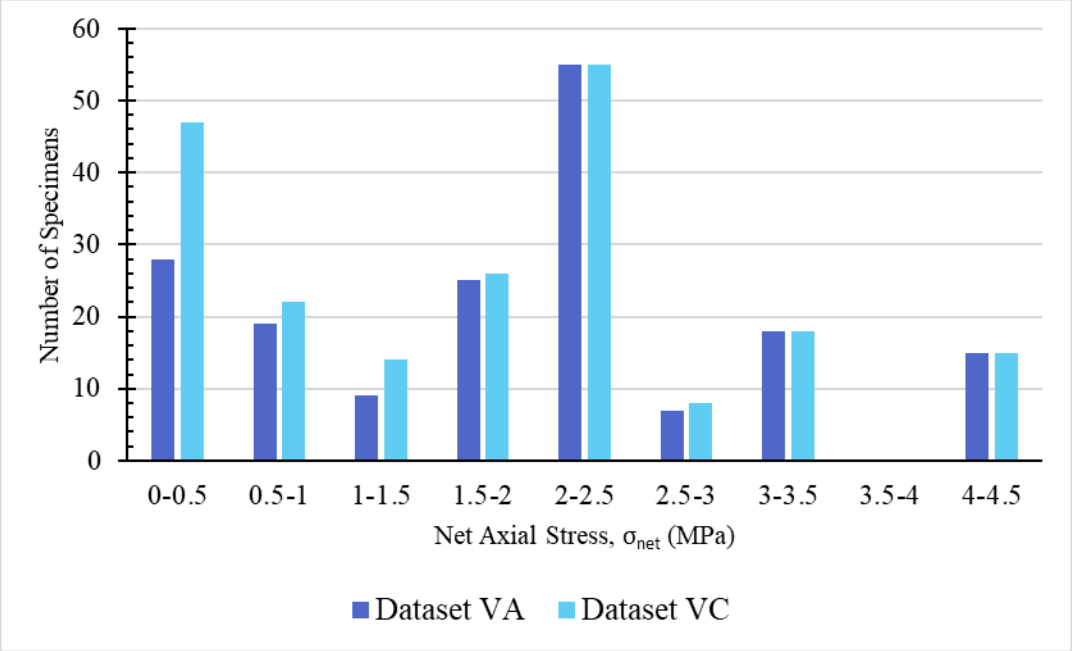

Figure 4.16 - Distribution of net axial stress

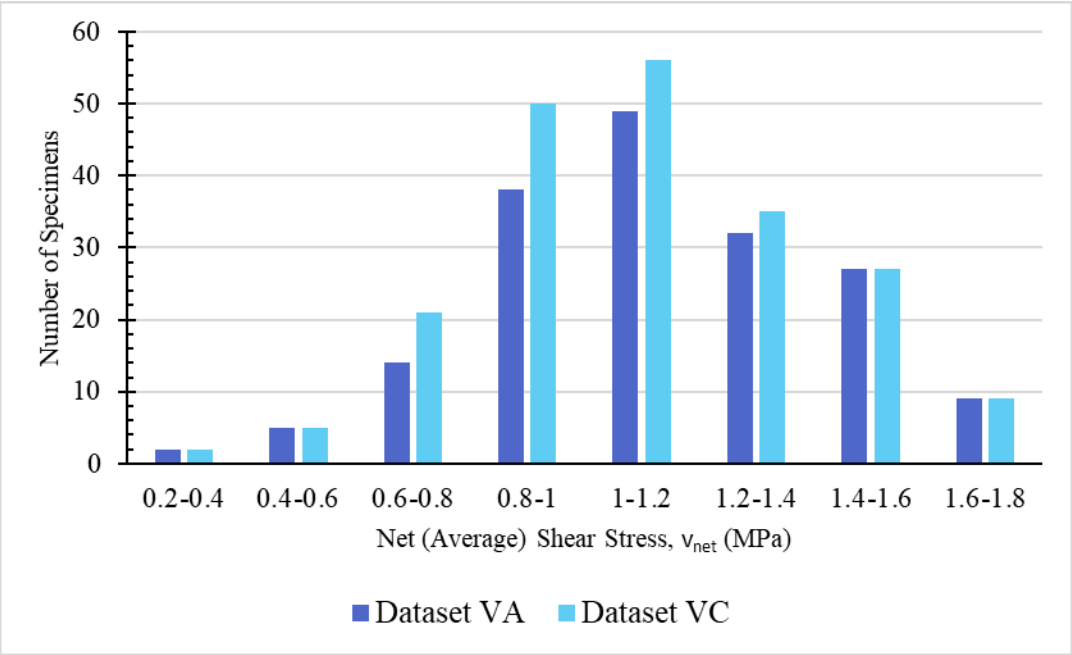

Figure 4.17 - Distribution of average net shear stress

4.6.1 Observed Gaps

Several observations can be made from the distributions presented in this section.

1. Almost all the specimens were tested under a quasi-static loading rate; in both Dataset VA and Dataset VC, only three dynamically tested specimens are included. All three specimens are from the study by Chen et al. (1978). This suggests a need for further research in dynamic testing of PG masonry shear walls.
2. The number of reduced-scale walls in both datasets is relatively small (20% for Dataset VA and 19% for Dataset VC), which is favourable considering the limited amount of research available comparing the shear strength of reduced-scale walls with full-scale prototypes.
3. Most of the tested walls have an area of 5 m^2 or less. This is not be representative of typical buildings and reflects a continued gap in the literature (Minaie, 2009). In fact,

close to half of the specimens with areas above 5 m^2 are reduced-scale models with areas that are much smaller than 5 m^2.

4. Most of the tested walls have aspect ratios of 1 or less. This is likely due to the tendency of masonry walls to fail in flexure at higher aspect ratios (Haider, 2007).
5. Limited experimental investigation has been performed on PG masonry walls built using high strength blocks, mortar, or grout.
6. Although several researchers have reported that increasing horizontal reinforcement ratios above 0.2% leads to negligible increases in shear strength, very few of the database walls have horizontal reinforcement ratios above 0.2%. This makes it difficult to study the effect of high horizontal reinforcement ratios using statistical analysis.

5 GENERATED MODELS

5.1 Introduction

Using the datasets described in Chapter 4, several stepwise regressions and model trees were generated and assessed for accuracy, precision, complexity, robustness, and interpretability. The methodology used is described in the following section, and then the resulting models are presented. Model comparison and selection of proposed models is done in Chapter 6.

5.2 Model Generation Procedure

Several datasets including different variable groups were used, as described in Chapter 4, to allow for investigation of various combinations of input variables. Dataset VA includes all possible input variables while Dataset VC includes only those input variables which are considered to be conventional, as they are generally available to designers and most of them are commonly used in existing code- and research-based shear strength equations for PG walls. The division of variables into the groups R, T and RT allowed for models to be generated using only raw or transformed variables, or both. Group T is made of variables with consistent units of kN.

For each dataset, 25% of the wall specimens were randomly selected and reserved for testing. Following model generation, each model was tested using the reserved 25% of the data to allow for model validation. The walls included in each dataset, as well as those selected for training and testing, are identified in Appendix B.

Based on the generated models, a few additions were made in the datasets over the course of the analysis. These additions are described in detail in Sections 5.3.3 and 5.4.

The following sections describe the model generation procedure in more detail for both stepwise regressions and model trees.

5.2.1 Stepwise Regressions

As explained in Section 2.4.1, stepwise regression allows the number of input variables to be reduced to an appropriate subset for predicting the output (Mohsenijam and Lu, 2016). It does this by identifying significant input variables while eliminating interdependencies between variables, or cases where an input variable does not need to be included in the model because it could be explained by other input variables (Leung et al., 2001; Mohsenijam and Lu, 2016). This is done objectively, without the researcher's opinions influencing the selection of variables from the candidates provided.

Stepwise regression models were generated in MATLAB (2018) using the function "stepwiselm". Intercepts were not allowed for any of the generated models. Model generation was done iteratively by adjusting variable inclusion and exclusion p-value thresholds (PEnter and PRemove) until a suitable number of terms was reached, so while many models were generated, only a few are presented in this chapter. The stepwise regression models selected for investigation were those that consisted of no more than 6 equation terms. This requirement ensures that selected models are not overly complex (although a few complex models were generated for comparison purposes, as discussed in Section 5.2.2) and reduces the chances of illogical variable relationships due to noise cancellation. Efforts were made to obtain at least one model with no illogical relationships for each variable group (R, T and RT) from both Dataset VA and Dataset VC. Following equation generation, each of the selected models was tested using the reserved 25% of the data. The selected models are presented in Section 5.3.

Stepwise regression facilitates testing different combinations of input variables, thus eliminating constraints on how many variables can be investigated (Dillon, 2015). All the variables that are present in the training data provided to the program are considered in the analysis.

The stepwise regressions generated were categorized into 4 types, shown in Table 5.1, depending on which variable groups were included in the training data.

Table 5.1 - Types of stepwise regressions generated

Model Type	Description
RS	Stepwise regression using the raw variables from Group R
TS	Stepwise regression using the variables with consistent units from Group T
RTS	Stepwise regression using the raw and transformed variables from Group RT
RTSi	Same as RTS, but interactions are also allowed

The model types listed in Table 5.1 allow for models of varying degrees of complexity to be generated, and for different groups of variables to be considered. The variables belonging to each of the 3 groups are listed in Sections 4.4.2 and 4.4.3. The RS models are simple linear regressions that contain no transformations, which makes them useful for comparison purposes. If a model containing transformations cannot outperform an RS model, it is difficult to justify the transformations. The RS models are also valuable because they are free of the assumptions required to create transformed variables. The RS models generated in the present study were found to generally perform quite well, in some cases outperforming the TS models. The TS models are of particular interest, however, as they contain only variables from Group T, which are designed to use consistent units, as would be expected in a typical code equation.

The RTSi model type differs from the RTS type in that it allows the program to add interactions between variables outside of the ones built into Group RT. Interactions in this context means that one variable (raw or transformed) is multiplied by another. RTSi models allow for more transformations to be potentially added to the models, allowing more non-linearities to appear in models. Because the interactions are chosen by the program based solely on the significance of the interaction compared to the other variables, the transformations may not have any physical meaning. For example, a TSi model may include a term that multiplies the axial load by the yield strength of bond beam reinforcement. Most of the RTSi models that were generated during analysis were identical to their RTS counterparts, meaning that the possible interactions were not

significant enough to be included in the models. The RTSi models that did include interactions contained too many terms for them to be considered as useful models.

5.2.2 Additional Regression Models

In addition to the model types listed in Table 5.1, a few more prediction models were generated that do not make use of stepwise variable selection. These models were generated using the MATLAB function "fitlm" and were of 4 types, as shown in Table 5.2.

Table 5.2 - Additional regression models generated

Model Type	Description
N	Naïve predictor (average of training set output)
RA	Regression including all variables from Group R
TA	Regression including all variables from Group T
RTA	Regression including all variables from Group RT

The model types shown in Table 5.2 were generated for the purpose of comparison with the stepwise regressions and model trees, and to illustrate the dangers of overfitting and underfitting. Unlike the model types in Table 5.1, these models were allowed to include intercepts. The models in Table 5.2 are discussed further in the following sections.

5.2.2.1 Naïve Predictor

Model type N is the simplest possible prediction model and is referred to by Sheiner and Beal (1981) as the "naïve predictor" because it makes the same prediction in all circumstances. It is a constant value—the average of the experimental values of shear strength from the training data set, which underfits the data. One model of this type was generated from Dataset VC (Model VC-N), and one was generated from Dataset VA (Model VA-N), with the values being 243.78 kN and 243.63, respectively. The performance indicators of VC-N and VA-N serve as a benchmark for any other models generated using the same data; if the generated models do not perform better

than the naïve predictor, then the models may not be of any value (Sheiner and Beal, 1981). The performance indicators of VC-N are given in Table 5.3.

Table 5.3 - Performance indicators for VC-N

		Training	Testing
GDF		0	
R^2		0	0
Adjusted R^2		0	0
RMSE (kN)		107	93.7
ME (kN)		-0.00248	-8.79
V_{exp}/V_n	Average	1.00	0.964
	Min	0.320	0.348
	Max	2.73	2.49
	Std. Dev.	0.439	0.386
	5th Percentile	0.411	0.408

Performance indicators for VA-N are given in Table 5.4.

Table 5.4 - Performance indicators for VA-N

		Training	Testing
GDF		0	
R^2		0	0
Adjusted R^2		0	0
RMSE (kN)		105	114
ME (kN)		0	-16.1
V_{exp}/V_n	Average	1.00	0.934
	Min	0.348	0.320
	Max	2.74	2.50
	Std. Dev.	0.433	0.470
	5th Percentile	0.411	0.404

The performance of the two naïve predictors is similar, with relatively high values of RMSE and standard deviation of V_{exp}/V_n.

5.2.2.2 Overly Complex Models

The RA, TA and RTA models do not use stepwise variable selection, so they include a large number of variables. In fact, these models will include all the variables present in the training data set, although they may assign a coefficient of 0 to some of the variables as the number of equation terms becomes larger and larger. This is generally the case for RTA models, which may have up to 87 terms, including the intercept.

These overly complex models generally perform well on training data but show poor generalization when tested on new data, an indication of overfitting. They are not useful as practical models for the shear behaviour of PG masonry walls, however they are useful in illustrating overfitting and in making comparisons with other models.

One model each of the RA, TA and RTA types was generated using Dataset VA. These models all contain a large number of terms, so the equations for these models will not be provided, but the performance indicators are presented here. The overly complex model VA-RA consists of 35 terms and has the performance indicators shown in Table 5.5.

Table 5.5 - Performance indicators for VA-RA

		Training	Testing
GDF		23.9	
R^2		0.960	0.786
Adjusted R^2		0.946	-0.0239
RMSE (kN)		21.1	63.1
ME (kN)		0	5.30
V_{exp}/V_n	Average	1.00	1.00
	Min	0.749	-0.955
	Max	1.70	2.02
	Std. Dev.	0.113	0.414
	5th Percentile	0.832	0.757

VA-RA shows obvious signs of overfitting, as the model performs very well on the training data, while the performance worsens severely for the testing data. The RMSE and standard deviation of

V_{exp}/V_n are relatively low for the training data, while the testing values of both of these indicators are three to four times larger.

VA-TA consists of 40 terms and has the performance indicators shown in Table 5.6.

Table 5.6 - Performance indicators for VA-TA

		Training	Testing
GDF		32.2	
R^2		0.970	0.837
Adjusted R^2		0.957	-0.751
RMSE (kN)		18.2	47.7
ME (kN)		0	-4.01
V_{exp}/V_n	Average	1.00	1.00
	Min	0.718	0.693
	Max	1.68	2.77
	Std. Dev.	0.103	0.303
	5th Percentile	0.859	0.730

Like VA-RA, the model VA-TA shows significant overfitting as made evident by the increase in values of RMSE and standard deviation of V_{exp}/V_n from training to testing data.

VA-RTA consists of 63 terms and has the performance indicators shown in Table 5.7.

Table 5.7 - Performance indicators for VA-RTA

		Training	Testing
GDF		62.2	
R^2		0.984	0.0172
Adjusted R^2		0.970	3.22
RMSE (kN)		13.2	234647
ME (kN)		0	21809
V_{exp}/V_n	Average	1.00	0.68
	Min	0.806	-0.015
	Max	1.39	1.72
	Std. Dev.	0.070	0.483
	5th Percentile	0.894	-0.003

VA-RTA is an extreme case of overfitting. Out of the three overly complex models tested, it has the lowest values of RMSE and standard deviation of V_{exp}/V_n for training data, while it has the largest values for both of these performance indicators when measured on testing data. In fact, some of the values of V_n calculated using VA-RTA on the testing data were negative. This illustrates the danger of using an overly complex model to predict the shear strength of PG masonry walls—the model performs deceptively well on the data that was used for training because it models the noise in the data. But when the model is used on new data, as Myung (2000) would say, "the conspiracy falls apart."

The performance of these overly complex equations will be compared to that of the existing code- and research-based shear strength equations and the proposed models in Chapter 6.

5.2.3 Model Trees

Model trees were generated in two main steps. First, the M5PrimeLab toolbox was used in MATLAB (2018) to generate an initial model tree (Jekabsons, 2016a). This was done using the functions "m5pbuild" and "m5pparams" with the default input arguments, except for the following (value used is indicated in brackets): minimum leaf size (30), smoothing (15). The minimum leaf size controls the number of observations that must be grouped together for a new branch to be formed. The default value for smoothing is 0, which disables smoothing and produces regressions trees (Jekabsons, 2016b). This is essentially the naïve predictor, but with one constant on each branch of a tree. When enabled, smoothing tries to compensate for sharp discontinuities occurring between adjacent tree branches (Jekabsons, 2016b). The larger the smoothing value, the more pronounced this effect becomes. Because different values of smoothing do not affect the structure of the tree or the splitting values, adjusting the "smoothingK" input argument has no effect on the MTs developed in this study.

Based on the initial tree generated by M5PrimeLab, branch splitting values were determined and rounded to more practical values. The analyzed dataset was then split manually in accordance with

these splitting values. Each data group was analyzed individually in MATLAB using the function "stepwiselm" to obtain several models, the same way as was described in Section 5.2.1. RS, TS, RTS and TSi models with less than six terms were generated for each branch. An optimum model was selected for each branch based on criteria of accuracy, simplicity and whether the model contained any illogical relationships. Then the final model tree was assembled by adding all the branch models to the tree structure. The completed MTs are presented in Section 5.3.4.

5.2.4 Model Naming

In the present study, each generated model is given a unique name to identify it. The model name identifies the overall model type, regression type(s) and dataset and variable group(s) used to generate the model, as well as the model iteration. The model naming used for stepwise regressions is shown in Figure 5.1.

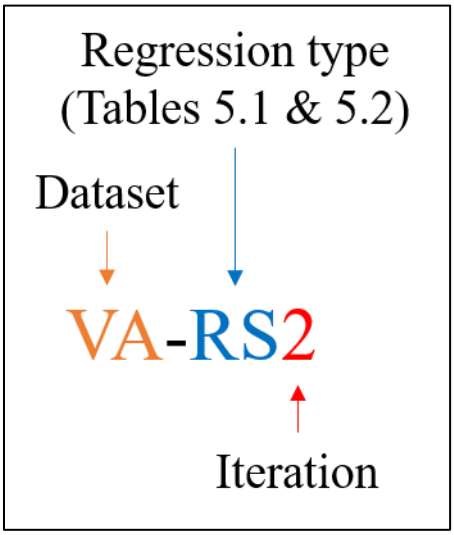

Figure 5.1 - Naming used for stepwise regression models

Here, iteration refers to the number of iterations of inclusion/exclusion thresholds made to reach the model. Although models with the same iteration number often have the same PEnter and PRemove values and models generally become less complex with each successive iteration, this

is not always the case. The iteration number simply refers to the order in which models were generated.

The model naming used for model trees is shown in Figure 5.2.

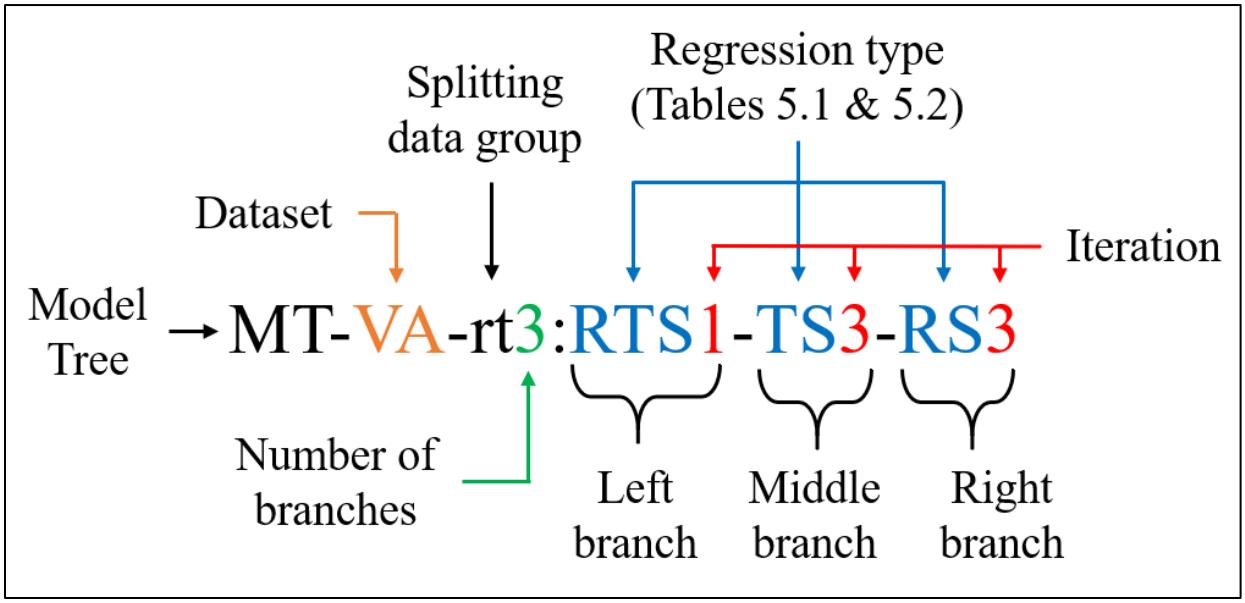

Figure 5.2 - Naming used for model trees

5.3 Results - Generated Shear Strength Models

The following sections present the stepwise regressions and model trees generated in the present study. For stepwise regressions, only those which include a maximum of 6 terms are presented. The inclusion and exclusion p-value thresholds used to generate each model are listed, as well as the performance indicators of each model.

R^2 and Adjusted R^2 values indicate the quality of fit of the model; the closer the values are to 1, the better the fit. Adjusted R^2 differs from R^2 in that it penalizes models of higher complexity based on the number of terms in the model. As discussed in Section 2.4.4.1, these indicators can be misleading in some cases, so they will not be relied on for model selection purposes.

RMSE and ME are measures of error: the lower the values, the lower the error is. RMSE is a measure of accuracy and is always positive, while ME is a measure of bias that can be positive or negative. Because ME is calculated by taking the average of observed values minus fitted values, a positive value of ME indicates the average value by which the model underestimates the shear strength. Conversely, a negative value of ME indicates the average value by which the model overestimates the shear strength.

Similarly, the average value of V_{exp}/V_n is an indication of model bias. A value above 1 indicates that the model underestimates the shear strength on average (conservative) while a value below 1 indicates that the model overestimates the shear strength on average. Minimum and maximum values of V_{exp}/V_n provide the range of overestimation and underestimation of the model. Standard deviation of V_{exp}/V_n indicates the spread of V_{exp}/V_n values for the given model, hence a low standard deviation combined with an average value of V_{exp}/V_n that is close to 1 is favourable. The fifth percentile of V_{exp}/V_n is the value of V_{exp}/V_n exceeded by 95% of the walls in the dataset. A high value of the fifth percentile of V_{exp}/V_n indicates a more conservative model.

GDF is an estimate of model complexity that facilitates comparisons between different model types. The higher the GDF is, the more complex the model is. During analysis, it was observed that the GDF tends to underestimate the complexity of models when it is calculated based on testing data, due to the high variance of errors. For this reason, GDF was calculated based on training data only. It should be noted that the GDF depends on the data provided; calculating the GDF of the same model based on two different sets of data would result in two different values of GDF. As such, GDF is not a perfect measure of complexity; it was observed that some of the differences in complexity between similar models were not well reflected by comparing the calculated GDF values.

For example, VC-RTS4 and VC-TS5 are very similar to each other. Both consist of two terms: one term is a raw variable, P, while the other term is a transformed variable. In the case of VC-

RTS4, the transformed variable is simply A_{net}, while for VC-TS5, the transformed variable is $f'_{m,eff}A_{net}$. Logic dictates that the model with the higher number of variables should be more flexible and more complex, however this is not reflected in the GDFs of the models; VC-RTS4 has a GDF of 3.27 while VC-TS5 has a GDF of 2.47. Despite this finding, the GDF values were observed to generally reflect the differences in complexity of various models relatively well.

Further information on the performance indicators used in the present study, as well as the equations used to calculate them, can be found in Section 2.4.4.

For raw variables, standard units of mm, mm^2 and MPa were used, except for the variable P, which was measured in kN. The transformed variables from Group T were multiplied by each other such that each term had units of kN (except for those terms which include a square root).

Selection of the proposed models and comparison with the existing code- and research-based shear strength expressions is done in Chapter 6.

5.3.1 Stepwise Regressions Generated - Dataset VA

Several stepwise regressions were generated which were permitted to include any variables, regardless of whether these variables had been used in previously developed shear strength expressions.

5.3.1.1 VA-RS2

VA-RS2 was generated using the p-value inclusion and exclusion thresholds shown in Table 5.8.

Table 5.8 - Inclusion and exclusion thresholds used to generate VA-RS2

	PEnter	PRemove
p-value threshold	0.0049	0.1

The equation for VA-RS2 is given here as Equation (4.1).

$$V_n = -0.0205H + 0.0337L + 6.00f_{mortar} + 0.0917A_{vi} + 0.289P \quad (5.1)$$

The performance indicators for VA-RS2 are shown in Table 5.9.

Table 5.9 - Performance indicators for VA-RS2

		Training	Testing
GDF		7.34	
R^2		0.880	0.900
Adjusted R^2		0.876	0.889
RMSE (kN)		36.5	37.6
ME (kN)		0.293	-10.6
V_{exp}/V_n	Average	1.00	0.953
	Min	0.478	0.598
	Max	1.54	1.46
	Std. Dev.	0.160	0.179
	5th Percentile	0.775	0.752

5.3.1.2 VA-RS3

VA-RS3 was generated using the p-value inclusion and exclusion thresholds shown in Table 5.10.

Table 5.10 - Inclusion and exclusion thresholds used to generate VA-RS3

	PEnter	PRemove
p-value threshold	0.0009	0.001

The equation for VA-RS3 is given here as Equation (5.2).

$$V_n = 0.0211L + 5.34f_{mortar} + 0.106A_{vi} + 0.29P \quad (5.2)$$

The performance indicators for VA-RS3 are shown in Table 5.11.

Table 5.11 - Performance indicators for VA-RS3

		Training	Testing
GDF		6.53	
R^2		0.871	0.904
Adjusted R^2		0.868	0.897
RMSE (kN)		37.9	38.3
ME (kN)		-1.18	-15.3
V_{exp}/V_n	Average	0.992	0.929
	Min	0.477	0.598
	Max	1.61	1.38
	Std. Dev.	0.164	0.174
	5th Percentile	0.789	0.682

5.3.1.3 VA-TS2

VA-TS2 was generated using the p-value inclusion and exclusion thresholds shown in Table 5.12.

Table 5.12 - Inclusion and exclusion thresholds used to generate VA-TS2

	PEnter	PRemove
p-value threshold	0.0049	0.005

The equation for VA-TS2 is given here as Equation (5.3).

$$V_n = 0.26P + 0.258f_{mortar}t_{fs}L_b + 0.222\sqrt{f_{mortar}}t_{fs}L + 0.0147f'_{m,eff}A_{net} + 0.459A_{vi}f_{yvi} - 0.281A_{vi,bar}f_{yvi}\frac{H}{s_{vi,max}} \quad (5.3)$$

It is not logical for the $A_{vi}f_{yvi}\frac{H}{s_{vi,ave}}$ term to have a negative coefficient, as the correlation of this term with the shear strength is expected to be positive. The presence of the term $A_{vi}f_{yvi}$ multiplied by a positive coefficient is likely an indication that these two terms are cancelling noise from each other.

The performance indicators for VA-TS2 are shown in Table 5.13.

Table 5.13 - Performance indicators for VA-TS2

		Training	Testing
GDF		9.13	
R^2		0.901	0.914
Adjusted R^2		0.897	0.903
RMSE (kN)		33.0	34.3
ME (kN)		-0.193	-8.1
V_{exp}/V_n	Average	1.00	0.969
	Min	0.514	0.637
	Max	1.86	1.48
	Std. Dev.	0.157	0.167
	5th Percentile	0.820	0.706

5.3.1.4 VA-TS3

VA-TS3 was generated using the p-value inclusion and exclusion thresholds shown in Table 5.14.

Table 5.14 - Inclusion and exclusion thresholds used to generate VA-TS3

	PEnter	PRemove
p-value threshold	0.0009	0.001

The equation for VA-TS3 is given here as Equation (5.4).

$$V_n = 0.278P + 0.296f_{mortar}t_{fs}L_b + 0.197\sqrt{f_{mortar}}t_{fs}L + 0.903A_{vi}f_{yvi} - 0.463A_{vi,bar}f_{yvi}\frac{L}{s_{vi,ave}} + 0.00769\frac{VL}{M}f'_{m,eff}A_{net} \quad (5.4)$$

Similar to VA-TS2, it is not logical for the $A_{vi}f_{yvi}\frac{L}{s_{vi,ave}}$ term to have a negative coefficient. The presence of the term $A_{vi}f_{yvi}$ multiplied by a positive coefficient may indicate noise cancelation.

The performance indicators for VA-TS3 are shown in Table 5.15.

Table 5.15 - Performance indicators for VA-TS3

		Training	Testing
GDF		9.75	
R^2		0.906	0.915
Adjusted R^2		0.902	0.904
RMSE (kN)		32.3	34.4
ME (kN)		0.670	-6.16
V_{exp}/V_n	Average	1.01	0.979
	Min	0.576	0.680
	Max	1.87	1.61
	Std. Dev.	0.157	0.168
	5th Percentile	0.806	0.739

5.3.1.5 VA-TS4

VA-TS4 was generated using the p-value inclusion and exclusion thresholds shown in Table 5.16.

Table 5.16 - Inclusion and exclusion thresholds used to generate VA-TS4

	PEnter	PRemove
p-value threshold	1E-05	2E-05

The equation for VA-TS4 is given here as Equation (5.5).

$$V_n = 0.305P + 0.508\sqrt{f_{mortar}}t_{fs}L \tag{5.5}$$

The performance indicators for VA-TS4 are shown in Table 5.17.

Table 5.17 - Performance indicators for VA-TS4

		Training	Testing
GDF		6.05	
R^2		0.853	0.872
Adjusted R^2		0.852	0.869
RMSE (kN)		41.3	44.0
ME (kN)		3.39	-7.0
V_{exp}/V_n	Average	1.08	1.05
	Min	0.474	0.597
	Max	3.23	2.03
	Std. Dev.	0.319	0.342
	5th Percentile	0.766	0.660

5.3.1.6 VA-TS5

VA-TS5 was generated using the p-value inclusion and exclusion thresholds shown in Table 5.18.

Table 5.18 - Inclusion and exclusion thresholds used to generate VA-TS5

	PEnter	PRemove
p-value threshold	9E-05	0.0001

The equation for VA-TS5 is given here as Equation (5.6).

$$V_n = 0.296P + 0.255f_{mortar}t_{fs}L_b + 0.291\sqrt{f_{mortar}}t_{fs}L + 0.209A_{vi}f_{yvi} \quad (5.6)$$

The performance indicators for VA-TS5 are shown in Table 5.19.

Table 5.19 - Performance indicators for VA-TS5

		Training	Testing
GDF		7.67	
R^2		0.884	0.895
Adjusted R^2		0.882	0.887
RMSE (kN)		35.8	38.9
ME (kN)		0.105	-9.8
V_{exp}/V_n	Average	1.01	0.970
	Min	0.539	0.645
	Max	2.03	1.58
	Std. Dev.	0.169	0.187
	5th Percentile	0.795	0.745

5.3.1.7 VA-RTS3

VA-RTS3 was generated using the p-value inclusion and exclusion thresholds shown in Table 5.20.

Table 5.20 - Inclusion and exclusion thresholds used to generate VA-RTS3

	PEnter	PRemove
p-value threshold	0.0009	0.001

The equation for VA-RTS3 is given here as Equation (5.7).

$$V_n = 0.296P + 0.000282A_{net} + 0.0746f_{mortar}t_{fs}L \quad (5.7)$$

The performance indicators for VA-RTS3 are shown in Table 5.21.

Table 5.21 - Performance indicators for VA-RTS3

		Training	Testing
GDF		6.18	
R^2		0.857	0.876
Adjusted R^2		0.855	0.870
RMSE (kN)		40.1	42.9
ME (kN)		1.83	-10.3
V_{exp}/V_n	Average	1.05	1.01
	Min	0.444	0.557
	Max	2.82	1.77
	Std. Dev.	0.260	0.278
	5th Percentile	0.782	0.663

5.3.2 Stepwise Regressions Generated - Dataset VC

Several stepwise regressions were generated which were only permitted to include conventional variables. Most notably, Dataset VC does not include any form of the variables f_{block}, f_{mortar} and f_{grout}.

5.3.2.1 VC-RS3

VC-RS3 was generated using the p-value inclusion and exclusion thresholds shown in Table 5.22.

Table 5.22 - Inclusion and exclusion thresholds used to generate VC-RS3

	PEnter	PRemove
p-value threshold	0.0009	0.001

The equation for VC-RS3 is given here as Equation (5.8).

$$V_n = 0.0568L + 5.18f'_{mg} + 0.175A_{vf,bar} - 0.0657s_{v,ave} + 0.23P \quad (5.8)$$

Here the negative coefficient in front of $s_{v,ave}$ is logical because as vertical bar spacing increases, one would expect to see a decrease in shear strength.

The performance indicators for VC-RS3 are shown in Table 5.23.

Table 5.23 - Performance indicators for VC-RS3

		Training	Testing
GDF		4.89	
R^2		0.840	0.823
Adjusted R^2		0.836	0.807
RMSE (kN)		43.0	41.1
ME (kN)		-2.23	-6.10
V_{exp}/V_n	Average	0.99	1.00
	Min	0.514	0.576
	Max	1.66	2.10
	Std. Dev.	0.193	0.231
	5th Percentile	0.658	0.768

5.3.2.2 VC-TS1

VC-TS1 was generated using the p-value inclusion and exclusion thresholds shown in Table 5.24.

Table 5.24 - Inclusion and exclusion thresholds used to generate VC-TS1

	PEnter	PRemove
p-value threshold	0.05	0.1

The equation for VC-TS1 is given here as Equation (5.9).

$$V_n = 0.187P + 0.0514f'_{m,g}t(1000\text{mm})\frac{n_g}{n_t} + 0.111A_{vi}f_{yvi} + 0.108\frac{M}{VL}\sqrt{f'_{m,eff}}A_{net} + 0.0514\frac{VL}{M}\sqrt{f'_{m,eff}}A_{net} \quad (5.9)$$

The shear span ratio $\frac{M}{VL}$ is expected to be negatively correlated with the shear strength, so it is not logical for the term $\frac{M}{VL}\sqrt{f'_{m,eff}}A_{net}$ to appear with a positive coefficient. Note that the presence of

the $\frac{VL}{M}\sqrt{f'_{m,eff}}A_{net}$ term indicates that there is likely noise cancellation occurring between the two terms.

The performance indicators for VC-TS1 are shown in Table 5.25.

Table 5.25 - Performance indicators for VC-TS1

		Training	Testing
GDF		5.00	
R^2		0.829	0.830
Adjusted R^2		0.825	0.815
RMSE (kN)		44.2	39.8
ME (kN)		0.962	0.269
V_{exp}/V_n	Average	1.02	1.03
	Min	0.490	0.691
	Max	2.06	1.95
	Std. Dev.	0.225	0.226
	5th Percentile	0.742	0.771

5.3.2.3 VC-TS2

VC-TS2 was generated using the p-value inclusion and exclusion thresholds shown in Table 5.26.

Table 5.26 - Inclusion and exclusion thresholds used to generate VC-TS2

	PEnter	PRemove
p-value threshold	0.0049	0.005

The equation for VC-TS2 is given here as Equation (5.10).

$$V_n = 0.186P + 0.0479f'_{m,g}t(1000\text{mm})\frac{n_g}{n_t} + 0.117\frac{M}{VL}\sqrt{f'_{m,eff}}A_{net} + 0.0581\frac{VL}{M}\sqrt{f'_{m,eff}}A_{net} \quad (5.10)$$

As with VC-TS2, it is not logical for the term $\frac{M}{VL}\sqrt{f'_{m,eff}}A_{net}$ to appear with a positive coefficient. The $\frac{VL}{M}\sqrt{f'_{m,eff}}A_{net}$ term may be attempting to cancel noise from the shear span ratio term.

The performance indicators for VC-TS2 are shown in Table 5.27.

Table 5.27 - Performance indicators for VC-TS2

		Training	Testing
GDF		4.63	
R^2		0.820	0.829
Adjusted R^2		0.817	0.818
RMSE (kN)		45.2	39.9
ME (kN)		0.529	-3.18
V_{exp}/V_n	Average	1.01	1.01
	Min	0.469	0.686
	Max	2.09	1.91
	Std. Dev.	0.227	0.223
	5th Percentile	0.731	0.754

5.3.2.4 VC-TS4

VC-TS4 was generated using the p-value inclusion and exclusion thresholds shown in Table 5.28.

Table 5.28 - Inclusion and exclusion thresholds used to generate VC-TS4

	PEnter	PRemove
p-value threshold	1E-05	2E-05

The equation for VC-TS4 is given here as Equation (5.11).

$$V_n = 0.190P + 0.156\frac{M}{VL}\sqrt{f'_{m,eff}}A_{net} + 0.0621\frac{VL}{M}\sqrt{f'_{m,eff}}A_{net} \quad (5.11)$$

As with VC-TS1 and VC-TS2, it is not logical for the term $\frac{M}{VL}\sqrt{f'_{m,eff}}A_{net}$ to appear with a positive coefficient. The $\frac{VL}{M}\sqrt{f'_{m,eff}}A_{net}$ term is likely attempting to cancel noise from the shear span ratio term.

The performance indicators for VC-TS4 are shown in Table 5.29.

Table 5.29 - Performance indicators for VC-TS4

		Training	Testing
GDF		4.42	
R^2		0.807	0.820
Adjusted R^2		0.804	0.813
RMSE (kN)		48.2	44.0
ME (kN)		4.41	-1.33
V_{exp}/V_n	Average	1.06	1.06
	Min	0.427	0.689
	Max	2.07	2.64
	Std. Dev.	0.268	0.328
	5th Percentile	0.741	0.741

5.3.2.5 VC-TS5

VC-TS5 was generated using the p-value inclusion and exclusion thresholds shown in Table 5.30.

Table 5.30 - Inclusion and exclusion thresholds used to generate VC-TS5

	PEnter	PRemove
p-value threshold	2E-12	5E-12

The equation for VC-TS5 is given here as Equation (5.12).

$$V_n = 0.256P + 0.0520f'_{m,eff}A_{net} \tag{5.12}$$

The performance indicators for VC-TS5 are shown in Table 5.31.

Table 5.31 - Performance indicators for VC-TS5

		Training	Testing
GDF		2.47	
R^2		0.692	0.680
Adjusted R^2		0.690	0.673
RMSE (kN)		62.3	58.9
ME (kN)		7.91	-2.99
V_{exp}/V_n	Average	1.14	1.12
	Min	0.639	0.595
	Max	2.63	3.38
	Std. Dev.	0.410	0.508
	5th Percentile	0.736	0.723

5.3.2.6 VC-RTS3

VC-RTS3 was generated using the inclusion and exclusion thresholds shown in Table 5.32.

Table 5.32 - Inclusion and exclusion thresholds used to generate VC-RTS3

	PEnter	PRemove
p-value threshold	0.0009	0.001

The equation for VC-RTS3 is given here as Equation (5.13).

$$V_n = 0.000649A_{net} - 0.383t + 8.19f'_{mg} + 0.237P \quad (5.13)$$

The negative coefficient in front of the variable t is not logical, as increasing the thickness of a PG shear wall should increase the shear strength of the wall.

The performance indicators for VC-RTS3 are shown in Table 5.33.

Table 5.33 - Performance indicators for VC-RTS3

		Training	Testing
GDF		4.46	
R^2		0.816	0.826
Adjusted R^2		0.813	0.815
RMSE (kN)		45.7	43.3
ME (kN)		0.0552	-7.79
V_{exp}/V_n	Average	1.04	1.04
	Min	0.446	0.643
	Max	1.90	2.94
	Std. Dev.	0.269	0.372
	5th Percentile	0.713	0.730

5.3.2.7 VC-RTS4

VC-RTS4 was generated using the inclusion and exclusion thresholds shown in Table 5.34.

Table 5.34 - Inclusion and exclusion thresholds used to generate VC-RTS4

	PEnter	PRemove
p-value threshold	1E-05	2E-05

The equation for VC-RTS4 is given here as Equation (5.14).

$$V_n = 0.000794A_{net} + 0.184P \tag{5.14}$$

The performance indicators for VC-RTS4 are shown in Table 5.35.

Table 5.35 - Performance indicators for VC-RTS4

		Training	Testing
GDF		3.27	
R^2		0.762	0.798
Adjusted R^2		0.760	0.793
RMSE (kN)		52.1	47.2
ME (kN)		0.903	-12.0
V_{exp}/V_n	Average	1.02	0.987
	Min	0.445	0.510
	Max	1.63	2.14
	Std. Dev.	0.227	0.244
	5th Percentile	0.610	0.689

5.3.3 Stepwise Regressions Generated - Dataset VCe

Over the course of analyzing Dataset VC, it was observed that the shear span ratio and inverse shear span ratio terms $\frac{M}{VL}\sqrt{f'_{m,eff}}A_{net}$ and $\frac{VL}{M}\sqrt{f'_{m,eff}}A_{net}$ frequently appeared together (Sections 5.3.2.2, 5.3.2.3 and 5.3.2.4) and seemed to be cancelling noise from each other. It was also observed that the term $f'_{m,eff}A_{net}$ was more significant than either of these terms, however it was removed by the stepwise regression procedure after the addition of the shear span ratio and inverse shear span ratio terms. Decreasing the inclusion threshold sufficiently resulted in a 2-term model without either of the shear span ratio terms (Section 5.3.2.5).

Based on these findings, a new variable, $\sqrt{f'_{m,eff}}A_{net}$, was added to Group T and subsequent models were generated. This expanded version of Dataset VC is referred to as Dataset VCe.

5.3.3.1 VCe-TS1

VCe-TS1 was generated using the p-value inclusion and exclusion thresholds shown in Table 5.36.

Table 5.36 - Inclusion and exclusion thresholds used to generate VCe-TS1

	PEnter	PRemove
p-value threshold	0.05	0.1

The equation for VCe-TS1 is given here as Equation (5.15).

$$V_n = 0.207P + 0.161\sqrt{f'_{m,eff}}A_{net} + 0.172A_{vi}f_{yvi} + 0.128A_{vf}f_{yvf} - 0.14A_vf_{yv} + 0.0229\frac{VL}{M}\sqrt{f'_{m,eff}}A_{net} \quad (5.15)$$

where $A_vf_{yv} = A_{vi}f_{yvi} + A_{vf}f_{yvf}$

$\frac{A_{vi}+A_{vf}}{Lt} \leq 0.0002$

Unlike VC-TS1, which used the same PEnter and PRemove variables (Section 5.3.2.2), this model doesn't include both shear span ratio terms. However, this model is still illogical because of the negative coefficient in front of the A_vf_{yv} term. It is also impractical to have a limit for one of the vertical reinforcement terms, but not for the others.

The performance indicators for VCe-TS1 are shown in Table 5.37.

Table 5.37 - Performance indicators for VCe-TS1

		Training	Testing
GDF		4.99	
R^2		0.829	0.806
Adjusted R^2		0.823	0.784
RMSE (kN)		44.3	44.5
ME (kN)		1.73	-1.04
V_{exp}/V_n	Average	1.04	1.07
	Min	0.587	0.630
	Max	1.96	2.78
	Std. Dev.	0.261	0.348
	5th Percentile	0.734	0.693

5.3.3.2 VCe-TS2

VCe-TS2 was generated using the p-value inclusion and exclusion thresholds shown in Table 5.38.

Table 5.38 - Inclusion and exclusion thresholds used to generate VCe-TS2

	PEnter	PRemove
p-value threshold	0.0049	0.005

The equation for VCe-TS2 is given here as Equation (5.16).

$$V_n = 0.21P + 0.155\sqrt{f'_{m,eff}}A_{net} + 0.0741A_{vf}f_{yvf} + 0.0195\frac{VL}{M}\sqrt{f'_{m,eff}}A_{net} \qquad (5.16)$$

The performance indicators for VCe-TS2 are shown in Table 5.39.

Table 5.39 - Performance indicators for VCe-TS2

		Training	Testing
GDF		4.43	
R^2		0.811	0.801
Adjusted R^2		0.807	0.789
RMSE (kN)		46.5	45.2
ME (kN)		1.90	-4.86
V_{exp}/V_n	Average	1.04	1.04
	Min	0.521	0.559
	Max	1.96	2.54
	Std. Dev.	0.247	0.310
	5th Percentile	0.682	0.692

5.3.3.3 VCe-TS3

VCe-TS3 was generated using the p-value inclusion and exclusion thresholds shown in Table 5.40.

Table 5.40 - Inclusion and exclusion thresholds used to generate VCe-TS3

	PEnter	PRemove
p-value threshold	0.0009	0.001

The equation for VCe-TS3 is given here as Equation (5.17).

$$V_n = 0.194P + 0.179\sqrt{f'_{m,eff}}A_{net} + 0.0228\frac{VL}{M}\sqrt{f'_{m,eff}}A_{net} \quad (5.17)$$

The performance indicators for VCe-TS3 are shown in Table 5.41.

Table 5.41 - Performance indicators for VCe-TS3

		Training	Testing
GDF		4.30	
R^2		0.803	0.811
Adjusted R^2		0.801	0.804
RMSE (kN)		48.2	44.8
ME (kN)		3.97	-5.09
V_{exp}/V_n	Average	1.07	1.05
	Min	0.538	0.639
	Max	2.17	2.67
	Std. Dev.	0.283	0.326
	5th Percentile	0.709	0.719

5.3.3.4 VCe-TS5

VCe-TS5 was generated using the p-value inclusion and exclusion thresholds shown in Table 5.42.

Table 5.42 - Inclusion and exclusion thresholds used to generate VCe-TS5

	PEnter	PRemove
p-value threshold	1E-05	2E-05

The equation for VCe-TS5 is given here as Equation (5.18).

$$V_n = 0.211P + 0.214\sqrt{f'_{m,eff}}A_{net} \tag{5.18}$$

The performance indicators for VCe-TS5 are shown in Table 5.43.

Table 5.43 - Performance indicators for VCe-TS5

		Training	Testing
GDF		3.34	
R^2		0.763	0.786
Adjusted R^2		0.761	0.781
RMSE (kN)		52.1	46.0
ME (kN)		1.70	-8.74
V_{exp}/V_n	Average	1.04	1.02
	Min	0.517	0.633
	Max	2.04	2.56
	Std. Dev.	0.270	0.317
	5th Percentile	0.710	0.714

5.3.4 Model Trees Generated

MT branch models were selected first on the basis of logic, so that models exhibiting illogical relationships between the input variables and the shear strength were not considered for implementation in the MTs. Among the branches with logical relationships, those with the best performance indicators were selected for implementation in the MTs.

5.3.4.1 MT-VA-rt3:RTS1-TS3-RS3

The model tree structure of MT-VA-rt3:RTS1-TS3-RS3 is shown in Figure 5.3.

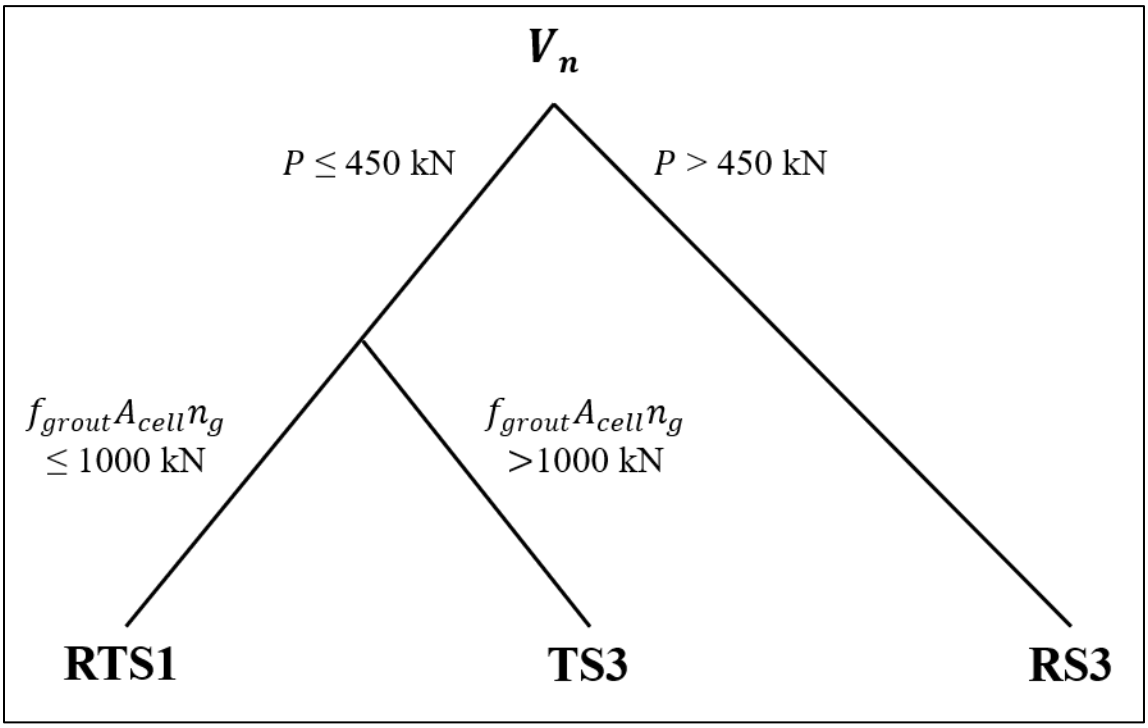

Figure 5.3 - Model tree structure of MT-VA-rt3:RTS1-TS3-RS3

MT-VA-rt3:RTS1-TS3-RS3 was generated using the p-value inclusion and exclusion thresholds shown in Table 5.44.

Table 5.44 - Inclusion and exclusion thresholds used for MT-VA-rt3:RTS1-TS3-RS3

p-value threshold	Left Branch	Middle Branch	Right Branch
PEnter	0.05	0.0009	0.0009
PRemove	0.1	0.001	0.001

The equation for MT-VA-rt3:RTS1-TS3-RS3 is given here as Equation (5.19).

$$V_n = \begin{cases} 0.167t + 0.668\sqrt{f_{mortar}}t_{fs}L & \text{if } P \leq 450 \;\&\; f_{grout}A_{cell}n_g \leq 1000 \\ 0.501\sqrt{f_{mortar}}t_{fs}L + 0.519P\dfrac{A_{net}}{A_{gross}} & \text{if } P \leq 450 \;\&\; f_{grout}A_{cell}n_g > 1000 \\ 0.461f_{ybb} - 0.0631s_{h,ave} + 0.417P & \text{if } P > 450 \end{cases} \quad (5.19)$$

The performance indicators for MT-VA-rt3:RTS1-TS3-RS3 are shown in Table 5.45.

Table 5.45 - Performance indicators for MT-VA-rt3:RTS1-TS3-RS3

		Training	Testing
GDF		8.58	
R^2		0.893	0.879
Adjusted R^2		0.888	0.859
RMSE (kN)		34.7	42.7
ME (kN)		1.76	-12.4
V_{exp}/V_n	Average	1.01	0.956
	Min	0.480	0.424
	Max	1.69	1.48
	Std. Dev.	0.154	0.197
	5th Percentile	0.818	0.656

5.3.4.2 VA-rt3:TS1-TS3-TS2

The model tree structure of MT-VA-rt3:TS1-TS3-TS2 is shown in Figure 5.4.

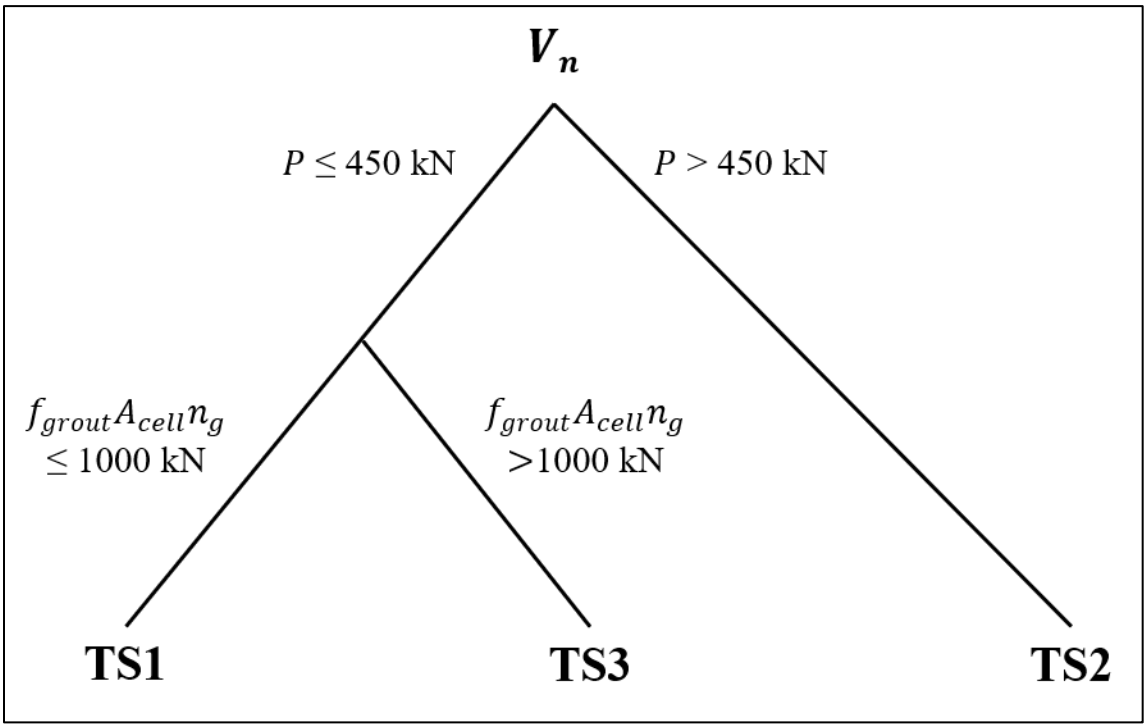

Figure 5.4 - Model tree structure of MT-VA-rt3:TS1-TS3-TS2

The performance indicators for MT-VA-rt3:TS1-TS3-TS2 are shown in Table 5.46.

Table 5.46 - Inclusion and exclusion thresholds used for MT-VA-rt3:TS1-TS3-TS2

p-value threshold	Left Branch	Middle Branch	Right Branch
PEnter	0.05	0.0009	0.0049
PRemove	0.1	0.001	0.005

The equation for MT-VA-rt3:TS1-TS3-TS2 is given here as Equation (5.20).

$$V_n = \begin{cases} 0.55\sqrt{f_{mortar}}t_{fs}L + 0.205f'_{mu}t_{fs}(1000mm)\left(1-\frac{n_g}{n_t}\right) & \text{if } P \leq 450 \;\&\; f_{grout}A_{cell}n_g \leq 1000 \\ 0.501\sqrt{f_{mortar}}t_{fs}L + 0.519P\frac{A_{net}}{A_{gross}} & \text{if } P \leq 450 \;\&\; f_{grout}A_{cell}n_g > 1000 \\ 0.311P + 0.493\sqrt{f_{mortar}}t_{fs}L & \text{if } P > 450 \end{cases} \quad (5.20)$$

The performance indicators for MT-VA-rt3:TS1-TS3-TS2 are shown in Table 5.47.

Table 5.47 - Performance indicators for MT-VA-rt3:TS1-TS3-TS2

		Training	Testing
GDF		7.47	
R^2		0.880	0.876
Adjusted R^2		0.875	0.859
RMSE (kN)		36.6	42.7
ME (kN)		1.01	-12.6
V_{exp}/V_n	Average	1.01	0.960
	Min	0.480	0.481
	Max	1.85	1.48
	Std. Dev.	0.158	0.196
	5th Percentile	0.815	0.688

It was observed that neither of the MTs generated using Dataset VA were able to outperform the stepwise regressions generated using the same dataset, and the models generated using Dataset VA performed better than those generated using Dataset VC. For these reasons, it was decided that no MTs would be generated using Dataset VC.

5.4 Investigation on the Influence of Horizontal Reinforcement

As was discussed in Section 2.2.2.4, it is widely accepted that horizontal reinforcement contributes to shear strength (Matsumura, 1987, Tomaževič and Lutman, 1988; Voon and Ingham, 2006). Almost all the existing code- and research-based equations presented in Chapter 2 contain a term to account for this contribution. However, none of the models presented in the previous sections (5.3.1 to 5.3.4) include a term accounting for the area of either bond beam or joint reinforcement. Additional analysis was undertaken to investigate this issue and attempt to produce an equation that includes the contribution of horizontal reinforcement so that the performance could be compared with the other generated models.

This section differs from the rest of Section 5.3 in that the models presented are not all stepwise regressions; some of the models were multiple linear regressions using the MATLAB function

"fitlm". In addition, some of the models presented contain more than 6 terms, as it was not possible to obtain stepwise regressions that included a term with the area of horizontal reinforcement with fewer terms.

Due to the high number of models that were generated, not all the models that were generated in this stage of the analysis are presented. Focus is placed on those models which included some form of the horizontal reinforcement area. A few models which did not include any horizontal reinforcement term are also presented, to illustrate the reasoning behind the analysis steps.

5.4.1 First Expansion of Dataset VA - Dataset VAe

To create more candidate variables that included the area of horizontal reinforcement, three new input variables that combine the contribution of bond beam and joint reinforcement were added to Dataset VA to create Dataset VAe. This expansion also included the raw variables that related to the horizontal reinforcement. The added variables are shown in Table 5.48.

Table 5.48 - Variables added to create Dataset VAe

Total horizontal reinforcement	$A_h f_{yh}$, $A_{h,m} f_{yh}$, $A_{h,m2} f_{yh}$
Raw areas of horizontal reinforcement	A_{hbb} , $A_{hbb,m}$, $A_{hbb,m2}$, A_{hj} , $A_{hbb,bar}$, $A_{hj,bar}$

Several variables were also removed from the dataset to reduce noise cancellation. The variables considered as candidates for each model will be indicated along with the other details regarding how the models were generated.

5.4.1.1 VAe-rTS2

VAe-rTS2 was generated using the input variable candidates shown in Table 5.48 as well as those shown in Table 4.6. It should be noted that although a few raw variables are included in Table 5.48, this model was not generated using all of the raw variables included in Data Group RT.

VAe-rTS2 was generated using the p-value inclusion and exclusion thresholds shown in Table 5.49.

Table 5.49 - Inclusion and exclusion thresholds used to generate VAe-rTS2

	PEnter	PRemove
p-value threshold	0.02	0.021

The equation for VAe-rTS2 is given here as Equation (5.21).

$$V_n = 0.239P - 0.0571f_{block}(L_b t)v + 0.452f_{mortar}t_{fs}L_b + 0.0298f'_{m,eff}A_{net} + 0.426A_{vi}f_{yvi} - 0.348\frac{A_{vi,bar}f_{yvi}H}{s_{vi,max}} + 0.124A_{h,m}f_{yh} + 0.024\frac{VL}{M}\sqrt{f'_{m,eff}}A_{net} \quad (5.21)$$

Although this model contains a horizontal reinforcement term, it is a relatively complex model as it contains 8 terms, most of which are transformed variables. There are some signs of noise cancellation between the positive and negative A_{vi} terms ($A_{vi}f_{yvi}$ and $\frac{A_{vi,bar}f_{yvi}H}{s_{vi,max}}$) and an illogical negative coefficient appearing before the $f_{block}A_{net}$ term. It is not possible to remove these illogical relationships by adjusting the PEnter and PRemove thresholds without also removing the $A_{h,m}f_{yh}$ term, as this is the least significant variable in the model.

The performance indicators for VAe-rTS2 are shown in Table 5.50.

Table 5.50 - Performance indicators for VAe-rTS2

		Training	Testing
GDF		11.3	
R^2		0.918	0.900
Adjusted R^2		0.915	0.887
RMSE (kN)		30.2	36.5
ME (kN)		0.392	-3.4
V_{exp}/V_n	Average	1.01	0.989
	Min	0.529	0.658
	Max	1.91	1.47
	Std. Dev.	0.150	0.159
	5th Percentile	0.812	0.746

5.4.1.2 VAe-F2-TS3

The data used to generate this model is distinguished from Dataset VAe because several of the variables were removed, in an attempt to force a reduction in model noise. The variables that were not removed were selected based on the ones that were included in VAe-rTS2 through the stepwise selection procedure. None of the horizontal reinforcement terms were removed. The variables used as input candidates for VAe-F2-TS3 are shown in Table 5.51.

Table 5.51 - Input variable candidates used to generate VAe-F2-TS3

Mortar strength	$f_{mortar}t_{fs}L_b$
Effective prism strength	$f'_{m,eff}A_{net}$
Flexural reinforcement	$A_{vf}f_{yvf}$
	$A_{vf}f_{yvf}$ & $\rho_{vf} \leq 0.02\%$, $A_{vf}f_{yvf} + A_{vi}f_{yvi}$ & $\rho_{vf} + \rho_{vi} \leq 0.02\%$
Interior vertical reinforcement	$A_{vi}f_{yvi}$
Joint reinforcement	$A_{hj}f_{yhj}$, $\frac{A_{hj,bar}f_{yhj}L}{s_{h,ave}}$
Bond beam reinforcement	$A_{hbb}f_{yhbb}$, $\frac{A_{hbb,bar}f_{yhbb}L}{s_{h,ave}}$, $\frac{A_{hbb,bar}f_{yhbb}L}{s_{h,max}}$
	$A_{hbb,m}f_{yhbb}$, $A_{hbb,m2}f_{yhbb}$
Total horizontal reinforcement	A_hf_{yh} , $A_{h,m}f_{yh}$, $A_{h,m2}f_{yh}$
Axial load	P , $P * \frac{A_{net}}{A_{gross}}$
Inverse of shear span depth ratio	$\frac{VL}{M}A_{net}\sqrt{f'_{m,eff}}$

VAe-F2-TS3 was generated using the p-value inclusion and exclusion thresholds shown in Table 5.52.

Table 5.52 - Performance indicators for VAe-F2-TS3

	PEnter	PRemove
p-value threshold	0.1	0.2

The equation for VAe-F2-TS3 is given here as Equation (5.22).

$$V_n = 0.238P + 0.387f_{mortar}t_{fs}L_b + 0.0123f'_{m,eff}A_{net} + 0.181A_{vi}f_{yvi} + 0.0000741\frac{A_{hj,bar}f_{yhj}L}{s_{h,ave}} + 0.00293\frac{VL}{M}\sqrt{f'_{m,eff}}A_{net} \quad (5.22)$$

This equation is an improvement over the previous one, as it does not include any illogical relationships. In terms of horizontal reinforcement, it only includes a contribution from the joint reinforcement. The contribution of the horizontal reinforcement is still relatively low, however, as the maximum value of this term is 25.9 kN while the average is 3.5 kN for both training and testing data.

The performance indicators for VAe-F2-TS3 are shown in Table 5.53.

Table 5.53 - Performance indicators for VAe-F2-TS3

		Training	Testing
GDF		3.38	
R^2		0.846	0.889
Adjusted R^2		0.840	0.874
RMSE (kN)		56.6	49.5
ME (kN)		32.32	24.2
V_{exp}/V_n	Average	1.14	1.100
	Min	0.707	0.742
	Max	1.81	2.04
	Std. Dev.	0.205	0.213
	5th Percentile	0.891	0.874

In this case the GDF seems to underestimate the complexity of the model. This was taken into account in selection of the optimum models.

5.4.2 Forced Series - Dataset VAe

The next series of generated models is characterized by a great deal of forcing. The models in this section were not generated using stepwise regression; they were generated using an assumed set of input variables, similar to what has been done for many of the existing code- and research-based equations. Hence, the variables considered as candidates for input are no different from the variables included in the following models, and PEnter and PRemove thresholds were not used. The assumed input variable sets were chosen based on the variables that were selected by the stepwise variable selection procedure for VAe-rTS2.

Because the horizontal reinforcement term was relatively insignificant compared to the other input variables, the number of input candidates was reduced one at a time so that the relative explanatory power of the horizontal reinforcement term would gradually increase.

5.4.2.1 VAe-F3-TA

The input variables for VAe-F3-TA were selected by reducing Dataset VAe to the 5 most significant variables and adding the term $A_{h,mod}f_{yh}$. The equation for VAe-F3-TA is given here as Equation (5.23).

$$V_n = 0.249P + 0.41f_{mortar}t_{fs}L_b + 0.0114f'_{m,eff}A_{net} + 0.177A_{vi}f_{yvi} + 0.00281A_{h,m}f_{yh} + 0.0278\frac{VL}{M}\sqrt{f'_{m,eff}A_{net}} \quad (5.23)$$

The horizontal reinforcement term was assigned a very low coefficient; the maximum value of this term is 1.0 kN while the average is 0.2 kN for both training and testing data. The reason for this is that $A_{h,mod}f_{yh}$ explains little of the output variable that is not already explained by the other input variables. This is confirmed by performing a stepwise regression using the 6 variables from Equation (5.23) with PEnter=0.1 and PRemove = 0.2. The resulting model, VAe-F3-TS, contains all of the variables except for $A_{h,mod}f_{yh}$ and the coefficients change very little from those in VAe-F3-TA (Equation (5.24)).

$$V_n = 0.249P + 0.411f_{mortar}t_{fs}L_b + 0.0114f'_{m,eff}A_{net} + 0.177A_{vi}f_{yvi} + 0.0278\frac{VL}{M}\sqrt{f'_{m,eff}A_{net}} \quad (5.24)$$

The performance indicators for VAe-F3-TA are shown in Table 5.54.

Table 5.54 - Performance indicators for VAe-F3-TA

		Training	Testing
GDF		7.02	
R^2		0.878	0.897
Adjusted R^2		0.879	0.899
RMSE (kN)		36.8	37.4
ME (kN)		-1.07	-8.24
V_{exp}/V_n	Average	0.993	0.960
	Min	0.614	0.693
	Max	1.59	1.72
	Std. Dev.	0.170	0.188
	5th Percentile	0.784	0.755

5.4.2.2 VAe-F4-TA

The input variables for VAe-F4-TA were selected by reducing Dataset VAe to the 4 most significant variables and adding the term $A_{h,mod}f_{yh}$. The equation for VAe-F4-TA is given here as Equation (5.25).

$$V_n = 0.279P + 0.487f_{mortar}t_{fs}L_b + 0.195A_{vi}f_{yvi} + 0.0112A_{h,m}f_{yh} + 0.0289\frac{VL}{M}\sqrt{f'_{m,eff}}A_{net} \quad (5.25)$$

Reducing the number of input variables increased the significance of the horizontal reinforcement term slightly, however the coefficient for this term is still relatively low; the maximum value of this term is 3.8 kN while the average is 0.9 kN for both training and testing data.

The performance indicators for VAe-F4-TA are shown in Table 5.55.

Table 5.55 - Performance indicators for VAe-F4-TA

		Training	Testing
GDF		6.64	
R^2		0.869	0.881
Adjusted R^2		0.870	0.884
RMSE (kN)		38.1	39.8
ME (kN)		-0.262	-5.93
V_{exp}/V_n	Average	1.00	0.971
	Min	0.613	0.679
	Max	1.65	1.86
	Std. Dev.	0.178	0.205
	5th Percentile	0.773	0.763

5.4.2.3 VAe-F5-TA

The input variables for VAe-F5-TA were selected by reducing Dataset VAe to the 3 most significant variables and adding the term $A_{h,mod}f_{yh}$. The equation for VAe-F5-TA is given here as Equation (5.26).

$$V_n = 0.282P + 0.474f_{mortar}t_{fs}L_b + 0.0245A_{h,m}f_{yh} + 0.0404\frac{VL}{M}\sqrt{f'_{m,eff}}A_{net} \qquad (5.26)$$

Again, reducing the number of input variables increased the significance of the horizontal reinforcement term, however the coefficient for this term is still relatively low; the maximum value of this term is 8.4 kN while the average is 2.1 kN for both training and testing data.

The performance indicators for VAe-F5-TA are shown in Table 5.56.

Table 5.56 - Performance indicators for VAe-F5-TA

		Training	Testing
GDF		5.77	
R^2		0.854	0.868
Adjusted R^2		0.855	0.871
RMSE (kN)		40.3	41.4
ME (kN)		-0.186	-4.40
V_{exp}/V_n	Average	1.00	0.971
	Min	0.644	0.675
	Max	1.65	1.85
	Std. Dev.	0.185	0.207
	5th Percentile	0.752	0.748

5.4.2.4 VAe-F6-TA

The input variables for VAe-F6-TA were selected by reducing Dataset VAe to the 2 most significant variables and adding the term $A_{h,m}f_{yh}$ ($f'_{m,eff}A_{net}$ is more significant when the terms $f_{mortar}t_{fs}L_b$ and $\frac{VL}{M}\sqrt{f'_{m,eff}}A_{net}$ are not included). The equation for VAe-F6-TA is given here as Equation (5.27).

$$V_n = 0.233P + 0.0479f'_{m,eff}A_{net} + 0.225A_{h,m}f_{yh} \quad (5.27)$$

The contribution of the horizontal reinforcement term is more significant in this case; the maximum value of this term is 77.3 kN while the average is 18.9 kN for both training and testing data.

The performance indicators for VAe-F6-TA are shown in Table 5.57.

Table 5.57 - Performance indicators for VAe-F6-TA

		Training	Testing
GDF		2.44	
R^2		0.689	0.769
Adjusted R^2		0.692	0.774
RMSE (kN)		61.1	57.1
ME (kN)		6.59	-1.52
V_{exp}/V_n	Average	1.14	1.12
	Min	0.593	0.553
	Max	3.67	2.31
	Std. Dev.	0.466	0.460
	5th Percentile	0.713	0.676

5.4.3 Second Expansion of Dataset VA - Dataset VAee

To create more candidate variables that included the area of horizontal reinforcement, several new input variables that combine the contribution of bond beam and joint reinforcement were added to Dataset VA to create Dataset VAee. The added variables are shown in Table 5.58.

Table 5.58 - Variables added to create Dataset VAee

Total horizontal reinforcement	$A_h f_{yh}$, $A_{h,m} f_{yh}$, $A_{h,m2} f_{yh}$
Combined interior vertical and horizontal reinforcement	$A_{vi} f_{yvi} + A_{hbb} f_{yhbb}$, $A_{vi} f_{yvi} + A_{hj} f_{yhj}$
	$A_{vi} f_{yvi} + A_{hbb,m2} f_{yhbb}$, $A_{vi} f_{yvi} + A_{hbb,m} f_{yhbb}$
	$A_{vi} f_{yvi} + A_h f_{yh}$, $A_{vi} f_{yvi} + A_{h,m} f_{yhbb}$, $A_{vi} f_{yvi} + A_{h,m2} f_{yh}$
Individual horizontal bars at average/maximum spacings	$\frac{A_{h,bar} f_{yh}L}{s_{h,max}}$, $\frac{A_{h,bar} f_{yh}L}{s_{h,ave}}$, $\frac{A_{h,bar} f_{yh}H}{s_{h,max}}$, $\frac{A_{h,bar} f_{yh}H}{s_{h,ave}}$
	$\frac{A_{hbb,bar} f_{yhbb}H}{s_{h,max}}$, $\frac{A_{hbb,bar} f_{yhbb}H}{s_{h,ave}}$, $\frac{A_{hj,bar} f_{yhj}H}{s_{h,ave}}$

Several variables were also removed from the dataset to reduce noise cancellation. The variables considered as candidates for each model will be indicated along with the other details regarding how the models were generated.

5.4.3.1 VAee-TS3

VAee-TS3 was generated using the input variable candidates shown in Table 5.58 as well as those shown in Table 4.6. This model was generated using the p-value inclusion and exclusion thresholds shown in Table 5.59.

Table 5.59 - Inclusion and exclusion thresholds used to generate VAee-TS3

	PEnter	PRemove
p-value threshold	0.02	0.03

The equation for VAee-TS3 is given here as Equation (5.28).

$$\begin{aligned} V_n = {} & 0.244P - 0.0727f_{block}(L_b t)v + 0.472f_{mortar}t_{fs}L_b + 0.0242f'_{m,eff}A_{net} \\ & + 0.531\left(A_{vi}f_{yvi} + A_{h,m}f_{yh}\right) - 0.443\frac{A_{vi,bar}f_{yvi}H}{s_{vi,max}} \\ & - 0.000334\frac{A_{h,bar}f_{yh}L}{s_{h,max}} + 0.0483\frac{VL}{M}\sqrt{f'_{m,eff}}A_{net} \end{aligned} \tag{5.28}$$

This model shows several instances of illogical relationships and noise cancelation, however it is not possible to remove these issues by adjusting the PEnter and PRemove thresholds.

The performance indicators for VAee-TS3 are shown in Table 5.60.

Table 5.60 - Performance indicators for VAee-TS3

		Training	Testing
GDF		11.73	
R^2		0.921	0.879
Adjusted R^2		0.918	0.863
RMSE (kN)		29.6	39.9
ME (kN)		-0.051	-0.7
V_{exp}/V_n	Average	1.01	1.003
	Min	0.514	0.640
	Max	2.01	1.42
	Std. Dev.	0.152	0.171
	5th Percentile	0.813	0.729

5.4.3.2 VAee-F1-2-TS2

This model was generated using a great deal of forcing to reduce the model noise. The variables used as input candidates for VAee-F1-2-TS2 are shown in Table 5.61.

Table 5.61 - Input variable candidates used to generate VAee-F1-2-TS2

Axial load / Material strengths	P , $f_{mortar}t_{fs}L_b$, $f'_{m,eff}A_{net}$
Reinforcement / Shear span ratio	$A_{h,m}f_{yh}$, $A_{vi}f_{yvi} + A_{h,m}f_{yh}$, $\frac{VL}{M}\sqrt{f'_{m,eff}}A_{net}$

VAee-F1-2-TS2 was generated using the p-value inclusion and exclusion thresholds shown in Table 5.62.

Table 5.62 - Inclusion and exclusion thresholds used to generate VAee-F1-2-TS2

	PEnter	PRemove
p-value threshold	0.012	0.013

The equation for VAee-F1-2-TS2 is given here as Equation (5.29).

$$V_n = 0.245P + 0.389f_{mortar}t_{fs}L_b + 0.0118f'_{m,eff}A_{net} + 0.0854\left(A_{vi}f_{yvi} + A_{h,m}f_{yh}\right) + 0.0311\frac{VL}{M}\sqrt{f'_{m,eff}}A_{net} \quad (5.29)$$

This model was essentially forced to include the combined contribution of the interior vertical reinforcement and horizontal reinforcement, because no separate term was included to account for the interior vertical reinforcement. If the interior vertical reinforcement term $A_{vi}f_{yvi}$ is included, with PEnter=0.5 and PRemove=0.6, the resulting model is as shown in Equation (5.30).

$$V_n = 0.249P + 0.411f_{mortar}t_{fs}L_b + 0.0114f'_{m,eff}A_{net} + 0.177A_{vi}f_{yvi} + 0.0278\frac{VL}{M}\sqrt{f'_{m,eff}}A_{net} \quad (5.30)$$

Of course, sufficiently high values of PEnter and PRemove would lead to the inclusion of the horizontal reinforcement term. However, the coefficient for the horizontal reinforcement term would be very low, as was seen in Sections 5.4.2.1 to 5.4.2.4. Such a model was generated and is shown in Equation (5.31).

$$V_n = 0.249P + 0.410f_{mortar}t_{fs}L_b + 0.0114f'_{m,eff}A_{net} + 0.177A_{vi}f_{yvi} + 0.00281A_{h,m}f_{yh} + 0.0278\frac{VL}{M}\sqrt{f'_{m,eff}}A_{net} \quad (5.31)$$

The performance indicators for VAee-F1-2-TS2 are shown in Table 5.63.

Table 5.63 - Performance indicators for VAee-F1-2-TS2

		Training	Testing
GDF		6.58	
R^2		0.873	0.891
Adjusted R^2		0.874	0.894
RMSE (kN)		37.7	38.1
ME (kN)		-1.56	-7.59
V_{exp}/V_n	Average	0.990	0.959
	Min	0.622	0.643
	Max	1.63	1.75
	Std. Dev.	0.174	0.186
	5th Percentile	0.782	0.718

5.4.4 Raw Stepwise Models

A few stepwise models were generated using raw variables to evaluate the influence of the raw areas of horizontal steel on the performance of the generated models. The raw variables were expanded on with additional horizontal reinforcement terms, while other raw variables were removed to reduce model noise.

5.4.4.1 VAe-F1-RS1

The variables used as input candidates for VAe-F1-RS1 are shown in Table 5.64.

Table 5.64 - Input variable candidates used to generate VAe-F1-RS1

Geometric properties	H , H_{eff} , L , d , t , H_b , L_b , t_{fs}
Material strengths / Axial load	n_g , n_t , f_{block} , f_{mortar} , f_{grout} , f'_{mg} , f'_{mu} , P
Horizontal / Vertical Steel	A_{hbb} , $A_{hbb,m}$, $A_{hbb,m2}$, A_{hj} , A_{vi} , A_{vf}
	$s_{v,max}$, $s_{v,ave}$, $s_{h,max}$, $s_{h,ave}$
	$A_{hbb} + A_{hj}$, $A_{hbb,m} + A_{hj}$, $A_{hbb,m2} + A_{hj}$
	$A_h + A_{vi}$, $A_{h,m} + A_{vi}$, $A_{h,m2} + A_{vi}$

VAe-F1-RS1 was generated using the p-value inclusion and exclusion thresholds shown in Table 5.65.

Table 5.65 - Inclusion and exclusion thresholds used to generate VAe-F1-RS1

	PEnter	PRemove
p-value threshold	0.1	0.15

The equation for VAe-F1-RS1 is given here as Equation (5.32).

$$V_n = -0.022H + 0.285L - 0.25d - 1.24f_{block} + 6.29f_{mortar} + 0.0911A_{vi} + 0.288P \quad (5.32)$$

This model does not include any contribution from the horizontal reinforcement, and it contains some illogical relationships (negative coefficients for variables d and f_{block}). The performance indicators for VAe-F1-RS1 are shown in Table 5.66.

Table 5.66 - Performance indicators for VAe-F1-RS1

		Training	Testing
GDF		7.80	
R^2		0.888	0.891
Adjusted R^2		0.889	0.893
RMSE (kN)		35.2	39.3
ME (kN)		-0.71	-11.5
V_{exp}/V_n	Average	1.00	0.95
	Min	0.441	0.552
	Max	1.63	1.41
	Std. Dev.	0.149	0.179
	5th Percentile	0.798	0.751

5.4.4.2 VAe-F1-2-RS3

All of the variables shown in Table 5.64 were used as input candidates for VAe-F1-2-RS3 except for the variable A_{vi}, which was removed to force the model to use a horizontal reinforcement term.

VAe-F1-2-RS3 was generated using the p-value inclusion and exclusion thresholds shown in Table 5.67.

Table 5.67 - Inclusion and exclusion thresholds used to generate VAe-F1-2-RS3

	PEnter	PRemove
p-value threshold	0.005	0.007

The equation for VAe-F1-2-RS3 is given here as Equation (5.33).

$$V_n = -0.0279H + 0.0386L + 6.00f_{mortar} + 0.0475(A_{vi} + A_h) + 0.289P \quad (5.33)$$

The performance indicators for VAe-F1-2-RS3 are shown in Table 5.68.

Table 5.68 - Performance indicators for VAe-F1-2-RS3

		Training	Testing
GDF		7.00	
R^2		0.875	0.896
Adjusted R^2		0.874	0.894
RMSE (kN)		37.1	37.7
ME (kN)		0.0283	0.0336
V_{exp}/V_n	Average	1.00	0.952
	Min	0.496	0.612
	Max	1.57	1.47
	Std. Dev.	0.162	0.165
	5th Percentile	0.773	0.676

6 DISCUSSION

6.1 Introduction

In this chapter, the best models are selected from those that were generated in Chapter 5. The proposed models are validated, and model checks are performed to ensure that the assumptions of the OLS regression method are satisfied. The proposed models are compared against the existing code- and research-based shear strength expressions that were introduced in Chapter 2. The performance of the proposed models is evaluated with the reduction factors from CSA S304-14

applied and compared with that of the CSA shear strength equation. Finally, observations are made regarding the generated models and the proposed models in particular.

6.2 Comparison of Generated Models

To assist with the selection of proposed models, error plots were produced for both Dataset VA and Dataset VC that compare the estimated variance and bias of the generated models according to model complexity. The estimated variance and bias are taken as the RMSE and ME, respectively, both calculated based on testing data. Model complexity is estimated using GDF.

Note that the models which were identified in Chapter 5 as including illogical variable relationships were not included in the error plots, to ensure that an illogical model would not be selected as an optimum model.

6.2.1 Dataset VA

Models that were generated using Dataset VA, which includes all of the raw variables, were grouped together for comparison purposes.

As discussed in Section 2.4.3 and illustrated in Figure 2.17, there is a trade-off between bias, variance and complexity. Bias generally decreases with increasing model complexity, while variance generally increases with increasing model complexity. These trends can be observed in Figure 6.1 and Figure 6.2, respectively.

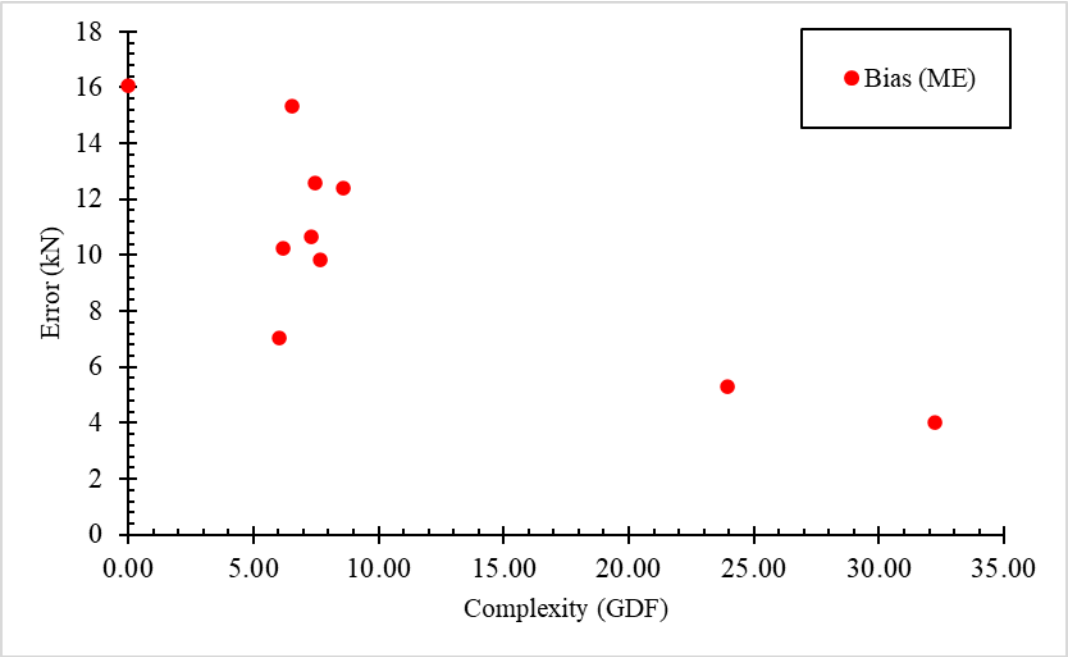

Figure 6.1 - Bias as a function of complexity for models generated using Dataset VA

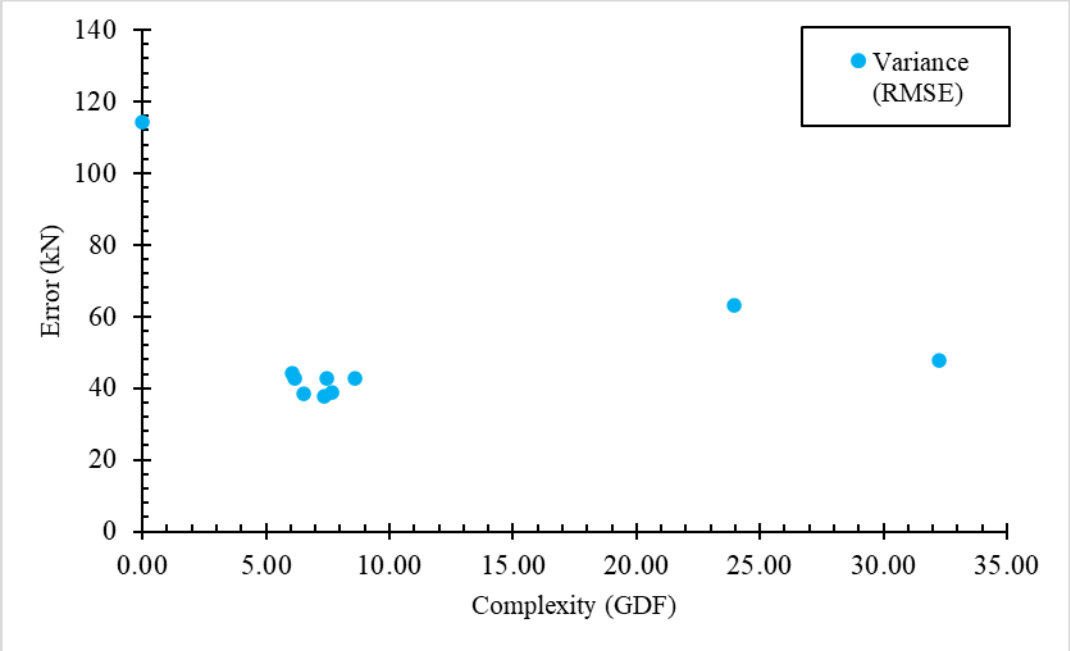

Figure 6.2 - Variance as a function of complexity for models generated using Dataset VA

In both figures, the point with a GDF of 0 represents VA-N, the naïve predictor generated using Dataset VA. This point appears to be an outlier in Figure 6.2, because VA-N had very high values of RMSE despite being the simplest possible prediction model. VA-RTA was not included in any of the plots, as the values of RMSE and ME were so high that including it changed the scale of the plots so significantly as to make it difficult to see the trends of the other models. VA-RA and VA-TA are represented by the two points on the right side of the plots.

In Figure 6.3, bias and variance are combined by adding RMSE and ME to obtain an estimate of total model error and determine which models minimize both RMSE and ME.

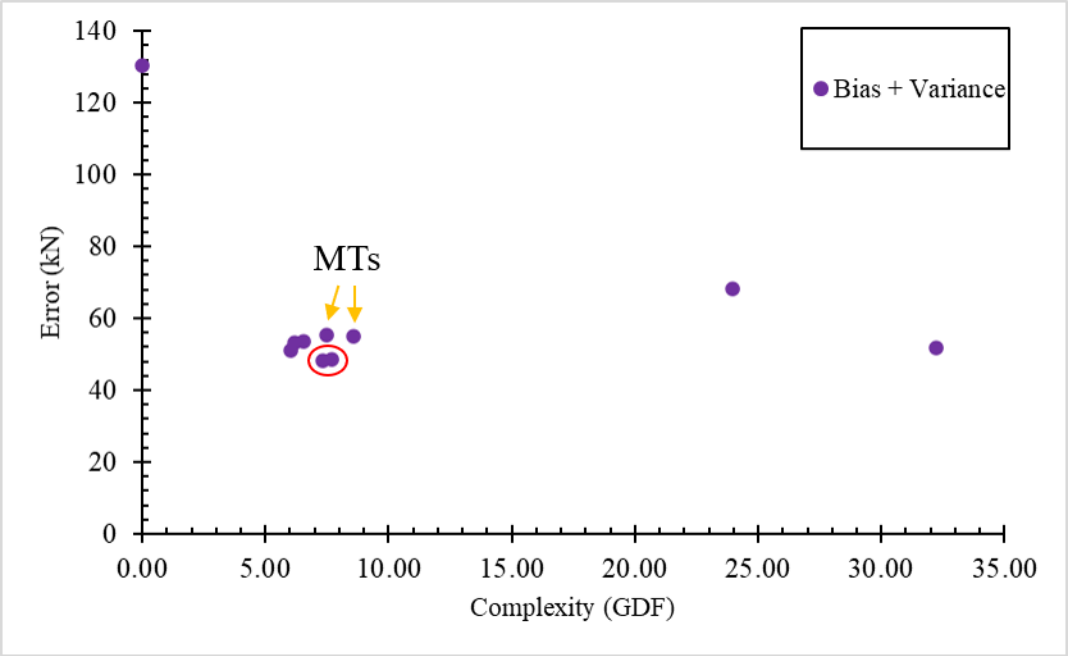

Figure 6.3 - Estimated total error as a function of complexity for models generated using Dataset VA

The circled models are those which minimize bias and variance: VA-RS2 and VA-TS5.

The models indicated by the arrows are the model trees MT-VA-rt3:RTS1-TS3-RS3 and MT-VA-rt3:TS1-TS3-TS2. As shown in Figure 6.3, both MTs perform well relative to the other generated

models, however they are outperformed slightly by VA-RS2 and VA-TS5. It is possible that the benefits of using MTs would be more visible with a larger amount of data, as the MT structures would be less constrained by the imposed minimum leaf number. There is still value in comparing the performance of MT-VA-rt3:RTS1-TS3-RS3 and MT-VA-rt3:TS1-TS3-TS2 to that of the existing code- and research-based shear strength expressions to evaluate the potential of this modeling method.

6.2.2 Datasets VC and VCe

Datasets VC differs from Dataset VA in that it does not include the variables f_{block}, f_{mortar}, and f_{grout}. Because Dataset VCe is the extended version of Dataset VC, the models generated from both versions of Dataset VC are grouped together in this section.

In the following plots, VA-RA, VA-TA and both models trees generated using Dataset VA are included despite not having been generated using Dataset VC, for comparison purposes. Figure 6.4 shows the downward trend in bias with increasing model complexity and Figure 6.5 shows the upward trend in variance with increasing model complexity.

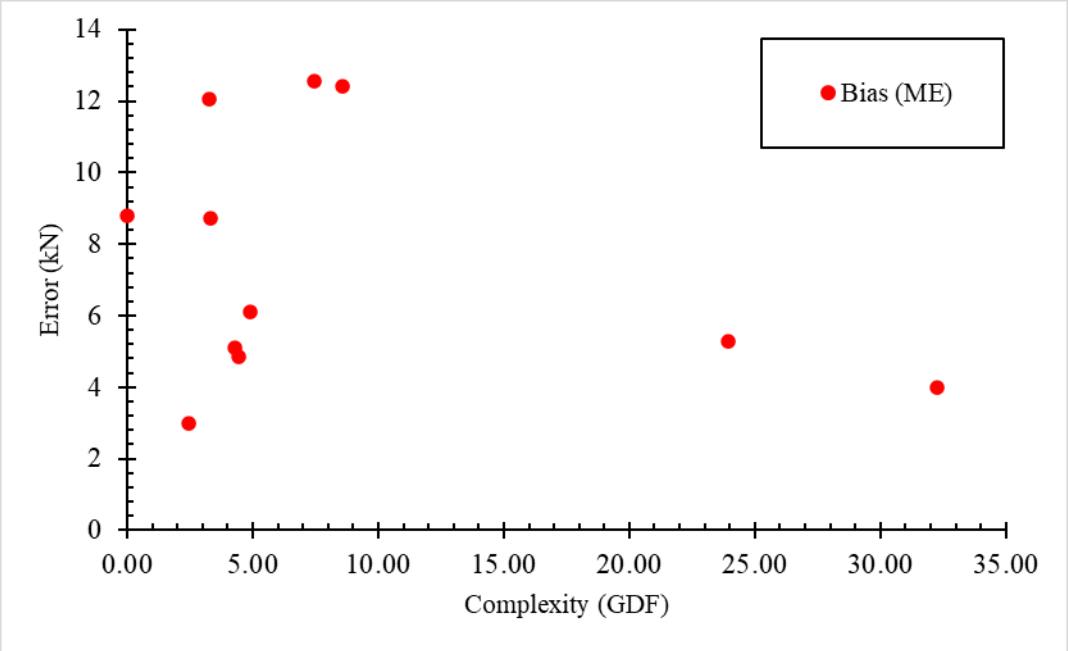

Figure 6.4 - Bias as a function of complexity for models generated using Datasets VC & VCe

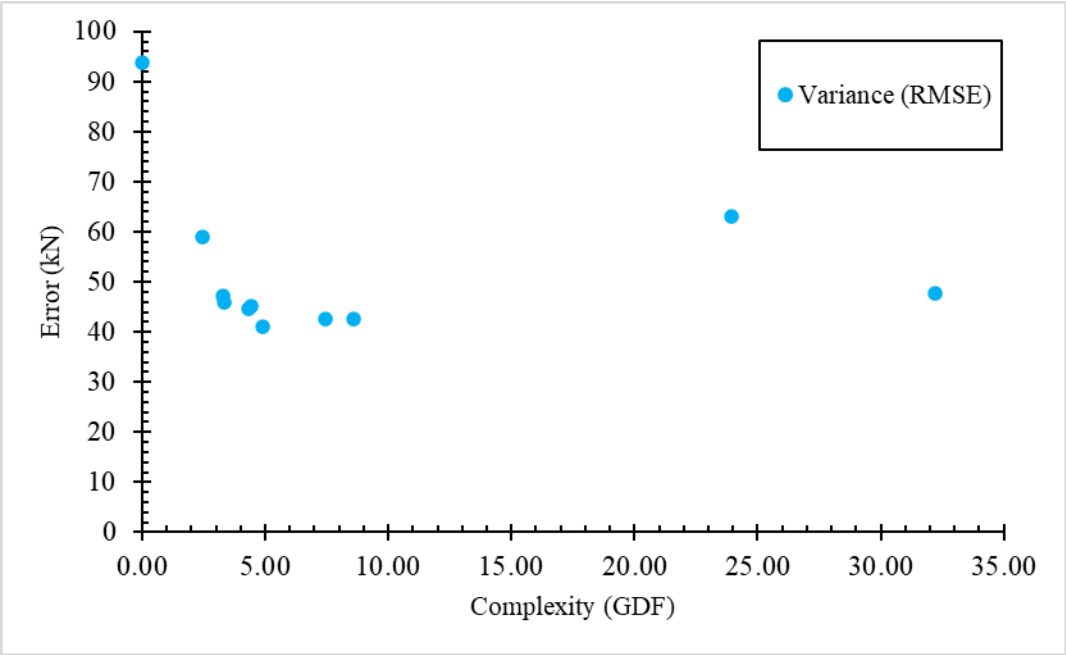

Figure 6.5 - Variance as a function of complexity for models generated using Datasets VC and VCe

As with Dataset VA, the models generated using Dataset VC show the same general trends in bias and variance. In both figures, the point with a GDF of 0 represents VC-N, the naïve predictor generated using Dataset VC. As was the case with VA-N in Figure 6.2, this point appears to be an outlier in Figure 6.5 because VC-N had very high values of RMSE despite being the simplest possible prediction model.

In Figure 6.6, bias and variance are combined by adding RMSE and ME to obtain an estimate of total model error and determine which models minimize both RMSE and ME.

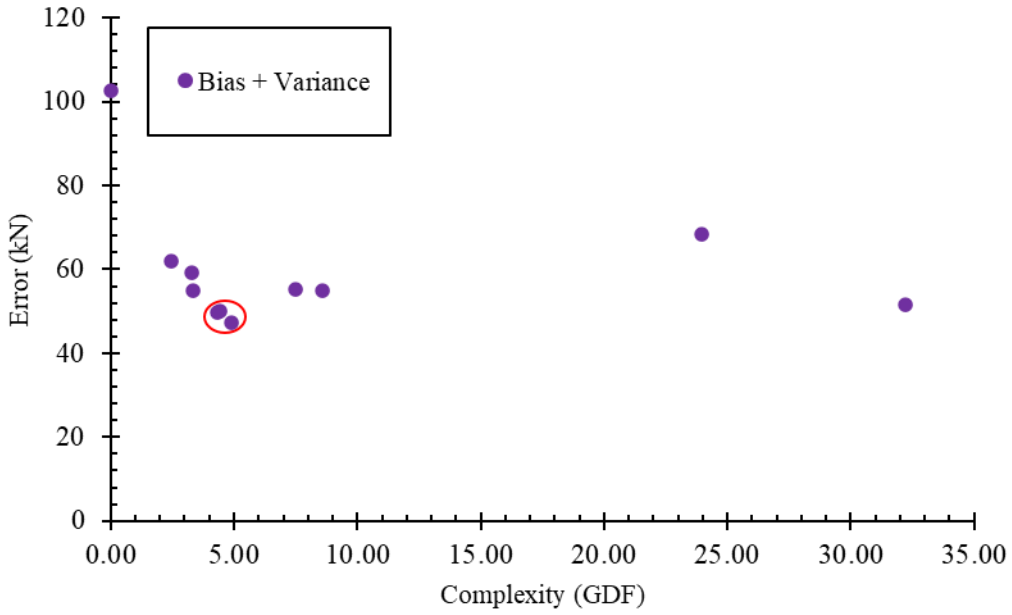

Figure 6.6 - Estimated total error as a function of complexity for models generated using Datasets VC and VCe

The circled models are those which minimize bias and variance: VC-RS3, VCe-TS2 and VCe-TS3.

VCe-TS2 and VCe-TS3 are similar in terms of model form and performance (Sections 5.3.3.2 and 5.3.3.3). Both equations include the same 3 terms, except that VCe-TS2 includes an additional term, $A_{vf} f_{yvf}$. All the performance indicators were close for both equations. However, VCe-TS2 is clearly the most complex of the two models, and the small increase in model precision is not enough to justify the increase in complexity.

6.2.3 Datasets VAe and VAee

Datasets VAe and VAee are the extended versions of Dataset VA that were used to investigate the influence of horizontal reinforcement on shear strength (Section 5.4). Because the horizontal reinforcement terms would not normally have appeared in the models based on the significance of

the variables, the models generated using Datasets VAe and VAee are not considered to be optimum models. They are investigated in this section for comparison purposes only.

In the following plots, VA-N, VA-RA, and VA-TA are included for comparison purposes. Figure 6.7 shows the downward trend in bias with increasing model complexity and Figure 6.8 shows the upward trend in variance with increasing model complexity.

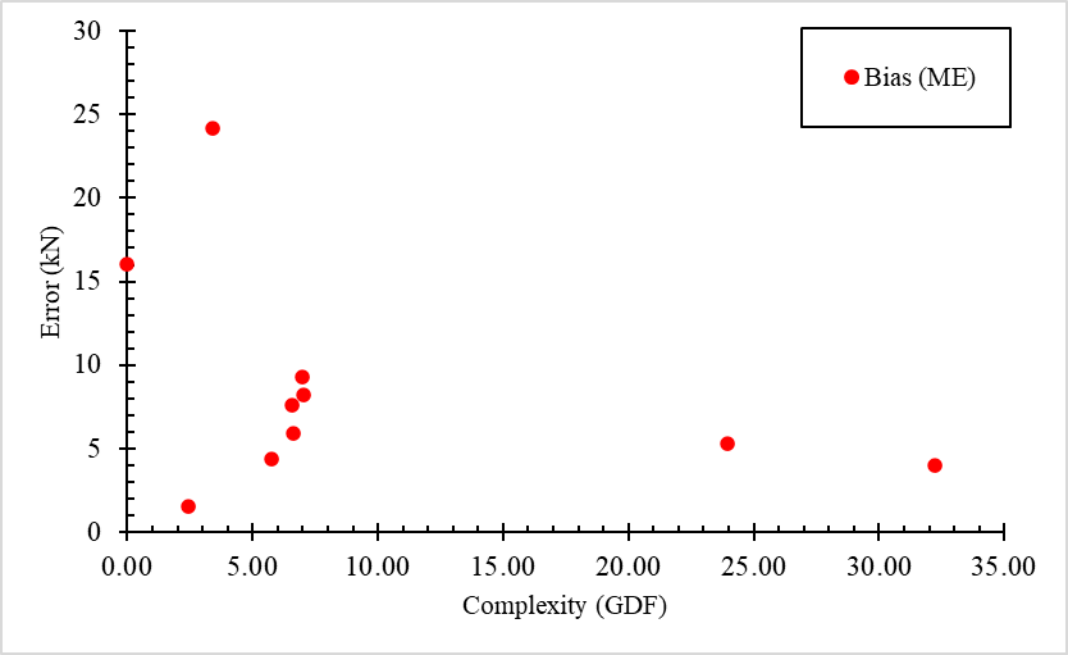

Figure 6.7 - Bias as a function of complexity for models generated using Datasets VAe & VAee

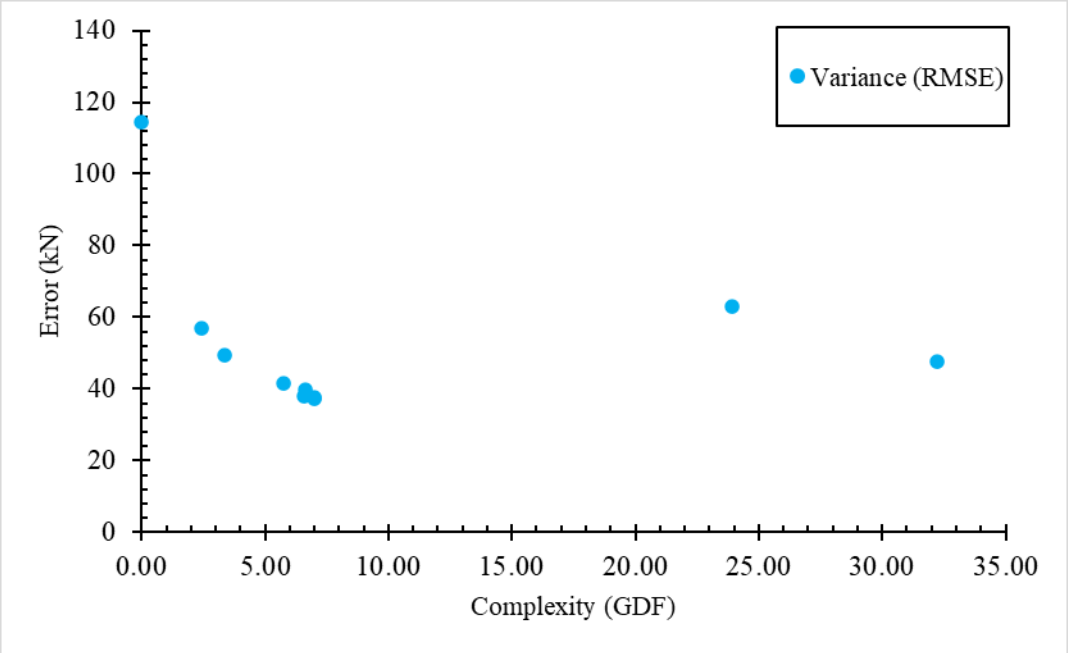

Figure 6.8 - Variance as a function of complexity for models generated using Datasets VAe & VAee

As with the other datasets, the models generated using Dataset VAe show the same downward trend in bias. The upward trend in variance is less visible, partly because of a few outliers. The point with a GDF of 0 represents VA-N, the naïve predictor generated using Dataset VA. As was the case in Figure 6.2, this point appears to be an outlier in Figure 6.8 because VA-N had very high values of RMSE despite being the simplest possible prediction model. It was also noted in Chapter 5 that the model VAe-F2-TS3 had a deceptively low value of GDF (3.38). The complexity of this model would be more accurately reflected in a GDF value closer to 7.

In Figure 6.9, bias and variance are combined by adding RMSE and ME to obtain an estimate of total model error and determine which models minimize both RMSE and ME.

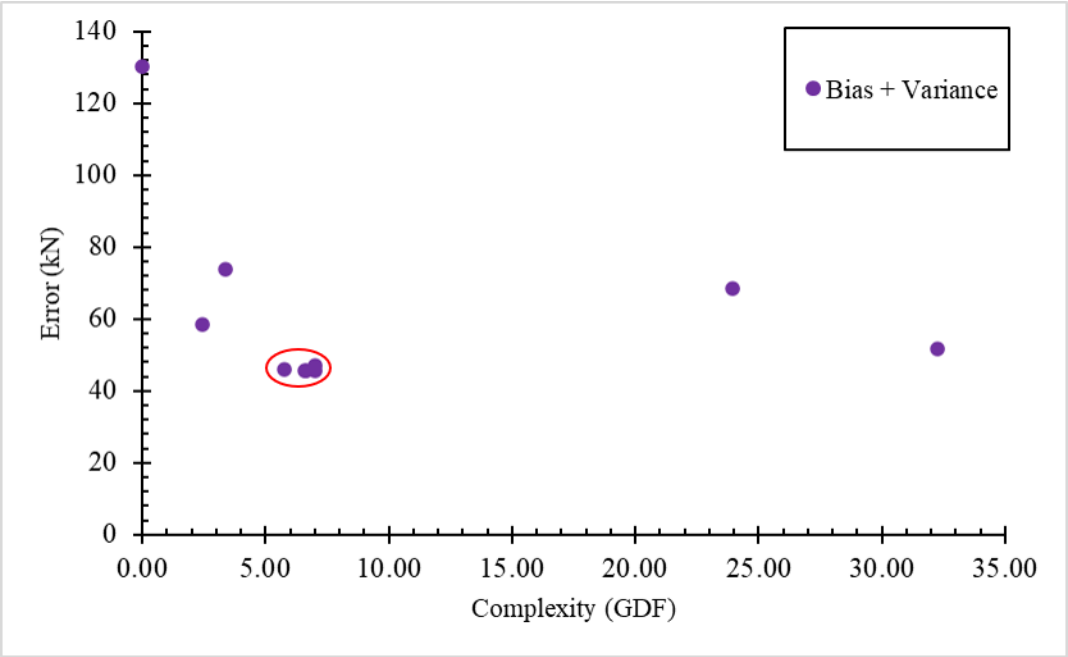

Figure 6.9 - Estimated total error as a function of complexity for models generated using Datasets VAe & VAee

In Figure 6.9, the circled models are those which minimize bias and variance: VAe-F3-TA, VAe-F4-TA, VAe-F5-TA, VAee-F1-2-TS2 and VAe-F1-2-RS3. As noted previously, none of these models is an optimum model. However, further investigation of some of these models will be performed for comparison purposes. The first three of the five models include only a very small contribution from the horizontal reinforcement, but the goal of this step of the analysis was to develop models that include a significant contribution from the horizontal reinforcement. For this reason, only VAee-F1-2-TS2 and VAe-F1-2-RS3 are investigated further in the following section.

6.2.4 Model Validation and Selection of Proposed Models

Using data for testing from the same studies used to train the models decreases the amount of variation between the testing and training sets. The method used to test the generated models is not the ideal way to illustrate the ability of the models ability to generalize to new data, however

the limited amount of data available is not conducive to reserving entire studies for testing purposes.

To further validate the selected models, they were tested using the experimental results of two walls (A2 and B2) tested by Ba Rahim (2020). Both walls were cantilevered and experienced a predominantly shear failure. The preliminary data from Ba Rahim (2020) is shown in Table 6.1.

Table 6.1 - Properties of walls tested by Ba Rahim (2020)

Variable	A2 & B2	Variable	A2	B2
H (mm)	2600	A_{vi} (mm^2)	200	
H_{eff} (mm)	2850†	$A_{vi,bar}$ (mm^2)	200	
L (mm)	2600	ρ_{vi}	0.000405	
H/L	1.00	A_{vf} (mm^2)	400	
t (mm)	190	$A_{vf,bar}$ (mm^2)	200	
H_b (mm)	190	ρ_{vf}	0.000810	
L_b (mm)	390	f_{yvi} (MPa)	400	
t_{fs} (mm)	32	f_{yvf} (MPa)	400	
n_g	3	$s_{v,max}$ (mm)	1200	
n_t	13	$s_{v,ave}$ (mm)	1200	
A_{net} (mm^2)	240110	A_{hbb} (mm^2)	300	100
A_{net}/A_{gross}	0.486	$A_{hbb,m}$ (mm^2)	300	100
f_{block} (MPa)	17.5*	$A_{hbb,m2}$ (mm^2)	200	0
f_{mortar} (MPa)	10*	$A_{hbb,bar}$ (mm^2)	100	100
f_{grout} (MPa)	27.5*	ρ_{hbb}	0.000607	0.000202
ν	0.486	A_{hj} (mm^2)	0	126
f'_{mg} (MPa)	16.8‡	$A_{hj,bar}$ (mm^2)	0	21
f'_{mu} (MPa)	20.2	ρ_{hj}	0	0.000255
$f'_{m,eff}$ (MPa)	19.4	f_{ybb} (MPa)	400	400
P (kN)	960†	f_{yj} (MPa)	-	530
σ_{gross} (MPa)	1.94	$s_{h,max}$ (mm)	1200	2400
σ_{net} (MPa)	4.00	$s_{h,ave}$ (mm)	1000	400
		V_{exp} (kN)	423‡	425‡

*taken as the average of the strength range provided by Ba Rahim (2020)
†exceeds the maximum unscaled value recorded in Dataset VA
‡exceeds the maximum unscaled value recorded in both Dataset VA and Dataset VC

In Table 6.1, the $s_{h,max}$ value given for wall B2 is the spacing of the single bond beam, since this wall contained both bond beam and joint reinforcement. A few of the values (H_{eff}, f'_{mg}, P and V_{exp}) exceeded the range of unscaled data used to train the models (Table 4.10), however none of them were greatly in excess of the appropriate ranges.

The estimates calculated using the models are compared with the observed shear strength for both walls in Table 6.2.

Table 6.2 - Performance of selected models on walls tested by Ba Rahim (2020)

Wall / Model	A2		B2	
	V_n (kN)	V_{exp}/V_n	V_n (kN)	V_{exp}/V_n
VA-RS2	390.1	1.09	390.1	1.09
VA-TS5	409.3	1.03	409.3	1.04
MT-VA-rt3:RTS1-TS3-RS3	521.6	0.812	559.5	0.760
MT-VA-rt3:TS1-TS3-TS2	428.3	0.988	428.3	0.993
VC-RS3	411.7	1.03	411.7	1.03
VCe-TS2	232.3	1.82	232.3	1.83
VCe-TS3	208.3	2.03	208.3	2.04
VAee-F1-2-TS2	385.9	1.10	384.8	1.10
VAe-F1-2-RS3	365.3	1.16	365.3	1.16
Observed Shear Strength, V_{exp} (kN)	**423.3**	**-**	**425.1**	**-**

It is observed that the nominal shear strength values determined using VCe-TS2 and VCe-TS3 were overly conservative for both walls. As discussed previously, VAee-F1-2-TS2 and VAe-F1-2-RS3 are not considered to be optimum models. Based on these results, models VA-RS2, VA-TS5, MT-VA-rt3:RTS1-TS3-RS3, MT-VA-rt3:TS1-TS3-TS2 and VC-RS3 were selected as the proposed models.

6.2.5 Model Verification

The assumptions used in modeling listed in Section 2.4.6 were verified as described in the following sections.

6.2.5.1 Checking for Homoscedasticity

To verify that the variance of the error is constant, residual plots were generated for each of the proposed models (Figures 6.10 to 6.14).

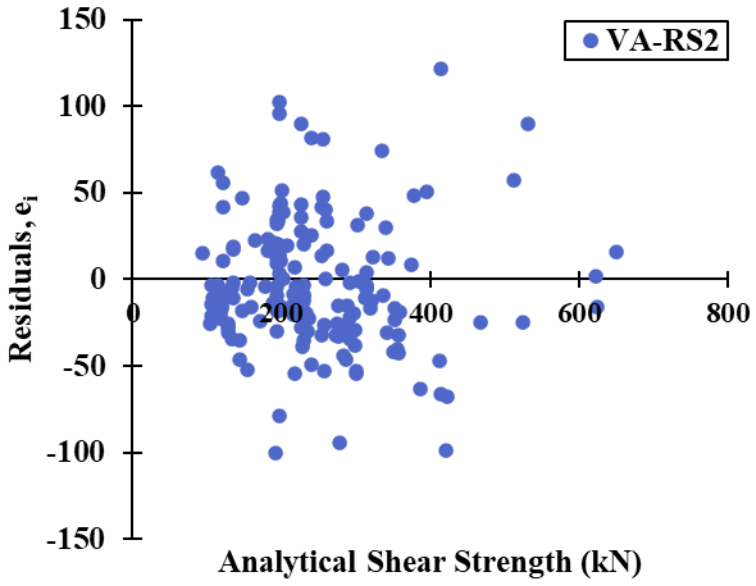

Figure 6.10 - Residual plot for VA-RS2

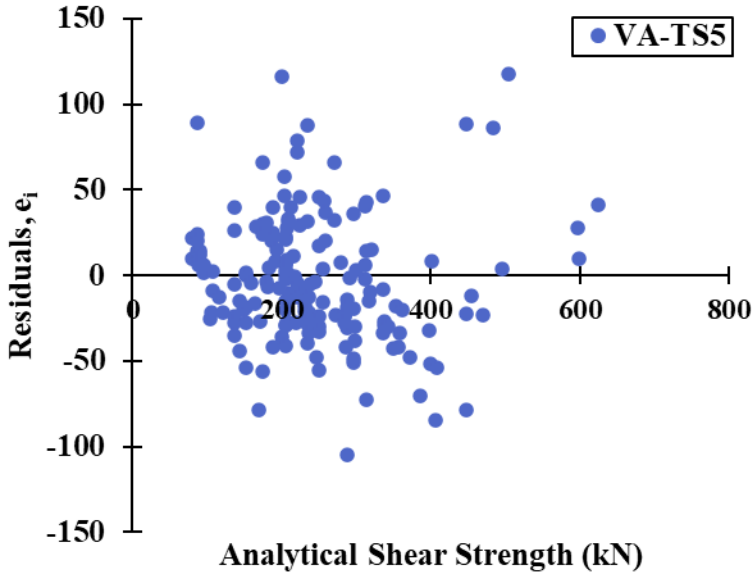

Figure 6.11 - Residual plot for VA-TS5

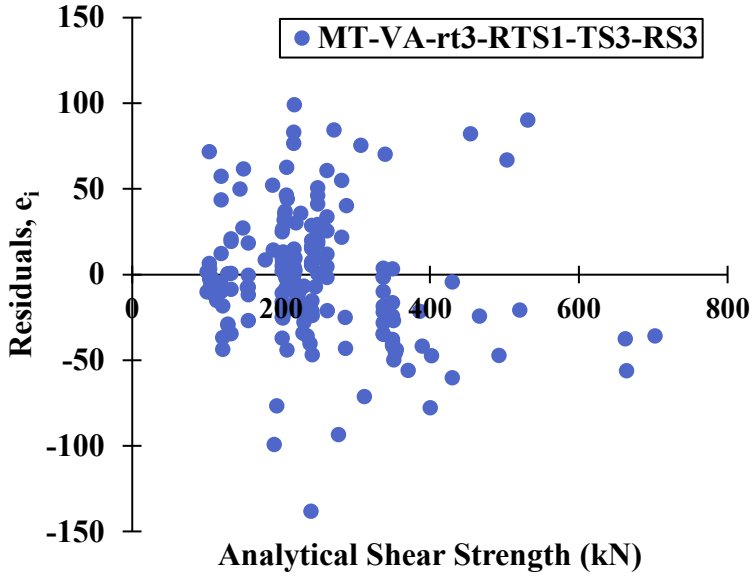

Figure 6.12 - Residual plot for MT-VA-rt3-RTS1-TS3-RS3

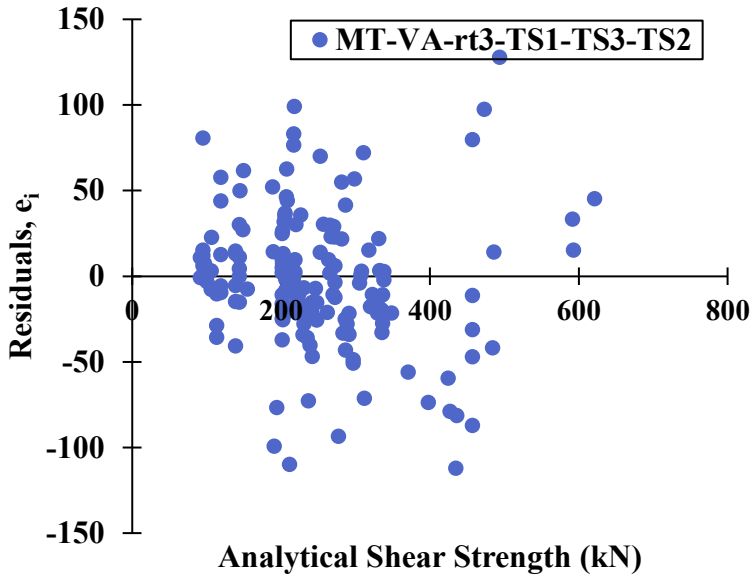

Figure 6.13 - Residual plot for MT-VA-rt3-TS1-TS3-RS3

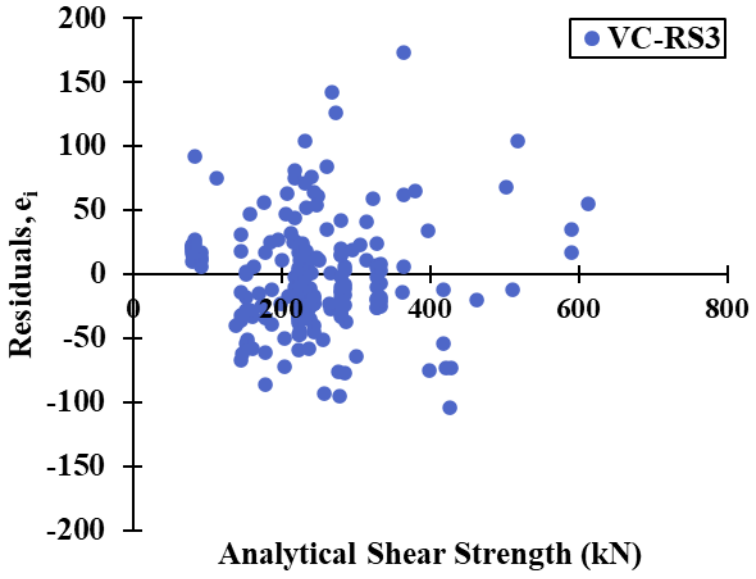

Figure 6.14 - Residual plot for VC-RS3

These plots show that the proposed models demonstrate homoscedasticity, meaning that the variance of the error is constant, as assumed.

6.2.5.2 Checking for Multicollinearity

The OLS regressions used for testing were generated using the full datasets (without dividing into training and testing data). For MTs, one OLS regression was generated for each of the branches for VIF testing. The VIF test results for each of the investigated models are shown in Table 6.3 to Table 6.7.

Table 6.3 - VIF test results for VA-RS2

Variable	VIF
H	2.03
L	3.29
f_{mortar}	1.68
A_{vi}	2.12
P	2.30

Table 6.4 - VIF test results for VA-TS5

Variable	VIF
P	2.05
$f_{mortar}t_{fs}L_b$	2.37
$\sqrt{f_{mortar}}t_{fs}L$	2.14
$A_{vi}f_{yvi}$	1.99

Table 6.5 - VIF test results for MT-VA-rt3-RTS1-TS3-RS3

Branch 1		Branch 2		Branch 3	
Variable	VIF	Variable	VIF	Variable	VIF
t	1.12	$\sqrt{f_{mortar}}t_{fs}L$	1.02	f_{ybb}	3.27
$\sqrt{f_{mortar}}t_{fs}L$	1.12	$P\frac{A_{net}}{A_{gross}}$	1.02	$s_{h,ave}$	3.39
				P	1.10

Table 6.6 - VIF test results for MT-VA-rt3-TS1-TS3-RS3

Branch 1		Branch 2		Branch 3	
Variable	VIF	Variable	VIF	Variable	VIF
$\sqrt{f_{mortar}}t_{fs}L$	1.00	$\sqrt{f_{mortar}}t_{fs}L$	1.02	P	1.00
$f'_{mu}t_{fs}(1000mm)\left(1-\frac{n_g}{n_t}\right)$	1.00	$P\frac{A_{net}}{A_{gross}}$	1.02	$\sqrt{f_{mortar}}t_{fs}L$	1.00

Table 6.7 - VIF test results for VC-RS3

Variable	VIF
L	1.84
f'_{mg}	1.34
$A_{vf,bar}$	2.40
$s_{v,ave}$	2.56
P	1.54

Because all the VIF values are relatively low and not in excess of 10, there is no significant multicollinearity in the proposed models, and the models satisfy the assumption of no perfect linear dependence between input variables. This is expected, as stepwise regression is designed to remove multicollinearities (Mohsenijam, 2019).

6.2.5.3 Checking for Normality of Error

Mohsenijam (2019) stated that the normality assumption is critical when the sample size is small (less than 100 observations). Because there is sufficient data in both datasets used to generate the models, checking the normality of the error term can be neglected.

6.2.6 Performance of Proposed Models

The performance of the proposed models, based on testing data, is compared in Table 6.8.

Table 6.8 - Performance of proposed models

Model	RMSE (kN)	ME (kN)	Average V_{exp}/V_n	Std. dev. V_{exp}/V_n
VA-RS2	37.6	-10.6	0.953	0.179
VA-TS5	38.9	-9.83	0.970	0.187
MT-VA-rt3:RTS1-TS3-RS3	42.7	-12.4	0.956	0.197
MT-VA-rt3:TS1-TS3-TS2	42.7	-12.6	0.960	0.196
VC-RS3	41.1	-6.10	1.00	0.231

Because neither VCe-TS2 nor VCe-TS3 had an acceptable performance when tested using the data from Ba Rahim (2020), no equation with only conventional variables and consistent units is provided.

6.2.7 Calculation Examples

To illustrate how the stepwise regressions and MTs are to be used in calculations, as well as how units should be handled for RS and TS models, the following calculation examples are provided.

6.2.7.1 Meli et al. (1968) Wall 309

The properties of “Muro 309”, which was tested as a cantilever wall by Meli et al. (1968), are provided in Table 6.9.

Table 6.9 - Selected properties of Muro 309

H (mm)	2650	A_{vi} (mm^2)	213
L (mm)	3200	$A_{vf,bar}$ (mm^2)	127
t (mm)	150	f_{yvi} (MPa)	245
L_b (mm)	390*	f_{yvf} (MPa)	245
t_{fs} (mm)	25.4*	$s_{v,ave}$ (mm)	650
n_g	7	f_{ybb} (MPa)	-
n_t	16	$s_{h,ave}$ (mm)	410
A_{net} (mm^2)	297968*	ν	0.57
f_{mortar} (MPa)	25.8	f'_{mg} (MPa)	11.8*
f_{grout} (MPa)	22.0	f'_{mu} (MPa)	9.66*
V_{exp} (kN)	189.0*	P (kN)	0

*assumed/calculated values

The shear strength estimation according to VA-RS2 is as shown in Equations (4.1) to (6.3).

$$V_n = -0.0205H + 0.0337L + 6.00f_{mortar} + 0.0917A_{vi} + 0.289P \tag{6.1}$$

$$V_n = -0.0205 * 2650 + 0.0337 * 3200 + 6 * 25.8 + 0.0917 * 213 + 0.289 * 0 \tag{6.2}$$

$$V_n = -54.3 + 107.8 + 154.8 + 19.5 + 0 = 227.8\text{kN} \tag{6.3}$$

The shear strength estimation according to VA-TS5 is as shown in Equations (5.6) to (6.6).

$$V_n = 0.296P + 0.255f_{mortar}t_{fs}L_b + 0.291\sqrt{f_{mortar}}t_{fs}L + 0.209A_{vi}f_{yvi} \tag{6.4}$$

$$V_n = 0.296 * 0 + 0.255(25.8 * 25.4 * 390)\text{N} + 0.291\left(\sqrt{25.8} * 25.4 * 3200\right)\text{N} + 0.209(213 * 245)\text{N} \tag{6.5}$$

$$V_n = 0 + 65.2 + 120 + 10.9 = 196.2\text{kN} \tag{6.6}$$

The shear strength estimation according to VC-RS3 is as shown in Equations (5.8) to (6.9).

$$V_n = 0.0568L + 5.18f'_{mg} + 0.175A_{vf,bar} - 0.0657s_{v,ave} + 0.23P \tag{6.7}$$

$$V_n = 0.0568 * 3200 + 5.18 * 11.8 + 0.175 * 127 - 0.0657 * 650 + 0.23 * 0 \quad (6.8)$$

$$V_n = 181.8 + 65.3 + 22.2 - 42.7 + 0 = 222.4\text{kN} \quad (6.9)$$

The shear strength is estimated according to MT-VA-rt3:RTS1-TS3-RS3 by first determining which branch of the tree to use (Equation (5.19)).

$$V_n = \begin{cases} 0.167t + 0.668\sqrt{f_{mortar}}t_{fs}L & \text{if } P \leq 450 \;\&\; f_{grout}A_{cell}n_g \leq 1000 \\ 0.501\sqrt{f_{mortar}}t_{fs}L + 0.519P\dfrac{A_{net}}{A_{gross}} & \text{if } P \leq 450 \;\&\; f_{grout}A_{cell}n_g > 1000 \\ 0.461f_{ybb} - 0.0631s_{h,ave} + 0.417P & \text{if } P > 450 \end{cases} \quad (6.10)$$

Because $P < 450$, it is necessary to determine the value of $f_{grout}A_{cell}n_g$ from Equation (6.11).

$$f_{grout}A_{cell}n_g = f_{grout}\left(L_b t\frac{1-v}{2}\right)n_g = \left[22.0\left(390 * 150 * \frac{1-0.57}{2}\right)7\right]\text{N} = 1937\text{kN} \quad (6.11)$$

Because $f_{grout}A_{cell}n_g > 1000$, the shear strength is estimated as shown in Equations (6.12) and (6.13).

$$V_n = 0.501\sqrt{f_{mortar}}t_{fs}L + 0.519P\frac{A_{net}}{A_{gross}} \quad (6.12)$$

$$V_n = 0.501\left(\sqrt{25.8} * 25.4 * 3200\right)\text{N} + 0.519(0) = 206.8\text{kN} \quad (6.13)$$

The branching of MT-VA-rt3:TS1-TS3-TS2 is the same as that of the previous MT, so the middle branch is used again to estimate the shear strength (Equation (5.20)).

$$V_n = \begin{cases} 0.55\sqrt{f_{mortar}}t_{fs}L + 0.205f'_{mu}t_{fs}(1000mm)\left(1-\frac{n_g}{n_t}\right) & \text{if } P \le 450 \;\&\; f_{grout}A_{cell}n_g \le 1000 \\ 0.501\sqrt{f_{mortar}}t_{fs}L + 0.519P\frac{A_{net}}{A_{gross}} & \text{if } P \le 450 \;\&\; f_{grout}A_{cell}n_g > 1000 \\ 0.311P + 0.493\sqrt{f_{mortar}}t_{fs}L & \text{if } P > 450 \end{cases} \quad (6.14)$$

The middle branches of both MTs are identical, such that the shear strength estimation according to MT-VA-rt3:TS1-TS3-TS2 is as shown in Equations (6.12) and (6.13).

6.2.7.2 Rizaee (2015) Wall 2-A

The properties of "Wall 2-A", which was tested under double curvature by Rizaee (2015), are provided in Table 6.10.

Table 6.10 - Selected properties of Wall 2-A

H (mm)	1800	A_{vi} (mm^2)	200
L (mm)	1800	$A_{vf,bar}$ (mm^2)	200
t (mm)	190	f_{yvi} (MPa)	448
L_b (mm)	390	f_{yvf} (MPa)	448
t_{fs} (mm)	37.75*	$s_{v,ave}$ (mm)	800
n_g	3	f_{ybb} (MPa)	448
n_t	9	$s_{h,ave}$ (mm)	850
A_{net} (mm^2)	202882.5*	ν	51.8*
f_{mortar} (MPa)	22.1	f'_{mg} (MPa)	10.3*
f_{grout} (MPa)	25.7	f'_{mu} (MPa)	16.5*
V_{exp} (kN)	302*	P (kN)	476*

*assumed/calculated values

The shear strength estimation according to VA-RS2 is as shown in Equations (6.15) to (6.17).

$$V_n = -0.0205H + 0.0337L + 6.00f_{mortar} + 0.0917A_{vi} + 0.289P \quad (6.15)$$

$$V_n = -0.0205 * 1800 + 0.0337 * 1800 + 6 * 22.1 + 0.0917 * 200 + 0.289 * 476 \quad (6.16)$$

$$V_n = -36.9 + 60.7 + 132.6 + 18.3 + 137.6 = 312.2\text{kN} \quad (6.17)$$

The shear strength estimation according to VA-TS5 is as shown in Equations (6.18) to (6.20).

$$V_n = 0.296P + 0.255f_{mortar}t_{fs}L_b + 0.291\sqrt{f_{mortar}}t_{fs}L + 0.209A_{vi}f_{yvi} \quad (6.18)$$

$$V_n = 0.296 * 476\text{kN} + 0.255(22.1 * 37.75 * 390)\text{N} + 0.291\left(\sqrt{22.1} * 37.75 * 1800\right)\text{N} + 0.209(200 * 448)\text{N} \quad (6.19)$$

$$V_n = 140.9\text{kN} + 83.0\text{kN} + 93.0 + 18.7 = 335.5\text{kN} \quad (6.20)$$

The shear strength estimation according to VC-RS3 is as shown in Equations (6.21) to (6.23).

$$V_n = 0.0568L + 5.18f'_{mg} + 0.175A_{vf,bar} - 0.0657s_{v,ave} + 0.23P \quad (6.21)$$

$$V_n = 0.0568 * 1800 + 5.18 * 10.3 + 0.175 * 200 - 0.0657 * 800 + 0.23 * 476 \quad (6.22)$$

$$V_n = 102.2 + 53.4 + 35.0 - 52.6 + 109.5 = 247.6\text{kN} \quad (6.23)$$

The shear strength is estimated according to MT-VA-rt3:RTS1-TS3-RS3 by first determining which branch of the tree to use (Equation (6.24)).

$$V_n = \begin{cases} 0.167t + 0.668\sqrt{f_{mortar}}t_{fs}L & \text{if } P \le 450 \;\&\; f_{grout}A_{cell}n_g \le 1000 \\ 0.501\sqrt{f_{mortar}}t_{fs}L + 0.519P\dfrac{A_{net}}{A_{gross}} & \text{if } P \le 450 \;\&\; f_{grout}A_{cell}n_g > 1000 \\ 0.461f_{ybb} - 0.0631s_{h,ave} + 0.417P & \text{if } P > 450 \end{cases} \quad (6.24)$$

Because $P > 450$, the shear strength is estimated as shown in Equations (6.25) to (6.27).

$$V_n = 0.461f_{ybb} - 0.0631s_{h,ave} + 0.417P \quad (6.25)$$

$$V_n = 0.461 * 448 - 0.0631 * 850 + 0.417 * 476 \tag{6.26}$$

$$V_n = 206.5 - 53.6 + 198.5 = 351.3 \text{ kN} \tag{6.27}$$

The shear strength is estimated according to MT-VA-rt3:TS1-TS3-TS2 by first determining which branch of the tree to use (Equation (6.28)).

$$V_n = \begin{cases} 0.55\sqrt{f_{mortar}}t_{fs}L + 0.205f'_{mu}t_{fs}(1000mm)\left(1 - \frac{n_g}{n_t}\right) & \text{if } P \leq 450 \;\&\; f_{grout}A_{cell}n_g \leq 1000 \\ 0.501\sqrt{f_{mortar}}t_{fs}L + 0.519P\frac{A_{net}}{A_{gross}} & \text{if } P \leq 450 \;\&\; f_{grout}A_{cell}n_g > 1000 \\ 0.311P + 0.493\sqrt{f_{mortar}}t_{fs}L & \text{if } P > 450 \end{cases} \tag{6.28}$$

Because $P > 450$, the shear strength is estimated as shown in Equations (6.29) to (6.31).

$$V_n = 0.311P + 0.493\sqrt{f_{mortar}}t_{fs}L \tag{6.29}$$

$$V_n = 0.311 * 476\text{kN} + 0.493(\sqrt{22.1} * 37.75 * 1800)\text{N} \tag{6.30}$$

$$V_n = 148.0\text{kN} + 157.5\text{kN} = 305.5\text{kN} \tag{6.31}$$

6.3 Comparison with Existing Code- and Research-Based Models

The performance of the existing code- and research-based shear strength equations that were discussed in Chapter 2 was evaluated so that they could be compared to the proposed models.

6.3.1 Performance of Existing Code- and Research-Based Models

In evaluating the existing code- and research-based shear strength equations, every effort was made to follow the original variable definitions as closely as possible. In some cases where variable definitions were unclear, multiple possibilities were tested to find the option that produced the best equation performance. Otherwise, assumptions were made.

For cases where the code or researcher did not specify a definition of f'_m to apply, $f'_{m,eff}$ was used. This assumption was made for the AIJ (1987), UBC (1988), Blondet et al. (1989), Shing et al. (1990), Anderson and Priestley (1992), Fattal (1993b), TCCMaR (1997), NZS 4230:2004, Voon and Ingham (2007), CSA S304-14 (2014), Dillon (2015), and TMS 402/602-16 (2016) models.

For cases where the code or researcher did not specify whether to use the maximum or average spacing of horizontal reinforcement, both variables were used to calculate V_n and the more favourable option was selected. This applies to the Matsumura (1987), AIJ (1987), Shing et al. (1990), Anderson and Priestley (1992), Fattal (1993b), TCCMaR (1997), NTC-2004, NZS 4230:2004, Voon and Ingham (2007), CSA S304-14 (2014), and TMS 402/602-16 (2016) models. For most of these equations, the equation performance was either the same or slightly better when the maximum horizontal reinforcement spacing was used. Thus, the maximum spacing definition was used for all the equations except for one, the Matsumura (1987) model. For this model, the performance was slightly better when the average horizontal reinforcement spacing was used. In all cases, the difference in performances was small (no more than a 3 kN difference in RMSE and ME values), which is explained in part because only 45 of the 205 tested walls had $s_{h,max}$ values that differed from the $s_{h,ave}$ values.

Masonry walls in Mexico do not normally use bond beam reinforcement, so three versions of the horizontal reinforcement term were used for the NTC-2004 model. One only considered joint reinforcement to be effective in resisting shear, one considered both types of reinforcement using average bond beam spacing, and one considered both types of reinforcement using maximum bond beam spacing. The performance of the equation was best when both types of reinforcement were included, while the definition of spacing used made little difference to the equation performance.

For cases where the code or researcher did not specify what definition of ρ_h to use, an overall reinforcement ratio based on total reinforcement area and gross wall area was used. This applies to the UBC (1988) and Blondet et al. (1989) models. For the Shing et al. (1990) model, it was

observed that the horizontal reinforcement term gave a slightly negative value for three of the tested walls. For these walls, the contribution of the horizontal reinforcement term was taken as 0.

Because the variable t_e in the AIJ (1987) model was described by Okamoto et al. (1987) simply as the "equivalent width of wall," two definitions of this variable were tested. For the first definition it was assumed that t_e should be taken as the wall thickness, while for the second definition it was assumed that t_e should be taken as 2 times the face shell thickness. Because the former definition produced much lower error values when implemented in the AIJ (1987) equation, t_e was taken as the wall thickness.

In the case of the Dillon (2015) model, it was observed that the upper limit provided was detrimental to the accuracy of the equation. Some of the maximum values of V_n predicted by the upper limit were negative when the flexural reinforcement was included in calculating the value of a. As a result, the equation produced negative values when considering the upper limit. In these cases, the upper limit was ignored. An alternative version of the upper limit was tested in which the flexural reinforcement was neglected in calculating a. The equation performance improved slightly when using this modified upper limit, and no negative shear strengths were predicted. The best equation performance was achieved by ignoring the upper limit completely.

Bolhassani et al. (2016) provided limited information on how to use their proposed equation. In particular, the methodology used to calculate the plastic moment, M_p, is unclear. From the example values provided by Bolhassani et al. (2016), it seems that M_p depends on the area of flexural reinforcement and possibly the area of exterior grouted cells. In testing this equation, M_p was taken as the yield strength of the flexural reinforcement multiplied by the plastic section modulus of this reinforcement. The resulting values of M_p are significantly lower than the ones provided by Bolhassani et al. (2016), suggesting that this assumption is overly conservative. Overall, this equation was found to be conservative, with an average V_{exp}/V_n value of 1.70, so a more accurate calculation of M_p would likely improve the equation performance.

To ensure that the ANN developed by Hung was implemented correctly in the program used to test its performance, the implementation was tested using the example calculation from Section 4.7.4 of Hung (2018). It was found that Hung's recorded value of 0.476 for x_5 is incorrect, as it did not lead to the correct value of $x_{5,norm}$ (-0.7067). When the value of -0.7067 was used for $x_{5,norm}$ and the values of x_1, x_2, x_3, x_4, x_6 and x_7 were used as reported in Table 4.13 of Hung (2018), a value of $v_{n,gross}$ of 0.484 MPa was obtained, which is in close agreement with the value provided by Hung.

The sensitivity to provided data of the ANN generated by Hung (2018) can be illustrated by investigating "Wall #5" tested by Maleki et al. (2009). This is one of the walls that Hung (2018) used to generate his ANN. If the value of gross axial stress for this wall is changed from its actual value of 0.74 MPa to a value of 0.2 MPa or less, the ANN produces a negative estimate of V_n. The fact that the ANN produces such an unrealistic shear strength estimate because of a change in the value of a single variable shows a lack of model robustness and may indicate that the model is overfitting.

6.3.2 Summary of Performance of All Models

The performance of the existing code- and research-based equations that were discussed in Chapter 2 is illustrated in Table 6.11 and compared with that of the proposed equations that were generated in the present study. The performance of the naïve predictor generated using Dataset VC (VC-N) is also provided as a benchmark, for comparison purposes.

Table 6.11 - Performance of existing code- and research-based shear strength equations and newly generated shear strength equations

Model			RMSE (kN)	ME (kN)	V_{exp}/V_n Average	Std. dev.	Min	Max
Code-based equations	AIJ (1987)		95.2	56.0	1.71	1.10	0.440	6.41
	UBC (1988)		108	55.7	1.64	0.807	0.428	5.04
	TCCMaR (1997)		107	-55.8	0.893	0.315	0.395	2.67
	NTC-2004		94.9	33.1	1.50	0.893	0.388	6.37
	NZS 4230:2004		118	93.0	1.81	0.723	0.786	5.70
	Eurocode 6 (2005)		175	-97.2	1.51	1.73	0.278	11.2
	CSA S304-14 (2014)		89.8	29.8	1.41	0.722	0.485	5.61
	TMS 402/602-16 (2016)		75.0	18.5	1.19	0.419	0.527	3.56
Research-based equations	Matsumura (1987)		119	105	2.41	1.74	0.760	12.4
	Blondet et al. (1989)		226	-201	0.559	0.137	0.264	1.28
	Shing et al. (1990)		123	-27.5	1.04	0.370	0.303	2.90
	Anderson and Priestley (1992)		311	-258	0.532	0.182	0.210	1.49
	Fattal (1993)		130	-58.5	0.979	0.467	0.326	3.50
	Voon and Ingham (2007)		80.5	-12.3	0.979	0.267	0.349	1.97
	Dillon (2015)		92.3	65.2	1.51	0.672	0.725	4.66
	Bolhassani et al. (2016)		106	84.2	1.70	0.609	0.951	4.51
	Hung (2018)		118	-46.4	1.02	0.719	0.290	7.39
Izquierdo (2020)	Proposed models	VA-RS2	37.6	-10.6	0.953	0.179	0.598	1.46
		VA-TS5	38.9	-9.83	0.970	0.187	0.645	1.58
		VA-rt3:RTS1-TS3-RS3	42.7	-12.4	0.956	0.197	0.424	1.48
		VA-rt3:TS1-TS3-TS2	42.7	-12.6	0.960	0.196	0.481	1.48
		VC-RS3	41.1	-6.10	1.00	0.231	0.576	2.10
	Naïve predictor, VC-N		93.7	-8.79	0.964	0.386	0.348	2.49

The performance indicators of the existing code- and research-based equations were calculated based on the data from Dataset VC, which contains 205 walls in total, however several of the equations could not be tested on all 205 walls due to the absence of needed data. The Matsumura (1987), NTC-2004, and NZS 4320:2004 models were tested on 193 walls, while the Bolhassani et al. (2016b) model was tested on 191 walls and the Eurocode 6 (2005) model was tested on 185

walls. The models generated in the present study were tested on the testing data for the dataset that was used to generate the model.

Of the existing code- and research-based shear strength equations, the TMS (2016) and Voon and Ingham (2007) equations had the best performance on the data. The RMSE and ME error values for both are lower than those of the other existing code- and research-based equations, the standard deviations of V_{exp}/V_n are relatively low and the average values of V_{exp}/V_n are close to 1. Although the Blondet et al. (1989) and Anderson and Priestley (1992) models have much lower standard deviations of V_{exp}/V_n, the average values of V_{exp}/V_n for these models are close to 0.5, indicating a high bias. These models tend to overestimate the shear strength.

The proposed models from the present study all vastly outperform the existing code- and research-based shear strength equations, as indicated by the low error values and low standard deviations of V_{exp}/V_n. The RMSE values of the proposed models are approximately half those of the TMS (2016) and Voon and Ingham (2007) equations, indicating that the variance of the proposed models is much lower. The ME values of the proposed models are comparable to that of the Voon and Ingham equation and close to two times lower than that of the TMS (2016) equation. The average values of V_{exp}/V_n are close to 1, indicating low bias. The low standard deviations of V_{exp}/V_n indicate a relatively small spread of shear strength estimates around the average value, meaning that the V_{exp}/V_n values of all the tested walls are relatively close to 1.

Most of the existing code- and research-based equations have higher RMSE values than the naïve predictor, meaning that they fail to estimate shear strength with greater precision than if the average shear strength value was used as the estimate for each wall. The naïve predictor is the simplest possible shear strength model, one which makes the same prediction in all circumstances, so the fact that most of the existing code- and research-based equations do not outperform it puts the merit of these equations into question (Sheiner and Beal, 1981). However, it should be noted that the naïve predictor was generated using Dataset VC while the existing code- and research-based

equations were generated using different data. There is some overlap in most cases, however slight differences should be expected in the overlapping data due to the use of different variable definitions. As pointed out by Dillon (2015), the principal reason for one model to perform better than another may be that it was developed using the same dataset used to test the models. The performance indicators are expected to vary somewhat between different datasets used for testing. The performance indicators also vary depending on the assumptions made regarding how to use the equations while testing them. The best way to compare all the models would be to test them on a large, representative dataset that was not used to train any of the models. Nevertheless, the results are promising thus far.

Notably, the performance of the ANN developed by Hung (2018) is significantly worse than what was observed by Hung (Table 6.12).

Table 6.12 - Performance of ANN "F-7-5-1" observed by Hung (2018) compared to results of testing on Dataset VC

	MSE (MPa^2)	V_{exp}/V_n	
		Average	Std. dev.
Reported by Hung (2018)	0.009	0.994	0.183
Tested on Dataset VC	0.0784	1.02	0.719

This illustrates the danger of using ANNs in estimating the shear strength of PG walls; the performance on the training data is excellent, but it generalizes poorly to previously unseen data (either training data that has been modified slightly or new data). This may indicate that the ANN is overfitting. The ANN performed particularly poorly on data that was not included in the datasets used to train it (such as the walls tested by Oan, 2013).

6.3.3 Performance and Residual Plots of Proposed Models

The performance plots of the proposed models are presented here and compared to the performance plots of several existing code- and research-based equations. The residual plots of the selected

existing code- and research-based equations are also provided, for comparison with the residual plots of the proposed models (Section 6.2.5.1).

VA-RS2 is provided as a simple, yet accurate shear strength prediction model for PG masonry walls. It does not include any transformations, and as a result the input variable units are not consistent. The performance of this model is illustrated in Figure 6.15.

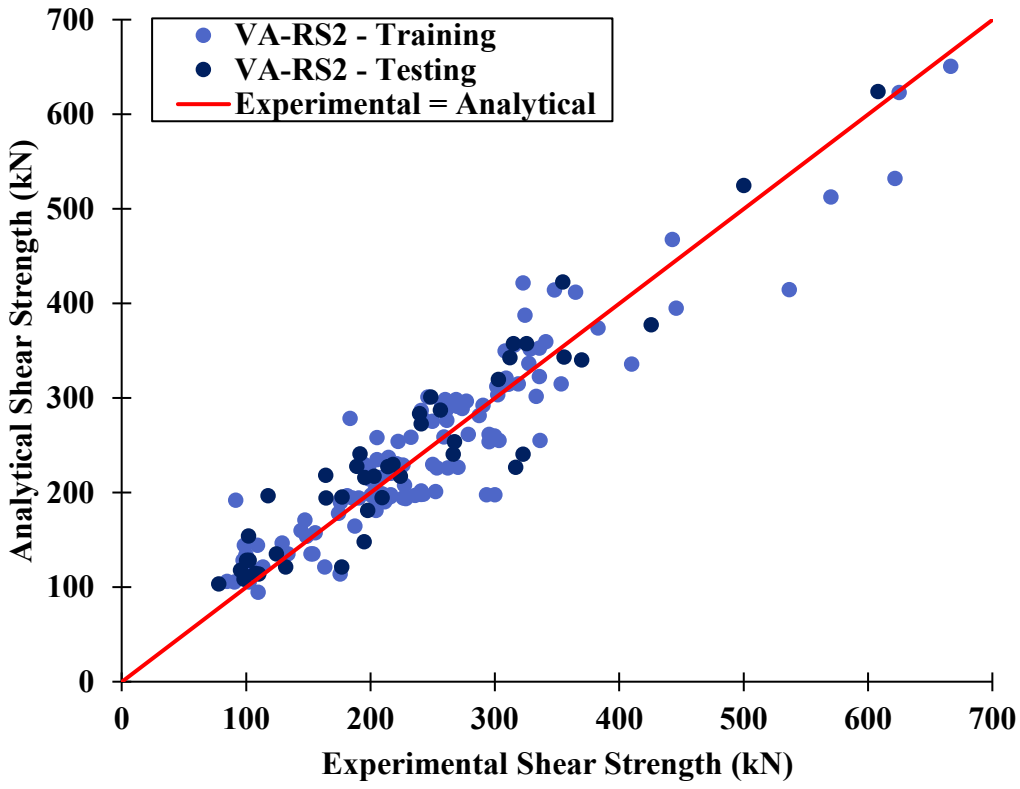

Figure 6.15 - Performance of VA-RS2

In Figure 6.15, and in subsequent plots of analytical shear strength against experimental shear strength, each point represents a wall from the dataset under investigation. The red line represents the ideal scenario, where fitted shear strength values are exactly equal to the observed shear strength values. Points above this line overestimate the shear strength while points below this line

underestimate the shear strength. The closer the points are to the red line, the better the performance of the model.

VA-TS5 is provided as an alternative to VA-RS2. The input variables have consistent units of kN for VA-TS5. The performance of this model is shown in Figure 6.16.

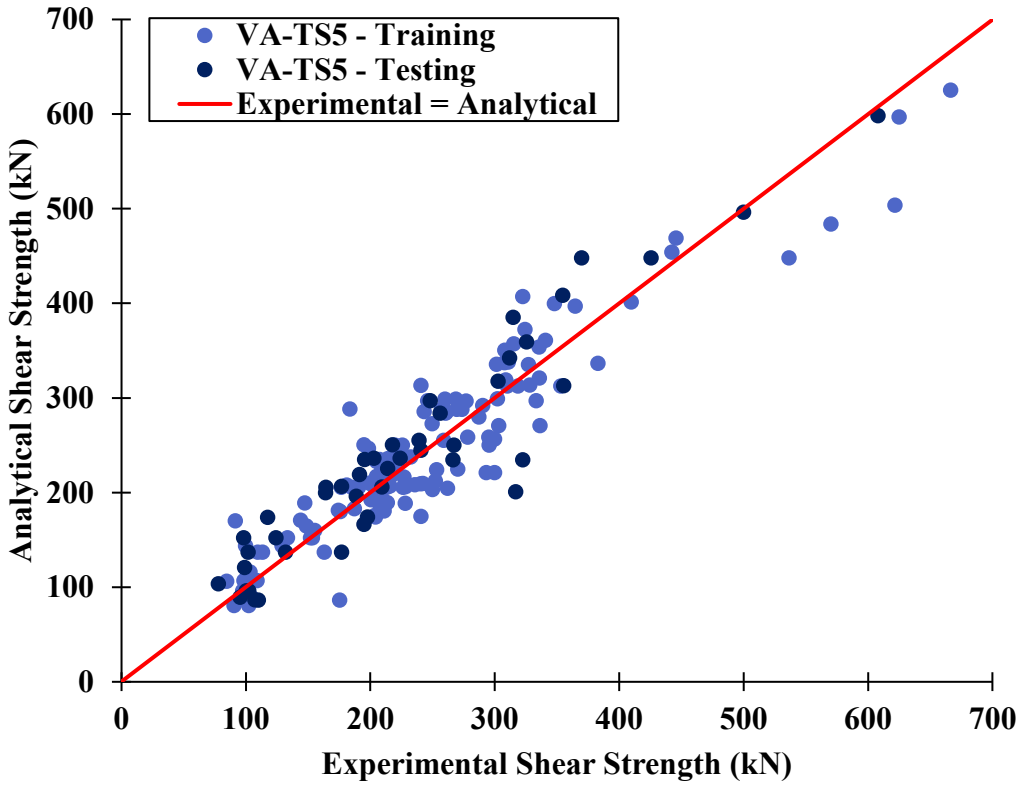

Figure 6.16 - Performance of VA-TS5

Although the proposed stepwise regressions outperform the model trees generated using Dataset VA, the model trees were selected for further investigation to evaluate their potential as a modeling method for PG masonry shear walls.

The performance of MT-VA-rt3:RTS1-TS3-RS3 is illustrated in Figure 6.17.

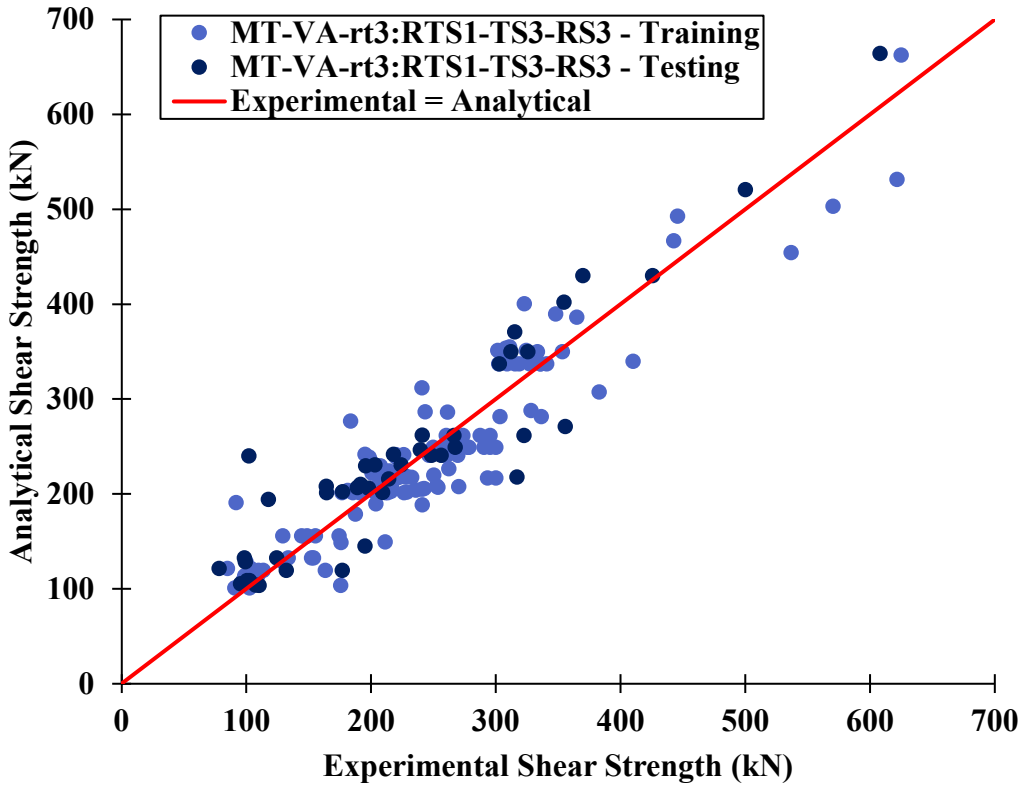

Figure 6.17 - Performance of MT-VA-rt3:RTS1-TS3-RS3

The performance of MT-VA-rt3:TS1-TS3-TS2 is illustrated in Figure 6.18.

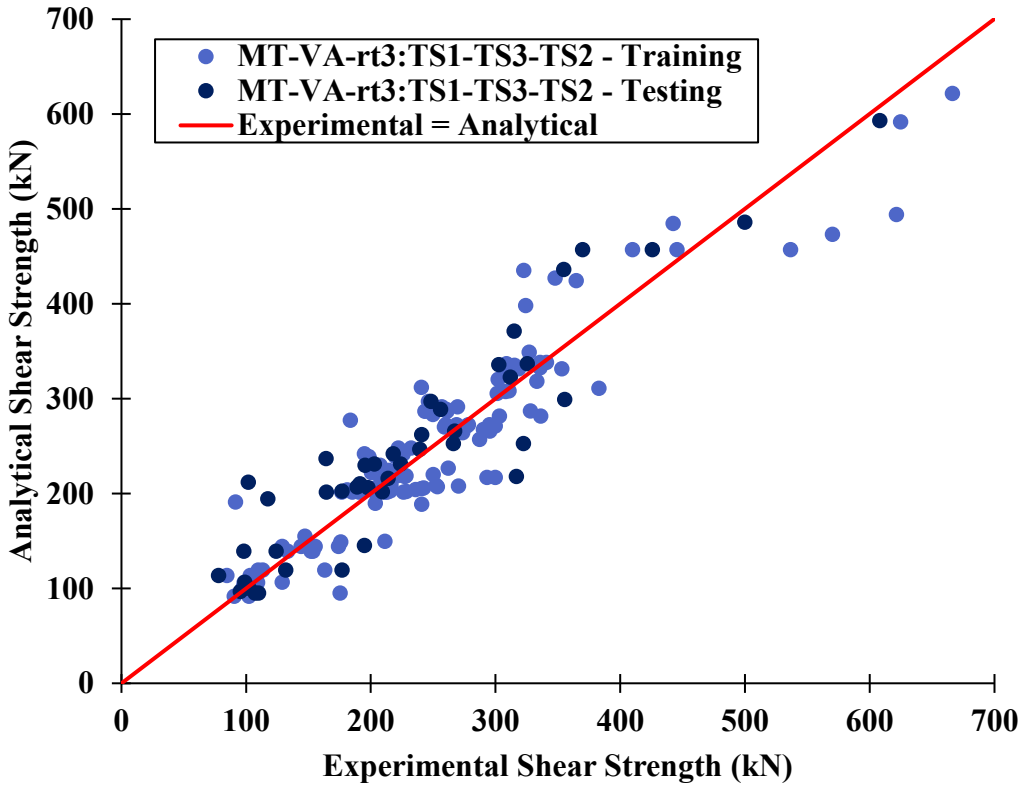

Figure 6.18 - Performance of MT-VA-rt3:TS1-TS3-TS2

VC-RS3 is provided as an alternative model that uses only conventional input variables, which was generated using Dataset VC. Most notably, the variable f_{mortar}, which appears in all of the proposed models that were generated from Dataset VA, was not allowed to appear in this model. VC-RS3 is relatively accurate and simple and contains input variables with inconsistent units.

The performance of VC-RS3 is shown in Figure 6.19.

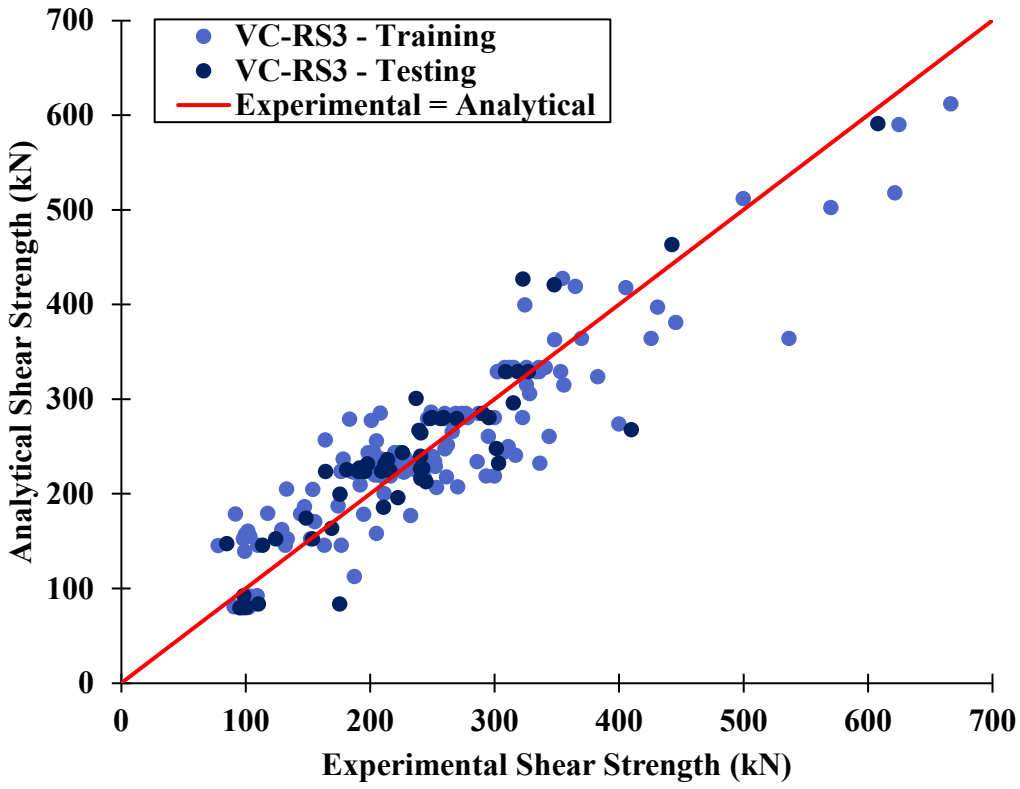

Figure 6.19 - Performance of VC-RS3

These figures show that the proposed models perform well in estimating the shear strength of PG walls. As illustrated in the residual plots for these models (Section 6.2.5.1), all five exhibited homoscedasticity, satisfying the OLS assumption of constant variance of the error.

For comparison, performance plots and residual plots, based on the data from Dataset VC, are provided for four existing code- and research-based shear strength models that are relevant to North American structural design (CSA S304-14, 2014; TMS 402/602-16, 2016; Dillon, 2015; Hung, 2018). The performance and residual plots of the Voon and Ingham (2007) equation are also presented, as the Voon and Ingham (2007) and TMS (2016) equations had the best overall performances among the existing code- and research-based shear strength equations.

The performance of the CSA S304-14 (2014) shear strength equation is shown in Figure 6.20.

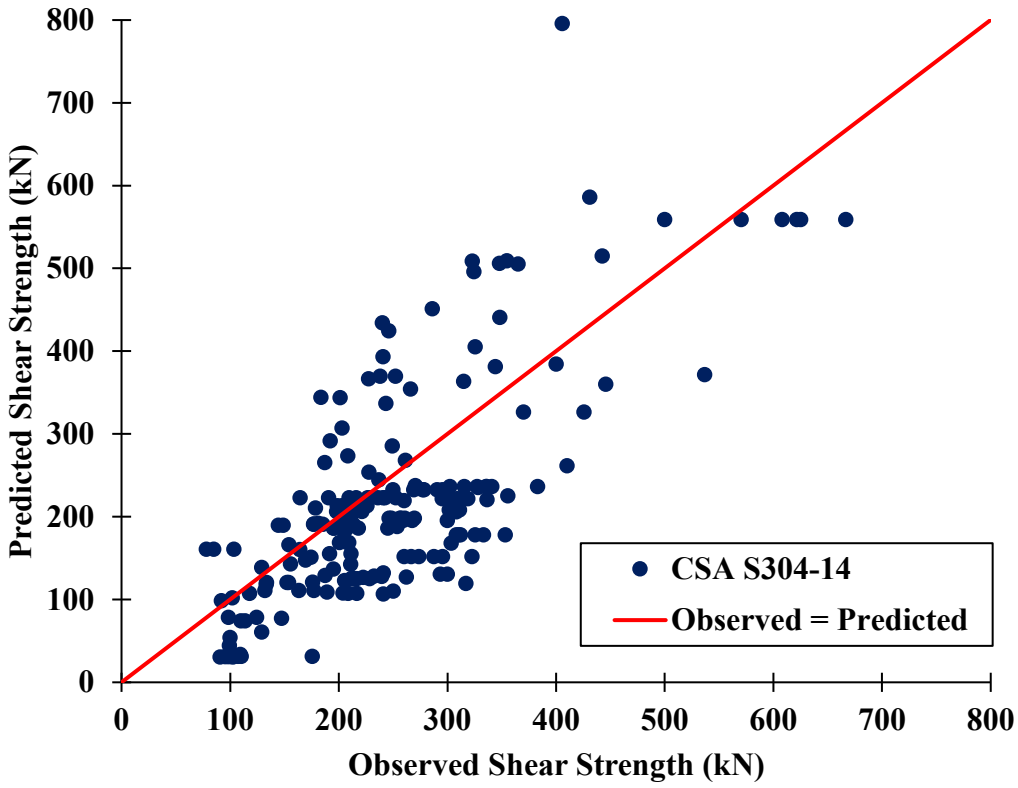

Figure 6.20 - Performance of the CSA S304-14 shear strength equation

The residual plot for this equation is shown in Figure 6.21.

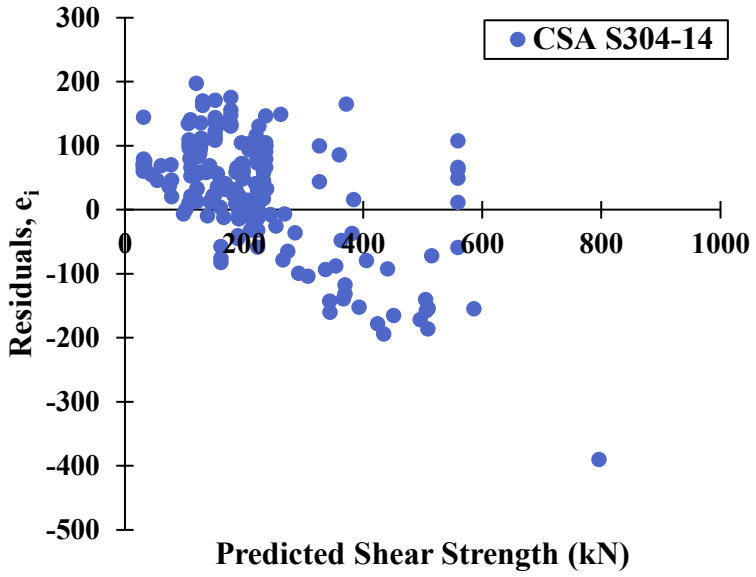

Figure 6.21 - Residual plot for the CSA S304-14 shear strength equation

The performance of the TMS 402/602-16 (2016) shear strength equation is shown in Figure 6.22.

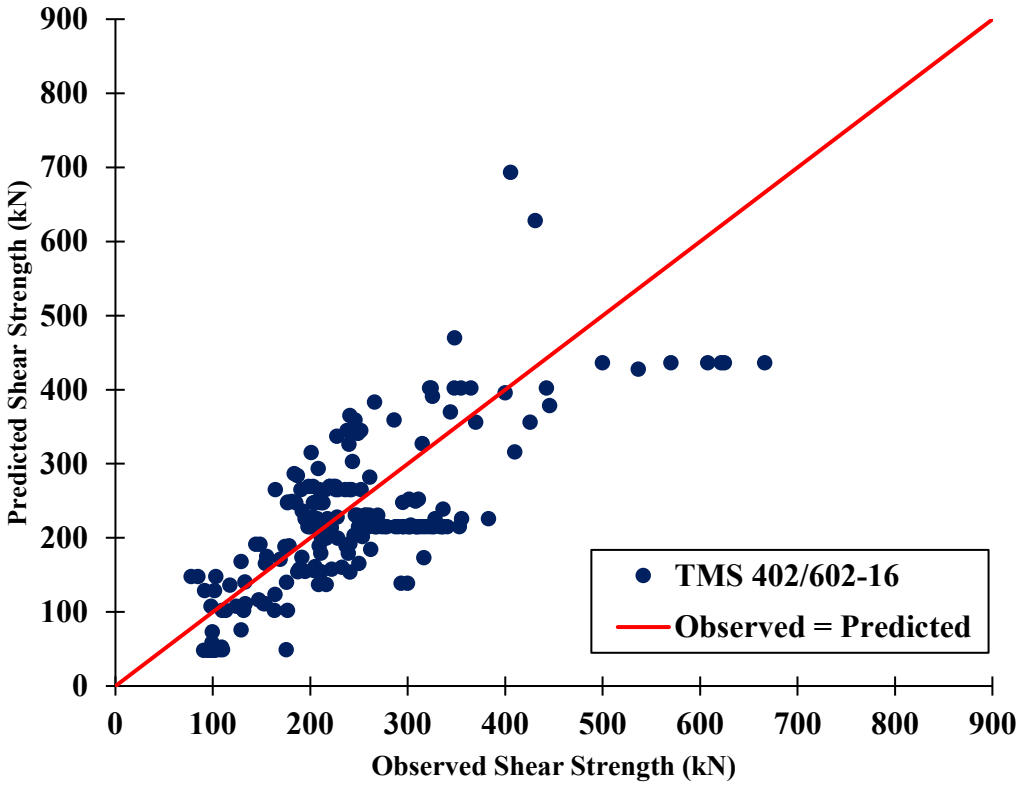

Figure 6.22 - Performance of the TMS 402/602-16 (2016) shear strength equation

The residual plot for this equation is shown in Figure 6.23.

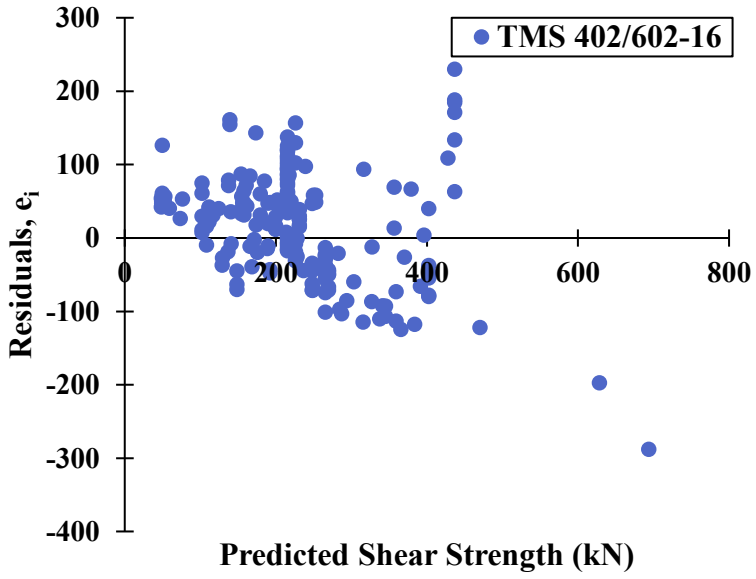

Figure 6.23 - Residual plot for the TMS 402/602-16 (2016) shear strength equation

The performance of the Dillon (2015) shear strength equation is shown in Figure 6.24.

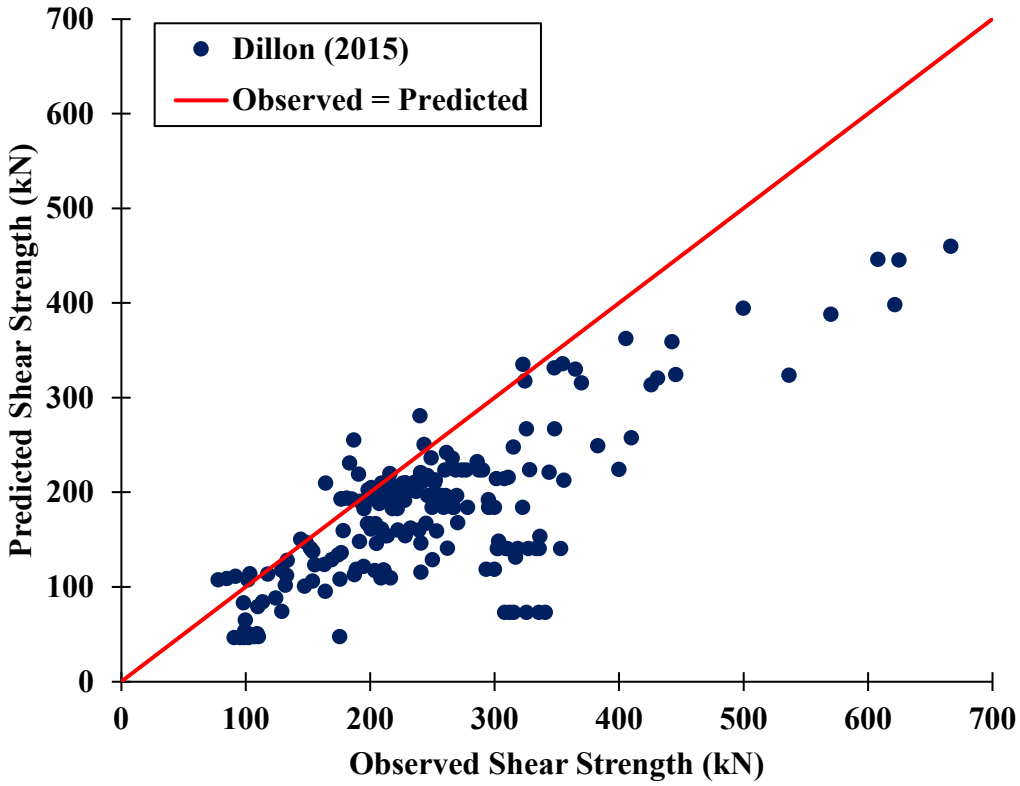

Figure 6.24 - Performance of the Dillon (2015) shear strength equation

The residual plot for this equation is shown in Figure 6.25.

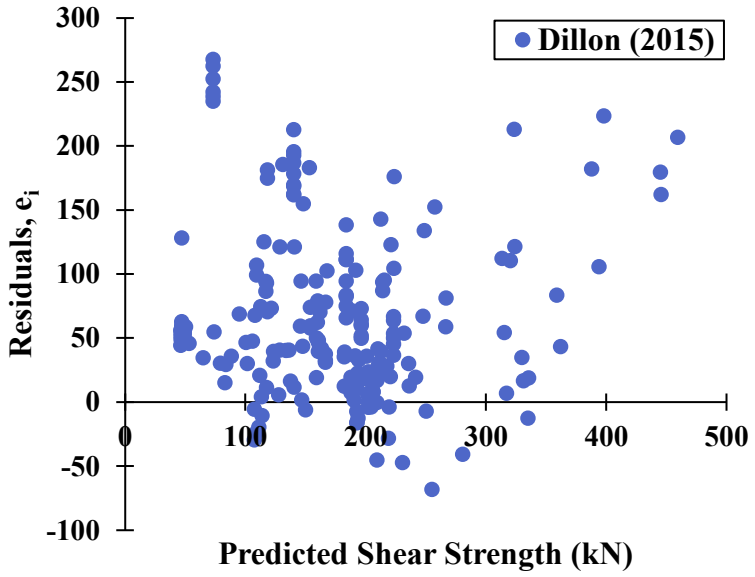

Figure 6.25 - Residual plot for the Dillon (2015) shear strength equation

The performance of the Hung (2018) shear strength model is shown in Figure 6.26.

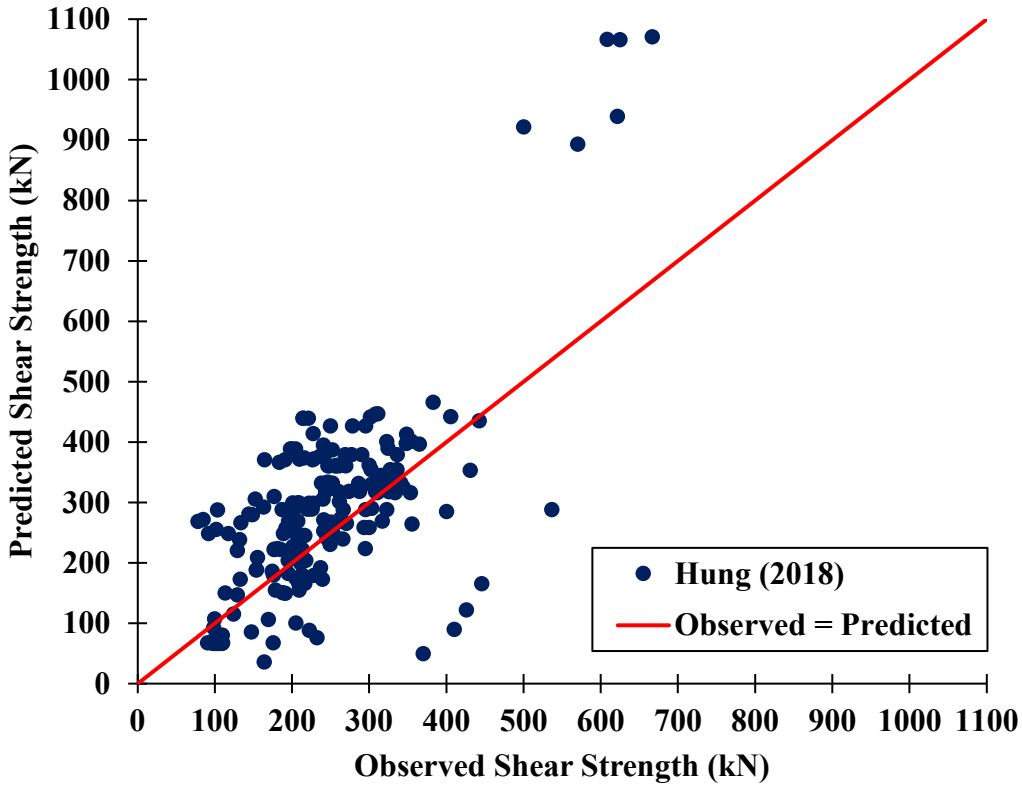

Figure 6.26 - Performance of the Hung (2018) shear strength model

The residual plot for this model is shown in Figure 6.27.

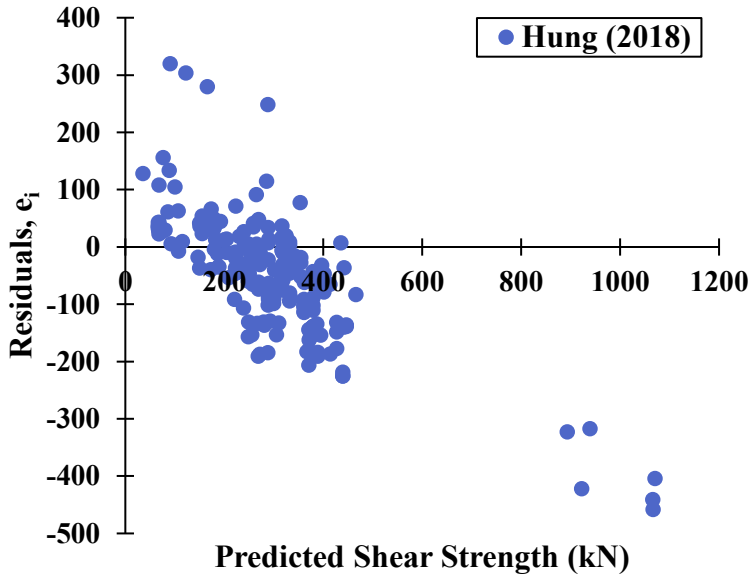

Figure 6.27 - Residual plot for the Hung (2018) shear strength model

The performance of the Voon and Ingham (2007) shear strength equation is shown in Figure 6.28.

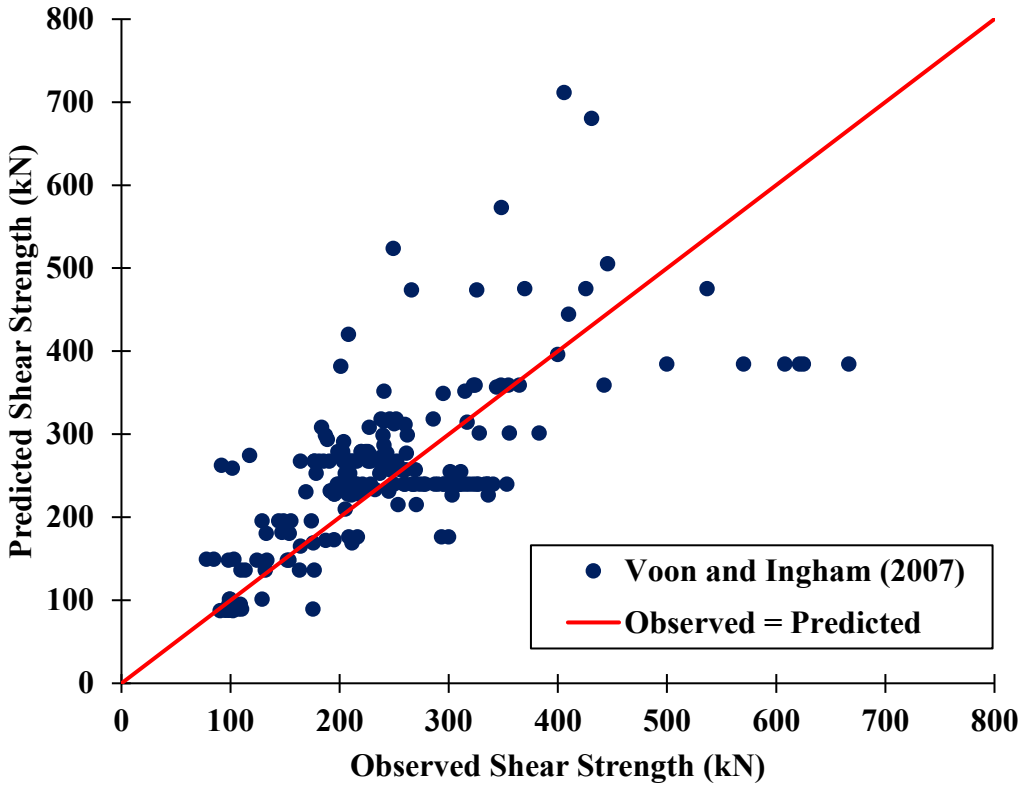

Figure 6.28 - Performance of the Voon and Ingham (2007) shear strength equation

The residual plot for this equation is shown in Figure 6.29.

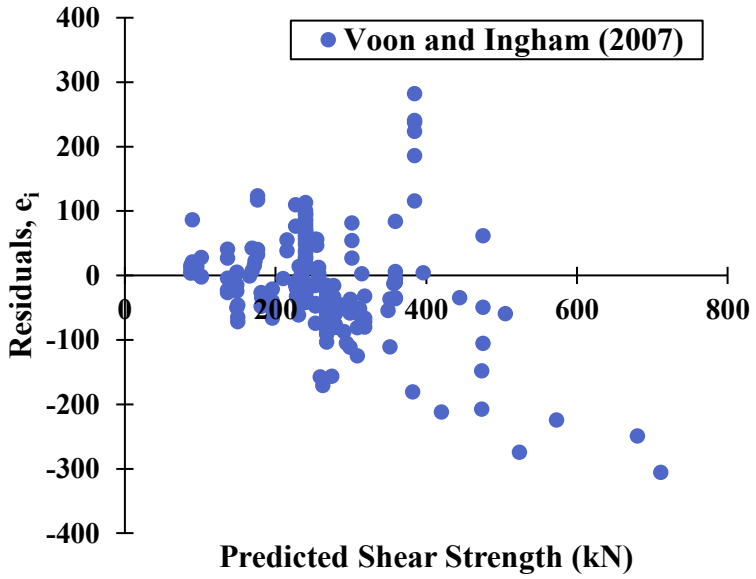

Figure 6.29 - Residual plot for the Voon and Ingham (2007) shear strength equation

The spread of shear strength estimates is much larger for these existing code- and research-based equations than it is for the proposed equations. Additionally, the residual plots of these equations all show some degree of heteroscedasticity, meaning that the variance of the error is not constant as it should be.

6.3.4 Factored Shear Strength

To evaluate the level of conservatism of the proposed models in a design scenario, the reduction factors $\varphi_m = 0.6$ and $\varphi_s = 0.85$ from CSA S304-14 were applied to the masonry and steel terms in the models, respectively. The performance of the factored shear strength models is presented in this section, as well as that of the factored CSA S304-14 shear strength equation, for comparison purposes.

The models with reduction factors applied are shown in Table 6.13.

Table 6.13 - Proposed models and CSA shear strength equation with reduction factors applied

Model	Factored Shear Strength Equation
VA-RS2	$V_r = \varphi_m(-0.0205H + 0.0337L + 6.00f_{mortar} + 0.289P) + 0.0917\varphi_s A_{vi}$
VA-TS5	$V_r = \varphi_m(0.296P + 0.255f_{mortar}t_{fs}L_b + 0.291\sqrt{f_{mortar}}t_{fs}L) + 0.209\varphi_s A_{vi}f_{yvi}$
VC-RS3	$V_r = \varphi_m(0.0568L + 5.18f'_{mg} + 0.23P) + \varphi_s(0.175A_{vf,bar} - 0.0657s_{v,ave})$
MT-VA-rt3:RTS1-TS3-RS3	$V_r = \begin{cases} \varphi_m(0.167t + 0.668\sqrt{f_{mortar}}t_{fs}L) & \text{if } P \le 450 \text{ \& } F_{grout} \le 1000 \\ \varphi_m\left(0.501\sqrt{f_{mortar}}t_{fs}L + 0.519P\frac{A_{net}}{A_{gross}}\right) & \text{if } P \le 450 \text{ \& } F_{grout} > 1000 \\ \varphi_s(0.461f_{ybb} - 0.0631s_{h,ave}) + 0.417\varphi_m P & \text{if } P > 450 \end{cases}$
MT-VA-rt3:TS1-TS3-TS2	$V_r = \begin{cases} \varphi_m\left(0.55\sqrt{f_{mortar}}t_{fs}L + 0.205f'_{mu}t_{fs}(1000mm)\left(1 - \frac{n_g}{n_t}\right)\right) & \text{if } P \le 450 \text{ \& } F_{grout} \le 1000 \\ \varphi_m\left(0.501\sqrt{f_{mortar}}t_{fs}L + 0.519P\frac{A_{net}}{A_{gross}}\right) & \text{if } P \le 450 \text{ \& } F_{grout} > 1000 \\ \varphi_m(0.311P + 0.493\sqrt{f_{mortar}}t_{fs}L) & \text{if } P > 450 \end{cases}$
CSA S304-14	$V_r = \varphi_m\left(0.16\left(2 - \frac{M_f}{V_f d_v}\right)\sqrt{f'_m}td_v + 0.25P\right)\gamma_g + 0.6\varphi_s A_h f_{yh}\frac{d_v}{s_h}$ $\le 0.4\varphi_m\sqrt{f'_m}td_v\gamma_g$

where $F_{grout} = f_{grout}A_{cell}n_g$

The performance of each of the models listed in Table 6.13 is summarized in Table 6.14. For the proposed models, the performance indicators were calculated based on testing data. The CSA equation was tested on Dataset VC.

Table 6.14 - Performance of models with reduction factors applied

Model	RMSE (kN)	ME (kN)	V_{exp}/V_n			
			Average	Std. dev.	Min	Max
CSA S304-14	129	107	2.27	1.23	0.748	9.34
VA-RS2	95.2	80.5	1.55	0.297	0.984	2.43
VA-TS5	95.1	81.1	1.59	0.316	1.08	2.57
VA-rt3:RTS1-TS3-RS3	93.2	79.6	1.57	0.330	0.707	2.46
VA-rt3:TS1-TS3-TS2	99.8	83.5	1.60	0.327	0.802	2.47
VC-RS3	109	96.1	1.75	0.450	1.04	3.60

The overly conservative nature of the CSA S304-14 shear strength equation is evident in the high average and maximum V_{exp}/V_n values. At the same time, despite the conservative values of reduction factors used, the factored CSA shear strength equation is unconservative in some cases, as evidenced by the minimum value of V_{exp}/V_n of 0.748. It appears that the number of unsafe PG shear wall designs made using VA-RS2, VA-TS5 or VC-RS3 would be lower than the number made using the CSA shear strength equation. The large spread of the factored CSA equation causes it to be overly conservative in most cases, while it produces unconservative estimates in a few cases.

The percentage of conservative shear strength estimates produced by each of the models is presented in Table 6.15.

Table 6.15 - Percentage of conservative shear strength estimates produced by the factored models

Model	Dataset	
	Training	Testing
CSA S304-14	-	94.1%
VA-RS2	99.2%	97.7%
VA-TS5	98.5%	100%
VA-rt3:RTS1-TS3-RS3	99.2%	97.7%
VA-rt3:TS1-TS3-TS2	99.2%	97.7%
VC-RS3	98.7%	100%

Overall, it appears that all the proposed models are safer, more economic alternatives to the CSA S304-14 shear strength equation. It should be remembered, however, that these equations require further testing using new data for validation purposes.

The performance of the factored CSA S304-14 shear strength equation is illustrated by Figure 6.30.

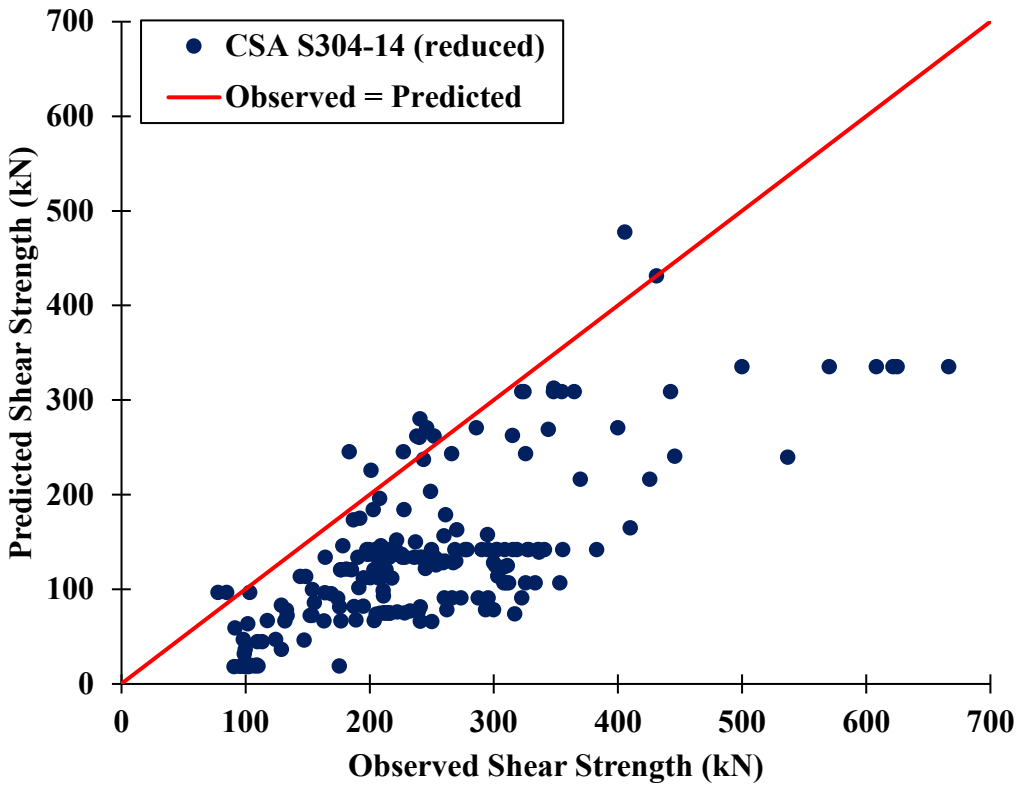

Figure 6.30 - Performance of the factored CSA S304-14 equation

The performance of VA-RS2 with the reduction factors applied is illustrated by Figure 6.31.

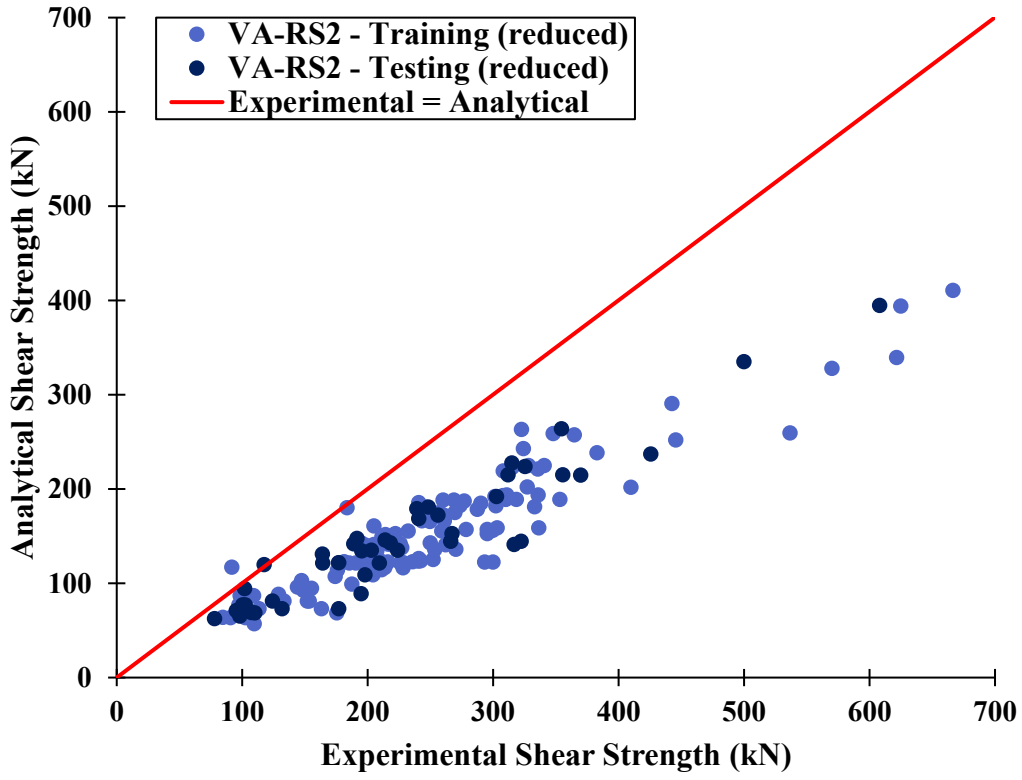

Figure 6.31 - Performance of VA-RS2 with reduction factors applied

The performance of VA-TS5 with the reduction factors applied is illustrated by Figure 6.32.

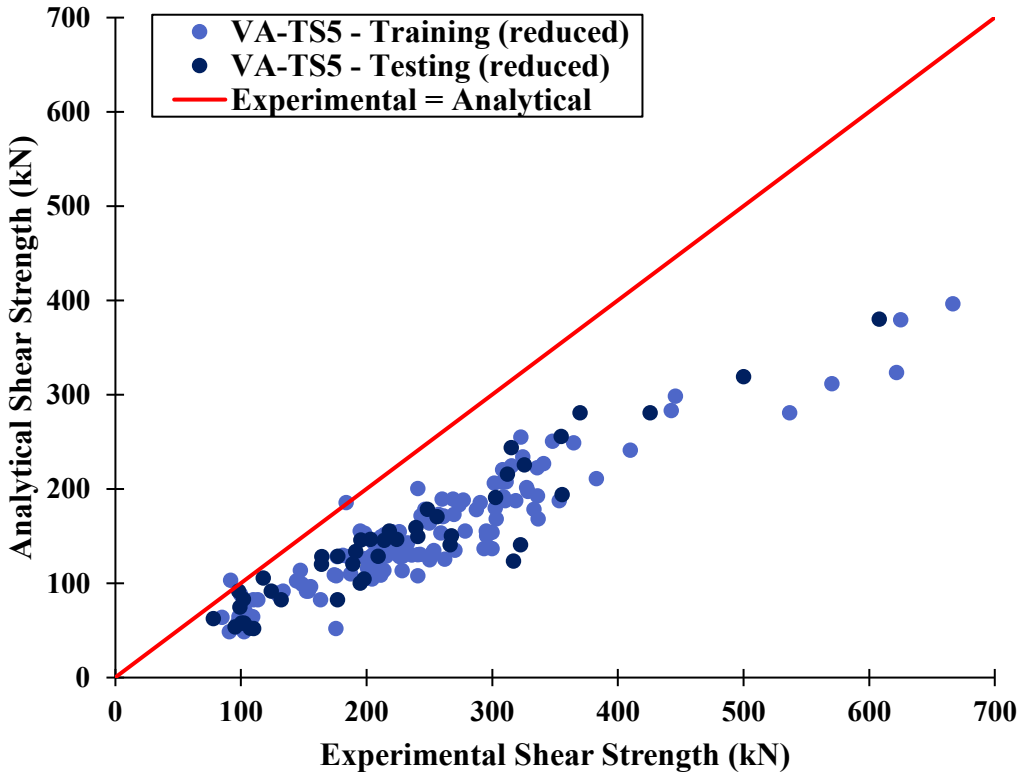

Figure 6.32 - Performance of VA-TS5 with reduction factors applied

The performance of VA-rt3:RTS1-TS3-RS3 with the reduction factors applied is illustrated by Figure 6.33.

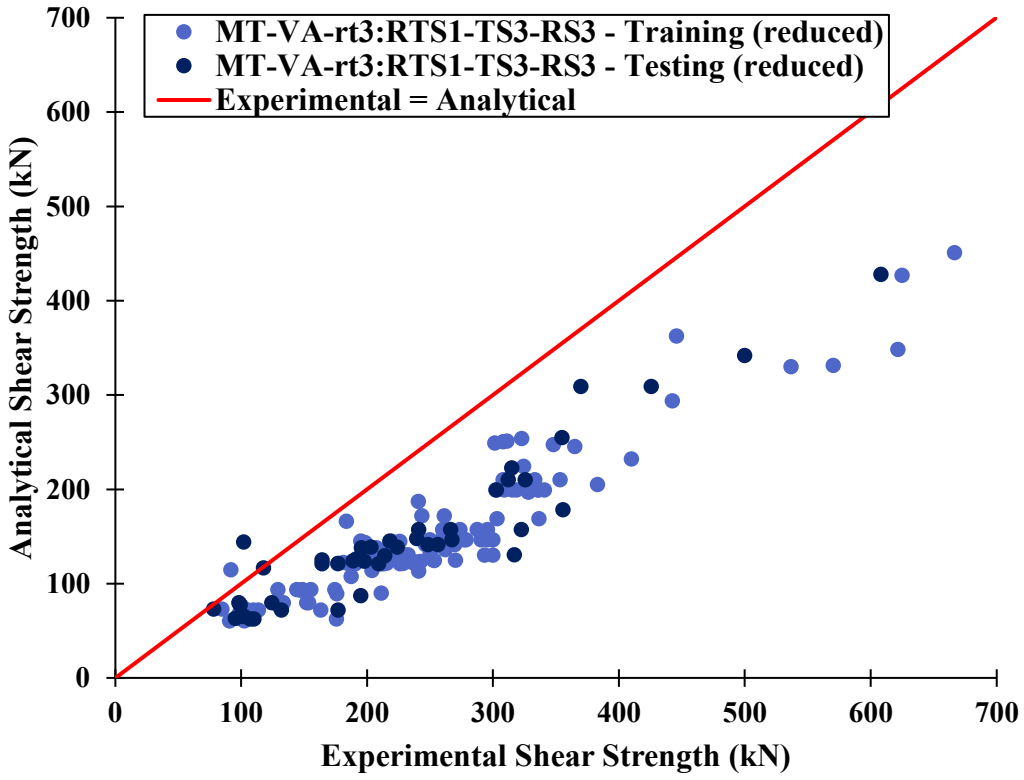

Figure 6.33 - Performance of MT-VA-rt3-RTS1-TS3-RS4 with reduction factors applied

The performance of VA-rt3:TS1-TS3-TS2 with the reduction factors applied is illustrated by Figure 6.34.

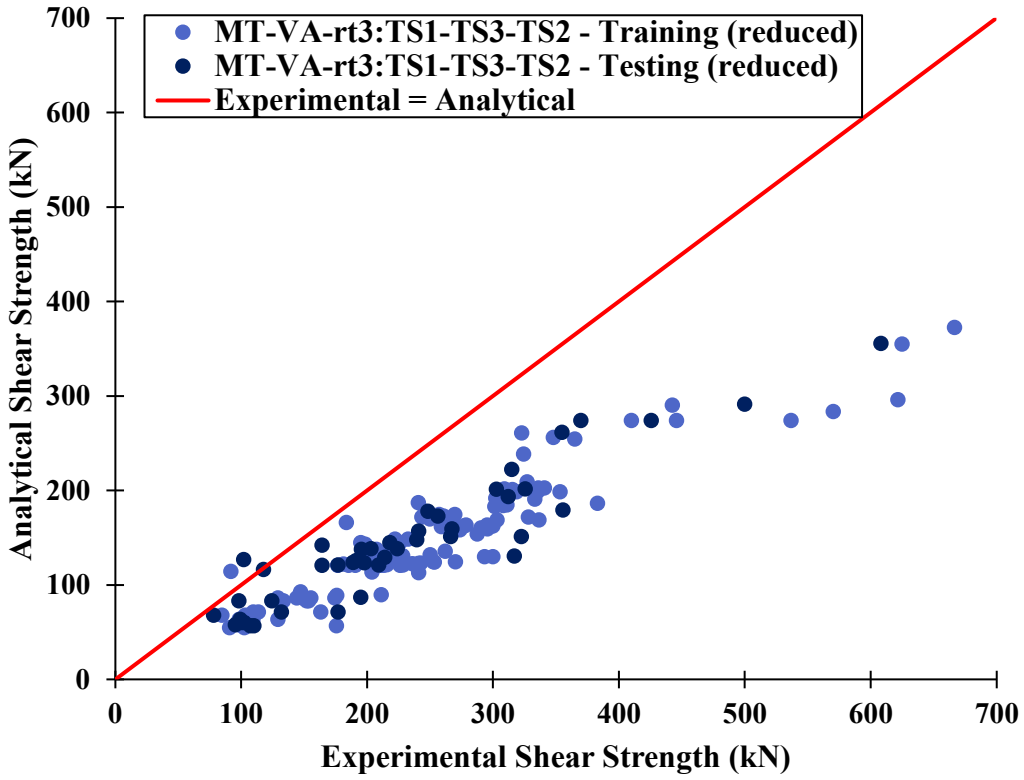

Figure 6.34 - Performance of MT-VA-rt3:TS1-TS3-TS2 with reduction factors applied

The performance of VC-RS3 with the reduction factors applied is illustrated by Figure 6.35.

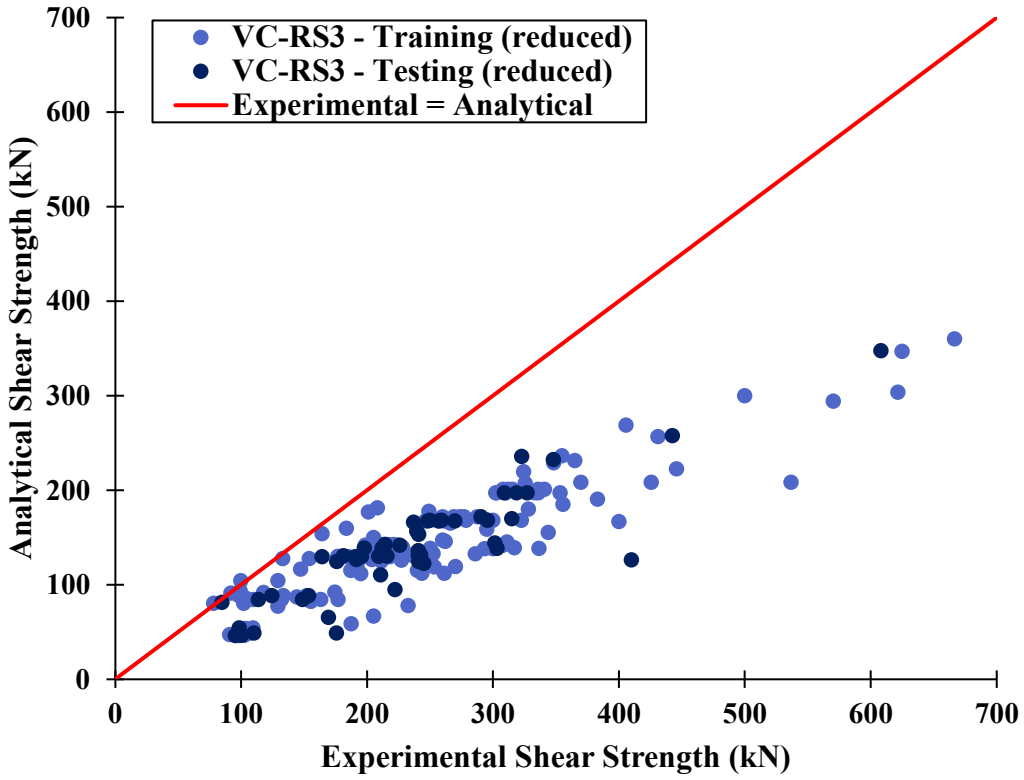

Figure 6.35 - Performance of VC-RS3 with reduction factors applied

6.4 Engineering Significance of Model Parameters

6.4.1 General Observations

By comparing the generated equations from Chapter 5, the following observations can be made:

- The models generated using Dataset VA generally performed better than the models generated using Dataset VC. The main difference between these datasets was the inclusion of the variables f_{block}, f_{mortar} and f_{grout} in Dataset VA, while Dataset VC only included conventional variables. All the models generated using Dataset VA included some form of

the variable f_{mortar}, which suggests that including the contribution of the mortar improves the model fit. This finding will be discussed in greater depth in Section 6.4.3.

- All the models generated using Dataset VC (except for VC-RTS4) included some form of either f'_{mg} or $f'_{m,eff}$. A correlation analysis of Dataset VA reveals that f'_{mg} and f_{mortar} are positively correlated to each other (correlation coefficient=0.630), however $f'_{m,eff}$ and f_{mortar} are very weakly correlated to each other (correlation coefficient=0.0923). The presence of f'_{mg} in the VC models may be due to the high correlation of this variable with f_{mortar}, but the same cannot be said of $f'_{m,eff}$.
- The RS models, which consisted of raw variables with inconsistent units, generally performed better than the TS models, which consisted of transformed variables with consistent units. This suggests that the raw variables may better capture the behaviour of PG masonry shear walls than the transformed variables with consistent units that were considered. There are likely better possible transformations that could be used, but discovering them empirically requires a tedious trial and error process.
- In terms of model structure, VC-TS5 and VCe-TS5 are almost identical, except that the term $f'_{m,eff}A_{net}$ is replaced in VCe-TS5 by $\sqrt{f'_{m,eff}}A_{net}$. Overall, VCe-TS5 performed better than VC-TS5. This suggests that the square root of $f'_{m,eff}$ provides a better model fit and supports the conclusion made by Matsumura (1987). A relatively low number of different transformations including the square root of $f'_{m,eff}$ were used in the datasets, so similar transformations should be investigated to find which ones are most beneficial for improving model fit.
- The appearance of the term $\frac{VL}{M}\sqrt{f'_{m,eff}}A_{net}$ in models VCe-TS1, VCe-TS2 and VCe-TS3 instead of the $\frac{M}{VL}\sqrt{f'_{m,eff}}A_{net}$ term supports the finding of Dillon (2015) that use of the inverse shear span ratio provides a better model fit than using the direct shear span ratio.

- Different definitions of the variables appear in the various generated models. Hence, the investigation of modified horizontal reinforcement terms, average bar spacing compared with maximum bar spacing and total reinforcement terms compared with single-bar terms was inconclusive. This is partially due to the limited amount of data available—the number of walls that had different values of A_{hbb} and $A_{hbb,m}$ was relatively low, for example.
- No terms related to the horizontal reinforcement appeared in any of the stepwise regressions unless they were forcefully included. This suggests that the form of the generated models is such that the contribution horizontal of reinforcement is less significant than the variables that were consistently included in the stepwise regression models. This finding will be discussed in more detail in Section 6.4.4.

6.4.2 Observations on Proposed Models

The proposed models are summarized in Table 6.16.

Table 6.16 - Summary of proposed stepwise regressions and model trees

Model	Equation
VA-RS2	$V_n = -0.0205H + 0.0337L + 6.00f_{mortar} + 0.0917A_{vi} + 0.289P$
VA-TS5	$V_n = 0.296P + 0.255f_{mortar}t_{fs}L_b + 0.291\sqrt{f_{mortar}}t_{fs}L + 0.209A_{vi}f_{yvi}$
VC-RS3	$V_n = 0.0568L + 5.18f'_{mg} + 0.175A_{vf,bar} - 0.0657s_{v,ave} + 0.23P$
MT-VA-rt3:RTS1-TS3-RS3	$V_n = \begin{cases} 0.167t + 0.668\sqrt{f_{mortar}}t_{fs}L & \text{if } P \le 450 \;\&\; f_{grout}A_{cell}n_g \le 1000 \\ 0.501\sqrt{f_{mortar}}t_{fs}L + 0.519P\dfrac{A_{net}}{A_{gross}} & \text{if } P \le 450 \;\&\; f_{grout}A_{cell}n_g > 1000 \\ 0.461f_{ybb} - 0.0631s_{h,ave} + 0.417P & \text{if } P > 450 \end{cases}$
MT-VA-rt3:TS1-TS3-TS2	$V_n = \begin{cases} 0.55\sqrt{f_{mortar}}t_{fs}L + 0.205f'_{mu}t_{fs}(1000mm)\left(1 - \dfrac{n_g}{n_t}\right) & \text{if } P \le 450 \;\&\; f_{grout}A_{cell}n_g \le 1000 \\ 0.501\sqrt{f_{mortar}}t_{fs}L + 0.519P\dfrac{A_{net}}{A_{gross}} & \text{if } P \le 450 \;\&\; f_{grout}A_{cell}n_g > 1000 \\ 0.311P + 0.493\sqrt{f_{mortar}}t_{fs}L & \text{if } P > 450 \end{cases}$

By comparing the proposed models shown in Table 6.16 the following observations can be made:

- All the proposed models included the variable P. This is consistent with the findings of numerous researchers that increasing axial load increases shear resistance (Meli and Salgado, 1969; Matsumura, 1987; Okamoto et al., 1987; Haach, 2009; Voon and Ingham, 2006; Oan, 2013).
- Other than the middle branch of both MTs, all of the proposed models used P rather than $P\frac{A_{net}}{A_{gross}}$. This suggests that a better model fit is achieved using P as a raw variable instead of including it in a transformation. More transformations using P should be investigated to verify this finding.
- All the proposed models include a geometry related variable (H or L). This reflects the importance of aspect ratio in determining shear strength, which has been observed by many researchers (Matsumura, 1988; Fattal, 1993a; Voon and Ingham, 2006; Hamedzadeh, 2013, Dillon, 2015; Ramírez et al., 2016)
- All the proposed models generated using Dataset VA included some form of the variable f_{mortar}. Those which considered transformations included a term with $\sqrt{f_{mortar}}$. This suggests that the relationship of shear strength with the compressive strength of mortar is better represented using $\sqrt{f_{mortar}}$.
- Both of the VA models include terms related to the interior vertical reinforcement. This is consistent with the findings of several researchers that interior vertical reinforcement has a positive influence on shear strength (Ghanem et al., 1992; Dillon, 2015; Ba Rahim et al., 2019).

By investigating the model trees, the following observations can be made:

- When axial load is low and the strength and area of grouting is low, the contribution of mortar is more important. MT-VA-rt3:TS1-TS3-TS2 also suggests that the ungrouted prism strength is more important in this case.

- As the strength and area of grouting increases, the strength of mortar becomes less important. This is consistent with the observation that mortar joints are more important in PG walls than in FG walls (Shing et al., 1990; Hassanli et al., 2014).
- As the axial load increases, the strength of mortar becomes less important. This can be explained considering that more of the lateral force is carried by the aggregate-interlock forces as the axial load becomes greater and crack openings are reduced.
- As the strength and area of grouting increase, the axial load becomes more important. This can be attributed to the fact that increasing the amount of grouting leads to more aggregate-interlock forces that are increased by axial stresses that minimize crack openings (Shing et al., 1990).

These findings are significant. In particular, the finding that the compressive strength of mortar contributes to the shear strength and the observation that the horizontal reinforcement terms were not significant are deserving of further discussion. These topics will be addressed in the following sections.

6.4.3 Contribution of Mortar

The inclusion of f_{mortar} is ground-breaking in that it has not been done in any of the existing code- and research-based expressions that were investigated in Chapter 2. This could be partly because many of those expressions were developed using FG wall data exclusively. As noted by Shing et al. (1990), in FG masonry cracks pass through the blocks more than the joints, and thus the mortar joints are thought to have little influence on the shear strength of FG walls. In PG walls, however, cracks pass through the mortar joints more frequently because the mortar typically plays the role of weak layers (Hassanli et al., 2014).

Hoque (2013) identified mortar bond strength as one of the material properties of mortar that influences the structural performance of masonry, stating that the compressive strength of mortar is less important. Oan (2013) attributed lower shear strengths of PG walls to a reduced bond

between mortar and masonry units. Although the compressive strength of mortar may not be the best variable to quantify the contribution of mortar to shear strength, it is possible that there is a correlation between f_{mortar} and the bond strength of mortar, which would explain the consistent appearance of f_{mortar} in the generated models. Woodward and Rankin (1985) found that at high axial stress, increasing the compressive strength of mortar led to noticeable increases in the shear strength of URM walls. This is an area that requires further research.

6.4.4 Contribution of Horizontal Reinforcement

The absence of the horizontal reinforcement term in most of the generated models is unexpected, as almost all the existing code- and research-based equations include a contribution from the horizontal reinforcement. However, researchers have noted that many of these equations overestimate the contribution of the horizontal reinforcement (Hassanli et al., 2014; Dillon, 2015). Unlike the other existing code- and research-based equations, the shear strength model developed by Bolhassani et al. (2016b) included no horizontal reinforcement term.

Several researchers have observed that increasing the amount of horizontal reinforcement has inconsistent effects on the shear strength of masonry walls. Shing (1990) found that increasing the amount of horizontal bond beam reinforcement can prevent shear failure in FG masonry walls and significantly improves the post-cracked ductility of shear-dominated walls. However, the influence of the amount of horizontal reinforcement was inconsistent, and it was found that doubling the amount of horizontal reinforcement will not necessarily lead to a substantial increase in shear strength (Shing, 1990). Schultz et al. (1998) observed increases in ultimate shear stress of 20% and 7% for PG walls with aspect ratios of 1 and 0.7, respectively, when horizontal joint reinforcement was increased from 0.056 to 0.11%. However, the same increase in joint reinforcement led to a 7% decrease in shear strength for walls with aspect ratios of 0.5 (Schultz et al., 1998). Haach et al. (2010) found that varying the percentage of horizontal joint reinforcement did not seem to improve the lateral strength of their PG walls. One of their tested walls with a horizontal reinforcement ratio of 0.053% presented higher lateral strength than an equivalent wall

with a horizontal reinforcement ratio of 0.094% (Haach et al., 2010). Oan (2013) found that increasing joint reinforcement diameter resulted in lower shear strengths, which was attributed to the reduced bond between the mortar and masonry units.

Other researchers have noted that horizontal reinforcement does not lead to any noticeable increase in the shear strength of masonry walls. Medeiros et al. (2013) developed a macro Finite Element Model (FEM) of several lightweight concrete block masonry walls reinforced horizontally with joint reinforcement that had been experimentally tested previously. Although the horizontal reinforcement caused greater distribution of cracking, greater ductility and a reduced width of the localised diagonal crack, both the experimental results and the FEM showed that the horizontal reinforcement did not have a noticeable contribution to the lateral peak load (Medeiros et al., 2013). Janaraj and Dhanasekar (2016) studied the contribution of horizontal reinforcement to in-plane shear strength using a homogenized macro FEM of a two-storey PG wall. They found that varying the level of reinforcement in the middle horizontal bond beam of the wall from 0.03% to 0.48% led to no increase in shear strength and concluded that shear strength contribution from the horizontal reinforcement was negligible.

Further, if the horizontal reinforcement term should be included in the generated equations, then one would expect the effectiveness of the equations to vary with respect to the horizontal reinforcement ratio. Hassanli et al. (2014) determined that several code-based equations overestimate the contribution of horizontal reinforcement to the shear strength of PG masonry walls. They illustrated this using plots of V_{exp}/V_n as a function of horizontal reinforcement ratio multiplied by yield strength (Figure 6.36).

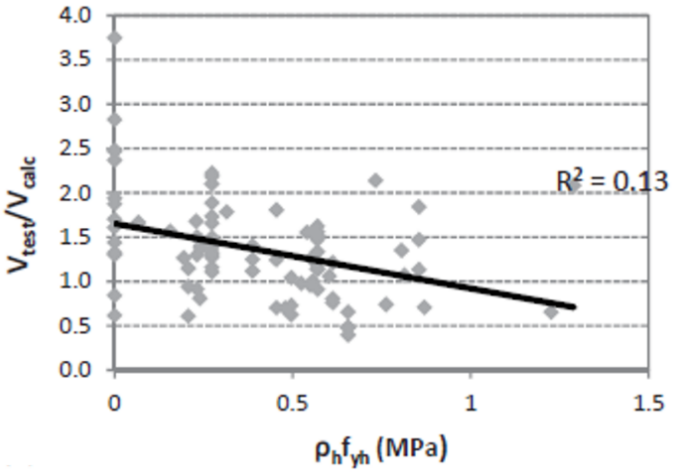

Figure 6.36 - Effect of horizontal reinforcement on V_{exp}/V_n of the CSA S304.1-04 shear strength equation (adapted from Hassanli et al., 2014)

Similar plots are provided for each of the proposed models (Figures 6.37 to 6.41).

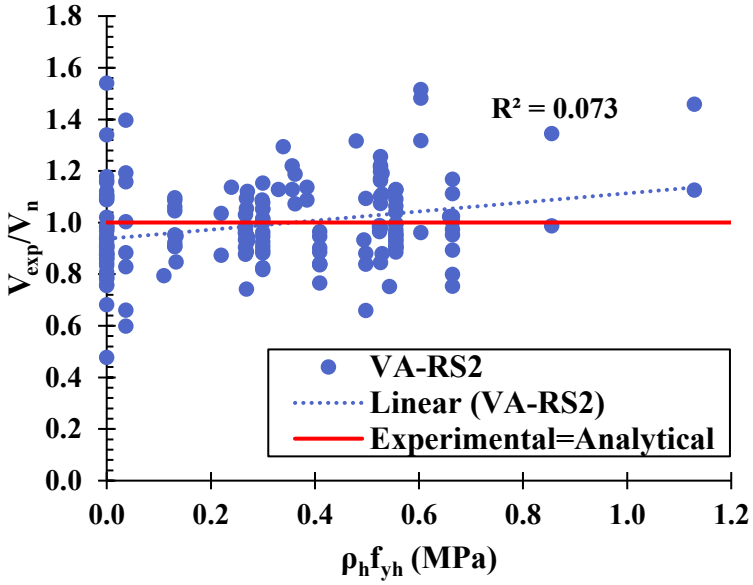

Figure 6.37 - Effect of horizontal reinforcement on V_{exp}/V_n of VA-RS2

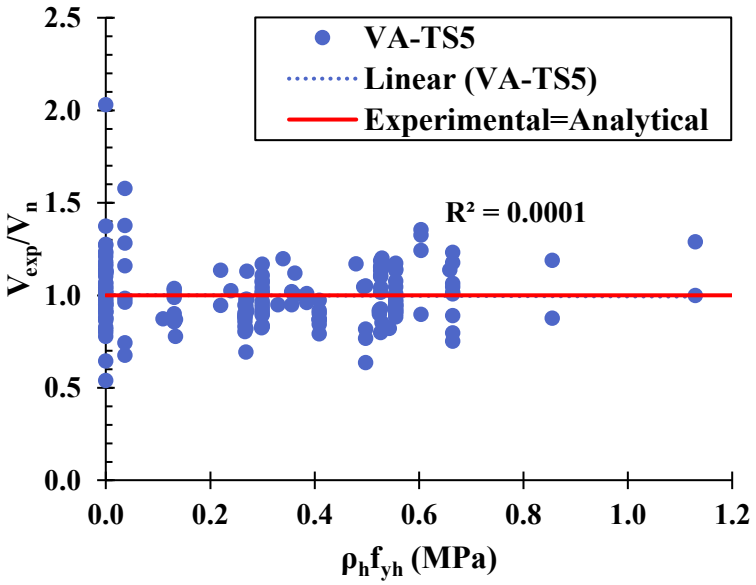

Figure 6.38 - Effect of horizontal reinforcement on V_{exp}/V_n of VA-TS5

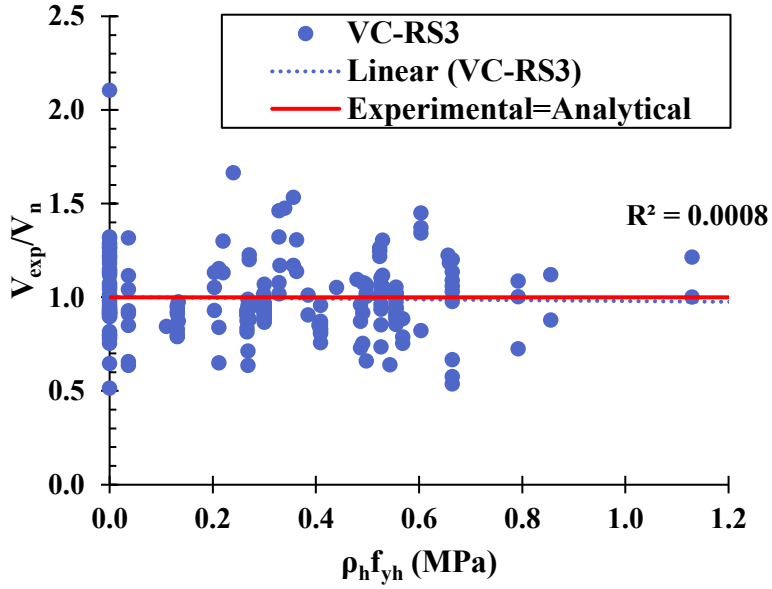

Figure 6.39 - Effect of horizontal reinforcement on V_{exp}/V_n of VC-RS3

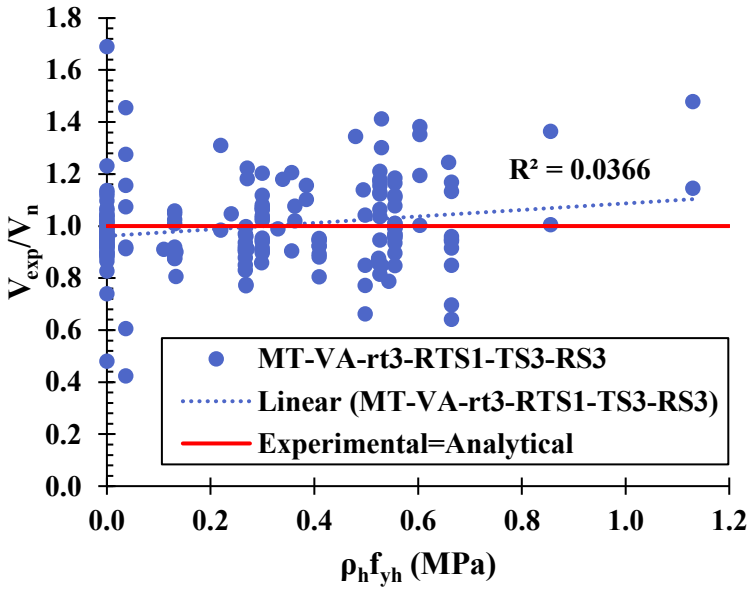

Figure 6.40 - Effect of horizontal reinforcement on V_{exp}/V_n of MT-VA-rt3-RTS1-TS3-RS3

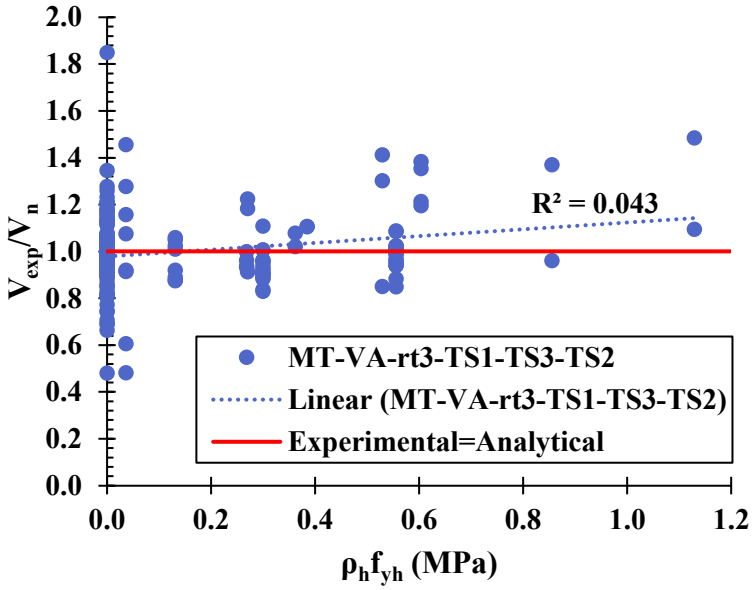

Figure 6.41 - Effect of horizontal reinforcement on V_{exp}/V_n of MT-VA-rt3-TS1-TS3-TS2

Figure 6.38 and Figure 6.39 show that the proposed models VA-TS5 and VC-RS3 do not show any significant change in values of V_{exp}/V_n as the amount and strength of horizontal reinforcement increases. The other three proposed models show slight upward trends (Figure 6.36, Figure 6.37, Figure 6.40 and Figure 6.41), however the associated R^2 values are quite low. These plots confirm that the proposed models are able to capture the behaviour of PG shear walls very well, even without considering any contribution from the horizontal reinforcement.

It should be noted that the addition of the horizontal reinforcement term does not worsen the performance of the generated models that included it (such as VAee-F1-2-TS2 and VAe-F1-2-RS3), as compared with those that did not. This is because the addition of a parameter to a linear regression cannot make the correlation worse, it can only improve the correlation or have no effect (Rencher and Schaalje, 2008; Dillon, 2015). The correct method to judge whether a parameter should be included is through inspection of the parameter's p-value, to verify if it is statistically significant (Dillon, 2015). The horizontal reinforcement terms were initially omitted from the stepwise regressions due to relatively low statistical significance, meaning that they should not be included in the models. The contribution of the horizontal reinforcement may be significant in existing code- and research-based equations because of the assumed forms of these equations.

7 CONCLUSIONS AND RECOMMENDATIONS

7.1 Summary

The objective of this study to develop an improved model to predict the in-plane shear strength of PG masonry walls was achieved according to the steps that follow.

1. Data were compiled, scrutinized, and synthesized to ensure consistency in the raw variables used and two datasets (Dataset VA and Dataset VC) were generated.
    a. Dataset VA consists of 176 PG walls and contains all 34 of the raw variables
    b. Dataset VC consists of 205 PG walls, contains only 31 conventional raw variables, and does not include the raw variables f_{block}, f_{mortar} and f_{grout}
2. The performance of 17 existing code- and research-based shear strength expressions were evaluated using the data in Dataset VC.
    a. The existing code-based equations generally showed high errors and a lack of consistency in predictions as indicated by high values of standard deviation of V_{exp}/V_n. The V_{exp}/V_n standard deviations for the CSA S304-14 (2014) and TMS 402/602-16 (2016) equations were found to be 0.722 and 0.419, respectively.
    b. The existing research-based equations also showed high errors and a lack of consistency in predictions. The V_{exp}/V_n standard deviation for the Dillon (2015) equation was found to be 0.672.
    c. The performance of the ANN developed by Hung (2018) was significantly worse than what was observed by Hung. The standard deviation of V_{exp}/V_n reported by Hung (2018) was 0.183 while the one calculated based on the data in Dataset VC was 0.719.
    d. Most of the existing code- and research-based equations were found to be overly conservative for nominal shear strength models. When reduction factors were applied to the CSA equation, the average V_{exp}/V_n value increased from 1.41 to 2.27, with the maximum V_{exp}/V_n value being 9.34. Even with this high degree of

conservatism, the factored CSA equation overestimated the shear strength of 6% of the walls from Dataset VC.

3. Several new models were generated using stepwise regression and model trees integrated with stepwise regression.
    a. A wide range of variables was used in Dataset VA to permit identification of important variables, even if these had previously not been accounted for in existing code- and research-based equations. Dataset VC was used to generate models with only conventional input variables.
    b. 25% of the data in each dataset was reserved for testing the generated models, to assess their performance on unseen data.
    c. The generated models were narrowed down to those which contained only logical relationships, and 5 models were selected as the proposed models based on accuracy, precision, and simplicity.
    d. The proposed models all outperformed the existing code- and research-based equations, as demonstrated by relatively low error values and V_{exp}/V_n standard deviation values. The V_{exp}/V_n standard deviation values of the stepwise regressions generated using Dataset VA were 0.179 and 0.187, while the standard deviation of V_{exp}/V_n for the stepwise regression generated using Dataset VC was 0.231. The standard deviation of V_{exp}/V_n for the MTs generated using Dataset VA were 0.196 and 0.197.
    e. After applying the reduction factors from the CSA S304-14 (2014) code to the proposed models, they all showed reasonable levels of conservatism with average V_{exp}/V_n values in the range of 1.55 to 1.75. The percentage of overestimated shear strength values was less than 3% for all the proposed models with reduction factors applied.

7.2 Conclusions

The results presented in this study demonstrate the ability of stepwise regression to produce models that are accurate and precise while selecting an appropriate, simple input variable set. The use of MTs also shows great potential for producing accurate shear strength estimates, as the MTs generated in this study showed improved performance over the existing code- and research-based equations. The following conclusions were made:

- All the proposed models included the variable P. This is consistent with the findings of numerous researchers that increasing axial load increases shear resistance (Meli and Salgado, 1969; Matsumura, 1987; Okamoto et al., 1987; Haach, 2009; Voon and Ingham, 2006; Oan, 2013).
- As the strength and area of grouting increase, the axial load becomes more important. This can be attributed to the fact that increasing the amount of grouting leads to more aggregate-interlock forces that are increased by axial stresses that minimize crack openings (Shing et al., 1990).
- All the proposed models include a geometry related variable (H or L). This reflects the importance of aspect ratio in determining shear strength, which has been observed by many researchers (Matsumura, 1988; Fattal, 1993a; Voon and Ingham, 2006; Hamedzadeh, 2013, Dillon, 2015; Ramírez et al., 2016).
- Both of the proposed stepwise regressions generated using Dataset VA include terms related to the interior vertical reinforcement. This is consistent with the findings of several researchers that interior vertical reinforcement has a positive influence on shear strength (Ghanem et al., 1992; Dillon, 2015; Ba Rahim et al., 2019).
- The models generated using Dataset VA generally performed better than the models generated using Dataset VC. The main difference between these datasets was the inclusion of the variables f_{block}, f_{mortar} and f_{grout} in Dataset VA, while Dataset VC only included conventional variables. All the models generated using Dataset VA included some form of

the variable f_{mortar}, which suggests that including the contribution of mortar improves the model fit.

- The VA models frequently included a term with $\sqrt{f_{mortar}}$. This suggests that the relationship of shear strength with the compressive strength of mortar is better represented using $\sqrt{f_{mortar}}$.
- As the strength and area of grouting increases, the strength of mortar becomes less important. This is consistent with the observation that mortar joints are more important in PG walls than in FG walls (Shing et al., 1990; Hassanli et al., 2014). Also, as the axial load increases, the strength of mortar becomes less important. A possible explanation is that more of the lateral force is carried by the aggregate-interlock forces as the axial load becomes greater and crack openings are reduced.
- No terms related to the horizontal reinforcement appeared in any of the selected stepwise regressions until steps were taken to force the inclusion of the horizontal reinforcement terms. This suggests that the form of the generated models is such that the contribution horizontal of reinforcement is less significant than the variables that were consistently included in the stepwise regression models.

The inclusion of f_{mortar} is ground-breaking in that it has not been done in any of the existing code- and research-based equations that were investigated. Although research in this area is limited, Woodward and Rankin (1985) observed that, at high axial stress, increasing the compressive strength of mortar led to increased shear strength.

Although the absence of the horizontal reinforcement term in most of the generated models is unexpected, it is not altogether inconsistent with findings of other researchers. Some have found that increases to the amount of horizontal reinforcement leads to inconsistent effects on the shear strength of masonry walls (Shing, 1990; Schultz et al., 1998; Haach et al., 2010). Others have suggested that horizontal reinforcement does not lead to any noticeable increase in the shear strength of masonry walls (Medeiros et al., 2013; Janaraj and Dhanasekar, 2016).

The models generated in this study are subject to certain limitations:

- The models are only dependable within the range of variables that were used for training and cannot be confidently used for extrapolation. The range of experimental shear strengths was 78 to 667 kN including scaled-up values or 78 to 383 kN (for Dataset VA) and 78 to 431 kN (for Dataset VC) considering only unscaled values.
- Approximately 20% of the walls in both datasets were reduced-scale walls. Some of the maximum values of variables (such as the maximum shear strength of 667 kN) are scaled-up versions of the reduced-scale wall properties. As such, these values may be less reliable than the values obtained from full-scale walls. There is a limited amount of research available on the effectiveness of modeling full-scale masonry shear walls using reduced-scale models. The only study that could be located that compared the shear strength of reduced-scale masonry walls with full-scale prototypes was a study that investigated FG masonry. This is an area where further research is needed, particularly in the case of PG walls.
- Although the proposed models significantly outperform the existing code- and research-based equations, it has been noted that the principle reason that one model outperforms another may be that it was generated from the same dataset used to test the models (Dillon, 2015). The models generated in this study were tested using 25% of the datasets which was randomly reserved prior to model training, however with such a limited amount of data, this is a relatively low amount of testing data. The proposed models should be validated with additional data to ensure that they generalize well to new data. Additionally, data from new studies would likely add variation due to differences in testing methodologies used by different researchers.

7.3 Recommendations

- The difficulty of scrutinizing and synthesizing the data used in this study highlights the need for researchers to be thorough and specific in their reporting on experimental studies.

Variables such as f_{mortar}, f_{block} and f_{grout} are frequently not reported, are sometimes given as a range, or are given as a single value for several different walls. This makes it difficult to determine the influence of these variables on the behaviour of masonry walls.

- Standard methods for testing f_{mortar} should be developed, and a synthesization method should be developed to account for the differences in testing methodologies used in previous experiments.
- The effects of f_{mortar} should be studied further in experimental studies to validate the conclusions made in this study. It may also be valuable to study other properties of mortar that may influence the shear behaviour of PG walls, such as mortar bond strength.
- The effects of horizontal reinforcement should be studied further in experimental studies to validate the conclusions made in this study.
- More data is needed to further validate the proposed models, as well as improve upon them. Additional data may also lead to improved results from MTs, as the MT structures would be less constrained by the imposed minimum leaf number.
- Hung (2018) pointed out that most existing shear strength equations do not consider the interaction between variables. For example, the influence of the axial load on shear strength increases as the aspect ratio decreases. MTs may be helpful in representing some of these interactions by applying logic and engineering judgement to the choice of variables used for MT splitting.
- Similar data analyses should explore more options for transformations that may better represent the behaviour of PG shear walls. In particular, more transformations involving the square root of f_{mortar} or the square root of $f'_{m,eff}$ may be beneficial.
- Applying techniques such as K-fold cross validation may lead to model improvements without the need for significant additions of data.

REFERENCES

Aguilar, V. (2013). *Estimation of shear strength of reinforced masonry walls. Comparative study and use of artificial neural networks.* [Universidad Austral de Chile]. Retrieved from https://www.researchgate.net/publication279286093_Estimation_of_shear_strength_of_reinforced_masonry_walls_Comparative_study_and_use_of_artificial_neural_networks

Aguilar, V., Sandoval, C., Adam, J. M., Garzón-Roca, J., and Valdebenito, G. (2016). Prediction of the shear strength of reinforced masonry walls using a large experimental database and artificial neural networks. *Structure and Infrastructure Engineering*, *12*(12), 1661–1674. https://doi.org/10.1080/15732479.2016.1157824

Alcocer, S. M., Cesín, J., Flores, L.E., Hernández, O., Meli, R., Tena, A and Vasconcelos, D. (2003). The new Mexico City building code requirements for design and construction of masonry structures, Ninth North American Masonry Conference, Clemson, SC. The Masonry Society.

Anderson, D. L., and Priestley, M. J. N. (1992). In plane shear strength of masonry walls. 6th Canadian Masonry Symposium, Saskatoon, Canada. University of Saskatchewan.

Angelus Block Co., Inc. (n.d.). Dimensions and Sizes for CMU. Retrieved August 20, 2020, from https://www.angelusblock.com/products/cmu_size.cfm

Baenziger, G. P. and Porter, M. L. (2010). In-plane structural testing of joint reinforcement in concrete masonry shear walls: Final report. Iowa State University.

Baenziger, G., and Porter, M. L. (2011). Joint reinforcement for masonry shear walls. Eleventh North American Masonry Conference, Minneapolis, MN. The Masonry Society.

Ba Rahim, A. (2020). *Shear strength of partially grouted (PG) masonry shear walls: Experimental and analytical study.* [Draft of doctoral dissertation, University of Alberta].

Ba Rahim, A., Hung, J., Pettit, C. and Cruz Noguez, C. (2019). Effect of vertical reinforcement on the performance of partially grouted masonry shear walls. 13th North American Masonry Conference, Salt Lake City, UT. The Masonry Society.

Blondet, J. M., Mayes, R. L., Kelly, T., Villablanca F., R. and Klingner, R. E. (1989). Performance of engineered masonry in the Chilean Earthquake of March 3, 1985: Implications for U.S. design practice. University of Texas at Austin.

Boehmers, (2005). Quality concrete masonry units: Product dimensions and data. Hargest Block Ltd. Retrieved August 20, 2020 from http://www.boehmerblock.com/pdf/2D&D.pdf

Bolhassani, M., Hamid, A. A., Lau, A. C. W., and Moon, F. L. (2016a). Simplified micro modeling of partially grouted masonry assemblages. *Journal of Structural Engineering*, *142*(12). https://doi.org/10.1061/(ASCE)ST.1943-541X.0001620

Bolhassani, M., Hamid, A. A., Johnson, C., and Schultz, A. E. (2016b). Shear strength expression for partially grouted masonry walls. *Engineering Structures*, *127*, 475–494. https://doi.org/10.1016/j.engstruct.2016.09.001

Boult, B. F. (1979). Concrete masonry prism testing. *American Concrete Institute Journal*, *76*(4), 513–536.

Burnham, K. P. and Anderson, D. R. (1998). *Model selection and multimodel inference: A practical information-theoretic approach* (2nd ed.). Springer-Verlag New York, Inc.

Chen, S. J., Hidalgo, P. A., Mayes, R. L., Clough, R. W., and McNiven, H. D. (1978). Cyclic loading tests of masonry single piers, Volume 2—Height to width ratio of 1. University of California.

CSA S304-14. (2014). *Design of masonry structures.* Canadian Standards Association.

D'Agostino, R. B. and Stephens, M. A. (1986). *Goodness-of-fit techniques.* M. Dekker.

Dhanasekar, M. (2011). Shear in reinforced and unreinforced masonry: Response, design and construction. *Procedia Engineering*, *14*, 2069–2076. https://doi.org/10.1016/j.proeng.2011.07.260

Dickie, J. E. and Lissel, S. L. (2009). Comparison of in-plane masonry shear models. 11th Canadian Masonry Symposium, Toronto, Canada. McMaster University.

Dickie, J. & Lissel, S., (2010). In-plane Shear Test Method for Reinforced Concrete Masonry and Preliminary Test Results. 8th International Masonry Conference, Dresden, Germany. International Masonry Society.

Dillon, P. (2015). *Shear strength prediction methods for grouted masonry shear walls*. (Paper 4395) [Doctoral dissertation, Brigham Young University]. All Theses and Dissertations.

Dillon, P., and Fonseca, F. (2014a). Preliminary Study into the Standardisation of Masonry Shear Wall Reporting Methods. 9th International Masonry Conference, Guimarães, Portugal. International Masonry Society.

Dillon, P., and Fonseca, F. (2014b). Analysing masonry research data in matrix form. 9th International Masonry Conference, Guimarães, Portugal. International Masonry Society.

Dillon, P. B., and Fonseca, F. S. (2017a). Uncertainty in partially grouted masonry shear strength predictions. 13th Canadian Masonry Symposium, Halifax, Canada. Canada Masonry Design Centre.

Dillon, P. B. and Fonseca, F. S. (2017b). Reevaluation of the current North American shear strength equations. 13th Canadian Masonry Symposium, Halifax, Canada. Canada Masonry Design Centre.

El-Dakhakhni, W. W., Banting, B. R., and Miller, S. C. (2013). Seismic performance parameter quantification of shear-critical reinforced concrete masonry squat walls. *Journal of Structural Engineering*, *139*, 957–973. https://doi.org/10.1061/(ASCE)ST.1943-541X.0000713

Elmapruk, J. H. (2010). *Shear strength of partially grouted squat masonry shear walls*. [Master's thesis, Washington State University]. http://citeseerx.ist.psu.edu/viewdoc/download?doi=10.1.1.666.9172&rep=rep1&type=pdf

EN 1996-1-1 (2005). *Eurocode 6: Design of masonry structures - Part 1-1: General rules for reinforced and unreinforced masonry structures.* European Committee for Standardization.

ESECMaSE (2005). Development of test methods for the determination of masonry properties under lateral loads in WP7, including test methods for European standardisation. Institute of Concrete and Masonry Structures.

Fattal, S. G. (1993a). The effect of critical parameters on the behavior of partially-grouted masonry shear walls under lateral loads. (NISTIR 5116), National Institute of Standards and Technology.

Fattal, S. G. (1993b). Strength of partially-grouted masonry shear walls under lateral loads. (NISTIR 5147), National Institute of Standards and Technology.

Frank, E., Wang, Y., Inglis, S., Holmes, G. and Witten, I. H. (1998). Using model trees for classification. *Machine Learning, 32*, 63-76. Kluwer Academic Publishers.

Gardner, B., Gransberg, D. D. and Jeong, H. D. (2016). Reducing data-collection efforts for conceptual cost estimating at a highway agency. *Journal of Construction Engineering and Management, 142*(11). https://doi.org/10.1061/(ASCE)CO.1943-7862.0001174

Geman, S., Bienenstock, E., and Doursat, R. (1992). Neural Networks and the Bias/Variance Dilemma. *Neural Computation, 4*, 1-58.

Ghanem, G. M., Essawy, A. S., and Hamid, A. A. (1992). Effect of steel distribution on the behavior of partially reinforced masonry shear walls. 6th Canadian Masonry Symposium, Saskatoon, Canada. University of Saskatchewan.

Ghanem, G. M., Salama, A. E., Shreif, E. A., and Hamid, A. A. (1993). "Effect of axial compression on the behavior of partially reinforced masonry shear walls." Sixth North American Masonry Conference, Philadelphia, PA. The Masonry Society.

Haach, V. G. (2009). *Development of a design method for reinforced masonry subjected to in-plane loading based on experimental and numerical analysis.* [Doctoral dissertation, Universidade de Minho]. http://hdl.handle.net/1822/9596

Haach, V. G., Vasconcelos, G., and Lourenço, P. B. (2007). Cyclic Behaviour of Truss Type Reinforced Concrete Masonry. 7° Congresso de Sismologia e Engenharia Sísmica, Porto, Portugal. Universidade do Porto.

Haach, V. G., Vasconcelos, G., and Lourenço, P. B. (2010). Experimental Analysis of Reinforced Concrete Block Masonry Walls Subjected to In-Plane Cyclic Loading. *Journal of Structural Engineering, 136*(4), 452–462. https://doi.org/10.1061/(ASCE)ST.1943-541X.0000125

Haider, W. (2007). *Inplane response of wide spaced reinforced masonry shear walls*. (PhD thesis, Central Queensland University, Rockhampton, Australia).

Hamedzadeh, A. (2013). *On the shear strength of partially grouted concrete masonry*. [Master's thesis, University of Calgary]. http://dx.doi.org/10.11575/PRISM/27195

Hassanli, R., ElGawady, M. A., and Mills, J. E. (2014). An evaluation of design code expressions for in-plane shear strength of partially grouted masonry walls. *Australian Journal of Structural Engineering, 15*(3), 299–320. https://doi.org/10.7158/S13-031.2014.15.3

Hauenstein, S., Wood, S. N., Dormann, C. F. (2018). Computing AIC for black-box models using generalized degrees of freedom: A comparison with cross-validation. *Communications in Statistics - Simulation and Computation, 47*(5), 1382-1396, https://doi.org/10.1080/03610918.2017.1315728

Hoei Company Ltd. (n.d.). Kenchikuyō konkurītoburokku: Kūdō burokku [Concrete blocks for construction: Hollow block]. JIS A5406 (Nintei bangō 474057 [Certification number 474057]).

Hoque, N. (2013). *In-Plane Cyclic Testing of Reinforced Concrete Masonry Walls to Assess the Effect of Varying Reinforcement Anchorage and Boundary Conditions.* [Master's thesis, University of Calgary]. http://dx.doi.org/10.11575/PRISM/26545

Hudson, K., Pettit, C., Ba Rahim, A., Hung, J. and Cruz-Noguez, C. (2019). An investigation of the Canadian code-based shear strength equation of partially grouted masonry shear walls. 13th North American Masonry Conference, Salt Lake City, UT. The Masonry Society.

Hung, J. R. (2018). *Artificial neural network model for analysis of in-plane shear strength of partially grouted masonry shear walls.* [Master's thesis, University of Alberta]. https://doi.org/10.7939/R3QN5ZS6M

Janaraj, T., and Dhanasekar, M. (2016). Design expressions for the in-plane shear capacity of confined masonry shear walls containing squat panels. *Journal of Structural Engineering, 142*(2), 1–12. https://doi.org/10.1061/(ASCE)ST.1943-541X.0001403

Jekabsons, G. (2016a). M5PrimeLab: M5' regression tree, model tree, and tree ensemble toolbox for Matlab/Octave (Version 1.7.0). Retrieved from http://www.cs.rtu.lv/jekabsons/regression.html

Jekabsons, G. (2016b). M5PrimeLab: M5' regression tree, model tree, and tree ensemble toolbox for Matlab/Octave: User's manual. Retrieved from http://www.cs.rtu.lv/jekabsons/Files/M5PrimeLab.pdf

Johal, P., and Anderson, E. (1988). Shear Strength of Masonry Piers Under Cyclic Loading. *Masonry: Materials, Design, Construction, and Maintenance*. (ASTM STP 992), 18–32. ASTM International. https://doi.org/10.1520/STP27258S

JR Blocks (n.d.). Prefabricados Ligeros de Concreto. JR. Blocks de Calidad S.A de C.V.

Leung, A. W. R., Tam, C. M. and Liu, D. K. (2001). Comparative study of artificial neural networks and multiple regression analysis for predicting hoisting times of tower cranes. *Building and Environment, 36*(4), 457-467.

Long, L. M. (2006). Behaviour of half-scale reinforced concrete masonry shear walls. [Master's thesis, McMaster University].

Maleki, M. (2008). Behaviour of partially grouted masonry shear walls under cyclic reversed loading. [Doctoral dissertation, McMaster University]. http://hdl.handle.net/11375/13702

Maleki, M., Drysdale, R. G., Hamid, A. A., and El-Damatty, A. A. (2009). Behaviour of partially grouted reinforced masonry shear walls - experimental study. 11th Canadian Masonry Symposium, Toronto, Canada. McMaster University.

MATLAB. (2018). Version 9.5 (R2018b). The Mathworks, Inc.

Matsumura, A. (1987). Shear strength of reinforced hollow unit masonry walls. 4th North American Masonry Conference, Los Angeles, CA. The Masonry Society.

Matsumura, A. (1988). Shear strength of reinforced masonry walls. Ninth World Conference on Earthquake Engineering, Tokyo-Kyoto, Japan. Japan Association for Earthquake Disaster Prevention.

Mayes, R. L., Omote, Y., and Clough, R. W. (1976). *Cyclic shear tests of masonry piers volume 1 - test results*. University of California.

Medeiros, P., Vasconcelos, G., Lourenço, P. B. and Gouveia, J. (2013). Numerical modelling of non-confined and confined masonry walls. *Construction and Building Materials, 41,* 968-976. https://doi.org/10.1016/j.conbuildmat.2012.07.013

Meli, R., and Salgado, G. (1969). Comportamiento de muros de mampostería sujetos a carga lateral: Segundo informe. Instituto de ingeniería.

Meli, R., Wolff, A. Z., and Esteve, L. (1968). Comportamiento de muros de mampostería hueca ante carga lateral alternada. *Revista ingeniera, 38*(3), 371–390.

Minaie, E. (2009). Behavior and vulnerability of reinforced masonry shear walls. [Doctoral dissertation, Drexel University]. http://hdl.handle.net/1860/3163

Minaie, E., Mota, M., Moon, F. L., and Hamid, A. A. (2010). In-plane behavior of partially grouted reinforced concrete masonry shear walls. *Journal of Structural Engineering, 136*(9), 1089–1097. 10.1061/(ASCE)ST.1943-541X.0000206

Mohsenijam, A. (2019). *Advancing regression based analytics for steel fabrication productivity modeling.* [Doctoral dissertation, University of Alberta]. https://era.library.ualberta.ca/items/c8c57003-5148-4825-b83a-4f15cc4ddc48/view/7de4cbf9-097e-4f45-a00c-25a55b1bf876/Mohsenijam_Arash_201903_PhD.pdf

Mohsenijam, A., and Lu, M. (2016). Achieving Sustainable Structural Steel Design by Estimating Fabrication Labor Cost Based on BIM Data. *Procedia Engineering, 145*, 654–661. 10.1016/j.proeng.2016.04.056

Mohsenijam, A., Siu, M. F. and Lu, M. (2016). Modified stepwise regression approach to streamlining predictive analytics for construction engineering applications. *Journal of Computing in Civil Engineering, 31*(3). 10.1061/(ASCE)CP.1943-5487.0000636

Montgometry, D. C., Peck, E. A., and Vining, G. G. (2012). *Introduction to linear regression analysis*. (Fifth ed.). John Wiley & Sons, Inc.

Myung, I. J. (2000). The importance of complexity in model selection. *Journal of Mathematical Psychology, 44*, 190-204. 10.1006/jmps.1999.1283

Myung, I. J., Pitt, M. A. (1996). Applying Occam's razor in modeling cognition: A Bayesian approach. *Psychonomic Bulletin & Review, 4*(1), 79–95.

National Concrete Masonry Association. (2012). ASTM specifications for concrete masonry units. NCMA TEK 1-1F.

NEHRP. (1997a). *Recommended provisions for seismic regulations for new buildings and other structures: Part 2: Commentary*. Building Seismic Safety Council.

NEHRP. (1997b). *Recommended provisions for seismic regulations for new buildings and other structures: Part 1: Provisions*. Building Seismic Safety Council.

Nolph, S. M. (2010). In-plane shear performance of partially grouted masonry shear walls. [Master's thesis, Washington State University].

Nolph, S. M., and ElGawady, M. A. (2012). Static cyclic response of partially grouted masonry shear walls. *Journal of Structural Engineering, 138*(7), 864–879. 10.1061/(ASCE)ST.1943-541X.0000529

NTC-2004. (2004). Normas técnicas complementarias para diseño y construcción de estructuras de mampostería. Gobierno del distrito federal.

NTC-2017. (2017). Administración pública de la ciudad de México. Ciudad de México.

NZS 4230:2004. (2004). *Design of reinforced concrete masonry structures*. New Zealand Standards Executive.

Oan, A. F. (2013). *Diagonal shear of partially grouted concrete masonry panels*. [Doctoral dissertation, University of Calgary]. 10.11575/PRISM/25700

Okamoto, S., Tamazaki, Y., Kaminosono, T., Teshigawara, M., and Hirashi, H. (1987). Seismic capacity of reinforced masonry walls and beams in wind and seismic effects. Proceedings of the 18th joint Meeting, U.S.-Japan Panel on Wind and Seismic Effects. National Institute of Standards and Technology.

Page, A. W. (1989). A parametric study of the behaviour of masonry. 5th Canadian Masonry Symposium, Vancouver, Canada. University of British Columbia.

Priestley, M. J. N., Verma, R., and Xiao, Y. (1994). Seismic shear strength of reinforced concrete columns. *Journal of Structural Engineering, 120*(8), 2310–2329. 10.1061/(ASCE)0733-9445(1994)120:8(2310)

Quinlan, J. R. (1992). Learning with continuous classes. 5th Australian Joint Conference on Artificial Intelligence, Hobart, Tasmania. World Scientific.

Ramírez, P., Sandoval, C., and Almazán, J. L. (2016). Experimental study on in-plane cyclic response of partially grouted reinforced concrete masonry shear walls. *Engineering Structures, 126*, 598–617. 10.1016/j.engstruct.2016.08.010

Rencher, A. C. and Schaalje, G. B. (2008). *Linear models in statistics* (2nd Ed). John Wiley & Sons. http://www.utstat.toronto.edu/~brunner/books/LinearModelsInStatistics.pdf

Rizaee, S. (2015). *Assessing bond beam horizontal reinforcement efficacy with different end anchorage conditions in concrete block masonry shear walls.* [Master's thesis, University of Calgary]. 10.11575/PRISM/25017

Schultz, A. E. (1994). NIST research program on the seismic resistance of partially-grouted masonry shear walls. (NISTIR 5481), National Institute of Standards and Technology.

Schultz, A. E. (1996). Seismic performance of partially-grouted masonry shear walls. Eleventh World Conference on Earthquake Engineering, Acapulco, Mexico. Elsevier Science Ltd.

Schultz, A. E., Hutchinson, R. S., and Cheok, G. C. (1998). Seismic performance of masonry walls with bed joint reinforcement. Paper Reference: T119-4. Elsevier Science Ltd.

Scrivener, J. C. (1967). Static racking tests on concrete masonry walls. International Conference on Masonry Structural Systems, Austin, TX. University of Texas at Austin.

Shedid, M. M. T. (2006). *Ductility of reinforced concrete masonry shear walls.* [Master's thesis, McMaster University]. http://hdl.handle.net/11375/17913

Sheiner, L. B. and Beal, S. L. (1981). Some suggestions for measuring predictive performance. *Journal of Pharmacokinetics and Biopharmaceutics, 9*, 503-512. 10.1007/BF01060893

Shing, B. P. B., Member, A., Noland, J. L., Klamerus, E., and Spaeh, H. (1989). Inelastic behavior of concrete masonry shear walls. *Journal of Structural Engineering, 115*(9), 2204–2225. 10.1061/(ASCE)0733-9445(1989)115:9(2204)

Shing, P. B., Schuller, M., and Hoskere, V. S. (1990). In-plane resistance of reinforced masonry shear walls. *Journal of Structural Engineering, 116*(3), 619–640. 10.1061/(ASCE)0733-9445(1990)116:3(619)

Sveinsson, B. I., McNiven, H. D., and Sucuoglu, H. (1985). *Cyclic loading tests of masonry single piers - Volume 4: Additional tests with height to width ratio of 1*. University of California.

Thurston, S. J., and Hutchinson, D. L. (1982). Reinforced masonry shear walls: Cyclic load tests in contraflexure. *Bulletin of the New Zealand Society for Earthquake Engineering, 15*(1), 27–45.

TMS 402/602-16. (2016). *Building code requirements and specifications for masonry structures*. The Masonry Society.

Tomaževič, M., and Lutman, M. (1988). Seismic resistance of reinforced masonry walls. Ninth World Conference on Earthquake Engineering, Tokyo-Kyoto, Japan. Japan Association for Earthquake Disaster Prevention.

Tomaževič, M., Lutman, M., and Petkovic, L. (1996). Seismic behavior of masonry walls: Experimental simulation. *Journal of Structural Engineering, 122*(9), 1040–1047. 10.1061/(ASCE)0733-9445(1996)122:9(1040)

Tomaževič, M., and Velechovsky, T. (1992). Some aspects of testing small-scale masonry building models on simple earthquake simulators. *Earthquake Engineering & Structural Dynamics, 21*(11), 945–963. https://doi.org/10.1002/eqe.4290211102

Tomaževič, M. (2009). Shear resistance of masonry walls and Eurocode 6: Shear versus tensile strength of masonry. *Materials and Structures*, *42*, 889-907. https://doi.org/10.1617/s11527-008-9430-6

UBC. (1988). *Uniform Building Code* (1998 ed.). International Conference of Building Officials.

UBC. (1997). *Uniform Building Code: Structural Engineering Design Provisions* (Vol. 2). International Conference of Building Officials.

Voon, K. C. (2007). *In-plane seismic design of concrete masonry structures*. (Paper 5037) [Doctoral dissertation, University of Auckland]. http://hdl.handle.net/2292/580

Voon, K. C., and Ingham, J. M. (2002). *Shear strength of masonry walls*. School of Engineering Report No. 611, University of Auckland.

Voon, K. C., and Ingham, J. M. (2006). Experimental in-plane shear strength investigation of reinforced concrete masonry walls. *Journal of Structural Engineering*, *132*(3), 400–408. https://doi.org/10.1061/(ASCE)0733-9445(2006)132:3(400)

Voon, K. C., and Ingham, J. M. (2007). Design expression for the in-plane shear strength of reinforced concrete masonry. *Journal of Structural Engineering*, *133*(5), 706–713. https://doi.org/10.1061/(ASCE)0733-9445(2007)133:5(706)

Wang, Y. and Witten, I. H. (1996). Induction of model trees for continuous classes. (Working paper 96/23). University of Waikato. https://hdl.handle.net/10289/1183

Woodward, K. and Rankin, F. (1985). Influence of Block and Mortar Strength on Shear Resistance of Concrete Block Masonry Walls. Report No. 85-3143, National Bureau of Standards. https://pdfs.semanticscholar.org/5707/e22ab46eb92fc0c4bcadb395acb18b859742.pdf

Yancey, C. W. C., and Scribner, C. F. (1989). Influence of horizontal reinforcement on shear resistance of concrete block masonry walls. (NISTIR 4202), National Institute of Standards and Technology.

Ye, J. (1998). On measuring and correcting the effects of data mining and model selection. *Journal of the American Statistical Association, 93*(441), 120-131. https://doi.org/10.2307/2669609

Yoo, W., Mayberry, R., Bae, S., Singh, K., Peter He, Q., & Lillard, J. W., Jr. (2014). A study of effects of multicollinearity in the multivariable analysis. *International Journal of Applied Science and Technology*, *4*(5), 9–19.

Yu, L., Lai, K. K., Wang, S., Huang, W. (2006). A bias-variance-complexity trade-off framework for complex system modeling. International Conference on Computational Science and its Applications, Glasgow, UK. Springer.

APPENDIX A: DATABASE ASSUMPTIONS

This appendix provides further information about key assumptions made in the data compilation step of the study. The full details of all assumptions made for each individual study are not provided. Only those assumptions which required extensive study of the experimental studies, or extensive calculations, are explained here.

A.1 Corrections and General Assumptions

A.1.1 Matsumura (1987)

Matsumura (1987) did not provide any information on what vertical and horizontal reinforcement was used in the PG walls he tested, or how it was spaced throughout the walls. As a result, these details had to be assumed based on the flexural reinforcement and horizontal reinforcement ratios that he provided. It was assumed that standard Japanese steel reinforcing bars were used. No interior vertical reinforcement ratios were provided, so it was assumed that the number of interior vertical bars in each wall was equal to the number of blocks (lengthwise) minus one, and that one D10 bar was used in each grouted cell.

Because Matsumura (1987) used 3-cell blocks to construct their PG walls, A_{net} could not be determined in the same way that was done for the 2-cell walls in the database. Based on the figures provided by Matsumura showing the blocks, it was assumed that the 3 cells were all equal in size. Thus, A_{net} was calculated using Equation (A.1).

$$A_{net} = n_g \frac{L_b}{4} t + \left(L - n_g \frac{L_b}{4}\right) * 2t_{fs} \quad \text{(A.1)}$$

A.1.2 Haach et al. (2007)

Because Haach et al. (2007) used 3-cell blocks to construct their PG walls and only the middle cells were grouted, A_{net} could not be determined in the same way that it was calculated for the 2-cell walls in the database. Instead, A_{net} was calculated using Equation (A.2).

$$A_{net} = n_g L_{wcc} t + \left(L - n_g L_{wcc}\right) * 2t_{fs} \quad \text{(A.2)}$$

Here L_{wcc} represents the centre-to-centre distance between the middle webs, which was taken as 27 mm for the blocks used by Haach et al.

A.1.3 Elmapruk (2010)

There are several mistakes in Table 2.1 of Elmapruk (2010). These mistakes were identified prior to compiling the corrected data with the data from other studies.

The identification of horizontal bars in Table 2.1 of Elmapruk (2010) contradicts what was stated on page 12: "For specimens PG180-48 and PG254-48… 1#6 (D 19) and 2#5 (D 16) were used, respectively." Elmapruk (2010) stated that the first three digits in the specimen name (for example, 180 for PG180-48) corresponded to the horizontal reinforcement ratio multiplied by 10^5. Based on this information, the correct horizontal reinforcement of PG180-48 and PG254-48 was identified by calculating the reinforcement ratio of both walls. This was done by dividing the total reinforcement area by the height from the base of the wall to the middle of the top reinforcing bar (60 in) multiplied by the wall thickness (8 in). It was found that the reinforcement of 2#5 bars corresponds to the reinforcement ratio of approximately 0.254% (meaning this is the reinforcement of PG254-48) while the reinforcement of 1#6 bar corresponds to the reinforcement ratio of 0.180% (and thus corresponds to wall PG180-48).

The corrected Table 2.1 is shown here as Table A.1, with corrections in bold font.

Table A.1 - Corrected distribution of vertical and horizontal reinforcement (adapted from Elmapruk, 2010)

Cell No.	PG 127-48	PG **254**-48	PG 180-48	PG 127-32	PG 127-24	PG 127-48I
1	2 No. 6	2 No. 6	2 No. 6	2 No. 6	2 No. 6	2 No. 6
4					1 No. 5	
5				1 No. 6		
7	2 No. 6	2 No. 6	2 No. 6		1 No. 5	2 No. 6
9				1 No. 6		
10					1 No. 5	
13	2 No. 6	2 No. 6	2 No. 6	2 No. 6	2 No. 6	2 No. 6
ρ_v %	0.332	0.332	0.332	0.332	0.332	0.332
Spacing In. (mm)	48 (1219)	48 (1219)	48 (1219)	**32 (813)**	24 (610)	48 (1219)
ρ_h %	0.127	**0.254**	0.180	**0.127**	0.127	0.127
HR	1 No. 5	**2 No. 5**	**1 No. 6**	1 No. 5	1 No. 5	1 No. 5

A.2 Variable Axial Loading

A few of the experimental studies used variable axial loading during the testing of PG masonry walls. In these cases, the axial load at the point of ultimate shear strength was determined as described in the following sections and used as the axial load for a given wall.

A.2.1 Scrivener (1967)

Scrivener (1967) stated the following:

> Racking load was increased from zero in 4000 lb. increments until failure, which was taken to be the maximum load that could be applied to and held by the wall. At each increment and prior to applying the racking load, a vertical load, just sufficient to balance the overturning moment of the racking load about the toe of the wall, was applied. The geometry of the set-up was such that the ratio of horizontal to vertical load was 0.9.

To determine the axial load that corresponds to the ultimate shear strength of these walls, the loading scheme used by Scrivener was investigated (Figure A.1).

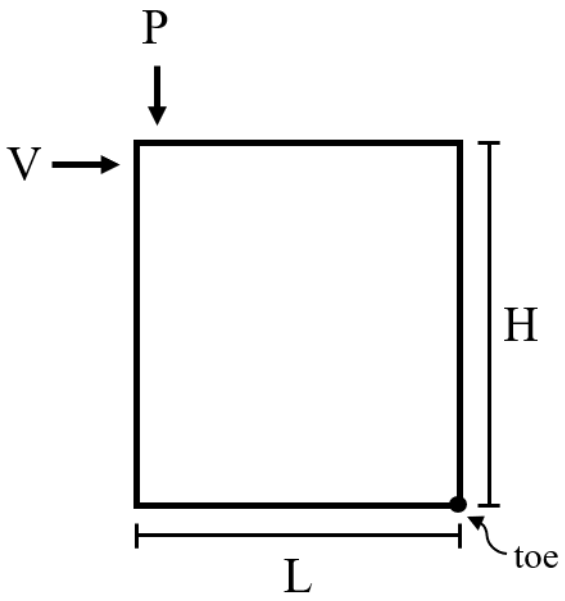

Figure A.1 - Wall loading scheme used by Scrivener (1967)

From this figure, the summation of moments about the toe of the wall is as shown in Equation (A.3).

$$\sum M = -VH + PL \tag{A.3}$$

Because all the walls tested by Scrivener (1967) have the same height and length, the axial load of these walls for any value of V can be determined using Equation (A.4).

$$P = \frac{VH}{L} = \frac{104\text{ in}}{96\text{ in}}V = 1.08V \tag{A.4}$$

A.2.2 Hoque (2013)

Hoque (2013) states:

> Loads applied at the top of the wall were varied in such a way as to ensure zero bending moment at the mid-height centre of the wall. The total applied vertical load remains constant at N = N_1 + N_2 with N_1 and N_2 varying dependent on the specimen being tested and the applied horizontal load. The determination of N_1 and N_2 is done in real time during the test to counter the moment due to the horizontal load.

Thus, the equations used to determine N_1 and N_2 are Equations (A.5) and (A.6).

$$N_1 + N_2 = 409 \text{ kN} \tag{A.5}$$

$$M = N_1 e_1 - N_2 e_2 = \frac{VH}{2} \tag{A.6}$$

Here e_1 and e_2 are both equal to 0.5 m. Hoque also states: "for the seventh set the load in both vertical actuators was held constant rather than being variable to maintain zero moment at the middle of the wall."

Based on this information, it is apparent that as the horizontal load increases, the difference between the vertical loads of the two actuators becomes greater until one of them becomes negative. In other words, one actuator will apply a compressive load higher than the total of 204.5 while the other is (theoretically) in tension. However, the actuators are on rollers, and are not capable of acting in tension. Therefore, the load applied by the actuator that should theoretically be in tension is 0 kN in reality.

The uncorrected values of peak shear strength in push and pull directions (V_{min} and V_{max}) were first used to determine corresponding values of N_1 and N_2 using Equations (A.5) and (A.6). The corresponding axial loads (P_{min} and P_{max}) were then determined by adding N_1 and N_2 if both were

positive. If either one was negative, then it was taken as 0 in determining the corresponding axial load. The average peak axial load in either direction (push or pull) was then calculated by taking the average of P_{min} and P_{max}. This value, P_{ave}, is the value that was used in the compiled database (Table A.2).

Table A.2 - Axial load values used for walls tested by Hoque (all values given in kN)

Wall	V_{min}	N_1	N_2	P_{min}	V_{max}	N_1	N_2	P_{max}	$\boldsymbol{P_{ave}}$
1A	189	375	34	409	230	411	-2	411	**410.1**
1B	226	408	1	409	227	409	0	409	**409.0**
2A	251	430	-21	430	254	433	-24	433	**431.7**
2B	225	407	2	409	232	414	-5	414	**411.3**
3A	234	415	-6	415	251	431	-22	431	**422.7**
3B	226	408	1	409	246	426	-17	426	**417.6**
3C	160	349	60	409	169	356	53	409	**409.0**
4A	195	380	29	409	237	418	-9	418	**413.3**
4B	231	412	-3	412	251	430	-21	430	**421.1**
4C	187	373	36	409	195	380	29	409	**409.0**
5A	205	389	20	409	208	392	17	409	**409.0**
5B	208	392	17	409	219	401	8	409	**409.0**
6A	202	386	23	409	205	389	20	409	**409.0**
6B	210	393	16	409	213	396	13	409	**409.0**
7A*	176	205	205	409	178	205	205	409	**409.0**
7B*	181	205	205	409	190	205	205	409	**409.0**
8A	-	-	-	-	230	412	-3	412	**411.8**
8B	-	-	-	-	236	417	-8	417	**416.7**

*walls 7A and 7B had constant axial load in both actuators

A.2.3 Rizaee (2015)

Rizaee (2015) used the same loading protocol as Dickie and Lissel (2011) and Hoque (2013). Rizaee states that Dickie and Lissel used a total load of 409 kN (equivalent to 2 MPa net stress). The axial load was not kept constant for any of Rizaee's walls, however, so the same procedure discussed in Section 0 must be used to calculate the axial loads at the point of ultimate shear strength.

For Groups A and B of Rizaee's walls, the goal was to maintain zero moment at the centre of the wall. However, as Rizaee points out, this method ignores the additional moment arm of 225 mm between the point of lateral load application (on a steel beam) and the top of the wall. He also points out that a problem arises when the horizontal load exceeds a critical value of 227.2, when one of the vertical actuators should theoretically go into tension to maintain zero moment at the desired location. He notes that the vertical actuators are not capable of applying a tensile force to the wall, so instead one actuator applies a higher compressive load while the other applies no load.

This implies one of two things: the actuator in compression (already exceeding 409 kN) must exert a higher load to maintain zero moment at the centre, or else there will be a small moment at the centre which is not balanced because the second actuator exerts no force. The latter case was assumed.

For Rizaee's Groups C through G, this problem was avoided by considering the additional 225 mm moment arm, and by changing the location of zero moment to a point 485 mm above the centre of the wall. This changes the critical horizontal load to 320 kN. Since none of the walls exceeded a shear strength of 320 kN, walls in groups C through G all have a total axial load of 409 kN.

For the walls belonging to Groups A and B, the axial loads corresponding to the ultimate shear strength were calculated using the procedure described in section 0 (Table A.3).

Table A.3 - Axial load values used for Rizaee's walls belonging to Groups A and B (all values given in kN)

Wall	V_{min}	N_1	N_2	P_{min}	V_{max}	N_1	N_2	P_{max}	$\boldsymbol{P_{ave}}$
1-A	232	413	-4.30	413	273	450	-41.2	450	432
2-A	276	453	-43.9	453	327	499	-89.8	499	476
3-B	276	453	-43.9	453	346	516	-107	516	484
4-B	282	458	-49.3	458	334	505	-96.1	505	482

A.2.4 Hamedzadeh (2013)

Hamedzadeh (2013) stated that, because the axial load varied during the tests, the axial load corresponding to the ultimate shear was used for the purpose of design.

For this study, the axial load at peak shear strength is estimated using the ratios given in Table 6-9 of Hamedzadeh (2013). These values represent "the ratio between the axial and shear stresses at the peak point" (Hamedzadeh, 2013), and are shown along with the axial load corresponding to ultimate shear strength in Table A.4.

Table A.4 - Axial load values used walls tested by Hamedzadeh (all values given in kN)

Wall	*V*	Ratio	***P***
1A	54.7	-	**-**
1B	51.6	1.67	**86.2**
2A	38.2	1.61	**61.5**
2B	46	1.52	**69.9**
3A	42.68	1.83	**78.1**
3B	44	1.67	**73.5**
4A	108	1.68	**181.4**
4B	103	1.78	**183.3**
4C	105	1.81	**190.1**
5A	96	1.69	**162.2**
5B	95.52	1.98	**189.1**
5C	131	1.72	**225.3**
6A	197.3	1.62	**319.6**
6B	168.8	1.25	**211.0**
6C	184	1.23	**226.3**
7A	180	1.66	**298.8**
7B	185	1.61	**297.9**
7C	148	1.49	**220.5**
8A	25.1	1.55	**38.9**
8B	23.1	1.6	**37.0**
8C	30.6	1.52	**46.5**

APPENDIX B: FULL DATABASE

This appendix consists of several tables containing the full database used in this study. The data was synthesized and scrutinized as described in Chapter 4. The tables show the unscaled (actual) wall properties; prototype values can be obtained using the process outlined in Section 4.2.8.2.

Note that some of the cells have been left blank for studies that were not included in Dataset VA or Dataset VC, as these studies were not investigated as thoroughly as those that were used in the data analysis.

Several values were not found or not explicitly stated in the original sources and had to be assumed. These values are identified using the colour scheme shown in Table B.1.

Table B.1 - Colour scheme used in database

Black	Values taken directly from the source papers
Blue	Values that were calculated based on information given in the source papers
Orange	Values that were assumed based on information provided in the source papers
Red	Values that were assumed based only on engineering judgement
Green	Indicates that the wall belongs to the testing data

The VA and VC columns indicate which walls were included (Y) and which walls were not included (N) in Dataset VA and Dataset VC, respectively. In these columns, a green "Y" indicates that the wall was part of the testing data group for the given dataset.

The full list of walls used for model testing is provided in Table B.2.

Table B.2 - Walls used for model testing

Dataset VA				Dataset VC				
3	76	170	236	5	95	176	230	263
5	78	175	246	7	97	182	234	266
8	80	183	256	8	108	186	236	270
9	84	184	263	14	111	190	237	275
13	87	185	265	21	119	196	238	279
14	90	204	267	72	126	203	239	287
15	94	209	273	73	138	205	247	289
16	97	211	274	77	147	208	253	
17	136	225	279	84	149	224	255	
39	140	229	282	85	166	225	258	
72	147	230	292	89	170	228	259	

The full database is given in the tables that follow.

Wall #	DATASET		Experimental Study	Wall ID	Scale	LOADING / BOUNDARY CONDITIONS		
	VA	VC				Loading Type	Loading Rate	Support Type
1	N	N	Scrivener (1967)	C1	1	Monotonic	Quasi-Static	Cantilever
2	Y	Y	Scrivener (1967)	D2	1	Monotonic	Quasi-Static	Cantilever
3	Y	Y	Scrivener (1967)	C10	1	Monotonic	Quasi-Static	Cantilever
4	Y	Y	Scrivener (1967)	C7	1	Monotonic	Quasi-Static	Cantilever
5	Y	Y	Scrivener (1967)	C8	1	Monotonic	Quasi-Static	Cantilever
6	Y	Y	Scrivener (1967)	C9	1	Monotonic	Quasi-Static	Cantilever
7	Y	Y	Scrivener (1967)	D11	1	Monotonic	Quasi-Static	Cantilever
8	Y	Y	Scrivener (1967)	C3	1	Monotonic	Quasi-Static	Cantilever
9	Y	Y	Scrivener (1967)	D12	1	Monotonic	Quasi-Static	Cantilever
10	N	N	Scrivener (1967)	D4	1	Monotonic	Quasi-Static	Cantilever
11	Y	Y	Scrivener (1967)	D13	1	Monotonic	Quasi-Static	Cantilever
12	Y	Y	Scrivener (1967)	D14	1	Monotonic	Quasi-Static	Cantilever
13	Y	Y	Meli et al. (1968)	Muro 309	1	Reverse Cyclic	Quasi-Static	Cantilever
14	Y	Y	Meli et al. (1968)	Muro 310	1	Reverse Cyclic	Quasi-Static	Cantilever
15	Y	Y	Meli et al. (1968)	Muro 311	1	Reverse Cyclic	Quasi-Static	Cantilever
16	Y	Y	Meli et al. (1968)	Muro 312	1	Reverse Cyclic	Quasi-Static	Cantilever
17	Y	Y	Meli et al. (1968)	Muro 313	1	Reverse Cyclic	Quasi-Static	Cantilever
18	Y	Y	Meli et al. (1968)	Muro 314	1	Reverse Cyclic	Quasi-Static	Cantilever
19	Y	Y	Meli et al. (1968)	Muro 315	1	Reverse Cyclic	Quasi-Static	Cantilever
20	Y	Y	Meli et al. (1968)	Muro 316	1	Reverse Cyclic	Quasi-Static	Cantilever
21	Y	Y	Meli et al. (1968)	Muro 317	1	Reverse Cyclic	Quasi-Static	Cantilever
22	Y	Y	Meli et al. (1968)	Muro 318	1	Reverse Cyclic	Quasi-Static	Cantilever
23	N	N	Meli et al. (1969)	Muro 501	1	Monotonic	Quasi-Static	Cantilever
24	N	N	Meli et al. (1969)	Muro 504	1	Monotonic	Quasi-Static	Cantilever
25	N	N	Meli et al. (1969)	Muro 505	1	Monotonic	Quasi-Static	Cantilever
26	N	N	Meli et al. (1969)	Muro 506	1	Monotonic	Quasi-Static	Cantilever

Wall #	DATASET		Experimental Study	Wall ID	Scale	LOADING / BOUNDARY CONDITIONS		
	VA	VC				Loading Type	Loading Rate	Support Type
27	N	N	Meli et al. (1969)	Muro 507	1	Monotonic	Quasi-Static	Cantilever
28	N	N	Meli et al. (1969)	Muro 508	1	Monotonic	Quasi-Static	Cantilever
29	N	N	Meli et al. (1969)	Muro 509	1	Monotonic	Quasi-Static	Cantilever
30	N	N	Meli et al. (1969)	Muro 510	1	Monotonic	Quasi-Static	Cantilever
31	N	N	Meli et al. (1969)	Muro 511	1	Monotonic	Quasi-Static	Cantilever
32	N	N	Meli et al. (1969)	Muro 514	1	Monotonic	Quasi-Static	Cantilever
33	N	N	Meli et al. (1969)	Muro 519	1	Monotonic	Quasi-Static	Cantilever
34	N	N	Mayes et al. (1976)	HCBL-21-11	1	Reverse Cyclic	Quasi-Static	Double Curvature
35	N	N	Mayes et al. (1976)	HCBL-21-12	1	Reverse Cyclic	Dynamic	Double Curvature
36	N	N	Chen et al. (1978)	HCBL-11-2	1	Reverse Cyclic	Dynamic	Double Curvature
37	Y	Y	Chen et al. (1978)	HCBL-11-5	1	Reverse Cyclic	Dynamic	Double Curvature
38	Y	Y	Chen et al. (1978)	HCBL-11-8	1	Reverse Cyclic	Dynamic	Double Curvature
39	Y	Y	Chen et al. (1978)	HCBL-11-10	1	Reverse Cyclic	Dynamic	Double Curvature
40	N	N	Thurston and Hutchison (1982)	UNIT NO. 2	1	Reverse Cyclic	Quasi-Static	Double Curvature
41	N	N	Thurston and Hutchison (1982)	UNIT NO. 4	1	Reverse Cyclic	Quasi-Static	Double Curvature
42	N	N	Thurston and Hutchison (1982)	UNIT NO. 5	1	Reverse Cyclic	Quasi-Static	Double Curvature
43	N	N	Matsumura (1987)	CW4-1-1	1	Reverse Cyclic	Quasi-Static	Double Curvature
44	N	N	Matsumura (1987)	CW4-1-2	1	Reverse Cyclic	Quasi-Static	Double Curvature
45	N	N	Matsumura (1987)	CW3-1-1	1	Reverse Cyclic	Quasi-Static	Double Curvature
46	N	N	Matsumura (1987)	CW3-1-2	1	Reverse Cyclic	Quasi-Static	Double Curvature
47	N	N	Matsumura (1987)	CW2-1-1	1	Reverse Cyclic	Quasi-Static	Double Curvature
48	N	N	Matsumura (1987)	CW2-1-2	1	Reverse Cyclic	Quasi-Static	Double Curvature
49	N	N	Matsumura (1987)	CW3-0-1	1	Reverse Cyclic	Quasi-Static	Double Curvature
50	N	N	Matsumura (1987)	CW3-0-2	1	Reverse Cyclic	Quasi-Static	Double Curvature
51	N	N	Matsumura (1987)	CW3-1'	1	Reverse Cyclic	Quasi-Static	Double Curvature
52	N	N	Matsumura (1987)	CW3-2	1	Reverse Cyclic	Quasi-Static	Double Curvature

Wall #	DATASET		Experimental Study	Wall ID	Scale	LOADING / BOUNDARY CONDITIONS		
	VA	VC				Loading Type	Loading Rate	Support Type
53	N	N	Matsumura (1987)	CW3-3	1	Reverse Cyclic	Quasi-Static	Double Curvature
54	N	N	Matsumura (1987)	CW3-1-A2	1	Reverse Cyclic	Quasi-Static	Double Curvature
55	N	N	Matsumura (1987)	CW3-1-A3	1	Reverse Cyclic	Quasi-Static	Double Curvature
56	N	N	Matsumura (1987)	CW3-1-A4	1	Reverse Cyclic	Quasi-Static	Double Curvature
57	N	N	Matsumura (1987)	CW3-0-A2	1	Reverse Cyclic	Quasi-Static	Double Curvature
58	N	N	Matsumura (1987)	CW3-2-A2	1	Reverse Cyclic	Quasi-Static	Double Curvature
59	N	N	Matsumura (1987)	CW3-3-A2	1	Reverse Cyclic	Quasi-Static	Double Curvature
60	N	N	Matsumura (1987)	CW3-4-A2	1	Reverse Cyclic	Quasi-Static	Double Curvature
61	N	N	Matsumura (1987)	CWB3-1'-A2	1	Reverse Cyclic	Quasi-Static	Double Curvature
62	N	N	Matsumura (1987)	CW3-0-A3	1	Reverse Cyclic	Quasi-Static	Double Curvature
63	N	N	Matsumura (1987)	CW3-0'-A3	1	Reverse Cyclic	Quasi-Static	Double Curvature
64	N	N	Matsumura (1987)	CW3-2-A3	1	Reverse Cyclic	Quasi-Static	Double Curvature
65	N	N	Matsumura (1987)	CW3-3-A3	1	Reverse Cyclic	Quasi-Static	Double Curvature
66	N	N	Matsumura (1987)	**CW5-2'-A2-1**	1	Reverse Cyclic	Quasi-Static	Double Curvature
67	N	N	Matsumura (1987)	**CW5-2'-A2-2**	1	Reverse Cyclic	Quasi-Static	Double Curvature
68	N	N	Matsumura (1987)	**CW4-2'-A2**	1	Reverse Cyclic	Quasi-Static	Double Curvature
69	N	N	Matsumura (1987)	**CW3-2'-A2**	1	Reverse Cyclic	Quasi-Static	Double Curvature
70	N	N	Matsumura (1987)	**CW2-2'-A2-1**	1	Reverse Cyclic	Quasi-Static	Double Curvature
71	N	N	Matsumura (1987)	**CW2-2'-A2-2**	1	Reverse Cyclic	Quasi-Static	Double Curvature
72	Y	Y	Tomaževic and Lutman (1988)	CN-0	0.5	Reverse Cyclic	Quasi-Static	Cantilever
73	Y	Y	Tomaževic and Lutman (1988)	CN-14	0.5	Reverse Cyclic	Quasi-Static	Cantilever
74	Y	Y	Tomaževic and Lutman (1988)	CN-28	0.5	Reverse Cyclic	Quasi-Static	Cantilever
75	Y	Y	Tomaževic and Lutman (1988)	CN-50	0.5	Reverse Cyclic	Quasi-Static	Cantilever
76	Y	Y	Tomaževic and Lutman (1988)	CV-0	0.5	Reverse Cyclic	Quasi-Static	Cantilever
77	Y	Y	Tomaževic and Lutman (1988)	DN-0	0.5	Reverse Cyclic	Quasi-Static	Cantilever
78	Y	Y	Tomaževic and Lutman (1988)	DN-14	0.5	Reverse Cyclic	Quasi-Static	Cantilever

Wall #	DATASET		Experimental Study	Wall ID	Scale	LOADING / BOUNDARY CONDITIONS		
	VA	VC				Loading Type	Loading Rate	Support Type
79	Y	Y	Tomaževic and Lutman (1988)	DN-28	0.5	Reverse Cyclic	Quasi-Static	Cantilever
80	Y	Y	Tomaževic and Lutman (1988)	DN-50	0.5	Reverse Cyclic	Quasi-Static	Cantilever
81	Y	Y	Tomaževic and Lutman (1988)	DV-0	0.5	Reverse Cyclic	Quasi-Static	Cantilever
82	Y	Y	Johal and Anderson (1988)	DM1	1	Reverse Cyclic	Quasi-Static	Double Curvature
83	Y	Y	Johal and Anderson (1988)	DM2	1	Reverse Cyclic	Quasi-Static	Double Curvature
84	Y	Y	Johal and Anderson (1988)	DM3	1	Reverse Cyclic	Quasi-Static	Double Curvature
85	Y	Y	Johal and Anderson (1988)	DM4	1	Reverse Cyclic	Quasi-Static	Double Curvature
86	Y	Y	Johal and Anderson (1988)	DM5	1	Reverse Cyclic	Quasi-Static	Double Curvature
87	Y	Y	Johal and Anderson (1988)	DM6	1	Reverse Cyclic	Quasi-Static	Double Curvature
88	Y	Y	Johal and Anderson (1988)	DP1	1	Reverse Cyclic	Quasi-Static	Double Curvature
89	Y	Y	Johal and Anderson (1988)	DP2	1	Reverse Cyclic	Quasi-Static	Double Curvature
90	Y	Y	Johal and Anderson (1988)	DS1	1	Reverse Cyclic	Quasi-Static	Double Curvature
91	Y	Y	Johal and Anderson (1988)	DS2	1	Reverse Cyclic	Quasi-Static	Double Curvature
92	Y	Y	Johal and Anderson (1988)	DS3	1	Reverse Cyclic	Quasi-Static	Double Curvature
93	Y	Y	Johal and Anderson (1988)	DS4	1	Reverse Cyclic	Quasi-Static	Double Curvature
94	Y	Y	Johal and Anderson (1988)	DS5	1	Reverse Cyclic	Quasi-Static	Double Curvature
95	Y	Y	Johal and Anderson (1988)	DS6	1	Reverse Cyclic	Quasi-Static	Double Curvature
96	Y	Y	Johal and Anderson (1988)	DP3	1	Reverse Cyclic	Quasi-Static	Double Curvature
97	Y	Y	Johal and Anderson (1988)	DP4	1	Reverse Cyclic	Quasi-Static	Double Curvature
98	N	N	Yancey and Scribner (1989)	R1	1	Reverse Cyclic	Quasi-Static	Double Curvature
99	N	N	Yancey and Scribner (1989)	R2	1	Reverse Cyclic	Quasi-Static	Double Curvature
100	N	N	Yancey and Scribner (1989)	R4	1	Reverse Cyclic	Quasi-Static	Double Curvature
101	N	N	Yancey and Scribner (1989)	R5	1	Reverse Cyclic	Quasi-Static	Double Curvature
102	N	N	Yancey and Scribner (1989)	R6	1	Reverse Cyclic	Quasi-Static	Double Curvature
103	N	N	Yancey and Scribner (1989)	R7	1	Reverse Cyclic	Quasi-Static	Double Curvature
104	N	N	Yancey and Scribner (1989)	R8	1	Reverse Cyclic	Quasi-Static	Double Curvature

Wall #	DATASET		Experimental Study	Wall ID	Scale	LOADING / BOUNDARY CONDITIONS		
	VA	VC				Loading Type	Loading Rate	Support Type
105	N	N	Yancey and Scribner (1989)	R9	1	Reverse Cyclic	Quasi-Static	Double Curvature
106	N	N	Yancey and Scribner (1989)	R10	1	Reverse Cyclic	Quasi-Static	Double Curvature
107	N	N	Yancey and Scribner (1989)	R11	1	Reverse Cyclic	Quasi-Static	Double Curvature
108	N	Y	Ghanem et al (1992)	SWA	0.33	Monotonic	Quasi-Static	Cantilever
109	N	Y	Ghanem et al (1992)	SWB	0.33	Monotonic	Quasi-Static	Cantilever
110	N	Y	Ghanem et al (1993)	SWA-2	0.33	Monotonic	Quasi-Static	Cantilever
111	N	Y	Ghanem et al (1993)	SWA-3	0.33	Monotonic	Quasi-Static	Cantilever
112	N	N	Tomazevic et al. (1996)	V2-BS	0.5	Reverse Cyclic	Quasi-Static	Cantilever
113	N	N	Tomazevic et al. (1996)	V2-BD	0.5	Reverse Cyclic	Dynamic	Cantilever
114	N	N	Tomazevic et al. (1996)	V2-CS	0.5	Phased-Sequential	Quasi-Static	Cantilever
115	N	N	Tomazevic et al. (1996)	V2-CD	0.5	Phased-Sequential	Dynamic	Cantilever
116	N	N	Tomazevic et al. (1996)	V2-DS	0.5	Simulated Seismic	Quasi-Static	Cantilever
117	N	N	Tomazevic et al. (1996)	V2-DD	0.5	Simulated Seismic	Dynamic	Cantilever
118	N	Y	Schultz (1996)	1	1	Phased-Sequential	Quasi-Static	Double Curvature
119	N	Y	Schultz (1996)	3	1	Phased-Sequential	Quasi-Static	Double Curvature
120	N	Y	Schultz (1996)	5	1	Phased-Sequential	Quasi-Static	Double Curvature
121	N	Y	Schultz (1996)	7	1	Phased-Sequential	Quasi-Static	Double Curvature
122	N	Y	Schultz (1996)	9	1	Phased-Sequential	Quasi-Static	Double Curvature
123	N	Y	Schultz (1996)	11	1	Phased-Sequential	Quasi-Static	Double Curvature
124	Y	Y	Schultz et al. (1998)	2	1	Phased-Sequential	Quasi-Static	Double Curvature
125	Y	Y	Schultz et al. (1998)	4	1	Phased-Sequential	Quasi-Static	Double Curvature
126	Y	Y	Schultz et al. (1998)	6	1	Phased-Sequential	Quasi-Static	Double Curvature
127	Y	Y	Schultz et al. (1998)	8	1	Phased-Sequential	Quasi-Static	Double Curvature
128	Y	Y	Schultz et al. (1998)	10	1	Phased-Sequential	Quasi-Static	Double Curvature
129	Y	Y	Schultz et al. (1998)	12	1	Phased-Sequential	Quasi-Static	Double Curvature
130	N	N	Voon and Ingham (2006)	5	1	Reverse Cyclic	Quasi-Static	Cantilever

Wall #	DATASET		Experimental Study	Wall ID	Scale	LOADING / BOUNDARY CONDITIONS		
	VA	VC				Loading Type	Loading Rate	Support Type
131	N	N	Voon and Ingham (2006)	6	1	Reverse Cyclic	Quasi-Static	Cantilever
132	N	N	Haach et al. (2007)	N60-B1	0.5	Reverse Cyclic	Quasi-Static	Cantilever
133	N	N	Haach et al. (2007)	N60-B2	0.5	Reverse Cyclic	Quasi-Static	Cantilever
134	N	N	Haach et al. (2007)	N150-B1	0.5	Reverse Cyclic	Quasi-Static	Cantilever
135	N	N	Haach et al. (2007)	N150-B2	0.5	Reverse Cyclic	Quasi-Static	Cantilever
136	Y	Y	Maleki et al. (2009)	Wall #1	0.47	Reverse Cyclic	Quasi-Static	Cantilever
137	Y	Y	Maleki et al. (2009)	Wall #2	0.47	Reverse Cyclic	Quasi-Static	Cantilever
138	Y	Y	Maleki et al. (2009)	Wall #3	0.47	Reverse Cyclic	Quasi-Static	Cantilever
139	Y	Y	Maleki et al. (2009)	Wall #4	0.47	Reverse Cyclic	Quasi-Static	Cantilever
140	Y	Y	Maleki et al. (2009)	Wall #5	0.47	Reverse Cyclic	Quasi-Static	Cantilever
141	N	Y	Elmapruk (2010)	PG127-48	1	Reverse Cyclic	Quasi-Static	Double Curvature
142	N	Y	Elmapruk (2010)	PG127-48I	1	Reverse Cyclic	Quasi-Static	Double Curvature
143	N	Y	Elmapruk (2010)	PG180-48	1	Reverse Cyclic	Quasi-Static	Double Curvature
144	N	Y	Elmapruk (2010)	PG254-48	1	Reverse Cyclic	Quasi-Static	Double Curvature
145	N	Y	Elmapruk (2010)	PG127-32	1	Reverse Cyclic	Quasi-Static	Double Curvature
146	N	Y	Elmapruk (2010)	PG127-24	1	Reverse Cyclic	Quasi-Static	Double Curvature
147	Y	Y	Minaie et al. (2010)	PCL 1	1	Reverse Cyclic	Quasi-Static	Cantilever
148	Y	Y	Minaie et al. (2010)	MC 1	1	Reverse Cyclic	Quasi-Static	Cantilever
149	Y	Y	Minaie et al. (2010)	PCL 2	1	Reverse Cyclic	Quasi-Static	Double Curvature
150	Y	Y	Minaie et al. (2010)	MC 2	1	Reverse Cyclic	Quasi-Static	Double Curvature
151	N	Y	Baenziger & Porter (2011)	A-1 (DR)	1	Reverse Cyclic	Quasi-Static	Cantilever
152	N	Y	Baenziger & Porter (2011)	A-2 (JR)	1	Reverse Cyclic	Quasi-Static	Cantilever
153	N	Y	Baenziger & Porter (2011)	A-6 (JRx2)	1	Reverse Cyclic	Quasi-Static	Cantilever
154	N	Y	Baenziger & Porter (2011)	B-7 (DR)	1	Reverse Cyclic	Quasi-Static	Cantilever
155	N	Y	Baenziger & Porter (2011)	B-5 (JR)	1	Reverse Cyclic	Quasi-Static	Cantilever
156	N	Y	Baenziger & Porter (2011)	D-3 (DR)	1	Reverse Cyclic	Quasi-Static	Cantilever

Wall #	DATASET		Experimental Study	Wall ID	Scale	LOADING / BOUNDARY CONDITIONS		
	VA	VC				Loading Type	Loading Rate	Support Type
157	N	Y	Baenziger & Porter (2011)	D-4 (JR)	1	Reverse Cyclic	Quasi-Static	Cantilever
158	N	Y	Baenziger & Porter (2011)	D-8 (JRx2)	1	Reverse Cyclic	Quasi-Static	Cantilever
159	N	Y	Nolph et al. (2012)	PG085-48	1	Reverse Cyclic	Quasi-Static	Cantilever
160	N	Y	Nolph et al. (2012)	PG120-48	1	Reverse Cyclic	Quasi-Static	Cantilever
161	N	Y	Nolph et al. (2012)	PG169-48	1	Reverse Cyclic	Quasi-Static	Cantilever
162	N	Y	Nolph et al. (2012)	PG085-32	1	Reverse Cyclic	Quasi-Static	Cantilever
163	N	Y	Nolph et al. (2012)	PG085-24	1	Reverse Cyclic	Quasi-Static	Cantilever
164	Y	Y	Oan (2013)	1	1	Monotonic	Quasi-Static	Cantilever
165	Y	Y	Oan (2013)	2	1	Monotonic	Quasi-Static	Cantilever
166	Y	Y	Oan (2013)	3	1	Monotonic	Quasi-Static	Cantilever
167	Y	Y	Oan (2013)	4	1	Monotonic	Quasi-Static	Cantilever
168	Y	Y	Oan (2013)	5	1	Monotonic	Quasi-Static	Cantilever
169	Y	Y	Oan (2013)	6	1	Monotonic	Quasi-Static	Cantilever
170	Y	Y	Oan (2013)	7	1	Monotonic	Quasi-Static	Cantilever
171	Y	Y	Oan (2013)	8	1	Monotonic	Quasi-Static	Cantilever
172	Y	Y	Oan (2013)	9	1	Monotonic	Quasi-Static	Cantilever
173	Y	Y	Oan (2013)	10	1	Monotonic	Quasi-Static	Cantilever
174	Y	Y	Oan (2013)	11	1	Monotonic	Quasi-Static	Cantilever
175	Y	Y	Oan (2013)	12	1	Monotonic	Quasi-Static	Cantilever
176	Y	Y	Oan (2013)	13	1	Monotonic	Quasi-Static	Cantilever
177	Y	Y	Oan (2013)	14	1	Monotonic	Quasi-Static	Cantilever
178	Y	Y	Oan (2013)	15	1	Monotonic	Quasi-Static	Cantilever
179	N	N	Oan (2013)	16	1	Monotonic	Quasi-Static	Cantilever
180	N	N	Oan (2013)	17	1	Monotonic	Quasi-Static	Cantilever
181	N	N	Oan (2013)	18	1	Monotonic	Quasi-Static	Cantilever
182	Y	Y	Oan (2013)	19	1	Monotonic	Quasi-Static	Cantilever

Wall #	DATASET		Experimental Study	Wall ID	Scale	LOADING / BOUNDARY CONDITIONS		
	VA	VC				Loading Type	Loading Rate	Support Type
183	Y	Y	Oan (2013)	20	1	Monotonic	Quasi-Static	Cantilever
184	Y	Y	Oan (2013)	21	1	Monotonic	Quasi-Static	Cantilever
185	Y	Y	Oan (2013)	22	1	Monotonic	Quasi-Static	Cantilever
186	Y	Y	Oan (2013)	23	1	Monotonic	Quasi-Static	Cantilever
187	Y	Y	Oan (2013)	24	1	Monotonic	Quasi-Static	Cantilever
188	Y	Y	Oan (2013)	25	1	Monotonic	Quasi-Static	Cantilever
189	Y	Y	Oan (2013)	26	1	Monotonic	Quasi-Static	Cantilever
190	Y	Y	Oan (2013)	27	1	Monotonic	Quasi-Static	Cantilever
191	Y	Y	Oan (2013)	28	1	Monotonic	Quasi-Static	Cantilever
192	Y	Y	Oan (2013)	29	1	Monotonic	Quasi-Static	Cantilever
193	Y	Y	Oan (2013)	30	1	Monotonic	Quasi-Static	Cantilever
194	Y	Y	Oan (2013)	31	1	Monotonic	Quasi-Static	Cantilever
195	Y	Y	Oan (2013)	32	1	Monotonic	Quasi-Static	Cantilever
196	Y	Y	Oan (2013)	33	1	Monotonic	Quasi-Static	Cantilever
197	N	N	Oan (2013)	34	1	Monotonic	Quasi-Static	Cantilever
198	N	N	Oan (2013)	35	1	Monotonic	Quasi-Static	Cantilever
199	N	N	Oan (2013)	36	1	Monotonic	Quasi-Static	Cantilever
200	Y	Y	Oan (2013)	37	1	Monotonic	Quasi-Static	Cantilever
201	Y	Y	Oan (2013)	38	1	Monotonic	Quasi-Static	Cantilever
202	Y	Y	Oan (2013)	39	1	Monotonic	Quasi-Static	Cantilever
203	Y	Y	Oan (2013)	40	1	Monotonic	Quasi-Static	Cantilever
204	Y	Y	Oan (2013)	41	1	Monotonic	Quasi-Static	Cantilever
205	Y	Y	Oan (2013)	42	1	Monotonic	Quasi-Static	Cantilever
206	Y	Y	Oan (2013)	43	1	Monotonic	Quasi-Static	Cantilever
207	Y	Y	Oan (2013)	44	1	Monotonic	Quasi-Static	Cantilever
208	Y	Y	Oan (2013)	45	1	Monotonic	Quasi-Static	Cantilever

Wall #	DATASET		Experimental Study	Wall ID	Scale	LOADING / BOUNDARY CONDITIONS		
	VA	VC				Loading Type	Loading Rate	Support Type
209	Y	Y	Oan (2013)	46	1	Monotonic	Quasi-Static	Cantilever
210	Y	Y	Oan (2013)	47	1	Monotonic	Quasi-Static	Cantilever
211	Y	Y	Oan (2013)	48	1	Monotonic	Quasi-Static	Cantilever
212	Y	Y	Oan (2013)	49	1	Monotonic	Quasi-Static	Cantilever
213	Y	Y	Oan (2013)	50	1	Monotonic	Quasi-Static	Cantilever
214	Y	Y	Oan (2013)	51	1	Monotonic	Quasi-Static	Cantilever
215	N	N	Oan (2013)	52	1	Monotonic	Quasi-Static	Cantilever
216	N	N	Oan (2013)	53	1	Monotonic	Quasi-Static	Cantilever
217	N	N	Oan (2013)	54	1	Monotonic	Quasi-Static	Cantilever
218	N	N	Oan (2013)	P2-55	1	Monotonic	Quasi-Static	Cantilever
219	N	N	Oan (2013)	P2-56	1	Monotonic	Quasi-Static	Cantilever
220	N	N	Oan (2013)	P2-57	1	Monotonic	Quasi-Static	Cantilever
221	N	N	Oan (2013)	P2-58	1	Monotonic	Quasi-Static	Cantilever
222	N	N	Oan (2013)	P2-59	1	Monotonic	Quasi-Static	Cantilever
223	N	N	Oan (2013)	P2-60	1	Monotonic	Quasi-Static	Cantilever
224	Y	Y	Oan (2013)	P2-61	1	Monotonic	Quasi-Static	Cantilever
225	Y	Y	Oan (2013)	P2-62	1	Monotonic	Quasi-Static	Cantilever
226	Y	Y	Oan (2013)	P2-63	1	Monotonic	Quasi-Static	Cantilever
227	Y	Y	Oan (2013)	P2-64	1	Monotonic	Quasi-Static	Cantilever
228	Y	Y	Oan (2013)	P2-65	1	Monotonic	Quasi-Static	Cantilever
229	Y	Y	Oan (2013)	P2-66	1	Monotonic	Quasi-Static	Cantilever
230	Y	Y	Hoque (2013)	1A	1	Reverse Cyclic	Quasi-Static	Double Curvature
231	Y	Y	Hoque (2013)	1B	1	Reverse Cyclic	Quasi-Static	Double Curvature
232	Y	Y	Hoque (2013)	2A	1	Reverse Cyclic	Quasi-Static	Double Curvature
233	Y	Y	Hoque (2013)	2B	1	Reverse Cyclic	Quasi-Static	Double Curvature
234	Y	Y	Hoque (2013)	3A	1	Reverse Cyclic	Quasi-Static	Double Curvature

Wall #	DATASET		Experimental Study	Wall ID	Scale	LOADING / BOUNDARY CONDITIONS		
	VA	VC				Loading Type	Loading Rate	Support Type
235	Y	Y	Hoque (2013)	3B	1	Reverse Cyclic	Quasi-Static	Double Curvature
236	Y	Y	Hoque (2013)	3C	1	Reverse Cyclic	Quasi-Static	Double Curvature
237	Y	Y	Hoque (2013)	4A	1	Reverse Cyclic	Quasi-Static	Double Curvature
238	Y	Y	Hoque (2013)	4B	1	Reverse Cyclic	Quasi-Static	Double Curvature
239	Y	Y	Hoque (2013)	4C	1	Reverse Cyclic	Quasi-Static	Double Curvature
240	Y	Y	Hoque (2013)	5A	1	Reverse Cyclic	Quasi-Static	Double Curvature
241	Y	Y	Hoque (2013)	5B	1	Reverse Cyclic	Quasi-Static	Double Curvature
242	Y	Y	Hoque (2013)	6A	1	Reverse Cyclic	Quasi-Static	Double Curvature
243	Y	Y	Hoque (2013)	6B	1	Reverse Cyclic	Quasi-Static	Double Curvature
244	Y	Y	Hoque (2013)	7A	1	Reverse Cyclic	Quasi-Static	Double Curvature
245	Y	Y	Hoque (2013)	7B	1	Reverse Cyclic	Quasi-Static	Double Curvature
246	Y	Y	Hoque (2013)	8A	1	Monotonic	Quasi-Static	Double Curvature
247	Y	Y	Hoque (2013)	8B	1	Monotonic	Quasi-Static	Double Curvature
248	N	N	Hamedzadeh (2013)	1A (Type A)	0.477	Monotonic	Quasi-Static	Double Curvature
249	Y	Y	Hamedzadeh (2013)	1B (Type A)	0.477	Monotonic	Quasi-Static	Double Curvature
250	Y	Y	Hamedzadeh (2013)	2A (Type A)	0.477	Monotonic	Quasi-Static	Double Curvature
251	Y	Y	Hamedzadeh (2013)	2B (Type A)	0.477	Monotonic	Quasi-Static	Double Curvature
252	Y	Y	Hamedzadeh (2013)	3A (Type A)	0.477	Monotonic	Quasi-Static	Double Curvature
253	Y	Y	Hamedzadeh (2013)	3B (Type A)	0.477	Monotonic	Quasi-Static	Double Curvature
254	Y	Y	Hamedzadeh (2013)	4A (Type B)	0.477	Monotonic	Quasi-Static	Double Curvature
255	Y	Y	Hamedzadeh (2013)	4B (Type B)	0.477	Monotonic	Quasi-Static	Double Curvature
256	Y	Y	Hamedzadeh (2013)	4C (Type B)	0.477	Monotonic	Quasi-Static	Double Curvature
257	Y	Y	Hamedzadeh (2013)	5A (Type B)	0.477	Monotonic	Quasi-Static	Double Curvature
258	Y	Y	Hamedzadeh (2013)	5B (Type B)	0.477	Monotonic	Quasi-Static	Double Curvature
259	Y	Y	Hamedzadeh (2013)	5C (Type B)	0.477	Monotonic	Quasi-Static	Double Curvature
260	Y	Y	Hamedzadeh (2013)	6A (Type C)	0.477	Monotonic	Quasi-Static	Double Curvature

Wall #	DATASET		Experimental Study	Wall ID	Scale	LOADING / BOUNDARY CONDITIONS		
	VA	VC				Loading Type	Loading Rate	Support Type
261	Y	Y	Hamedzadeh (2013)	6B (Type C)	0.477	Monotonic	Quasi-Static	Double Curvature
262	Y	Y	Hamedzadeh (2013)	6C (Type C)	0.477	Monotonic	Quasi-Static	Double Curvature
263	Y	Y	Hamedzadeh (2013)	7A (Type C)	0.477	Monotonic	Quasi-Static	Double Curvature
264	Y	Y	Hamedzadeh (2013)	7B (Type C)	0.477	Monotonic	Quasi-Static	Double Curvature
265	Y	Y	Hamedzadeh (2013)	7C (Type C)	0.477	Monotonic	Quasi-Static	Double Curvature
266	Y	Y	Hamedzadeh (2013)	8A (Type D)	0.477	Monotonic	Quasi-Static	Double Curvature
267	Y	Y	Hamedzadeh (2013)	8B (Type D)	0.477	Monotonic	Quasi-Static	Double Curvature
268	Y	Y	Hamedzadeh (2013)	8C (Type D)	0.477	Monotonic	Quasi-Static	Double Curvature
269	N	N	Rizaee (2015)	Wall 1-A	1	Reverse Cyclic	Quasi-Static	Double Curvature
270	Y	Y	Rizaee (2015)	Wall 2-A	1	Reverse Cyclic	Quasi-Static	Double Curvature
271	Y	Y	Rizaee (2015)	Wall 3-B	1	Reverse Cyclic	Quasi-Static	Double Curvature
272	Y	Y	Rizaee (2015)	Wall 4-B	1	Reverse Cyclic	Quasi-Static	Double Curvature
273	Y	Y	Rizaee (2015)	Wall 5-C	1	Reverse Cyclic	Quasi-Static	Double Curvature
274	Y	Y	Rizaee (2015)	Wall 6-C	1	Reverse Cyclic	Quasi-Static	Double Curvature
275	Y	Y	Rizaee (2015)	Wall 7-D	1	Reverse Cyclic	Quasi-Static	Double Curvature
276	Y	Y	Rizaee (2015)	Wall 8-D	1	Reverse Cyclic	Quasi-Static	Double Curvature
277	Y	Y	Rizaee (2015)	Wall 9-E	1	Reverse Cyclic	Quasi-Static	Double Curvature
278	Y	Y	Rizaee (2015)	Wall 10-E	1	Reverse Cyclic	Quasi-Static	Double Curvature
279	Y	Y	Rizaee (2015)	Wall 11-F	1	Reverse Cyclic	Quasi-Static	Double Curvature
280	Y	Y	Rizaee (2015)	Wall 12-F	1	Reverse Cyclic	Quasi-Static	Double Curvature
281	Y	Y	Rizaee (2015)	Wall 13-G	1	Reverse Cyclic	Quasi-Static	Double Curvature
282	Y	Y	Rizaee (2015)	Wall 14-G	1	Reverse Cyclic	Quasi-Static	Double Curvature
283	Y	Y	Ramirez et al. (2016)	M1	1	Reverse Cyclic	Quasi-Static	Cantilever
284	Y	Y	Ramirez et al. (2016)	M2	1	Reverse Cyclic	Quasi-Static	Cantilever
285	Y	Y	Ramirez et al. (2016)	M3	1	Reverse Cyclic	Quasi-Static	Cantilever
286	Y	Y	Ramirez et al. (2016)	M4	1	Reverse Cyclic	Quasi-Static	Cantilever

Wall #	DATASET		Experimental Study	Wall ID	Scale	LOADING / BOUNDARY CONDITIONS		
	VA	VC				Loading Type	Loading Rate	Support Type
287	Y	Y	Ramirez et al. (2016)	M5	1	Reverse Cyclic	Quasi-Static	Cantilever
288	Y	Y	Ramirez et al. (2016)	M6	1	Reverse Cyclic	Quasi-Static	Cantilever
289	Y	Y	Ramirez et al. (2016)	M7	1	Reverse Cyclic	Quasi-Static	Cantilever
290	Y	Y	Ramirez et al. (2016)	M8	1	Reverse Cyclic	Quasi-Static	Cantilever
291	Y	Y	Ramirez et al. (2016)	M9	1	Reverse Cyclic	Quasi-Static	Cantilever
292	Y	Y	Ramirez et al. (2016)	M10	1	Reverse Cyclic	Quasi-Static	Cantilever

Wall #	WALL GEOMETRY											PARTIAL GROUTING					
	H [mm]	H_v [mm]	H_{eff} [mm]	L [mm]	t [mm]	H_b [mm]	L_b [mm]	t_{fs} [mm]	n_g	n_t	d [mm]	A_{net} [mm^2]	A_{net}/A_{gross}	$s_{gv,max}$	$s_{gv,ave}$	$s_{gh,max}$	$s_{gh,ave}$
1	2438	2540	2540	2438	143	194	397	25.4	0	12	2388	123871	0.36	2438	2438	2642	2642
2	2438	2540	2540	2438	143	194	397	25.4	2	12	2388	160413	0.46	2438	2235	2642	2642
3	2438	2540	2540	2438	143	194	397	25.4	0	12	2388	123871	0.36	2438	2438	1016	813
4	2438	2540	2540	2438	143	194	397	25.4	2	12	2388	160413	0.46	2235	2235	1321	1219
5	2438	2540	2540	2438	143	194	397	25.4	3	12	2388	178684	0.51	1219	1118	1321	1219
6	2438	2540	2540	2438	143	194	397	25.4	4	12	2388	196955	0.57	813	745	2642	2642
7	2438	2540	2540	2438	143	194	397	25.4	2	12	2388	160413	0.46	2235	2235	2642	2642
8	2438	2540	2540	2438	143	194	397	25.4	5	12	2388	215226	0.62	813	745	2642	2642
9	2438	2540	2540	2438	143	194	397	25.4	5	12	2388	215226	0.62	813	745	1321	1219
10	2438	2540	2540	2438	143	194	397	25.4	5	12	2388	215226	0.62	813	745	1016	813
11	2438	2540	2540	2438	143	194	397	25.4	5	12	2388	215226	0.62	813	745	813	610
12	2438	2540	2540	2438	143	194	397	25.4	5	12	2388	215226	0.62	813	745	1016	813
13	2650	2750	2750	3200	150	190	390	25.4	7	16	3100	297968	0.62	800	650	2650	2650
14	2650	2750	2750	3200	150	190	390	25.4	7	16	3100	297968	0.62	800	650	2650	2650
15	2650	2750	2750	3200	150	190	390	25.4	7	16	3100	297968	0.62	800	650	2650	2650
16	2650	2750	2750	3200	150	190	390	25.4	5	16	3100	259280	0.54	1400	1300	2650	2650
17	2650	2750	2750	3200	150	190	390	25.4	5	16	3100	259280	0.54	1400	1300	2650	2650
18	2650	2750	2750	3200	150	190	390	25.4	7	16	3100	297968	0.62	800	650	2650	2650
19	2650	2750	2750	3200	150	190	390	25.4	5	16	3100	259280	0.54	1400	1300	2650	2650
20	2650	2750	2750	3200	150	190	390	25.4	7	16	3100	297968	0.62	800	650	2650	2650
21	2650	2750	2750	3200	150	190	390	25.4	7	16	3100	297968	0.62	800	650	2650	2650
22	2650	2750	2750	3200	150	190	390	25.4	7	16	3100	297968	0.62	800	650	2650	2650
23	2000	2100	2100	2000	150	190	390	25.4	4	10	1900	178976	0.60	1800		2000	
24	2000	2100	2100	2000	150	190	390	25.4	4	10	1900	178976	0.60	1800		2000	
25	2000	2100	2100	2000	150	190	390	25.4	4	10	1900	178976	0.60	1800		2000	

Wall #	WALL GEOMETRY											PARTIAL GROUTING					
	H [mm]	H_v [mm]	H_{eff} [mm]	L [mm]	t [mm]	H_b [mm]	L_b [mm]	t_{fs} [mm]	n_g	n_t	d [mm]	A_{net} [mm^2]	A_{net}/A_{gross}	$s_{gv,max}$	$s_{gv,ave}$	$s_{gh,max}$	$s_{gh,ave}$
26	2000	2100	2100	2000	150	190	390	25.4	4	10	1900	178976	0.60	1800		2000	
27	2000	2100	2100	2000	150	190	390	25.4	4	10	1900	178976	0.60	1800		2000	
28	2000	2100	2100	2000	150	190	390	25.4	6	10	1900	217664	0.73	900		2000	
29	2000	2100	2100	2000	150	190	390	25.4	4	10	1900	178976	0.60	1800		2000	
30	2000	2100	2100	2000	150	190	390	25.4	6	10	1900	217664	0.73	900		2000	
31	2000	2100	2100	2000	150	190	390	25.4	4	10	1900	178976	0.60	1800		2000	
32	2000	2100	2100	2000	150	190	390	25.4	4	10	1900	178976	0.60	1800		2000	
33	2000	2100	2100	2000	150	190	390	25.4	4	10	1900	178976	0.60	1800		2000	
34	1626		0	813	143							83045		613		1626	
35	1626		0	813	143							83045		613		1626	
36	1422	1830	915	1219	194	197	397	41.3	0		1168	100645	0.43	1219	1219	1422	1422
37	1422	1830	915	1219	194	197	397	41.3	2	6	1168	144748	0.61	1067	1067	711	711
38	1422	1830	915	1219	194	197	397	41.3	2	6	1168	144748	0.61	1067	1067	1422	1422
39	1422	1830	915	1219	194	197	397	41.3	2	6	1168	144748	0.61	1067	1067	508	474
40	2400		0	1600	140							158400	0.71	400		1000	
41	2400		0	1600	140							158400	0.71	400		2400	
42	2400		0	1600	140							158400	0.71	400		600	
43	1800	2475	1238	1720	150	190	390	35.0	5		1655	159400	0.62	400	350	600	600
44	1800	2475	1238	1720	150	190	390	35.0	5		1655	159400	0.62	400	350	600	600
45	1800	2475	1238	1320	150	190	390	35.0	4		1255	123600	0.62	400	333	600	600
46	1800	2475	1238	1320	150	190	390	35.0	4		1255	123600	0.62	400	333	600	600
47	1800	2475	1238	920	150	190	390	35.0	3		855	87800	0.64	300	300	600	600
48	1800	2475	1238	920	150	190	390	35.0	3		855	87800	0.64	300	300	600	600
49	1800	2475	1238	1320	150	190	390	35.0	4		1255	123600	0.62	400	333	0	0
50	1800	2475	1238	1320	150	190	390	35.0	4		1255	123600	0.62	400	333	0	0

Wall #	WALL GEOMETRY											PARTIAL GROUTING					
	H [mm]	H_v [mm]	H_{eff} [mm]	L [mm]	t [mm]	H_b [mm]	L_b [mm]	t_{fs} [mm]	n_g	n_t	d [mm]	A_{net} [mm^2]	A_{net}/A_{gross}	$s_{gv,max}$	$s_{gv,ave}$	$s_{gh,max}$	$s_{gh,ave}$
51	1800	2475	1238	1320	150	190	390	35.0	4		1255	123600	0.62	400	333	600	600
52	1800	2475	1238	1320	150	190	390	35.0	4		1255	123600	0.62	400	333	600	600
53	1800	2475	1238	1320	150	190	390	35.0	4		1255	123600	0.62	400	333	600	600
54	1800	2475	1238	1320	150	190	390	35.0	4		1255	123600	0.62	400	333	600	600
55	1800	2475	1238	1320	150	190	390	35.0	4		1255	123600	0.62	400	333	600	600
56	1800	2475	1238	1320	150	190	390	35.0	4		1255	123600	0.62	400	333	600	600
57	1800	2475	1238	1370	150	190	390	35.0	4		1293	127100	0.62	400	333	0	0
58	1800	2475	1238	1370	150	190	390	35.0	4		1293	127100	0.62	400	333	600	600
59	1800	2475	1238	1370	150	190	390	35.0	4		1293	127100	0.62	400	333	600	600
60	1800	2475	1238	1370	150	190	390	35.0	4		1293	127100	0.62	400	333	400	400
61	1800	2475	1238	1370	150	190	390	35.0	4		1293	127100	0.62	400	333	600	600
62	1800	2475	1238	1320	150	190	390	35.0	4		1255	123600	0.62	400	333	0	0
63	1800	2475	1238	1320	150	190	390	35.0	4		1255	123600	0.62	400	333	0	0
64	1800	2475	1238	1320	150	190	390	35.0	4		1255	123600	0.62	400	333	600	600
65	1800	2475	1238	1320	150	190	390	35.0	4		1255	123600	0.62	400	333	600	600
66	1800	2475	1238	1970	150	190	390	35.0	6		1880	184700	0.63	400	360	600	600
67	1800	2475	1238	1970	150	190	390	35.0	6		1880	184700	0.63	400	360	600	600
68	1800	2475	1238	1770	150	190	390	35.0	5		1680	162900	0.61	400	350	600	600
69	1800	2475	1238	1370	150	190	390	35.0	4		1280	127100	0.62	400	333	600	600
70	1800	2475	1238	970	150	190	390	35.0	3		880	91300	0.63	300	300	600	600
71	1800	2475	1238	970	150	190	390	35.0	3		880	91300	0.63	300	300	600	600
72	760	860	860	610	100	100	200	20	2	6	560	36400	0.60	510	510	760	760
73	760	860	860	610	100	100	200	20	2	6	560	36400	0.60	510	510	760	760
74	760	860	860	610	100	100	200	20	2	6	560	36400	0.60	510	510	760	760
75	760	860	860	610	100	100	200	20	2	6	560	36400	0.60	510	510	760	760

Wall #	WALL GEOMETRY											PARTIAL GROUTING					
	H [mm]	H_v [mm]	H_{eff} [mm]	L [mm]	t [mm]	H_b [mm]	L_b [mm]	t_{fs} [mm]	n_g	n_t	d [mm]	A_{net} [mm^2]	A_{net}/A_{gross}	$s_{gv,max}$	$s_{gv,ave}$	$s_{gh,max}$	$s_{gh,ave}$
76	1405	1505	1505	610	100	100	200	20	2	6	560	36400	0.60	510	510	1405	1405
77	760	860	860	610	100	100	200	20	2	6	560	36400	0.60	510	510	760	760
78	760	860	860	610	100	100	200	20	2	6	560	36400	0.60	510	510	760	760
79	760	860	860	610	100	100	200	20	2	6	560	36400	0.60	510	510	760	760
80	760	860	860	610	100	100	200	20	2	6	560	36400	0.60	510	510	760	760
81	1405	1505	1505	610	100	100	200	20	2	6	560	36400	0.60	510	510	1405	1405
82	813	1422	711	813	194	194	397	32	2	4	762	103276	0.66	610	610	813	813
83	813	1422	711	813	194	194	397	32	2	4	762	103276	0.66	610	610	813	813
84	813	1422	711	813	194	194	397	32	2	4	762	103276	0.66	610	610	813	813
85	813	1422	711	813	194	194	397	32	2	4	762	103276	0.66	610	610	813	813
86	813	1422	711	813	194	194	397	32	2	4	762	103276	0.66	610	610	813	813
87	813	1422	711	813	194	194	397	32	2	4	762	103276	0.66	610	610	813	813
88	813	1422	711	813	194	194	397	32	2	4	762	103276	0.66	610	610	813	813
89	813	1422	711	813	194	194	397	32	2	4	762	103276	0.66	610	610	813	813
90	813	1422	711	813	194	194	397	32	2	4	762	103276	0.66	610	610	813	813
91	813	1422	711	813	194	194	397	32	2	4	762	103276	0.66	610	610	813	813
92	813	1422	711	813	194	194	397	32	2	4	762	103276	0.66	610	610	813	813
93	813	1422	711	813	194	194	397	32	2	4	762	103276	0.66	610	610	813	813
94	813	1422	711	813	194	194	397	32	2	4	762	103276	0.66	610	610	813	813
95	813	1422	711	813	194	194	397	32	2	4	762	103276	0.66	610	610	813	813
96	813	1422	711	813	194	194	397	32	2	4	762	103276	0.66	610	610	813	813
97	813	1422	711	813	194	194	397	32	2	4	762	103276	0.66	610	610	813	813
98	1422		0	1219	194							126774	0.54	1219		1422	
99	1422		0	1219	194							126774	0.54	1219		1422	
100	1422		0	1219	194							126774	0.54	1219		1422	

Wall #	WALL GEOMETRY											PARTIAL GROUTING					
	H [mm]	H_v [mm]	H_{eff} [mm]	L [mm]	t [mm]	H_b [mm]	L_b [mm]	t_{fs} [mm]	n_g	n_t	d [mm]	A_{net} [mm^2]	A_{net}/A_{gross}	$s_{gv,max}$	$s_{gv,ave}$	$s_{gh,max}$	$s_{gh,ave}$
101	1422		0	1219	194							126774	0.54	1219		711	
102	1422		0	1219	194							126774	0.54	1219		711	
103	1422		0	1219	194							126774	0.54	1219		800	
104	1422		0	1219	194							126774	0.54	1219		711	
105	1422		0	1219	194							126774	0.54	1219		711	
106	1422		0	1219	194							126774	0.54	1219		711	
107	1422		0	1219	194							126774	0.54	1219		800	
108	920	1022	1022	939	47.8	64.6	132	8.5	2	14	906	19974	0.45	871	871	874	874
109	920	1022	1022	939	47.8	64.6	132	8.5	3	14	906	22012	0.49	470	436	432	432
110	920	1022	1022	939	47.8	64.6	132	8.5	3	14	906	22012	0.49	470	436	432	432
111	920	1022	1022	939	47.8	64.6	132	8.5	3	14	906	22012	0.49	470	436	432	432
112	760		0	610	100							42300	0.69	510		760	
113	760		0	610	100							42300	0.69	510		760	
114	760		0	610	100							42300	0.69	510		760	
115	760		0	610	100							42300	0.69	510		760	
116	760		0	610	100							42300	0.69	510		760	
117	760		0	610	100							42300	0.69	510		760	
118	1422	2032	1016	2845	195	194	396	33.7	2	7	2794	242283	0.44	2642	2642	711	711
119	1422	2032	1016	2032	195	194	396	33.7	2	7	1981	187486	0.47	1829	1829	711	711
120	1422	2032	1016	1422	195	194	396	33.7	2	7	1371	146372	0.53	1219	1219	711	711
121	1422	2032	1016	2845	195	194	396	33.7	2	7	2794	242283	0.44	2642	2642	711	711
122	1422	2032	1016	2032	195	194	396	33.7	2	7	1981	187486	0.47	1829	1829	711	711
123	1422	2032	1016	1422	195	194	396	33.7	2	7	1371	146372	0.53	1219	1219	711	711
124	1422	2032	1016	2845	195	194	396	33.7	2	7	2794	242283	0.44	2642	2642	1422	1422
125	1422	2032	1016	2032	195	194	396	33.7	2	7	1981	187486	0.47	1829	1829	1422	1422

Wall #	WALL GEOMETRY											PARTIAL GROUTING					
	H [mm]	H_v [mm]	H_{eff} [mm]	L [mm]	t [mm]	H_b [mm]	L_b [mm]	t_{fs} [mm]	n_g	n_t	d [mm]	A_{net} [mm^2]	A_{net}/A_{gross}	$s_{gv,max}$	$s_{gv,ave}$	$s_{gh,max}$	$s_{gh,ave}$
126	1422	2032	1016	1422	195	194	396	33.7	2	7	1371	146372	0.53	1219	1219	1422	1422
127	1422	2032	1016	2845	195	194	396	33.7	2	7	2794	242283	0.44	2642	2642	1422	1422
128	1422	2032	1016	2032	195	194	396	33.7	2	7	1981	187486	0.47	1829	1829	1422	1422
129	1422	2032	1016	1422	195	194	396	33.7	2	7	1371	146372	0.53	1219	1219	1422	1422
130	1800			1800	140							186000	0.74	400		1800	
131	1800		0	1800	140							186000	0.74	800		1800	
132	808	948	948	1200	100	93	200	16	3		1150	43908	0.37	500	500	808	808
133	808	948	948	1200	100	93	200	16	3		1150	43908	0.37	500	500	808	808
134	808	948	948	1200	100	93	200	16	3		1150	43908	0.37	500	500	808	808
135	808	948	948	1200	100	93	200	16	3		1150	43908	0.37	500	500	808	808
136	1800	1820	1820	1800	90	90	185	15.5	3	19	1755	72173	0.45	855	855	855	855
137	1800	1820	1820	1800	90	90	185	15.5	4	19	1755	77630	0.48	570	570	570	570
138	1800	1820	1820	1800	90	90	185	15.5	2	19	1755	66715	0.41	1710	1710	1710	1710
139	945	965	965	1800	90	90	185	15.5	3	19	1755	72173	0.45	855	855	855	855
140	2655	2675	2675	1800	90	90	185	15.5	3	19	1755	72173	0.45	855	855	855	855
141	1422	1524	762	2642	194	194	397	31.8	3	13	2591	245236	0.48	1219	1219	711.2	711.2
142	1422	1524	762	2642	194	194	397	31.8	3	13	2591	245236	0.48	1219	1219	711.2	711.2
143	1422	1524	762	2642	194	194	397	31.8	3	13	2591	245236	0.48	1219	1219	711.2	711.2
144	1422	1524	762	2642	194	194	397	31.8	3	13	2591	245236	0.48	1219	1219	711.2	711.2
145	1422	1524	762	2642	194	194	397	31.8	4	13	2591	271068	0.53	812.8	812.8	711.2	711.2
146	1422	1524	762	2642	194	194	397	31.8	5	13	2591	296900	0.58	609.6	609.6	711.2	711.2
147	2438	2642	2642	3861	194	194	397	31.8	4	19	3810	348487	0.47	1219	1219	1200	1168
148	2438	2642	2642	3861	194	194	397	31.8	4	19	3810	348487	0.47	1219	1219	1200	1168
149	2438	2642	1321	3861	194	194	397	31.8	4	19	3810	348487	0.47	1219	1219	1200	1168
150	2438	2642	1321	3861	194	194	397	31.8	4	19	3810	348487	0.47	1219	1219	1200	1168

Wall #	WALL GEOMETRY											PARTIAL GROUTING					
	H [mm]	H_v [mm]	H_{eff} [mm]	L [mm]	t [mm]	H_b [mm]	L_b [mm]	t_{fs} [mm]	n_g	n_t	d [mm]	A_{net} [mm^2]	A_{net}/A_{gross}	$s_{gv,max}$	$s_{gv,ave}$	$s_{gh,max}$	$s_{gh,ave}$
151	2438	2540	2540	2844.8	193.7	194	397	38.1	4	14	2794	310020	0.56	1219	881	1219	1168
152	2438	2540	2540	2844.8	193.7	194	397	38.1	4	14	2794	310020	0.56	1219	881	203	203
153	2438	2540	2540	2844.8	193.7	194	397	38.1	6	14	2794	356642	0.65	1016	745	203	203
154	2438	2540	2540	2844.8	193.7	194	397	38.1	6	14	2794	356642	0.65	1016	745	1219	1168
155	2438	2540	2540	2844.8	193.7	194	397	38.1	6	14	2794	356642	0.65	1016	745	203	203
156	2438	2540	2540	4267.2	193.7	194	397	38.1	6	21	4216	465029	0.56	1219	813	1219	1168
157	2438	2540	2540	4267.2	193.7	194	397	38.1	8	21	4216	511652	0.62	1219	732	203	203
158	2438	2540	2540	4267.2	193.7	194	397	38.1	8	21	4216	511652	0.62	1219	732	203	203
159	2235	2337	2337	2631	193.7	194	397	31.8	3	13	2535	244563	0.48	1219	1219	1118	1118
160	2235	2337	2337	2631	193.7	194	397	31.8	3	13	2535	244563	0.48	1219	1219	1118	1118
161	2235	2337	2337	2631	193.7	194	397	31.8	3	13	2535	244563	0.48	1219	1219	1118	1118
162	2235	2337	2337	2631	193.7	194	397	31.8	4	13	2535	270395	0.53	813	813	1118	1118
163	2235	2337	2337	2631	193.7	194	397	31.8	5	13	2535	296227	0.58	610	610	1118	1118
164	1000	1200	1200	1600	190	190	390	35	4	8	1500	205600	0.68	600	466.7	1200	1200
165	1000	1200	1200	1600	190	190	390	35	4	8	1500	205600	0.68	600	466.7	1200	1200
166	1000	1200	1200	1600	190	190	390	35	4	8	1500	205600	0.68	600	466.7	1200	1200
167	1000	1200	1200	1600	190	190	390	35	4	8	1500	205600	0.68	600	466.7	1200	1200
168	1000	1200	1200	1600	190	190	390	35	4	8	1500	205600	0.68	600	466.7	1200	1200
169	1000	1200	1200	1600	190	190	390	35	4	8	1500	205600	0.68	600	466.7	1200	1200
170	1000	1200	1200	1600	190	190	390	35	4	8	1500	205600	0.68	600	466.7	1200	1200
171	1000	1200	1200	1600	190	190	390	35	4	8	1500	205600	0.68	600	466.7	1200	1200
172	1000	1200	1200	1600	190	190	390	35	4	8	1500	205600	0.68	600	466.7	1200	1200
173	1000	1200	1200	1600	190	190	390	35	4	8	1500	205600	0.68	600	466.7	1200	1200
174	1000	1200	1200	1600	190	190	390	35	4	8	1500	205600	0.68	600	466.7	1200	1200
175	1000	1200	1200	1600	190	190	390	35	4	8	1500	205600	0.68	600	466.7	1200	1200

Wall #	WALL GEOMETRY											PARTIAL GROUTING					
	H [mm]	**H_v [mm]**	**H_{eff} [mm]**	**L [mm]**	**t [mm]**	**H_b [mm]**	**L_b [mm]**	**t_{fs} [mm]**	**n_g**	**n_t**	**d [mm]**	**A_{net} [mm^2]**	**A_{net}/A_{gross}**	**$s_{gv,max}$**	**$s_{gv,ave}$**	**$s_{gh,max}$**	**$s_{gh,ave}$**
176	1000	1200	1200	1600	190	190	390	35	4	8	1500	205600	0.68	600	466.7	1200	1200
177	1000	1200	1200	1600	190	190	390	35	4	8	1500	205600	0.68	600	466.7	1200	1200
178	1000	1200	1200	1600	190	190	390	35	4	8	1500	205600	0.68	600	466.7	1200	1200
179	1000	1200	1200	1600	190	190	390	35	0	8	1500	112000	0.37	1600	1600	1200	1200
180	1000	1200	1200	1600	190	190	390	35	0	8	1500	112000	0.37	1600	1600	1200	1200
181	1000	1200	1200	1600	190	190	390	35	0	8	1500	112000	0.37	1600	1600	1200	1200
182	1000	1200	1200	1600	190	190	390	35	4	8	1500	205600	0.68	600	466.7	1200	1200
183	1000	1200	1200	1600	190	190	390	35	4	8	1500	205600	0.68	600	466.7	1200	1200
184	1000	1200	1200	1600	190	190	390	35	4	8	1500	205600	0.68	600	466.7	1200	1200
185	1000	1200	1200	1600	190	190	390	35	4	8	1500	205600	0.68	600	466.7	1200	1200
186	1000	1200	1200	1600	190	190	390	35	4	8	1500	205600	0.68	600	466.7	1200	1200
187	1000	1200	1200	1600	190	190	390	35	4	8	1500	205600	0.68	600	466.7	1200	1200
188	1000	1200	1200	1600	190	190	390	35	4	8	1500	205600	0.68	600	466.7	1200	1200
189	1000	1200	1200	1600	190	190	390	35	4	8	1500	205600	0.68	600	466.7	1200	1200
190	1000	1200	1200	1600	190	190	390	35	4	8	1500	205600	0.68	600	466.7	1200	1200
191	1000	1200	1200	1600	190	190	390	35	4	8	1500	205600	0.68	600	466.7	1200	1200
192	1000	1200	1200	1600	190	190	390	35	4	8	1500	205600	0.68	600	466.7	1200	1200
193	1000	1200	1200	1600	190	190	390	35	4	8	1500	205600	0.68	600	466.7	1200	1200
194	1000	1200	1200	1600	190	190	390	35	4	8	1500	205600	0.68	600	466.7	1200	1200
195	1000	1200	1200	1600	190	190	390	35	4	8	1500	205600	0.68	600	466.7	1200	1200
196	1000	1200	1200	1600	190	190	390	35	4	8	1500	205600	0.68	600	466.7	1200	1200
197	1000	1200	1200	1600	190	190	390	35	0	8	1500	112000	0.37	1600	1600	1200	1200
198	1000	1200	1200	1600	190	190	390	35	0	8	1500	112000	0.37	1600	1600	1200	1200
199	1000	1200	1200	1600	190	190	390	35	0	8	1500	112000	0.37	1600	1600	1200	1200
200	1000	1200	1200	1600	190	190	390	35	4	8	1500	205600	0.68	600	466.7	1200	1200

Wall #	WALL GEOMETRY											PARTIAL GROUTING					
	H [mm]	**H_v [mm]**	**H_{eff} [mm]**	**L [mm]**	**t [mm]**	**H_b [mm]**	**L_b [mm]**	**t_{fs} [mm]**	**n_g**	**n_t**	**d [mm]**	**A_{net} [mm^2]**	**A_{net}/A_{gross}**	**$s_{gv,max}$**	**$s_{gv,ave}$**	**$s_{gh,max}$**	**$s_{gh,ave}$**
201	1000	1200	1200	1600	190	190	390	35	4	8	1500	205600	0.68	600	466.7	1200	1200
202	1000	1200	1200	1600	190	190	390	35	4	8	1500	205600	0.68	600	466.7	1200	1200
203	1000	1200	1200	1600	190	190	390	35	4	8	1500	205600	0.68	600	466.7	1200	1200
204	1000	1200	1200	1600	190	190	390	35	4	8	1500	205600	0.68	600	466.7	1200	1200
205	1000	1200	1200	1600	190	190	390	35	4	8	1500	205600	0.68	600	466.7	1200	1200
206	1000	1200	1200	1600	190	190	390	35	4	8	1500	205600	0.68	600	466.7	1200	1200
207	1000	1200	1200	1600	190	190	390	35	4	8	1500	205600	0.68	600	466.7	1200	1200
208	1000	1200	1200	1600	190	190	390	35	4	8	1500	205600	0.68	600	466.7	1200	1200
209	1000	1200	1200	1600	190	190	390	35	4	8	1500	205600	0.68	600	466.7	1200	1200
210	1000	1200	1200	1600	190	190	390	35	4	8	1500	205600	0.68	600	466.7	1200	1200
211	1000	1200	1200	1600	190	190	390	35	4	8	1500	205600	0.68	600	466.7	1200	1200
212	1000	1200	1200	1600	190	190	390	35	4	8	1500	205600	0.68	600	466.7	1200	1200
213	1000	1200	1200	1600	190	190	390	35	4	8	1500	205600	0.68	600	466.7	1200	1200
214	1000	1200	1200	1600	190	190	390	35	4	8	1500	205600	0.68	600	466.7	1200	1200
215	1000	1200	1200	1600	190	190	390	35	0	8	1500	112000	0.37	1600	1600	1200	1200
216	1000	1200	1200	1600	190	190	390	35	0	8	1500	112000	0.37	1600	1600	1200	1200
217	1000	1200	1200	1600	190	190	390	35	0	8	1500	112000	0.37	1600	1600	1200	1200
218	1000	1200	1200	1600	190	190	390	35	0	8	1500	112000	0.37	1600	1600	1200	1200
219	1000	1200	1200	1600	190	190	390	35	0	8	1500	112000	0.37	1600	1600	1200	1200
220	1000	1200	1200	1600	190	190	390	35	0	8	1500	112000	0.37	1600	1600	1200	1200
221	1000	1200	1200	1600	190	190	390	35	0	8	1500	112000	0.37	1600	1600	1200	1200
222	1000	1200	1200	1600	190	190	390	35	0	8	1500	112000	0.37	1600	1600	1200	1200
223	1000	1200	1200	1600	190	190	390	35	0	8	1500	112000	0.37	1600	1600	1200	1200
224	1000	1200	1200	1600	190	190	390	35	4	8	1500	205600	0.68	600	466.7	1200	1200
225	1000	1200	1200	1600	190	190	390	35	4	8	1500	205600	0.68	600	466.7	1200	1200

Wall #	WALL GEOMETRY											PARTIAL GROUTING					
	H [mm]	**H_v [mm]**	**H_{eff} [mm]**	**L [mm]**	**t [mm]**	**H_b [mm]**	**L_b [mm]**	**t_{fs} [mm]**	**n_g**	**n_t**	**d [mm]**	**A_{net} [mm^2]**	**A_{net}/A_{gross}**	**$s_{gv,max}$**	**$s_{gv,ave}$**	**$s_{gh,max}$**	**$s_{gh,ave}$**
226	1000	1200	1200	1600	190	190	390	35	4	8	1500	205600	0.68	600	466.7	1200	1200
227	1000	1200	1200	1600	190	190	390	35	4	8	1500	205600	0.68	600	466.7	1200	1200
228	1000	1200	1200	1600	190	190	390	35	4	8	1500	205600	0.68	600	466.7	1200	1200
229	1000	1200	1200	1600	190	190	390	35	4	8	1500	205600	0.68	600	466.7	1200	1200
230	1800	2025	1013	1800	190	190	390	36.2	3	9	1700	199116	0.58	800	800	900	850
231	1800	2025	1013	1800	190	190	390	36.2	3	9	1700	199116	0.58	800	800	900	850
232	1800	2025	1013	1800	190	190	390	36.2	3	9	1700	199116	0.58	800	800	900	850
233	1800	2025	1013	1800	190	190	390	36.2	3	9	1700	199116	0.58	800	800	900	850
234	1800	2025	1013	1800	190	190	390	36.2	3	9	1700	199116	0.58	800	800	900	850
235	1800	2025	1013	1800	190	190	390	36.2	3	9	1700	199116	0.58	800	800	900	850
236	1800	2025	1013	1800	190	190	390	36.2	3	9	1700	199116	0.58	800	800	900	850
237	1800	2025	1013	1800	190	190	390	36.2	3	9	1700	199116	0.58	800	800	700	600
238	1800	2025	1013	1800	190	190	390	36.2	3	9	1700	199116	0.58	800	800	700	600
239	1800	2025	1013	1800	190	190	390	36.2	3	9	1700	199116	0.58	800	800	700	600
240	1800	2025	1013	1800	190	190	390	36.2	3	9	1700	199116	0.58	800	800	1800	1800
241	1800	2025	1013	1800	190	190	390	36.2	3	9	1700	199116	0.58	800	800	1800	1800
242	1800	2025	1013	1800	190	190	390	36.2	3	9	1700	199116	0.58	800	800	1800	1800
243	1800	2025	1013	1800	190	190	390	36.2	3	9	1700	199116	0.58	800	800	1800	1800
244	1800	2025	1013	1800	190	190	390	36.2	3	9	1700	199116	0.58	800	800	1800	1800
245	1800	2025	1013	1800	190	190	390	36.2	3	9	1700	199116	0.58	800	800	1800	1800
246	1800	2025	1013	1800	190	190	390	36.2	3	9	1700	199116	0.58	800	800	1800	1800
247	1800	2025	1013	1800	190	190	390	36.2	3	9	1700	199116	0.58	800	800	1800	1800
248	1045	1140	570	1233	90.7	90.8	186.1	16.3	2	13	1187	51008	0.46	1140	1140	1235	1235
249	1045	1140	570	1233	90.7	90.8	186.1	16.3	2	13	1187	51008	0.46	1140	1140	1235	1235
250	1045	1140	570	1233	90.7	90.8	186.1	16.3	2	13	1187	51008	0.46	1140	1140	1235	1235

Wall #	WALL GEOMETRY											PARTIAL GROUTING					
	H [mm]	**H_v [mm]**	**H_{eff} [mm]**	**L [mm]**	**t [mm]**	**H_b [mm]**	**L_b [mm]**	**t_{fs} [mm]**	**n_g**	**n_t**	**d [mm]**	**A_{net} [mm^2]**	**A_{net}/A_{gross}**	**$s_{gv,max}$**	**$s_{gv,ave}$**	**$s_{gh,max}$**	**$s_{gh,ave}$**
251	1045	1140	570	1233	90.7	90.8	186.1	16.3	2	13	1187	51008	0.46	1140	1140	1235	1235
252	1235	1437	719	1233	90.7	90.8	186.1	16.3	2	13	1187	51008	0.46	1140	1140	1190	1190
253	1235	1437	719	1233	90.7	90.8	186.1	16.3	2	13	1187	51008	0.46	1140	1140	1190	1190
254	1235	1437	719	2372	90.7	90.8	186.1	16.3	3	25	2326	93546	0.43	1140	1140	1190	1190
255	1235	1437	719	2372	90.7	90.8	186.1	16.3	3	25	2326	93546	0.43	1140	1140	1190	1190
256	1235	1437	719	2372	90.7	90.8	186.1	16.3	3	25	2326	93546	0.43	1140	1140	1190	1190
257	1235	1437	719	2372	90.7	90.8	186.1	16.3	3	25	2326	93546	0.43	1140	1140	1190	1190
258	1235	1437	719	2372	90.7	90.8	186.1	16.3	3	25	2326	93546	0.43	1140	1140	1190	1190
259	1235	1437	719	2372	90.7	90.8	186.1	16.3	3	25	2326	93546	0.43	1140	1140	1190	1190
260	760	962	481	2372	90.7	90.8	186.1	16.3	4	25	2326	98952	0.46	760	760	714.6	714.6
261	760	962	481	2372	90.7	90.8	186.1	16.3	4	25	2326	98952	0.46	760	760	714.6	714.6
262	760	962	481	2372	90.7	90.8	186.1	16.3	4	25	2326	98952	0.46	760	760	714.6	714.6
263	760	962	481	2372	90.7	90.8	186.1	16.3	4	25	2326	98952	0.46	760	760	714.6	714.6
264	760	962	481	2372	90.7	90.8	186.1	16.3	4	25	2326	98952	0.46	760	760	714.6	714.6
265	760	962	481	2372	90.7	90.8	186.1	16.3	4	25	2326	98952	0.46	760	760	714.6	714.6
266	760	962	481	853	90.7	90.8	186.1	16.3	2	9	807	38620	0.50	760	760	714.6	714.6
267	760	962	481	853	90.7	90.8	186.1	16.3	2	9	807	38620	0.50	760	760	714.6	714.6
268	760	962	481	853	90.7	90.8	186.1	16.3	2	9	807	38620	0.50	760	760	714.6	714.6
269	1800	2025	1013	1800	190	190	390	37.8	3	9	1700	202883	0.59	800	800	900	850
270	1800	2025	1013	1800	190	190	390	37.8	3	9	1700	202883	0.59	800	800	900	850
271	1800	2025	1013	1800	190	190	390	37.8	3	9	1700	202883	0.59	800	800	900	850
272	1800	2025	1013	1800	190	190	390	37.8	3	9	1700	202883	0.59	800	800	900	850
273	1800	2025	1013	1800	190	190	390	37.8	3	9	1700	202883	0.59	800	800	900	850
274	1800	2025	1013	1800	190	190	390	37.8	3	9	1700	202883	0.59	800	800	900	850
275	1800	2025	1013	1800	190	190	390	37.8	3	9	1700	202883	0.59	800	800	900	850

Wall #	WALL GEOMETRY											PARTIAL GROUTING					
	H [mm]	**H_v [mm]**	**H_{eff} [mm]**	**L [mm]**	**t [mm]**	**H_b [mm]**	**L_b [mm]**	**t_{fs} [mm]**	**n_g**	**n_t**	**d [mm]**	**A_{net} [mm^2]**	**A_{net}/A_{gross}**	**$s_{gv,max}$**	**$s_{gv,ave}$**	**$s_{gh,max}$**	**$s_{gh,ave}$**
276	1800	2025	1013	1800	190	190	390	37.8	3	9	1700	202883	0.59	800	800	900	850
277	1800	2025	1013	1800	190	190	390	37.8	3	9	1700	202883	0.59	800	800	900	850
278	1800	2025	1013	1800	190	190	390	37.8	3	9	1700	202883	0.59	800	800	900	850
279	1800	2025	1013	1800	190	190	390	37.8	3	9	1700	202883	0.59	800	800	700	600
280	1800	2025	1013	1800	190	190	390	37.8	3	9	1700	202883	0.59	800	800	700	600
281	1800	2025	1013	1800	190	190	390	37.8	3	9	1700	202883	0.59	800	800	800	850
282	1800	2025	1013	1800	190	190	390	37.8	3	9	1700	202883	0.59	800	800	800	850
283	1800	1930	1930	1990	140	190	390	37.5	4	10	1890	199950	0.72	597	597	1930	1930
284	1800	1930	1930	1990	140	190	390	37.5	4	10	1890	199950	0.72	597	597	1930	1930
285	1800	1930	1930	1990	140	190	390	37.5	4	10	1890	199950	0.72	597	597	1930	1930
286	1800	1930	1930	1990	140	190	390	37.5	4	10	1890	199950	0.72	597	597	1930	1930
287	1000	1130	1130	2590	140	190	390	37.5	5	13	2490	257625	0.71	598	598	1130	1130
288	1000	1130	1130	2590	140	190	390	37.5	5	13	2490	257625	0.71	598	598	1130	1130
289	1000	1130	1130	2590	140	190	390	37.5	5	13	2490	257625	0.71	598	598	1130	1130
290	1800	1930	1930	990	140	190	390	37.5	3	5	890	112275	0.81	396	396	1930	1930
291	1800	1930	1930	990	140	190	390	37.5	3	5	890	112275	0.81	396	396	1930	1930
292	1800	1930	1930	990	140	190	390	37.5	3	5	890	112275	0.81	396	396	1930	1930

Wall #	MASONRY MATERIALS											
	f_{block} [MPa]	**f_{mortar} [MPa]**	**f_{grout} [MPa]**	***v***	**$f'_{mg,u}$**	**$f'_{mu,u}$**	**# of courses in Prism**	**Prism h/t**	**Corr. factor, k**	**f'_{mg}**	**f'_{mu}**	**$f'_{m,eff}$**
1	22.8	19.9	31.5	62%	12.6	16.3	-	-	1	12.6	16.3	16.3
2	30.0	21.9	36.1	62%	14.5	20.4	-	-	1	14.5	20.4	19.4
3	22.8	19.9	31.5	62%	12.6	16.3	-	-	1	12.6	16.3	16.3
4	22.8	19.9	31.5	62%	12.6	16.3	-	-	1	12.6	16.3	15.7
5	22.8	19.9	31.5	62%	12.6	16.3	-	-	1	12.6	16.3	15.4
6	22.8	19.9	31.5	62%	12.6	16.3	-	-	1	12.6	16.3	15.1
7	30.0	21.9	36.1	62%	14.5	20.4	-	-	1	14.5	20.4	19.4
8	22.8	19.9	31.5	62%	12.6	16.3	-	-	1	12.6	16.3	14.8
9	30.0	21.9	36.1	62%	14.5	20.4	-	-	1	14.5	20.4	18.0
10	30.0	21.9	36.1	62%	14.5	20.4	-	-	1	14.5	20.4	18.0
11	30.0	21.9	36.1	62%	14.5	20.4	-	-	1	14.5	20.4	18.0
12	30.0	21.9	36.1	62%	14.5	20.4	-	-	1	14.5	20.4	18.0
13	12.3	25.8	22.0	0.57	12.6	10.3	3	3.93	0.938	11.8	9.7	10.6
14	12.3	23.8	21.0	0.57	11.9	10.3	3	3.93	0.938	11.1	9.7	10.3
15	12.3	20.9	29.4	0.57	11.7	10.3	3	3.93	0.938	11.0	9.7	10.2
16	12.3	15.7	14.8	0.57	8.6	10.3	3	3.93	0.938	8.1	9.7	9.2
17	12.3	22.8	30.6	0.57	12.5	10.3	3	3.93	0.938	11.7	9.7	10.3
18	12.3	21.4	24.3	0.57	11.4	10.3	3	3.93	0.938	10.7	9.7	10.1
19	12.3	22.0	32.3	0.57	12.3	10.3	3	3.93	0.938	11.6	9.7	10.2
20	12.3	16.1	21.0	0.57	9.3	10.3	3	3.93	0.938	8.7	9.7	9.3
21	12.3	21.5	22.8	0.57	11.3	10.3	3	3.93	0.938	10.6	9.7	10.0
22	12.3	21.7	30.4	0.57	12.1	10.3	3	3.93	0.938	11.3	9.7	10.4
23	-	15.2	29.3	0.57	-	10.3	3	3.93	0.938	-	9.7	-
24	-	20.4	33.1	0.57	-	10.3	3	3.93	0.938	-	9.7	-
25	-	25.7	13.3	0.57	-	14.4	3	3.93	0.938	-	13.5	-

Wall #	MASONRY MATERIALS											
	f_{block} [MPa]	**f_{mortar} [MPa]**	**f_{grout} [MPa]**	***v***	**$f'_{mg,u}$**	**$f'_{mu,u}$**	**# of courses in Prism**	**Prism h/t**	**Corr. factor, k**	**f'_{mg}**	**f'_{mu}**	**$f'_{m,eff}$**
26	-	23.1	15.9	0.57	-	14.4	3	3.93	0.938	-	13.5	-
27	-	24.8	18.8	0.57	-	14.4	3	3.93	0.938	-	13.5	-
28	-	20.4	10.6	0.57	-	14.4	3	3.93	0.938	-	13.5	-
29	-	17.6	8.1	0.57	-	14.4	3	3.93	0.938	-	13.5	-
30	-	17.5	11.9	0.57	-	14.4	3	3.93	0.938	-	13.5	-
31	-	17.7	14.5	0.57	-	14.4	3	3.93	0.938	-	13.5	-
32	-	24.1	23.2	0.57	-	14.4	3	3.93	0.938	-	13.5	-
33		11.6	12.3	0.57		14.4	3	3.93	0.938		13.5	
34	20.3	15.9	14.0	-	15.5	17.8	5	7.00	1	15.5	17.8	16.7
35	20.3	15.9	14.0	-	15.5	17.8	5	7.00	1	15.5	17.8	16.7
36	21.4	19.0	26.3	58%	9.2	14.8	5	5.00	1.000	9.2	14.8	14.8
37	21.4	19.0	26.3	58%	9.2	14.8	5	5.00	1.000	9.2	14.8	13.0
38	21.4	20.3	47.3	58%	13.1	15.1	5	5.00	1.000	13.1	15.1	14.5
39	21.4	16.0	47.5	58%	11.2	14.0	5	5.00	1.000	11.2	14.0	13.1
40	-	-	26	-	14.9	16.0	3	4.21	0.955	14.2	15.3	14.9
41	-	-	26	-	14.9	16.0	3	4.21	0.955	14.2	15.3	14.9
42	-	-	26	-	14.9	16.0	3	4.21	0.955	14.2	15.3	14.9
43	-	-	23	58%	-	16.4	3	3.93	0.938	-	15.4	-
44	-	-	23	58%	-	27.0	3	3.93	0.938	-	25.3	-
45	-	-	23	58%	-	16.4	3	3.93	0.938	-	15.4	-
46	-	-	23	58%	-	27.0	3	3.93	0.938	-	25.3	-
47	-	-	23	58%	-	16.4	3	3.93	0.938	-	15.4	-
48	-	-	23	58%	-	27.0	3	3.93	0.938	-	25.3	-
49	-	-	23	58%	-	16.4	3	3.93	0.938	-	15.4	-
50	-	-	23	58%	-	16.4	3	3.93	0.938	-	15.4	-

Wall #	MASONRY MATERIALS											
	f_{block} [MPa]	**f_{mortar} [MPa]**	**f_{grout} [MPa]**	***v***	**$f'_{mg,u}$**	**$f'_{mu,u}$**	**# of courses in Prism**	**Prism h/t**	**Corr. factor, k**	**f'_{mg}**	**f'_{mu}**	**$f'_{m,eff}$**
51	-	-	23	58%	-	16.4	3	3.93	0.938	-	15.4	-
52	-	-	23	58%	-	16.4	3	3.93	0.938	-	15.4	-
53	-	-	23	58%	-	16.4	3	3.93	0.938	-	15.4	-
54	-	-	23	58%	-	27.0	3	3.93	0.938	-	25.3	-
55	-	-	23	58%	-	27.0	3	3.93	0.938	-	25.3	-
56	-	-	23	58%	-	27.0	3	3.93	0.938	-	25.3	-
57	-	-	23	58%	-	14.0	3	3.93	0.938	-	13.1	-
58	-	-	23	58%	-	14.0	3	3.93	0.938	-	13.1	-
59	-	-	23	58%	-	14.0	3	3.93	0.938	-	13.1	-
60	-	-	23	58%	-	14.0	3	3.93	0.938	-	13.1	-
61	-	-	23	58%	-	14.0	3	3.93	0.938	-	13.1	-
62	-	-	23	58%	-	27.0	3	3.93	0.938	-	25.3	-
63	-	-	23	58%	-	14.0	3	3.93	0.938	-	13.1	-
64	-	-	23	58%	-	27.0	3	3.93	0.938	-	25.3	-
65	-	-	23	58%	-	27.0	3	3.93	0.938	-	25.3	-
66	-	-	23	58%	-	15.2	3	3.93	0.938	-	14.3	-
67	-	-	23	58%	-	15.2	3	3.93	0.938	-	14.3	-
68	-	-	23	58%	-	15.2	3	3.93	0.938	-	14.3	-
69	-	-	23	58%	-	15.2	3	3.93	0.938	-	14.3	-
70	-	-	23	58%	-	15.2	3	3.93	0.938	-	14.3	-
71	-	-	23	58%	-	15.2	3	3.93	0.938	-	14.3	-
72	17.4	9.3	9.3	60%	7.7	10.5	-	-	1	7.7	10.5	9.5
73	17.4	9.3	9.3	60%	7.7	10.5	-	-	1	7.7	10.5	9.5
74	17.4	9.3	9.3	60%	7.7	10.5	-	-	1	7.7	10.5	9.5
75	17.4	9.3	9.3	60%	7.7	10.5	-	-	1	7.7	10.5	9.5

Wall #	MASONRY MATERIALS											
	f_{block} [MPa]	**f_{mortar} [MPa]**	**f_{grout} [MPa]**	***v***	**$f'_{mg,u}$**	**$f'_{mu,u}$**	**# of courses in Prism**	**Prism h/t**	**Corr. factor, k**	**f'_{mg}**	**f'_{mu}**	**$f'_{m,eff}$**
76	17.4	9.3	9.3	60%	7.7	10.5	-	-	1	7.7	10.5	9.5
77	15.5	7.0	7.0	60%	6.4	8.8	-	-	1	6.4	8.8	8.0
78	15.5	7.0	7.0	60%	6.4	8.8	-	-	1	6.4	8.8	8.0
79	15.5	7.0	7.0	60%	6.4	8.8	-	-	1	6.4	8.8	8.0
80	15.5	7.0	7.0	60%	6.4	8.8	-	-	1	6.4	8.8	8.0
81	15.5	7.0	7.0	60%	6.4	8.8	-	-	1	6.4	8.8	8.0
82	19.3	15.8	19.3	53%	8.61	12.2	3	3.10	0.885	7.6	10.8	9.2
83	19.3	15.8	19.3	53%	8.61	12.2	3	3.10	0.885	7.6	10.8	9.2
84	19.3	17.2	19.3	53%	9.23	12.5	3	3.10	0.885	8.2	11.1	9.7
85	19.3	17.2	19.3	53%	9.23	12.5	3	3.10	0.885	8.2	11.1	9.7
86	19.3	19.6	19.3	53%	8.41	13.1	3	3.10	0.885	7.4	11.6	9.5
87	19.3	19.6	19.3	53%	8.41	13.1	3	3.10	0.885	7.4	11.6	9.5
88	19.3	22.3	19.3	53%	11.2	13.6	3	3.10	0.885	9.9	12.0	11.0
89	19.3	22.3	19.3	53%	11.2	13.6	3	3.10	0.885	9.9	12.0	11.0
90	19.3	17.3	19.3	53%	9.23	12.6	3	3.10	0.885	8.2	11.1	9.7
91	19.3	17.3	19.3	53%	9.23	12.6	3	3.10	0.885	8.2	11.1	9.7
92	19.3	18.1	19.3	53%	11	12.7	3	3.10	0.885	9.7	11.3	10.5
93	19.3	18.1	19.3	53%	11	12.7	3	3.10	0.885	9.7	11.3	10.5
94	19.3	19.6	19.3	53%	8.41	13.1	3	3.10	0.885	7.4	11.6	9.5
95	19.3	19.6	19.3	53%	8.41	13.1	3	3.10	0.885	7.4	11.6	9.5
96	19.3	17.9	19.3	53%	8.34	12.7	3	3.10	0.885	7.4	11.2	9.3
97	19.3	17.9	19.3	53%	8.34	12.7	3	3.10	0.885	7.4	11.2	9.3
98	12.5	-	10.7	52%	-	-	2	2.00	0.812	-	-	-
99	12.5	-	10.7	52%	-	-	2	2.00	0.812	-	-	-
100	12.5	-	10.7	52%	-	-	2	2.00	0.812	-	-	-

Wall #	MASONRY MATERIALS											
	f_{block} [MPa]	**f_{mortar} [MPa]**	**f_{grout} [MPa]**	***v***	**$f'_{mg,u}$**	**$f'_{mu,u}$**	**# of courses in Prism**	**Prism h/t**	**Corr. factor, k**	**f'_{mg}**	**f'_{mu}**	**$f'_{m,eff}$**
101	12.5	-	10.7	52%	-	-	2	2.00	0.812	-	-	-
102	12.5	-	10.7	52%	-	-	2	2.00	0.812	-	-	-
103	12.5	-	10.7	52%	-	-	2	2.00	0.812	-	-	-
104	12.5	-	10.7	52%	-	-	2	2.00	0.812	-	-	-
105	12.5	-	10.7	52%	-	-	2	2.00	0.812	-	-	-
106	12.5	-	10.7	52%	-	-	2	2.00	0.812	-	-	-
107	12.5	-	10.7	52%	-	-	2	2.00	0.812	-	-	-
108	19.3	15.5	31.0	-	13.8	15.9	3	4.45	0.969	13.4	15.4	15.1
109	19.3	15.5	31.0	-	13.8	15.9	3	4.45	0.969	13.4	15.4	14.9
110	19.3	15.5	31.0	-	13.8	15.9	3	4.45	0.969	13.4	15.4	14.9
111	19.3	15.5	31.0	-	13.8	15.9	3	4.45	0.969	13.4	15.4	14.9
112	-	-	-	-	-	13.0	-	-	1.00	-	13.0	-
113	-	-	-	-	-	13.0	-	-	1.00	-	13.0	-
114	-	-	-	-	-	13.0	-	-	1.00	-	13.0	-
115	-	-	-	-	-	13.0	-	-	1.00	-	13.0	-
116	-	-	-	-	-	13.0	-	-	1.00	-	13.0	-
117	-	-	-	-	-	13.0	-	-	1.00	-	13.0	-
118	-	21.7	29.6	51%	17.6	17.1	2	2.00	0.812	14.3	13.9	13.9
119	-	21.7	29.6	51%	17.6	17.1	2	2.00	0.812	14.3	13.9	14.0
120	-	21.7	29.6	51%	17.6	17.1	2	2.00	0.812	14.3	13.9	14.0
121	-	21.7	29.6	51%	17.6	17.1	2	2.00	0.812	14.3	13.9	13.9
122	-	21.7	29.6	51%	17.6	17.1	2	2.00	0.812	14.3	13.9	14.0
123	-	21.7	29.6	51%	17.6	17.1	2	2.00	0.812	14.3	13.9	14.0
124	23.3	22.2	28.2	51%	16.5	14.5	2	2.00	0.812	13.4	11.8	12.0
125	23.3	22.2	28.2	51%	16.5	14.5	2	2.00	0.812	13.4	11.8	12.1

Wall #	MASONRY MATERIALS											
	f_{block} [MPa]	f_{mortar} [MPa]	f_{grout} [MPa]	v	$f'_{mg,u}$	$f'_{mu,u}$	# of courses in Prism	Prism h/t	Corr. factor, k	f'_{mg}	f'_{mu}	$f'_{m,eff}$
126	23.3	22.2	28.2	51%	16.5	14.5	2	2.00	0.812	13.4	11.8	12.2
127	23.3	22.2	28.2	51%	16.5	14.5	2	2.00	0.812	13.4	11.8	12.0
128	23.3	22.2	28.2	51%	16.5	14.5	2	2.00	0.812	13.4	11.8	12.1
129	23.3	22.2	28.2	51%	16.5	14.5	2	2.00	0.812	13.4	11.8	12.2
130	-	-	-	-	18.5	-	3	4.21	0.955	-	-	-
131	-	-	-	-	18.5	-	3	4.21	0.955	-	-	-
132	26.3	3.82	3.82	46%	7.7	8.9	3	3.00	0.878	6.8	7.8	7.71
133	26.3	7.11	7.11	46%	8.9	10.8	3	3.00	0.878	7.8	9.5	9.35
134	26.3	8.62	8.62	46%	9.4	11.5	3	3.00	0.878	8.2	10.1	9.94
135	26.3	7.72	7.72	46%	9.1	11.1	3	3.00	0.878	8.0	9.7	9.60
136	29.2	21.4	37.6	51.2%	12.4	21.6	4	4.33	0.962	11.9	20.8	19.4
137	29.2	21.4	37.6	51.2%	12.4	21.6	4	4.33	0.962	11.9	20.8	19.0
138	29.2	21.4	37.6	51.2%	12.4	21.6	4	4.33	0.962	11.9	20.8	19.9
139	29.2	21.4	37.6	51.2%	12.4	21.6	4	4.33	0.962	11.9	20.8	19.4
140	29.2	21.4	37.6	51.2%	12.4	21.6	4	4.33	0.962	11.9	20.8	19.4
141	-	14.9	35.85	56.3%	24.47	17.49	2	1.99	0.811	19.9	14.2	15.5
142	-	14.9	35.85	56.3%	24.47	17.49	2	1.99	0.811	19.9	14.2	15.5
143	-	14.9	35.85	56.3%	24.47	17.49	2	1.99	0.811	19.9	14.2	15.5
144	-	14.9	35.85	56.3%	24.47	17.49	2	1.99	0.811	19.9	14.2	15.5
145	-	14.9	35.85	56.3%	24.47	17.49	2	1.99	0.811	19.9	14.2	15.9
146	-	14.9	35.85	56.3%	24.47	17.49	2	1.99	0.811	19.9	14.2	16.3
147	13.8	25.8	22.0	53%	12.1	11.4	2	2.00	0.812	9.8	9.2	9.4
148	13.8	12.6	22.0	53%	8.0	9.1	2	2.00	0.812	6.5	7.4	7.2
149	13.8	25.8	22.0	53%	12.1	11.4	2	2.00	0.812	9.8	9.2	9.4
150	13.8	12.6	22.0	53%	8.0	9.1	2	2.00	0.812	6.5	7.4	7.2

Wall #	MASONRY MATERIALS											
	f_{block} [MPa]	f_{mortar} [MPa]	f_{grout} [MPa]	v	$f'_{mg,u}$	$f'_{mu,u}$	# of courses in Prism	Prism h/t	Corr. factor, k	f'_{mg}	f'_{mu}	$f'_{m,eff}$
151	-	9.5	19.7	-	19.5	21.2	2	2.00	0.812	15.8	17.2	16.9
152	-	9.7	23.7	-	17.7	17.0	2	2.00	0.812	14.3	13.8	13.9
153	-	8.8	32.5	-	19.2	20.5	2	2.00	0.812	15.6	16.6	16.2
154	-	10.8	38.6	-	24.1	24.6	2	2.00	0.812	19.5	20.0	19.8
155	-	8.8	32.5	-	19.2	20.5	2	2.00	0.812	15.6	16.6	16.2
156	-	10.8	18.3	-	17.7	17.0	2	2.00	0.812	14.3	13.8	13.9
157	-	8.8	32.5	-	19.2	20.5	2	2.00	0.812	15.6	16.6	16.2
158	-	9.7	38.6	-	24.1	20.5	2	2.00	0.812	19.5	16.7	17.7
159	18.1	-	29.2	52.0%	19.7	11.3	3	3.05	0.881	17.4	9.9	11.6
160	18.1	-	29.2	52.0%	19.7	11.3	3	3.05	0.881	17.4	9.9	11.6
161	18.1	-	29.2	52.0%	19.7	11.3	3	3.05	0.881	17.4	9.9	11.6
162	18.1	-	29.2	52.0%	19.7	11.3	3	3.05	0.881	17.4	9.9	12.2
163	18.1	-	29.2	52.0%	19.7	11.3	3	3.05	0.881	17.4	9.9	12.8
164	18.4	6.7	21.8	49%	9.82	18.22	3	3.11	0.885	8.7	16.1	12.5
165	18.4	6.8	25.7	49%	9.82	18.22	3	3.11	0.885	8.7	16.1	12.5
166	18.4	6.8	25.7	49%	9.82	18.22	3	3.11	0.885	8.7	16.1	12.5
167	18.4	6.5	23.7	49%	9.82	18.22	3	3.11	0.885	8.7	16.1	12.5
168	18.4	7.3	25.1	49%	9.82	18.22	3	3.11	0.885	8.7	16.1	12.5
169	18.4	7.5	21.9	49%	9.82	18.22	3	3.11	0.885	8.7	16.1	12.5
170	18.4	4.6	24.7	49%	9.82	18.22	3	3.11	0.885	8.7	16.1	12.5
171	18.4	4.6	24.7	49%	9.82	18.22	3	3.11	0.885	8.7	16.1	12.5
172	18.4	10.1	22.9	49%	9.82	18.22	3	3.11	0.885	8.7	16.1	12.5
173	18.4	7.2	26.3	49%	9.82	18.22	3	3.11	0.885	8.7	16.1	12.5
174	18.4	5.0	25.2	49%	9.82	18.22	3	3.11	0.885	8.7	16.1	12.5
175	18.4	6.2	22.8	49%	9.82	18.22	3	3.11	0.885	8.7	16.1	12.5

Wall #	MASONRY MATERIALS											
	f_{block} [MPa]	**f_{mortar} [MPa]**	**f_{grout} [MPa]**	***v***	**$f'_{mg,u}$**	**$f'_{mu,u}$**	**# of courses in Prism**	**Prism h/t**	**Corr. factor, k**	**f'_{mg}**	**f'_{mu}**	**$f'_{m,eff}$**
176	18.4	7.2	26.3	49%	9.82	18.22	3	3.11	0.885	8.7	16.1	12.5
177	18.4	6.7	23.8	49%	9.82	18.22	3	3.11	0.885	8.7	16.1	12.5
178	18.4	7.8	23	49%	9.82	18.22	3	3.11	0.885	8.7	16.1	12.5
179	18.4	6.1	-	49%	9.82	18.22	3	3.11	0.885	8.7	16.1	16.1
180	18.4	7.8	-	49%	9.82	18.22	3	3.11	0.885	8.7	16.1	16.1
181	18.4	5.5	-	49%	9.82	18.22	3	3.11	0.885	8.7	16.1	16.1
182	18.4	6.5	21	49%	9.82	18.22	3	3.11	0.885	8.7	16.1	12.5
183	18.4	4.3	20	49%	9.82	18.22	3	3.11	0.885	8.7	16.1	12.5
184	18.4	4.3	20	49%	9.82	18.22	3	3.11	0.885	8.7	16.1	12.5
185	18.4	6.5	23.7	49%	9.82	18.22	3	3.11	0.885	8.7	16.1	12.5
186	18.4	7.3	25.1	49%	9.82	18.22	3	3.11	0.885	8.7	16.1	12.5
187	18.4	7.5	21.9	49%	9.82	18.22	3	3.11	0.885	8.7	16.1	12.5
188	18.4	7.8	23.2	49%	9.82	18.22	3	3.11	0.885	8.7	16.1	12.5
189	18.4	7.8	23.2	49%	9.82	18.22	3	3.11	0.885	8.7	16.1	12.5
190	18.4	10.1	22.9	49%	9.82	18.22	3	3.11	0.885	8.7	16.1	12.5
191	18.4	7.8	23	49%	9.82	18.22	3	3.11	0.885	8.7	16.1	12.5
192	18.4	6.2	22.8	49%	9.82	18.22	3	3.11	0.885	8.7	16.1	12.5
193	18.4	5.0	25.2	49%	9.82	18.22	3	3.11	0.885	8.7	16.1	12.5
194	18.4	7.5	21.4	49%	9.82	18.22	3	3.11	0.885	8.7	16.1	12.5
195	18.4	7.8	23	49%	9.82	18.22	3	3.11	0.885	8.7	16.1	12.5
196	18.4	6.8	25.7	49%	9.82	18.22	3	3.11	0.885	8.7	16.1	12.5
197	18.4	6.1	-	49%	9.82	18.22	3	3.11	0.885	8.7	16.1	16.1
198	18.4	6.1	-	49%	9.82	18.22	3	3.11	0.885	8.7	16.1	16.1
199	18.4	7.8	-	49%	9.82	18.22	3	3.11	0.885	8.7	16.1	16.1
200	18.4	6.5	21	49%	9.82	18.22	3	3.11	0.885	8.7	16.1	12.5

Wall #	MASONRY MATERIALS											
	f_{block} [MPa]	**f_{mortar} [MPa]**	**f_{grout} [MPa]**	***v***	**$f'_{mg,u}$**	**$f'_{mu,u}$**	**# of courses in Prism**	**Prism h/t**	**Corr. factor, k**	**f'_{mg}**	**f'_{mu}**	**$f'_{m,eff}$**
201	18.4	6.5	21	49%	9.82	18.22	3	3.11	0.885	8.7	16.1	12.5
202	18.4	4.3	20	49%	9.82	18.22	3	3.11	0.885	8.7	16.1	12.5
203	18.4	6.5	23.7	49%	9.82	18.22	3	3.11	0.885	8.7	16.1	12.5
204	18.4	7.3	25.1	49%	9.82	18.22	3	3.11	0.885	8.7	16.1	12.5
205	18.4	7.5	21.9	49%	9.82	18.22	3	3.11	0.885	8.7	16.1	12.5
206	18.4	7.8	23.2	49%	9.82	18.22	3	3.11	0.885	8.7	16.1	12.5
207	18.4	4.6	24.7	49%	9.82	18.22	3	3.11	0.885	8.7	16.1	12.5
208	18.4	10.1	22.9	49%	9.82	18.22	3	3.11	0.885	8.7	16.1	12.5
209	18.4	7.5	21.4	49%	9.82	18.22	3	3.11	0.885	8.7	16.1	12.5
210	18.4	6.2	22.8	49%	9.82	18.22	3	3.11	0.885	8.7	16.1	12.5
211	18.4	5.0	25.2	49%	9.82	18.22	3	3.11	0.885	8.7	16.1	12.5
212	18.4	7.2	26.3	49%	9.82	18.22	3	3.11	0.885	8.7	16.1	12.5
213	18.4	6.7	23.8	49%	9.82	18.22	3	3.11	0.885	8.7	16.1	12.5
214	18.4	7.8	23	49%	9.82	18.22	3	3.11	0.885	8.7	16.1	12.5
215	18.4	6.1	-	49%	9.82	18.22	3	3.11	0.885	8.7	16.1	16.1
216	18.4	7.8	-	49%	9.82	18.22	3	3.11	0.885	8.7	16.1	16.1
217	18.4	5.5	-	49%	9.82	18.22	3	3.11	0.885	8.7	16.1	16.1
218	18.4	12.8	-	49%	10.60	21.60	3	3.11	0.885	9.4	19.1	19.1
219	18.4	13.2	-	49%	10.60	21.60	3	3.11	0.885	9.4	19.1	19.1
220	18.4	15.0	-	49%	10.60	21.60	3	3.11	0.885	9.4	19.1	19.1
221	18.4	12.5	-	49%	10.60	21.60	3	3.11	0.885	9.4	19.1	19.1
222	18.4	13.2	-	49%	10.60	21.60	3	3.11	0.885	9.4	19.1	19.1
223	18.4	15.0	-	49%	10.60	21.60	3	3.11	0.885	9.4	19.1	19.1
224	18.4	13.7	18.4	49%	10.60	21.60	3	3.11	0.885	9.4	19.1	14.4
225	18.4	15.3	18.2	49%	10.60	21.60	3	3.11	0.885	9.4	19.1	14.4

Wall #	MASONRY MATERIALS											
	f_{block} [MPa]	**f_{mortar} [MPa]**	**f_{grout} [MPa]**	***v***	**$f'_{mg,u}$**	**$f'_{mu,u}$**	**# of courses in Prism**	**Prism h/t**	**Corr. factor, k**	**f'_{mg}**	**f'_{mu}**	**$f'_{m,eff}$**
226	18.4	13.0	24.5	49%	10.60	21.60	3	3.11	0.885	9.4	19.1	14.4
227	18.4	15.3	18.4	49%	10.60	21.60	3	3.11	0.885	9.4	19.1	14.4
228	18.4	13.7	18.4	49%	10.60	21.60	3	3.11	0.885	9.4	19.1	14.4
229	18.4	13.0	24.5	49%	10.60	21.60	3	3.11	0.885	9.4	19.1	14.4
230	16.5	5.7	24.2	50%	8.7	20.4	5	5.21	1	8.65	20.4	16.6
231	16.5	5.7	24.2	50%	8.7	20.4	5	5.21	1	8.65	20.4	16.6
232	16.5	5.7	24.2	50%	8.7	20.4	5	5.21	1	8.65	20.4	16.6
233	16.5	5.7	24.2	50%	8.7	20.4	5	5.21	1	8.65	20.4	16.6
234	16.5	5.7	24.2	50%	8.7	20.4	5	5.21	1	8.65	20.4	16.6
235	16.5	5.7	24.2	50%	8.7	20.4	5	5.21	1	8.65	20.4	16.6
236	16.5	5.7	24.2	50%	8.7	20.4	5	5.21	1	8.65	20.4	16.6
237	16.5	5.7	24.2	50%	8.7	20.4	5	5.21	1	8.65	20.4	16.6
238	16.5	5.7	24.2	50%	8.7	20.4	5	5.21	1	8.65	20.4	16.6
239	16.5	5.7	24.2	50%	8.7	20.4	5	5.21	1	8.65	20.4	16.6
240	16.5	5.7	24.2	50%	8.7	20.4	5	5.21	1	8.65	20.4	16.6
241	16.5	5.7	24.2	50%	8.7	20.4	5	5.21	1	8.65	20.4	16.6
242	16.5	5.7	24.2	50%	8.7	20.4	5	5.21	1	8.65	20.4	16.6
243	16.5	5.7	24.2	50%	8.7	20.4	5	5.21	1	8.65	20.4	16.6
244	16.5	5.7	24.2	50%	8.7	20.4	5	5.21	1	8.65	20.4	16.6
245	16.5	5.7	24.2	50%	8.7	20.4	5	5.21	1	8.65	20.4	16.6
246	16.5	5.7	24.2	50%	8.7	20.4	5	5.21	1	8.65	20.4	16.6
247	16.5	5.7	24.2	50%	8.7	20.4	5	5.21	1	8.65	20.4	16.6
248	26.9	4.43	12.23	51.2%	7.15	7.93	3	3.22	0.893	6.38	7.08	7.0
249	26.9	4.43	12.23	51.2%	7.15	7.93	3	3.22	0.893	6.38	7.08	7.0
250	26.9	4.43	12.23	51.2%	7.15	7.93	3	3.22	0.893	6.38	7.08	7.0

Wall #	MASONRY MATERIALS											
	f_{block} [MPa]	**f_{mortar} [MPa]**	**f_{grout} [MPa]**	***v***	**$f'_{mg,u}$**	**$f'_{mu,u}$**	**# of courses in Prism**	**Prism h/t**	**Corr. factor, k**	**f'_{mg}**	**f'_{mu}**	**$f'_{m,eff}$**
251	26.9	4.43	12.23	51.2%	7.15	7.93	3	3.22	0.893	6.38	7.08	7.0
252	26.9	4.43	12.23	51.2%	7.15	7.93	3	3.22	0.893	6.38	7.08	7.0
253	26.9	4.43	12.23	51.2%	7.15	7.93	3	3.22	0.893	6.38	7.08	7.0
254	26.9	4.43	12.23	51.2%	7.15	7.93	3	3.22	0.893	6.38	7.08	7.0
255	26.9	4.43	12.23	51.2%	7.15	7.93	3	3.22	0.893	6.38	7.08	7.0
256	26.9	4.43	12.23	51.2%	7.15	7.93	3	3.22	0.893	6.38	7.08	7.0
257	26.9	4.43	12.23	51.2%	7.15	7.93	3	3.22	0.893	6.38	7.08	7.0
258	26.9	4.43	12.23	51.2%	7.15	7.93	3	3.22	0.893	6.38	7.08	7.0
259	26.9	4.43	12.23	51.2%	7.15	7.93	3	3.22	0.893	6.38	7.08	7.0
260	26.9	4.85	11.22	51.2%	7.39	8.15	3	3.22	0.893	6.60	7.28	7.2
261	26.9	4.85	11.22	51.2%	7.39	8.15	3	3.22	0.893	6.60	7.28	7.2
262	26.9	4.85	11.22	51.2%	7.39	8.15	3	3.22	0.893	6.60	7.28	7.2
263	26.9	4.85	11.22	51.2%	7.39	8.15	3	3.22	0.893	6.60	7.28	7.2
264	26.9	4.85	11.22	51.2%	7.39	8.15	3	3.22	0.893	6.60	7.28	7.2
265	26.9	4.85	11.22	51.2%	7.39	8.15	3	3.22	0.893	6.60	7.28	7.2
266	26.9	4.85	11.22	51.2%	7.39	8.15	3	3.22	0.893	6.60	7.28	7.1
267	26.9	4.85	11.22	51.2%	7.39	8.15	3	3.22	0.893	6.60	7.28	7.1
268	26.9	4.85	11.22	51.2%	7.39	8.15	3	3.22	0.893	6.60	7.28	7.1
269	35.7	22.1	25.7	51.8%	11.7	18.6	3	3.11	0.885	10.3	16.5	14.5
270	35.7	22.1	25.7	51.8%	11.7	18.6	3	3.11	0.885	10.3	16.5	14.5
271	35.7	22.1	25.7	51.8%	11.7	18.6	3	3.11	0.885	10.3	16.5	14.5
272	35.7	22.1	21.7	51.8%	10.6	18.6	3	3.11	0.885	9.3	16.5	14.1
273	29.3	9.5	25.2	51.8%	14.1	22.3	3	3.11	0.885	12.5	19.7	17.4
274	29.3	9.5	25.2	51.8%	14.1	22.3	3	3.11	0.885	12.5	19.7	17.4
275	29.3	11.5	31.7	51.8%	14.1	22.3	3	3.11	0.885	12.5	19.7	17.4

Wall #	MASONRY MATERIALS											
	f_{block} [MPa]	**f_{mortar} [MPa]**	**f_{grout} [MPa]**	***v***	**$f'_{mg,u}$**	**$f'_{mu,u}$**	**# of courses in Prism**	**Prism h/t**	**Corr. factor, k**	**f'_{mg}**	**f'_{mu}**	**$f'_{m,eff}$**
276	29.3	11.5	31.7	51.8%	14.1	22.3	3	3.11	0.885	12.5	19.7	17.4
277	29.3	11	31.8	51.8%	14.1	22.3	3	3.11	0.885	12.5	19.7	17.4
278	29.3	11	31.8	51.8%	14.1	22.3	3	3.11	0.885	12.5	19.7	17.4
279	20.1	9.3	24.7	51.8%	9.78	14.7	3	3.11	0.885	8.65	13.0	11.6
280	20.1	9.3	24.7	51.8%	9.78	14.7	3	3.11	0.885	8.65	13.0	11.6
281	20.1	11.6	29.3	51.8%	9.78	14.7	3	3.11	0.885	8.65	13.0	11.6
282	20.1	11.6	29.3	51.8%	9.78	14.7	3	3.11	0.885	8.65	13.0	11.6
283	6.36	18.0	31.7	64%	11.0	8.65	1	1	0.744	8.20	6.44	7.1
284	6.36	18.0	31.7	64%	11.0	8.65	1	1	0.744	8.20	6.44	7.1
285	6.36	18.0	31.7	64%	11.0	8.65	1	1	0.744	8.20	6.44	7.1
286	6.36	18.0	31.7	64%	11.0	8.65	1	1	0.744	8.20	6.44	7.1
287	6.36	18.0	31.7	64%	11.0	8.65	1	1	0.744	8.20	6.44	7.1
288	6.36	18.0	31.7	64%	11.0	8.65	1	1	0.744	8.20	6.44	7.1
289	6.36	18.0	31.7	64%	11.0	8.65	1	1	0.744	8.20	6.44	7.1
290	6.36	18.0	31.7	64%	11.0	8.65	1	1	0.744	8.20	6.44	7.5
291	6.36	18.0	31.7	64%	11.0	8.65	1	1	0.744	8.20	6.44	7.5
292	6.36	18.0	31.7	64%	11.0	8.65	1	1	0.744	8.20	6.44	7.5

Wall #	VERTICAL REINFORCEMENT										
	Vertical (Interior) Reinf.	**A_{vi}**	**Flexural Reinf.**	**A_{vf}**	**$A_{vi,bar}$ [mm^2]**	**$A_{vf,bar}$ [mm^2]**	**A_v [mm^2]**	**f_{yvi} [MPa]**	**f_{yvf} [MPa]**	**$s_{v,max}$ [mm]**	**$s_{v,ave}$ [mm]**
1	-	0	-	0	0	0	0	0	0	0	0
2	-	0	5/8"	396	0	198	396	0	290	2235	2235
3	-	0	-	0	0	0	0	0	0	0	0
4	-	0	5/8"	396	0	198	396	0	285	2235	2235
5	(1)1/2"	127	5/8"	396	127	198	523	302	285	1219	1118
6	(2)1/2"	253	5/8"	396	127	198	649	302	285	813	745
7	-	0	5/8"+1/2"	649	0	325	649	0	295	2235	2235
8	(3)1/2"	380	5/8"	396	127	198	776	302	285	813	745
9	(3)1/2"	380	5/8"	396	127	198	776	302	290	813	745
10	(3)1/2"	380	5/8"	396	127	198	776	302	290	813	745
11	(3)5/8"	594	5/8"	396	198	198	990	290	290	813	745
12	(3)5/8"	594	5/8"	396	198	198	990	290	290	813	745
13	(3)#3	213	(2)2#4	1016	71	127	1229	245	245	800	650
14	(3)#3	213	(2)2#4	1016	71	127	1229	245	245	800	650
15	(3)#3	213	(2)2#4	1016	71	127	1229	245	245	800	650
16	#3	71	(2)#4	508	71	127	579	245	245	1400	1300
17	#3	71	(2)#4	508	71	127	579	245	245	1400	1300
18	(3)#3	213	(2)2#4	1016	71	127	1229	245	245	800	650
19	#3	71	(2)#4	508	71	127	579	245	245	1400	1300
20	(3)#3	213	(2)2#4	1016	71	127	1229	245	245	800	650
21	(3)#3	213	(2)4#4	1016	71	127	1229	245	245	800	650
22	(3)#3	213	(2)2#4	1016	71	127	1229	245	245	800	650
23	-	0	(2)2#5	796	0	199	796	0	392	1400	1400
24	-	0	(2)2#5	796	0	199	796	0	392	1400	1400

Wall #	VERTICAL REINFORCEMENT										
	Vertical (Interior) Reinf.	**A_{vi}**	**Flexural Reinf.**	**A_{vf}**	**$A_{vi,bar}$ [mm^2]**	**$A_{vf,bar}$ [mm^2]**	**A_v [mm^2]**	**f_{yvi} [MPa]**	**f_{yvf} [MPa]**	**$s_{v,max}$ [mm]**	**$s_{v,ave}$ [mm]**
25	-	0	(2)2#5	796	0	199	796	0	392	1400	1400
26	-	0	(2)2#5	796	0	199	796	0	392	1400	1400
27	-	0	(2)2#5	796	0	199	796	0	392	1400	1400
28	(2)#4	254	(2)2#5	796	127	199	1050	392	392	600	467
29	-	0	(2)2#4	508	0	127	508	0	392	1400	1400
30	(2)#4	254	(2)2#5	796	127	199	1050	392	392	600	467
31	-	0	(2)2#5	796	0	199	796	0	392	1400	1400
32	-	0	(2)#3	142	0	71	142	0	392	1400	1400
33	-	0	(2)2#5	796	0	199	796	0	392	1400	1400
34	-	0	2#6	568			568	0	516	1626	
35	-	0	2#6	568			568	0	516	1626	
36	-	0	-	0	0	0	0	0	0	0	0
37	-	0	#5	400	0	200	400	0	488	1067	1067
38	-	0	#8	1020	0	510	1020	0	477	1067	1067
39	-	0	#8	1020	0	510	1020	0	477	1067	1067
40	D10	157	D12	148			305	275	353	800	
41	D16	201	D16	402			603	454	454	800	
42	D16	201	D16	402			603	454	454	800	
43	(3)D10	213	2D22	1548	71	774	1761	385	385	400	350
44	(3)D10	213	D13&D32	1896	71	948	2109	385	385	400	350
45	(2)D10	142	2D22	1548	71	774	1690	385	385	400	333
46	(2)D10	142	D16&D25	1420	71	710	1562	385	385	400	333
47	D10	71	2D22	1548	71	774	1619	385	385	300	300
48	D10	71	D25	1020	71	510	1091	385	385	300	300

Wall #	VERTICAL REINFORCEMENT										
	Vertical (Interior) Reinf.	**A_{vi}**	**Flexural Reinf.**	**A_{vf}**	**$A_{vi,bar}$ [mm^2]**	**$A_{vf,bar}$ [mm^2]**	**A_v [mm^2]**	**f_{yvi} [MPa]**	**f_{yvf} [MPa]**	**$s_{v,max}$ [mm]**	**$s_{v,ave}$ [mm]**
49	(2)D10	142	2D22	1548	71	774	1690	385	385	400	333
50	(2)D10	142	2D22	1548	71	774	1690	385	385	400	333
51	(2)D10	142	2D22	1548	71	774	1690	385	385	400	333
52	(2)D10	142	2D22	1548	71	774	1690	385	385	400	333
53	(2)D10	142	2D22	1548	71	774	1690	385	385	400	333
54	(2)D10	142	2D22	1548	71	774	1690	385	385	400	333
55	(2)D10	142	2D22	1548	71	774	1690	385	385	400	333
56	(2)D10	142	2D22	1548	71	774	1690	385	385	400	333
57	(2)D10	142	2D22	1548	71	774	1690	385	385	400	333
58	(2)D10	142	2D22	1548	71	774	1690	385	385	400	333
59	(2)D10	142	2D22	1548	71	774	1690	385	385	400	333
60	(2)D10	142	2D22	1548	71	774	1690	385	385	400	333
61	(2)D10	142	D19	568	71	284	710	385	385	400	333
62	(2)D10	142	2D22	1548	71	774	1690	385	385	400	333
63	(2)D10	142	2D22	1548	71	774	1690	385	385	400	333
64	(2)D10	142	2D22	1548	71	774	1690	385	385	400	333
65	(2)D10	142	2D22	1548	71	774	1690	385	385	400	333
66	(4)D10	284	2D22	1548	71	774	1832	385	385	400	360
67	(4)D10	284	2D22	1548	71	774	1832	385	385	400	360
68	(3)D10	213	D29	1290	71	645	1503	385	385	400	350
69	(2)D10	142	D25	1020	71	510	1162	385	385	400	333
70	D10	71	D22	774	71	774	845	385	385	300	300
71	D10	71	D22	774	71	774	845	385	385	300	300
72	-	0	Ø10mm	157.1	0.0	78.5	157.1	0	522	510	510

Wall #	VERTICAL REINFORCEMENT										
	Vertical (Interior) Reinf.	**A_{vi}**	**Flexural Reinf.**	**A_{vf}**	**$A_{vi,bar}$ [mm^2]**	**$A_{vf,bar}$ [mm^2]**	**A_v [mm^2]**	**f_{yvi} [MPa]**	**f_{yvf} [MPa]**	**$s_{v,max}$ [mm]**	**$s_{v,ave}$ [mm]**
73	-	0	Ø10mm	157.1	0.0	78.5	157.1	0	522	510	510
74	-	0	Ø10mm	157.1	0.0	78.5	157.1	0	522	510	510
75	-	0	Ø10mm	157.1	0.0	78.5	157.1	0	522	510	510
76	-	0	Ø10mm	157.1	0.0	78.5	157.1	0	522	510	510
77	-	0	2Ø10mm	314.2	0.0	78.5	314.2	0	522	510	510
78	-	0	2Ø10mm	314.2	0.0	78.5	314.2	0	522	510	510
79	-	0	2Ø10mm	314.2	0.0	78.5	314.2	0	522	510	510
80	-	0	2Ø10mm	314.2	0.0	78.5	314.2	0	522	510	510
81	-	0	2Ø10mm	314.2	0.0	78.5	314.2	0	522	510	510
82	-	0	#5	400	0	200	400	0	414	609.6	609.6
83	-	0	#5	400	0	200	400	0	414	609.6	609.6
84	-	0	#5	400	0	200	400	0	414	609.6	609.6
85	-	0	#5	400	0	200	400	0	414	609.6	609.6
86	-	0	#5	400	0	200	400	0	414	609.6	609.6
87	-	0	#5	400	0	200	400	0	414	609.6	609.6
88	-	0	#5	400	0	200	400	0	414	609.6	609.6
89	-	0	#5	400	0	200	400	0	414	609.6	609.6
90	-	0	#5	400	0	200	400	0	414	609.6	609.6
91	-	0	#5	400	0	200	400	0	414	609.6	609.6
92	-	0	#5	400	0	200	400	0	414	609.6	609.6
93	-	0	#5	400	0	200	400	0	414	609.6	609.6
94	-	0	#5	400	0	200	400	0	414	609.6	609.6
95	-	0	#5	400	0	200	400	0	414	609.6	609.6
96	-	0	#5	400	0	200	400	0	414	609.6	609.6

Wall #	VERTICAL REINFORCEMENT										
	Vertical (Interior) Reinf.	**A_{vi}**	**Flexural Reinf.**	**A_{vf}**	**$A_{vi,bar}$ [mm^2]**	**$A_{vf,bar}$ [mm^2]**	**A_v [mm^2]**	**f_{yvi} [MPa]**	**f_{yvf} [MPa]**	**$s_{v,max}$ [mm]**	**$s_{v,ave}$ [mm]**
97	-	0	#5	400	0	200	400	0	414	609.6	609.6
98	-	0	-	0			0	0	0	0	
99	-	0	-	0			0	0	0	0	
100	-	0	-	0			0	0	0	0	
101	-	0	-	0			0	0	0	0	
102	-	0	-	0			0	0	0	0	
103	-	0	-	0			0	0	0	0	
104	-	0	-	0			0	0	0	0	
105	-	0	-	0			0	0	0	0	
106	-	0	-	0			0	0	0	0	
107	-	0	-	0			0	0	0	0	
108	-	0	2#4/3	53.2	0.0	26.6	53	0	443	871	871
109	#5/3	18.6	#5/3	37.3	18.6	18.6	56	447	447	470	436
110	#5/3	18.6	#5/3	37.3	18.6	18.6	56	447	447	470	436
111	#5/3	18.6	#5/3	37.3	18.6	18.6	56	447	447	470	436
112	-	0	D10	157.1			157	0	522	410	
113	-	0	D10	157.1			157	0	522	410	
114	-	0	D10	157.1			157	0	522	410	
115	-	0	D10	157.1			157	0	522	410	
116	-	0	D10	157.1			157	0	522	410	
117	-	0	D10	157.1			157	0	522	410	
118	-	0	2#6	1136	0	568	1136	0	414	2642	2642
119	-	0	2#6	1136	0	568	1136	0	414	1829	1829
120	-	0	2#6	1136	0	568	1136	0	414	1219	1219

Wall #	VERTICAL REINFORCEMENT										
	Vertical (Interior) Reinf.	**A_{vi}**	**Flexural Reinf.**	**A_{vf}**	**$A_{vi,bar}$ [mm^2]**	**$A_{vf,bar}$ [mm^2]**	**A_v [mm^2]**	**f_{yvi} [MPa]**	**f_{yvf} [MPa]**	**$s_{v,max}$ [mm]**	**$s_{v,ave}$ [mm]**
121	-	0	2#6	1136	0	568	1136	0	414	2642	2642
122	-	0	2#6	1136	0	568	1136	0	414	1829	1829
123	-	0	2#6	1136	0	568	1136	0	414	1219	1219
124	-	0	2#6	1136	0	568	1136	0	414	2642	2642
125	-	0	2#6	1136	0	568	1136	0	414	1829	1829
126	-	0	2#6	1136	0	568	1136	0	414	1219	1219
127	-	0	2#6	1136	0	568	1136	0	414	2642	2642
128	-	0	2#6	1136	0	568	1136	0	414	1829	1829
129	-	0	2#6	1136	0	568	1136	0	414	1219	1219
130	(3)D20	942	D20	628			1570	318	318	400	
131	D20	314	D20	628			942	318	318	800	
132	Ø5mm truss	39.3	Ø5mm tr.	78.5	39	39	118	580	580	500	500
133	Ø5mm truss	39.3	Ø5mm tr.	78.5	39	39	118	580	580	500	500
134	Ø5mm truss	39.3	Ø5mm tr.	78.5	39	39	118	580	580	500	500
135	Ø5mm truss	39.3	Ø5mm tr.	78.5	39	39	118	580	580	500	500
136	#10	100	#10	200	100	100	300	492	492	855	855
137	2#3	142	#3	142	71	71	284	503	503	570	570
138	-	0	#4	258	0	129	258	0	565	1710	1710
139	#10	100	#10	200	100	100	300	492	492	855	855
140	#10	100	#10	200	100	100	300	492	492	855	855
141	2#6	568	2#6	1136	284	284	1704	427	427	1219	1219
142	2#6	568	2#6	1136	284	284	1704	427	427	1219	1219
143	2#6	568	2#6	1136	284	284	1704	427	427	1219	1219
144	2#6	568	2#6	1136	284	284	1704	427	427	1219	1219

Wall #	VERTICAL REINFORCEMENT										
	Vertical (Interior) Reinf.	**A_{vi}**	**Flexural Reinf.**	**A_{vf}**	**$A_{vi,bar}$ [mm^2]**	**$A_{vf,bar}$ [mm^2]**	**A_v [mm^2]**	**f_{yvi} [MPa]**	**f_{yvf} [MPa]**	**$s_{v,max}$ [mm]**	**$s_{v,ave}$ [mm]**
145	(2)#6	568	2#6	1136	284	284	1704	427	427	812.8	812.8
146	(3)#5	600	2#6	1136	200	284	1736	452	427	609.6	609.6
147	(2)#6	568	#6	568	284	284	1136	414	414	1219	1219
148	(2)#6	568	#6	568	284	284	1136	414	414	1219	1219
149	(2)#6	568	#6	568	284	284	1136	414	414	1219	1219
150	(2)#6	568	#6	568	284	284	1136	414	414	1219	1219
151	(2)#4	258	2#6	1136	129	568	1394	449	449	1219.2	880.5
152	(2)#4	258	2#6	1136	129	568	1394	449	449	1219.2	880.5
153	(2)#4	258	2#6, 1#4	1394	129	697	1652	449	449	1016.0	745.1
154	(2)#4	258	#6, #4	826	129	413	1084	449	449	1016.0	745.1
155	(2)#4	258	#6, #4	826	129	413	1084	449	449	1016.0	745.1
156	(4)#4	516	2#6	1136	129	568	1652	449	449	1219.2	812.8
157	(4)#4	516	2#6, 1#4	1394	129	697	1910	449	449	1219.2	731.5
158	(4)#4	516	2#6, 1#4	1394	129	697	1910	449	449	1219.2	731.5
159	2#7	774	2#7	1548	387	387	2322	439	439	1219	1219
160	2#7	774	2#7	1548	387	387	2322	439	439	1219	1219
161	2#7	774	2#7	1548	387	387	2322	439	439	1219	1219
162	(2)2#6	1136	2#6	1136	284	284	2272	439	439	813	813
163	(3)2#5	1200	2#6	1136	200	284	2336	439	439	610	610
164	-	0	-	0	0	0	0	0	0	0	0
165	-	0	-	0	0	0	0	0	0	0	0
166	-	0	-	0	0	0	0	0	0	0	0
167	-	0	-	0	0	0	0	0	0	0	0
168	-	0	-	0	0	0	0	0	0	0	0

Wall #	VERTICAL REINFORCEMENT										
	Vertical (Interior) Reinf.	**A_{vi}**	**Flexural Reinf.**	**A_{vf}**	**$A_{vi,bar}$ [mm^2]**	**$A_{vf,bar}$ [mm^2]**	**A_v [mm^2]**	**f_{yvi} [MPa]**	**f_{yvf} [MPa]**	**$s_{v,max}$ [mm]**	**$s_{v,ave}$ [mm]**
169	-	0	-	0	0	0	0	0	0	0	0
170	-	0	-	0	0	0	0	0	0	0	0
171	-	0	-	0	0	0	0	0	0	0	0
172	-	0	-	0	0	0	0	0	0	0	0
173	2-15M	400	15M	400	200	200	800	480	480	600	466.7
174	2-15M	400	15M	400	200	200	800	480	480	600	466.7
175	2-15M	400	15M	400	200	200	800	480	480	600	466.7
176	2-15M	400	15M	400	200	200	800	480	480	600	466.7
177	2-15M	400	15M	400	200	200	800	480	480	600	466.7
178	2-15M	400	15M	400	200	200	800	480	480	600	466.7
179	-	0		0	0	0	0	0	0	0	0
180	-	0		0	0	0	0	0	0	0	0
181	-	0		0	0	0	0	0	0	0	0
182	-	0	-	0	0	0	0	0	0	0	0
183	-	0	-	0	0	0	0	0	0	0	0
184	-	0	-	0	0	0	0	0	0	0	0
185	-	0	-	0	0	0	0	0	0	0	0
186	-	0	-	0	0	0	0	0	0	0	0
187	-	0	-	0	0	0	0	0	0	0	0
188	-	0	-	0	0	0	0	0	0	0	0
189	-	0	-	0	0	0	0	0	0	0	0
190	-	0	-	0	0	0	0	0	0	0	0
191	2-15M	400	15M	400	200	200	800	480	480	600	466.7
192	2-15M	400	15M	400	200	200	800	480	480	600	466.7

Wall #	VERTICAL REINFORCEMENT										
	Vertical (Interior) Reinf.	**A_{vi}**	**Flexural Reinf.**	**A_{vf}**	**$A_{vi,bar}$ [mm^2]**	**$A_{vf,bar}$ [mm^2]**	**A_v [mm^2]**	**f_{yvi} [MPa]**	**f_{yvf} [MPa]**	**$s_{v,max}$ [mm]**	**$s_{v,ave}$ [mm]**
193	2-15M	400	15M	400	200	200	800	480	480	600	466.7
194	2-15M	400	15M	400	200	200	800	480	480	600	466.7
195	2-15M	400	15M	400	200	200	800	480	480	600	466.7
196	2-15M	400	15M	400	200	200	800	480	480	600	466.7
197	-	0	-	0	0	0	0	0	0	0	0
198	-	0	-	0	0	0	0	0	0	0	0
199	-	0	-	0	0	0	0	0	0	0	0
200	-	0	-	0	0	0	0	0	0	0	0
201	-	0	-	0	0	0	0	0	0	0	0
202	-	0	-	0	0	0	0	0	0	0	0
203	-	0	-	0	0	0	0	0	0	0	0
204	-	0	-	0	0	0	0	0	0	0	0
205	-	0	-	0	0	0	0	0	0	0	0
206	-	0	-	0	0	0	0	0	0	0	0
207	-	0	-	0	0	0	0	0	0	0	0
208	-	0	-	0	0	0	0	0	0	0	0
209	2-15M	400	15M	400	200	200	800	480	480	600	466.7
210	2-15M	400	15M	400	200	200	800	480	480	600	466.7
211	2-15M	400	15M	400	200	200	800	480	480	600	466.7
212	2-15M	400	15M	400	200	200	800	480	480	600	466.7
213	2-15M	400	15M	400	200	200	800	480	480	600	466.7
214	2-15M	400	15M	400	200	200	800	480	480	600	466.7
215	-	0	-	0	0	0	0	0	0	0	0
216	-	0	-	0	0	0	0	0	0	0	0

Wall #	VERTICAL REINFORCEMENT										
	Vertical (Interior) Reinf.	**A_{vi}**	**Flexural Reinf.**	**A_{vf}**	**$A_{vi,bar}$ [mm^2]**	**$A_{vf,bar}$ [mm^2]**	**A_v [mm^2]**	**f_{yvi} [MPa]**	**f_{yvf} [MPa]**	**$s_{v,max}$ [mm]**	**$s_{v,ave}$ [mm]**
217	-	0	-	0	0	0	0	0	0	0	0
218	-	0	-	0	0	0	0	0	0	0	0
219	-	0	-	0	0	0	0	0	0	0	0
220	-	0	-	0	0	0	0	0	0	0	0
221	-	0	-	0	0	0	0	0	0	0	0
222	-	0	-	0	0	0	0	0	0	0	0
223	-	0	-	0	0	0	0	0	0	0	0
224	-	0	-	0	0	0	0	0	0	0	0
225	-	0	-	0	0	0	0	0	0	0	0
226	-	0	-	0	0	0	0	0	0	0	0
227	-	0	-	0	0	0	0	0	0	0	0
228	-	0	-	0	0	0	0	0	0	0	0
229	-	0	-	0	0	0	0	0	0	0	0
230	15M	200	15M	400	200	200	600	450	450	800	800
231	15M	200	15M	400	200	200	600	450	450	800	800
232	15M	200	15M	400	200	200	600	450	450	800	800
233	15M	200	15M	400	200	200	600	450	450	800	800
234	15M	200	15M	400	200	200	600	450	450	800	800
235	15M	200	15M	400	200	200	600	450	450	800	800
236	15M	200	15M	400	200	200	600	450	450	800	800
237	15M	200	15M	400	200	200	600	450	450	800	800
238	15M	200	15M	400	200	200	600	450	450	800	800
239	15M	200	15M	400	200	200	600	450	450	800	800
240	15M (no splice)	200	15M (no splice)	400	200	200	600	450	450	800	800

Wall #	VERTICAL REINFORCEMENT										
	Vertical (Interior) Reinf.	**A_{vi}**	**Flexural Reinf.**	**A_{vf}**	**$A_{vi,bar}$ [mm^2]**	**$A_{vf,bar}$ [mm^2]**	**A_v [mm^2]**	**f_{yvi} [MPa]**	**f_{yvf} [MPa]**	**$s_{v,max}$ [mm]**	**$s_{v,ave}$ [mm]**
241	15M (no splice)	200	15M (no splice)	400	200	200	600	450	450	800	800
242	15M (top splice)	200	15M (top splice)	400	200	200	600	450	450	800	800
243	15M (top splice)	200	15M (top splice)	400	200	200	600	450	450	800	800
244	15M	200	15M	400	200	200	600	450	450	800	800
245	15M	200	15M	400	200	200	600	450	450	800	800
246	15M	200	15M	400	200	200	600	450	450	800	800
247	15M	200	15M	400	200	200	600	450	450	800	800
248	-	0	10M	200	0	100	200	0	458	1140	1140
249	-	0	10M	200	0	100	200	0	458	1140	1140
250	-	0	10M	200	0	100	200	0	458	1140	1140
251	-	0	10M	200	0	100	200	0	458	1140	1140
252	-	0	10M	200	0	100	200	0	458	1140	1140
253	-	0	10M	200	0	100	200	0	458	1140	1140
254	10M	100	10M	200	100	100	300	458	458	1140	1140
255	10M	100	10M	200	100	100	300	458	458	1140	1140
256	10M	100	10M	200	100	100	300	458	458	1140	1140
257	10M	100	10M	200	100	100	300	458	458	1140	1140
258	10M	100	10M	200	100	100	300	458	458	1140	1140
259	10M	100	10M	200	100	100	300	458	458	1140	1140
260	(2)10M	200	10M	200	100	100	400	458	458	760	760
261	(2)10M	200	10M	200	100	100	400	458	458	760	760
262	(2)10M	200	10M	200	100	100	400	458	458	760	760
263	(2)10M	200	10M	200	100	100	400	458	458	760	760
264	(2)10M	200	10M	200	100	100	400	458	458	760	760

Wall #	VERTICAL REINFORCEMENT										
	Vertical (Interior) Reinf.	**A_{vi}**	**Flexural Reinf.**	**A_{vf}**	**$A_{vi,bar}$ [mm^2]**	**$A_{vf,bar}$ [mm^2]**	**A_v [mm^2]**	**f_{yvi} [MPa]**	**f_{yvf} [MPa]**	**$s_{v,max}$ [mm]**	**$s_{v,ave}$ [mm]**
265	(2)10M	200	10M	200	100	100	400	458	458	760	760
266	-	0	10M	200	0	100	200	0	458	760	760
267	-	0	10M	200	0	100	200	0	458	760	760
268	-	0	10M	200	0	100	200	0	458	760	760
269	15M	200	15M	400	200	200	600	448	448	800	800
270	15M	200	15M	400	200	200	600	448	448	800	800
271	15M	200	15M	400	200	200	600	448	448	800	800
272	15M	200	15M	400	200	200	600	448	448	800	800
273	15M	200	15M	400	200	200	600	448	448	800	800
274	15M	200	15M	400	200	200	600	448	448	800	800
275	15M	200	15M	400	200	200	600	448	448	800	800
276	15M	200	15M	400	200	200	600	448	448	800	800
277	15M	200	15M	400	200	200	600	448	448	800	800
278	15M	200	15M	400	200	200	600	448	448	800	800
279	15M	200	15M	400	200	200	600	448	448	800	800
280	15M	200	15M	400	200	200	600	448	448	800	800
281	15M	200	15M	400	200	200	600	448	448	800	800
282	15M	200	15M	400	200	200	600	448	448	800	800
283	2Ø10mm	157	1Ø22mm	760	79	380	917	474	474	597	597
284	2Ø10mm	157	1Ø22mm	760	79	380	917	474	474	597	597
285	2Ø10mm	157	1Ø22mm	760	79	380	917	474	474	597	597
286	2Ø10mm	157	1Ø22mm	760	79	380	917	474	474	597	597
287	3Ø10mm	236	1Ø16mm	402	79	201	638	474	474	597.7	597.7
288	3Ø10mm	236	1Ø16mm	402	79	201	638	474	474	597.7	597.7

Wall #	VERTICAL REINFORCEMENT										
	Vertical (Interior) Reinf.	**A_{vi}**	**Flexural Reinf.**	**A_{vf}**	**$A_{vi,bar}$ [mm^2]**	**$A_{vf,bar}$ [mm^2]**	**A_v [mm^2]**	**f_{yvi} [MPa]**	**f_{yvf} [MPa]**	**$s_{v,max}$ [mm]**	**$s_{v,ave}$ [mm]**
289	3Ø10mm	236	1Ø16mm	402	79	201	638	474	474	597.7	597.7
290	1Ø10mm	79	1Ø22mm	760	79	380	839	474	474	396	396
291	1Ø10mm	79	1Ø22mm	760	79	380	839	474	474	396	396
292	1Ø10mm	79	1Ø22mm	760	79	380	839	474	474	396	396

Wall #	HORIZONTAL (SHEAR) REINFORCEMENT												
	Bond Beam Reinf	**A_{hbb} [mm^2]**	**$A_{hbb,m}$ [mm^2]**	**$A_{hbb,m2}$ [mm^2]**	**Joint Reinf**	**A_{hj} [mm^2]**	**$A_{hbb,bar}$ [mm^2]**	**$A_{hj,bar}$ [mm^2]**	**A_h [mm^2]**	**f_{ybb}**	**f_{yj}**	**$s_{h,max}$ [mm]**	**$s_{h,ave}$ [mm]**
1	-	0	0	0	-	0	0.0	0	0	0	0	0	0
2	-	0	0	0	-	0	0.0	0	0	0	0	0	0
3	(2)5/8"+(2)1/2"	649	649	649	-	0	324.6	0	649	291.6	0	1016	812.8
4	2-1/2"	253	253	253	-	0	253.4	0	253	302	0	1321	1219
5	(1)1/2"	127	127	127	-	0	126.7	0	127	302	0	1321	1219
6	-	0	0	0	-	0	0.0	0	0	0	0	0	0
7	-	0	0	0	-	0	0.0	0	0	0	0	0	0
8	-	0	0	0	-	0	0.0	0	0	0	0	0	0
9	2-1/2"	253	253	253	-	0	253.4	0	253	302	0	1321	1219
10	(2)2-1/2"	507	507	507	-	0	253.4	0	507	302	0	1016	812.8
11	(3)5/8"	594	594	594	-	0	197.9	0	594	290	0	812.8	609.6
12	(2)2-5/8"	792	792	792	-	0	395.9	0	792	290	0	1016	812.8
13	-	0	0	0	Ø2.5mm	58.9		9.82	58.9	0	245	410	410
14	-	0	0	0	Ø2.5mm	58.9		9.82	58.9	0	245	410	410
15	-	0	0	0	Ø2.5mm	58.9		9.82	58.9	0	245	410	410
16	-	0	0	0	Ø2.5mm	58.9		9.82	58.9	0	245	410	410
17	-	0	0	0	Ø2.5mm	58.9		9.82	58.9	0	245	410	410
18	-	0	0	0	-	0.0		0.00	0.0	0	0	0	0
19	-	0	0	0	-	0.0		0.00	0.0	0	0	0	0
20	-	0	0	0	Ø2.5mm	58.9		9.82	58.9	0	245	410	410
21	-	0	0	0	Ø2.5mm	58.9		9.82	58.9	0	245	410	410
22	-	0	0	0	Ø2.5mm	58.9		9.82	58.9	0	245	410	410
23	-	0	0	0	-	0		0	0	0	0	0	0
24	-	0	0	0	-	0		0	0	0	0	0	0
25	-	0	0	0	-	0		0	0	0	0	0	0

Wall #	HORIZONTAL (SHEAR) REINFORCEMENT												
	Bond Beam Reinf	**A_{hbb} [mm^2]**	**$A_{hbb,m}$ [mm^2]**	**$A_{hbb,m2}$ [mm^2]**	**Joint Reinf**	**A_{hj} [mm^2]**	**$A_{hbb,bar}$ [mm^2]**	**$A_{hj,bar}$ [mm^2]**	**A_h [mm^2]**	**f_{ybb}**	**f_{yj}**	**$s_{h,max}$ [mm]**	**$s_{h,ave}$ [mm]**
26	-	0	0	0	-	0		0	0	0	0	0	0
27	-	0	0	0	-	0		0	0	0	0	0	0
28	-	0	0	0	-	0		0	0	0	0	0	0
29	-	0	0	0	-	0		0	0	0	0	0	0
30	-	0	0	0	-	0		0	0	0	0	0	0
31	-	0	0	0	-	0		0	0	0	0	0	0
32	-	0	0	0	-	0		0	0	0	0	0	0
33	-	0	0	0	-	0		0	0	0	0	0	0
34	-	0	0	0	-	0		0	0	0	0	0	
35	-	0	0	0	-	0		0	0	0	0	0	
36	-	0	0	0	-	0	0	0	0	0	0	0	0
37	#5	200	200	200	-	0	200	0	200	330	0	711	711
38	-	0	0	0	-	0	0	0	0	0	0	0	0
39	(2)#5	400	400	400	-	0	200	0	400	330	0	508	474
40	(2)D12	226	226	226	-	0	113	0	226	353	0	2000	
41	-	0	0	0	-	0	0	0	0	0	0	0	
42	(4)D12	452	452	452	-	0	113	0	452	454	0	800	
43	D10	213	213	213	-	0	71	0.0	213	385	0	600	600
44	D10	213	213	213	-	0	71	0.0	213	385	0	600	600
45	D10	213	213	213	-	0	71	0.0	213	385	0	600	600
46	D10	213	213	213	-	0	71	0.0	213	385	0	600	600
47	D10	213	213	213	-	0	71	0.0	213	385	0	600	600
48	D10	213	213	213	-	0	71	0.0	213	385	0	600	600
49	-	0	0	0	-	0	0	0.0	0	0	0	0	0
50	-	0	0	0	-	0	0	0.0	0	0	0	0	0

Wall #	HORIZONTAL (SHEAR) REINFORCEMENT												
	Bond Beam Reinf	**A_{hbb} [mm^2]**	**$A_{hbb,m}$ [mm^2]**	**$A_{hbb,m2}$ [mm^2]**	**Joint Reinf**	**A_{hj} [mm^2]**	**$A_{hbb,bar}$ [mm^2]**	**$A_{hj,bar}$ [mm^2]**	**A_h [mm^2]**	**f_{ybb}**	**f_{yj}**	**$s_{h,max}$ [mm]**	**$s_{h,ave}$ [mm]**
51	D10	213	213	213	-	0	71	0.0	213	385	0	600	600
52	D13	387	387	387	-	0	129	0.0	387	385	0	600	600
53	D16	600	600	600	-	0	200	0.0	600	385	0	600	600
54	D10	213	213	213	-	0	71	0.0	213	385	0	600	600
55	D10	213	213	213	-	0	71	0.0	213	385	0	600	600
56	D10	213	213	213	-	0	71	0.0	213	385	0	600	600
57	-	0	0	0	-	0	0	0.0	0	0	0	0	0
58	D13	387	387	387	-	0	129	0.0	387	385	0	600	600
59	D16	600	600	600	-	0	200	0.0	600	385	0	600	600
60	D16	800	800	800	-	0	200	0.0	800	385	0	400	400
61	D10	213	213	213	-	0	71	0.0	213	385	0	600	600
62	-	0	0	0	-	0	0	0.0	0	0	0	0	0
63	-	0	0	0	-	0	0	0.0	0	0	0	0	0
64	D13	387	387	387	-	0	129	0.0	387	385	0	600	600
65	D16	600	600	600	-	0	200	0.0	600	385	0	600	600
66	D13	387	387	387	-	0	129	0.0	387	385	0	600	600
67	D13	387	387	387	-	0	129	0.0	387	385	0	600	600
68	D13	387	387	387	-	0	129	0.0	387	385	0	600	600
69	D13	387	387	387	-	0	129	0.0	387	385	0	600	600
70	D13	387	387	387	-	0	129	0.0	387	385	0	600	600
71	D13	387	387	387	-	0	129	0.0	387	385	0	600	600
72	-	0	0	0	-	0.0		0.0	0.0	0	0	0	0
73	-	0	0	0	2Ø3.1mm	90.6		15.1	90.6	0	323	100	100
74	-	0	0	0	2Ø4.2mm	166.3		27.7	166.3	0	391	100	100
75	-	0	0	0	2Ø6mm	339.3		56.5	339.3	0	253	100	100

Wall #	HORIZONTAL (SHEAR) REINFORCEMENT												
	Bond Beam Reinf	**A_{hbb} [mm^2]**	**$A_{hbb,m}$ [mm^2]**	**$A_{hbb,m2}$ [mm^2]**	**Joint Reinf**	**A_{hj} [mm^2]**	**$A_{hbb,bar}$ [mm^2]**	**$A_{hj,bar}$ [mm^2]**	**A_h [mm^2]**	**f_{ybb}**	**f_{yj}**	**$s_{h,max}$ [mm]**	**$s_{h,ave}$ [mm]**
76	-	0	0	0	-	0.0		0.0	0.0	0	0	0	0
77	-	0	0	0	-	0.0		0.0	0.0	0	0	0	0
78	-	0	0	0	2Ø3.1mm	90.6		15.1	90.6	0	323	100	100
79	-	0	0	0	2Ø4.2mm	166.3		27.7	166.3	0	391	100	100
80	-	0	0	0	2Ø6mm	339.3		56.5	339.3	0	253	100	100
81	-	0	0	0	-	0.0		0.0	0.0	0	0	0	0
82	-	0	0	0	-	0		0	0	0	0	0	0
83	-	0	0	0	-	0		0	0	0	0	0	0
84	-	0	0	0	-	0		0	0	0	0	0	0
85	-	0	0	0	-	0		0	0	0	0	0	0
86	-	0	0	0	-	0		0	0	0	0	0	0
87	-	0	0	0	-	0		0	0	0	0	0	0
88	-	0	0	0	-	0		0	0	0	0	0	0
89	-	0	0	0	-	0		0	0	0	0	0	0
90	-	0	0	0	-	0		0	0	0	0	0	0
91	-	0	0	0	-	0		0	0	0	0	0	0
92	-	0	0	0	-	0		0	0	0	0	0	0
93	-	0	0	0	-	0		0	0	0	0	0	0
94	-	0	0	0	-	0		0	0	0	0	0	0
95	-	0	0	0	-	0		0	0	0	0	0	0
96	-	0	0	0	-	0		0	0	0	0	0	0
97	-	0	0	0	-	0		0	0	0	0	0	0
98	-	0	0		-	0		0.0	0	0	0	0	
99	-	0	0		9-ga Ladder	40		13.3	40	0	693	406.4	
100	-	0	0		9-ga Ladder	40		13.3	40	0	693	203.2	

Wall #	HORIZONTAL (SHEAR) REINFORCEMENT												
	Bond Beam Reinf	**A_{hbb} [mm²]**	**$A_{hbb,m}$ [mm²]**	**$A_{hbb,m2}$ [mm²]**	**Joint Reinf**	**A_{hj} [mm²]**	**$A_{hbb,bar}$ [mm²]**	**$A_{hj,bar}$ [mm²]**	**A_h [mm²]**	**f_{ybb}**	**f_{yj}**	**$s_{h,max}$ [mm]**	**$s_{h,ave}$ [mm]**
101	(2)#4	258	258		-	0		0.0	258	336	0	0	
102	(3)#5	600	600		-	0		0.0	600	439	0	0	
103	(1)#5	200	200		-	0		0.0	200	385	0	0	
104	(3)#5	600	600		-	0		0.0	600	374	0	0	
105	(1)#3	71	71		9-ga Ladder	40		13.3	111	373	693	406.4	
106	(2)#4, (1)#5	458	458		9-ga Ladder	40		13.3	498	341	693	203.2	
107	(1)#5	200	200		-	0		0	200	373	0	0	
108	(2)2#4/3	53	27	27	-	0	13.3	0	53	443	0	874	874
109	(3)#5/3	56	37	37	-	0	18.6	0	56	447	0	432	432
110	(3)#5/3	56	37	37	-	0	18.6	0	56	447	0	432	432
111	(3)#5/3	56	37	37	-	0	18.6	0	56	447	0	432	432
112	-	0	0	0	6mm Ladder	57		28.3	57	0	253	100	
113	-	0	0	0	6mm Ladder	57		28.3	57	0	253	100	
114	-	0	0	0	6mm Ladder	57		28.3	57	0	253	100	
115	-	0	0	0	6mm Ladder	57		28.3	57	0	253	100	
116	-	0	0	0	6mm Ladder	57		28.3	57	0	253	100	
117	-	0	0	0	6mm Ladder	57		28.3	57	0	253	100	
118	2#3	142	142	142	-	0	71	0	142	414	0	711	711
119	2#3	142	142	142	-	0	71	0	142	414	0	711	711
120	2#3	142	142	142	-	0	71	0	142	414	0	711	711
121	1#4 & 1#5	329	329	329	-	0	329	0	329	414	0	711	711
122	1#4 & 1#5	329	329	329	-	0	329	0	329	414	0	711	711
123	1#4 & 1#5	329	329	329	-	0	329	0	329	414	0	711	711
124	-	0	0	0	9-ga Ladder	155		22.2	155	0	482.6	203.2	203.2
125	-	0	0	0	9-ga Ladder	155		22.2	155	0	482.6	203.2	203.2

Wall #	HORIZONTAL (SHEAR) REINFORCEMENT												
	Bond Beam Reinf	**A_{hbb} [mm²]**	**$A_{hbb,m}$ [mm²]**	**$A_{hbb,m2}$ [mm²]**	**Joint Reinf**	**A_{hj} [mm²]**	**$A_{hbb,bar}$ [mm²]**	**$A_{hj,bar}$ [mm²]**	**A_h [mm²]**	**f_{ybb}**	**f_{yj}**	**$s_{h,max}$ [mm]**	**$s_{h,ave}$ [mm]**
126	-	0	0	0	9-ga Ladder	155		22.2	155	0	482.6	203.2	203.2
127	-	0	0	0	5-ga Ladder	304		43.5	304	0	482.6	203.2	203.2
128	-	0	0	0	5-ga Ladder	304		43.5	304	0	482.6	203.2	203.2
129	-	0	0	0	5-ga Ladder	304		43.5	304	0	482.6	203.2	203.2
130	-	0	0	0	-	0		0	0	0	0	0	
131	-	0	0	0	-	0		0	0	0	0	0	
132	-	0	0	0	Ø4mm truss	75.4		25.1	75	0	580	303	303
133	-	0	0	0	Ø4mm truss	75.4		25.1	75	0	580	303	303
134	-	0	0	0	Ø4mm truss	75.4		25.1	75	0	580	303	303
135	-	0	0	0	Ø4mm truss	75.4		25.1	75	0	580	303	303
136	(3)D4	77	52	52	-	0	25.8	0	77	690.7	0	855	855
137	(4)D3	78	58	58	-	0	19.4	0	78	743.7	0	570	570
138	(2)2D3	78	39	39	-	0	19.4	0	78	743.7	0	1710	1710
139	(2)D3	39	19	19	-	0	19.4	0	39	743.7	0	855	855
140	(4)D4	103	77	77	-	0	25.8	0	103	690.7	0	855	855
141	#5	200	200	200	-	0	200	0	200	452	0	711.2	711.2
142	#5	200	200	200	-	0	200	0	200	452	0	711.2	711.2
143	#6	284	284	284	-	0	284	0	284	427	0	711.2	711.2
144	2#5	400	400	400	-	0	400	0	400	452	0	711.2	711.2
145	#5	200	200	200	-	0	200	0	200	452	0	711.2	711.2
146	#5	200	200	200	-	0	200	0	200	452	0	711.2	711.2
147	(2)#6	568	284	568	-	0	284	0	568	414	0	1219	1168
148	(2)#6	568	284	568	-	0	284	0	568	414	0	1219	1168
149	(2)#6	568	284	568	-	0	284	0	568	414	0	1219	1168
150	(2)#6	568	284	568	-	0	284	0	568	414	0	1219	1168

Wall #	HORIZONTAL (SHEAR) REINFORCEMENT												
	Bond Beam Reinf	**A_{hbb} [mm^2]**	**$A_{hbb,m}$ [mm^2]**	**$A_{hbb,m2}$ [mm^2]**	**Joint Reinf**	**A_{hj} [mm^2]**	**$A_{hbb,bar}$ [mm^2]**	**$A_{hj,bar}$ [mm^2]**	**A_h [mm^2]**	**f_{ybb}**	**f_{yj}**	**$s_{h,max}$ [mm]**	**$s_{h,ave}$ [mm]**
151	(2)2#4	516	258	516	-	0	258	0	516	445	0	1219	1168
152	(1)2#4	258	0	258	(2)3/16"	428	258	35.6	686	445	606.4	203.2	203.2
153	(1)2#4	258	0	258	(4)3/16"	855	258	71.3	1113	445	606.4	203.2	203.2
154	(2)2#4	516	258	516	-	0	258	0	516	445	0	1219	1168
155	(1)2#4	258	0	258	(2)3/16"	428	258	35.6	686	445	606.4	203.2	203.2
156	(2)2#4	516	258	516	-	0	258	0	516	445	0	1219	1168
157	(1)2#4	258	0	258	(2)3/16"	428	258	35.6	686	445	606.4	203.2	203.2
158	(1)2#4	258	0	258	(4)3/16"	855	258	71.3	1113	445	606.4	203.2	203.2
159	#5	200	200	200	-	0	200.0	0	200	439	0	1118	1118
160	#6	284	284	284	-	0	284.0	0	284	439	0	1118	1118
161	2#5	400	400	400	-	0	400.0	0	400	439	0	1118	1118
162	#5	200	200	200	-	0	200.0	0	200	439	0	1118	1118
163	#5	200	200	200	-	0	200.0	0	200	439	0	1118	1118
164	-	0	0	0	-	0		0.0	0	0	0	0	0
165	-	0	0	0	-	0		0.0	0	0	0	0	0
166	-	0	0	0	-	0		0.0	0	0	0	0	0
167	-	0	0	0	Ø3.7mm	107.5		21.5	108	0	530	200	200
168	-	0	0	0	Ø3.7mm	107.5		21.5	108	0	530	200	200
169	-	0	0	0	Ø3.7mm	107.5		21.5	108	0	530	200	200
170	-	0	0	0	Ø4.9mm	188.5		37.7	189	0	560	200	200
171	-	0	0	0	Ø4.9mm	188.5		37.7	189	0	560	200	200
172	-	0	0	0	Ø4.9mm	188.5		37.7	189	0	560	200	200
173	-	0	0	0	-	0		0.0	0	0	0	0	0
174	-	0	0	0	-	0		0.0	0	0	0	0	0
175	-	0	0	0	-	0		0.0	0	0	0	0	0

Wall #	HORIZONTAL (SHEAR) REINFORCEMENT												
	Bond Beam Reinf	**A_{hbb} [mm^2]**	**$A_{hbb,m}$ [mm^2]**	**$A_{hbb,m2}$ [mm^2]**	**Joint Reinf**	**A_{hj} [mm^2]**	**$A_{hbb,bar}$ [mm^2]**	**$A_{hj,bar}$ [mm^2]**	**A_h [mm^2]**	**f_{ybb}**	**f_{yj}**	**$s_{h,max}$ [mm]**	**$s_{h,ave}$ [mm]**
176	-	0	0	0	Ø4.9mm	188.5		37.7	189	0	560	200	200
177	-	0	0	0	Ø4.9mm	188.5		37.7	189	0	560	200	200
178	-	0	0	0	Ø4.9mm	188.5		37.7	189	0	560	200	200
179	-	0	0	0	-	0		0.0	0	0	0	0	0
180	-	0	0	0	-	0		0.0	0	0	0	0	0
181	-	0	0	0	-	0		0.0	0	0	0	0	0
182	-	0	0	0	-	0		0.0	0	0	0	0	0
183	-	0	0	0	-	0		0.0	0	0	0	0	0
184	-	0	0	0	-	0		0.0	0	0	0	0	0
185	-	0	0	0	Ø3.7mm	107.5		21.5	108	0	530	200	200
186	-	0	0	0	Ø3.7mm	107.5		21.5	108	0	530	200	200
187	-	0	0	0	Ø3.7mm	107.5		21.5	108	0	530	200	200
188	-	0	0	0	Ø4.9mm	188.5		37.7	189	0	560	200	200
189	-	0	0	0	Ø4.9mm	188.5		37.7	189	0	560	200	200
190	-	0	0	0	Ø4.9mm	188.5		37.7	189	0	560	200	200
191	-	0	0	0	-	0		0.0	0	0	0	0	0
192	-	0	0	0	-	0		0.0	0	0	0	0	0
193	-	0	0	0	-	0		0.0	0	0	0	0	0
194	-	0	0	0	Ø4.9mm	188.5		37.7	189	0	560	200	200
195	-	0	0	0	Ø4.9mm	188.5		37.7	189	0	560	200	200
196	-	0	0	0	Ø4.9mm	188.5		37.7	189	0	560	200	200
197	-	0	0	0	-	0		0.0	0	0	0	0	0
198	-	0	0	0	-	0		0.0	0	0	0	0	0
199	-	0	0	0	-	0		0.0	0	0	0	0	0
200	-	0	0	0	-	0		0.0	0	0	0	0	0

Wall #	HORIZONTAL (SHEAR) REINFORCEMENT												
	Bond Beam Reinf	**A_{hbb} [mm^2]**	**$A_{hbb,m}$ [mm^2]**	**$A_{hbb,m2}$ [mm^2]**	**Joint Reinf**	**A_{hj} [mm^2]**	**$A_{hbb,bar}$ [mm^2]**	**$A_{hj,bar}$ [mm^2]**	**A_h [mm^2]**	**f_{ybb}**	**f_{yj}**	**$s_{h,max}$ [mm]**	**$s_{h,ave}$ [mm]**
201	-	0	0	0	-	0		0.0	0	0	0	0	0
202	-	0	0	0	-	0		0.0	0	0	0	0	0
203	-	0	0	0	Ø3.7mm	107.5		21.5	108	0	530	200	200
204	-	0	0	0	Ø3.7mm	107.5		21.5	108	0	530	200	200
205	-	0	0	0	Ø3.7mm	107.5		21.5	108	0	530	200	200
206	-	0	0	0	Ø4.9mm	188.5		37.7	189	0	560	200	200
207	-	0	0	0	Ø4.9mm	188.5		37.7	189	0	560	200	200
208	-	0	0	0	Ø4.9mm	188.5		37.7	189	0	560	200	200
209	-	0	0	0	-	0		0.0	0	0	0	0	0
210	-	0	0	0	-	0		0.0	0	0	0	0	0
211	-	0	0	0	-	0		0.0	0	0	0	0	0
212	-	0	0	0	Ø4.9mm	188.5		37.7	189	0	560	200	200
213	-	0	0	0	Ø4.9mm	188.5		37.7	189	0	560	200	200
214	-	0	0	0	Ø4.9mm	188.5		37.7	189	0	560	200	200
215	-	0	0	0	-	0		0.0	0	0	0	0	0
216	-	0	0	0	-	0		0.0	0	0	0	0	0
217	-	0	0	0	-	0		0.0	0	0	0	0	0
218	-	0	0	0	Ø3.7mm	107.5		21.5	108	0	530	200	200
219	-	0	0	0	Ø3.7mm	107.5		21.5	108	0	530	200	200
220	-	0	0	0	Ø3.7mm	107.5		21.5	108	0	530	200	200
221	-	0	0	0	Ø3.7mm	107.5		21.5	108	0	530	200	200
222	-	0	0	0	Ø3.7mm	107.5		21.5	108	0	530	200	200
223	-	0	0	0	Ø3.7mm	107.5		21.5	108	0	530	200	200
224	-	0	0	0	Ø3.7mm	107.5		21.5	108	0	530	200	200
225	-	0	0	0	Ø3.7mm	107.5		21.5	108	0	530	200	200

Wall #	HORIZONTAL (SHEAR) REINFORCEMENT												
	Bond Beam Reinf	**A_{hbb} [mm^2]**	**$A_{hbb,m}$ [mm^2]**	**$A_{hbb,m2}$ [mm^2]**	**Joint Reinf**	**A_{hj} [mm^2]**	**$A_{hbb,bar}$ [mm^2]**	**$A_{hj,bar}$ [mm^2]**	**A_h [mm^2]**	**f_{ybb}**	**f_{yj}**	**$s_{h,max}$ [mm]**	**$s_{h,ave}$ [mm]**
226	-	0	0	0	Ø3.7mm	107.5		21.5	108	0	530	200	200
227	-	0	0	0	Ø3.7mm	107.5		21.5	108	0	530	200	200
228	-	0	0	0	Ø3.7mm	107.5		21.5	108	0	530	200	200
229	-	0	0	0	Ø3.7mm	107.5		21.5	108	0	530	200	200
230	15M	400	400	200	-	0	200	0	400	450	0	900	850
231	15M	400	400	200	-	0	200	0	400	450	0	900	850
232	15M	400	400	200	-	0	200	0	400	450	0	900	850
233	15M	400	400	200	-	0	200	0	400	450	0	900	850
234	15M	400	400	200	-	0	200	0	400	450	0	900	850
235	15M	400	400	200	-	0	200	0	400	450	0	900	850
236	15M	400	400	200	-	0	200	0	400	450	0	900	850
237	15M	400	400	200	-	0	200	0	400	450	0	700	600
238	15M	400	400	200	-	0	200	0	400	450	0	700	600
239	15M	400	400	200	-	0	200	0	400	450	0	700	600
240	-	0	0	0	Ø3.665mm	86	0	21.5	86	0	520.8	400	400
241	-	0	0	0	Ø3.665mm	86	0	21.5	86	0	520.8	400	400
242	-	0	0	0	Ø3.665mm	86	0	21.5	86	0	520.8	400	400
243	-	0	0	0	Ø3.665mm	86	0	21.5	86	0	520.8	400	400
244	-	0	0	0	Ø3.665mm	86	0	21.5	86	0	520.8	400	400
245	-	0	0	0	Ø3.665mm	86	0	21.5	86	0	520.8	400	400
246	-	0	0	0	Ø3.665mm	86	0	21.5	86	0	520.8	400	400
247	-	0	0	0	Ø3.665mm	86	0	21.5	86	0	520.8	400	400
248	-	0	0	0	-	0	0	0	0	0	0	0	0
249	-	0	0	0	-	0	0	0	0	0	0	0	0
250	-	0	0	0	-	0	0	0	0	0	0	0	0

Wall #	HORIZONTAL (SHEAR) REINFORCEMENT												
	Bond Beam Reinf	**A_{hbb} [mm^2]**	**$A_{hbb,m}$ [mm^2]**	**$A_{hbb,m2}$ [mm^2]**	**Joint Reinf**	**A_{hj} [mm^2]**	**$A_{hbb,bar}$ [mm^2]**	**$A_{hj,bar}$ [mm^2]**	**A_h [mm^2]**	**f_{ybb}**	**f_{yj}**	**$s_{h,max}$ [mm]**	**$s_{h,ave}$ [mm]**
251	-	0	0	0	-	0	0	0	0	0	0	0	0
252	10M	100	100	0	-	0	100	0	100	458.2	0	1190	1190
253	10M	100	100	0	-	0	100	0	100	458.2	0	1190	1190
254	10M	100	100	0	-	0	100	0	100	458.2	0	1190	1190
255	10M	100	100	0	-	0	100	0	100	458.2	0	1190	1190
256	10M	100	100	0	-	0	100	0	100	458.2	0	1190	1190
257	10M	100	100	0	-	0	100	0	100	458.2	0	1190	1190
258	10M	100	100	0	-	0	100	0	100	458.2	0	1190	1190
259	10M	100	100	0	-	0	100	0	100	458.2	0	1190	1190
260	10M	100	100	0	-	0	100	0	100	458.2	0	714.6	714.6
261	10M	100	100	0	-	0	100	0	100	458.2	0	714.6	714.6
262	10M	100	100	0	-	0	100	0	100	458.2	0	714.6	714.6
263	10M	100	100	0	-	0	100	0	100	458.2	0	714.6	714.6
264	10M	100	100	0	-	0	100	0	100	458.2	0	714.6	714.6
265	10M	100	100	0	-	0	100	0	100	458.2	0	714.6	714.6
266	10M	100	100	0	-	0	100	0	100	458.2	0	714.6	714.6
267	10M	100	100	0	-	0	100	0	100	458.2	0	714.6	714.6
268	10M	100	100	0	-	0	100	0	100	458.2	0	714.6	714.6
269	15M	400	400	200	-	0	200	0	400	448	0	900	850
270	15M	400	400	200	-	0	200	0	400	448	0	900	850
271	15M	400	400	200	-	0	200	0	400	448	0	900	850
272	15M	400	400	200	-	0	200	0	400	448	0	900	850
273	10M	200	200	100	-	0	100	0	200	456	0	900	850
274	10M	200	200	100	-	0	100	0	200	456	0	900	850
275	10M	200	200	100	-	0	100	0	200	456	0	900	850

Wall #	HORIZONTAL (SHEAR) REINFORCEMENT												
	Bond Beam Reinf	**A_{hbb} [mm^2]**	**$A_{hbb,m}$ [mm^2]**	**$A_{hbb,m2}$ [mm^2]**	**Joint Reinf**	**A_{hj} [mm^2]**	**$A_{hbb,bar}$ [mm^2]**	**$A_{hj,bar}$ [mm^2]**	**A_h [mm^2]**	**f_{ybb}**	**f_{yj}**	**$s_{h,max}$ [mm]**	**$s_{h,ave}$ [mm]**
276	10M	200	200	100	-	0	100	0	200	456	0	900	850
277	10M	200	200	100	-	0	100	0	200	456	0	900	850
278	10M	200	200	100	-	0	100	0	200	456	0	900	850
279	10M	200	200	200	-	0	100	0	200	456	0	700	600
280	10M	200	200	200	-	0	100	0	200	456	0	700	600
281	10M	100	100	100	-	0	100	0	100	456	0	900	900
282	10M	100	100	100	-	0	100	0	100	456	0	900	900
283	-	0	0	0	4-2Ø4.2mm	111		27.7	111	0	610	400	400
284	-	0	0	0	4-2Ø4.2mm	111		27.7	111	0	610	400	400
285	-	0	0	0	9-2Ø4.2mm	249		27.7	249	0	610	200	200
286	-	0	0	0	9-2Ø4.2mm	249		27.7	249	0	610	200	200
287	-	0	0	0	3-2Ø4.2mm	83		27.7	83	0	610	400	400
288	-	0	0	0	5-2Ø4.2mm	139		27.7	139	0	610	200	200
289	-	0	0	0	3-2Ø4.2mm	83		27.7	83	0	610	400	400
290	-	0	0	0	4-2Ø4.2mm	111		27.7	111	0	610	400	400
291	-	0	0	0	9-2Ø4.2mm	249		27.7	249	0	610	200	200
292	-	0	0	0	4-2Ø4.2mm	111		27.7	111	0	610	400	400

Wall #	AXIAL STRESS			EXPERIMENTAL SHEAR STRENGTH						
	P [kN]	**σ_{gross} [MPa]**	**σ_{net} [MPa]**	**V_{min} [kN]**	**V_{max} [kN]**	**V_{avg} [kN]**	**k_{avg}**	**k_{mono}**	**k_{rate}**	**V_{exp} [kN]**
1	134.929	0.39	1.09	-	125		0.9443	0.814	1	96
2	327.686	0.94	2.04	-	302		0.9443	0.814	1	233
3	231.307	0.66	1.87	-	214		0.9443	0.814	1	164
4	289.134	0.83	1.80	-	267		0.9443	0.814	1	205
5	269.859	0.77	1.51	-	249		0.9443	0.814	1	191
6	289.134	0.83	1.47	-	267		0.9443	0.814	1	205
7	313.229	0.90	1.95	-	289		0.9443	0.814	1	222
8	337.323	0.97	1.57	-	311		0.9443	0.814	1	239
9	501.166	1.44	2.33	-	463		0.9443	0.814	1	356
10	539.717	1.55	2.51	-	498		0.9443	0.814	1	383
11	462.615	1.33	2.15	-	427		0.9443	0.814	1	328
12	539.717	1.55	2.51	-	498		0.9443	0.814	1	383
13	0	0	0	-	200		0.9443	1	1	189
14	196	0.41	0.66	-	255		0.9443	1	1	241
15	98.1	0.20	0.33	-	336		0.9443	1	1	317
16	0	0	0	-	108		0.9443	1	1	102
17	0	0	0	-	125		0.9443	1	1	118
18	98.1	0.20	0.33	-	265		0.9443	1	1	250
19	0	0	0	-	97		0.9443	1	1	92
20	196	0.41	0.66	-	278		0.9443	1	1	262
21	0	0	0	-	255		0.9443	1	1	241
22	0	0	0	-	216		0.9443	1	1	204
23	0	0.00	0.00	-	159		0.9443	0.814	1	122
24	49.05	0.16	0.27	-	148		0.9443	0.814	1	114
25	98.1	0.33	0.55	-	237		0.9443	0.814	1	182

Wall #	AXIAL STRESS			EXPERIMENTAL SHEAR STRENGTH						
	P [kN]	**σ_{gross} [MPa]**	**σ_{net} [MPa]**	**V_{min} [kN]**	**V_{max} [kN]**	**V_{avg} [kN]**	**k_{avg}**	**k_{mono}**	**k_{rate}**	**V_{exp} [kN]**
26	196.2	0.65	1.10	-	285		0.9443	0.814	1	219
27	0	0.00	0.00	-	134		0.9443	0.814	1	103
28	0	0.00	0.00	-	197		0.9443	0.814	1	151
29	0	0.00	0.00	-	128		0.9443	0.814	1	98
30	294.3	0.98	1.35	-	308		0.9443	0.814	1	237
31	294.3	0.98	1.64	-	337		0.9443	0.814	1	259
32	294.3	0.98	1.64	-	317		0.9443	0.814	1	243
33	0	0.00	0.00	-	184		0.9443	0.814	1	141
34	200.2	1.72	2.41	-	-	78	0.9443	1	1	74
35	200.2	1.72	2.41	-	-	86	0.9443	1	0.9	73
36	187.7	0.79	1.87	107	117	112	1	1	0.9	101
37	134.3	0.57	0.93	196	221	208	1	1	0.9	187
38	129.9	0.55	0.90	159	169	164	1	1	0.9	147
39	138.8	0.59	0.96	210	223	217	1	1	0.9	195
40	0	0.00	0.00	74.6	77.5	76	1	1	1	76
41	0	0.00	0.00	94	106	100	1	1	1	100
42	0	0.00	0.00	146	152	149	1	1	1	149
43	0	0	0	108.4	118.7	114	1	1	1	114
44	0	0	0	157.4	157.4	157	1	1	1	157
45	0	0	0	87.1	93.1	90	1	1	1	90
46	0	0	0	142.6	93.1	118	1	1	1	118
47	0	0	0	84.2	73.1	79	1	1	1	79
48	0	0	0	73.1	73.1	73	1	1	1	73
49	0	0	0	59.4	57.4	58	1	1	1	58
50	0	0	0	79.2	65.3	72	1	1	1	72

Wall #	AXIAL STRESS			EXPERIMENTAL SHEAR STRENGTH						
	P [kN]	**σ_{gross} [MPa]**	**σ_{net} [MPa]**	**V_{min} [kN]**	**V_{max} [kN]**	**V_{avg} [kN]**	**k_{avg}**	**k_{mono}**	**k_{rate}**	**V_{exp} [kN]**
51	0	0	0	101.0	63.4	82	1	1	1	82
52	0	0	0	104.9	73.3	89	1	1	1	89
53	0	0	0	132.7	89.1	111	1	1	1	111
54	97.0	0.49	0.78	172.3	101.0	137	1	1	1	137
55	194.0	0.98	1.57	148.5	136.6	143	1	1	1	143
56	291.1	1.47	2.35	192.1	166.3	179	1	1	1	179
57	100.7	0.49	0.79	108.9	84.3	97	1	1	1	97
58	100.7	0.49	0.79	154.1	150.0	152	1	1	1	152
59	100.7	0.49	0.79	160.3	185.0	173	1	1	1	173
60	100.7	0.49	0.79	248.7	141.8	195	1	1	1	195
61	100.7	0.49	0.79	148.0	129.5	139	1	1	1	139
62	194.0	0.98	1.57	180.2	136.6	158	1	1	1	158
63	194.0	0.98	1.57	95.0	79.2	87	1	1	1	87
64	194.0	0.98	1.57	196.0	138.6	167	1	1	1	167
65	194.0	0.98	1.57	215.8	152.5	184	1	1	1	184
66	144.8	0.49	0.78	239.4	224.6	232	1	1	1	232
67	144.8	0.49	0.78	230.5	218.7	225	1	1	1	225
68	130.1	0.49	0.80	212.4	180.5	196	1	1	1	196
69	100.7	0.49	0.79	148.0	143.9	146	1	1	1	146
70	71.3	0.49	0.78	87.3	69.8	79	1	1	1	79
71	71.3	0.49	0.78	90.2	68.4	79	1	1	1	79
72	60	0.98	1.65	-	32.9		0.9443	1	1	31
73	60	0.98	1.65	-	40.7		0.9443	1	1	38
74	60	0.98	1.65	-	35.3		0.9443	1	1	33
75	60	0.98	1.65	-	40.3		0.9443	1	1	38

Wall #	AXIAL STRESS			EXPERIMENTAL SHEAR STRENGTH						
	P [kN]	**σ_{gross} [MPa]**	**σ_{net} [MPa]**	**V_{min} [kN]**	**V_{max} [kN]**	**V_{avg} [kN]**	**k_{avg}**	**k_{mono}**	**k_{rate}**	**V_{exp} [kN]**
76	60	0.98	1.65	-	26.0		0.9443	1	1	25
77	60	0.98	1.65	-	30.1		0.9443	1	1	28
78	60	0.98	1.65	-	34.9		0.9443	1	1	33
79	60	0.98	1.65	-	43.2		0.9443	1	1	41
80	60	0.98	1.65	-	46.8		0.9443	1	1	44
81	60	0.98	1.65	-	29.1		0.9443	1	1	27
82	0	0	0	-	96		0.9443	1	1	91
83	0	0	0	-	108		0.9443	1	1	102
84	0	0	0	-	117		0.9443	1	1	110
85	0	0	0	-	186		0.9443	1	1	176
86	0	0	0	-	103		0.9443	1	1	97
87	0	0	0	-	106		0.9443	1	1	100
88	0	0	0	-	116		0.9443	1	1	109
89	0	0	0	-	104		0.9443	1	1	98
90	0	0	0	-	114		0.9443	1	1	107
91	0	0	0	-	107		0.9443	1	1	101
92	0	0	0	-	111		0.9443	1	1	104
93	0	0	0	-	108		0.9443	1	1	102
94	0	0	0	-	108		0.9443	1	1	102
95	0	0	0	-	106		0.9443	1	1	100
96	0	0	0	-	104		0.9443	1	1	98
97	0	0	0	-	101		0.9443	1	1	95
98	174.8	0.74	1.38	105.9	122.3	114	1	1	1	114
99	174.8	0.74	1.38	128.6	156.1	142	1	1	1	142
100	174.8	0.74	1.38	141.9	148.6	145	1	1	1	145

Wall #	AXIAL STRESS			EXPERIMENTAL SHEAR STRENGTH						
	P [kN]	**σ_{gross} [MPa]**	**σ_{net} [MPa]**	**V_{min} [kN]**	**V_{max} [kN]**	**V_{avg} [kN]**	**k_{avg}**	**k_{mono}**	**k_{rate}**	**V_{exp} [kN]**
101	174.8	0.74	1.38	189.0	201.9	195	1	1	1	195
102	174.8	0.74	1.38	145.5	156.1	151	1	1	1	151
103	174.8	0.74	1.38	156.6	163.7	160	1	1	1	160
104	174.8	0.74	1.38	119.2	119.2	119	1	1	1	119
105	174.8	0.74	1.38	161.5	176.6	169	1	1	1	169
106	174.8	0.74	1.38	191.7	201.1	196	1	1	1	196
107	174.8	0.74	1.38	147.7	171.7	160	1	1	1	160
108	30.9	0.69	1.55	-	24.5		0.9443	0.814	1	19
109	30.9	0.69	1.40	-	30.2		0.9443	0.814	1	23
110	30.9	0.69	1.40	-	25.8		0.9443	0.814	1	20
111	61.8	1.38	2.81	-	34.3		0.9443	0.814	1	26
112	120	1.97	2.84	-	45.05		0.9443	1	1	43
113	120	1.97	2.84	-	50.45		0.9443	1	1	43
114	120	1.97	2.84	-	49.23		0.9443	1	1	46
115	120	1.97	2.84	-	57.26		0.9443	1	1	49
116	120	1.97	2.84	-	53.78		0.9443	1	1	51
117	120	1.97	2.84	-	60.19		0.9443	1	1	51
118	267	0.48	1.10	-	-	187	1	1	1	187
119	191	0.48	1.02	-	-	245	1	1	1	245
120	133	0.48	0.91	-	-	133	1	1	1	133
121	266	0.48	1.10	-	-	240	1	1	1	240
122	177	0.45	0.94	-	-	192	1	1	1	192
123	132	0.48	0.90	-	-	154	1	1	1	154
124	265	0.48	1.09	-	-	261.3	1	1	1	261
125	185.4	0.47	0.99	-	-	253.5	1	1	1	254

Wall #	AXIAL STRESS			EXPERIMENTAL SHEAR STRENGTH						
	P [kN]	**σ_{gross} [MPa]**	**σ_{net} [MPa]**	**V_{min} [kN]**	**V_{max} [kN]**	**V_{avg} [kN]**	**k_{avg}**	**k_{mono}**	**k_{rate}**	**V_{exp} [kN]**
126	130.2	0.47	0.89	-	-	175.9	1	1	1	176
127	265.5	0.48	1.10	-	-	243.4	1	1	1	243
128	187.6	0.47	1.00	-	-	270.3	1	1	1	270
129	133.2	0.48	0.91	-	-	211.3	1	1	1	211
130	357.5	1.42	1.92	-	143		0.9443	1	1	135
131	145.3	0.58	0.78	-	93		0.9443	1	1	88
132	60.0	0.5	1.37	52.73	52.75	52.7	1	1	1	53
133	60.0	0.5	1.37	62.09	65.18	63.6	1	1	1	64
134	150.0	1.25	3.42	92.98	93.22	93.1	1	1	1	93
135	150.0	1.25	3.42	93.28	93.8	93.5	1	1	1	94
136	120	0.74	1.66	91.2	96.9	94.1	1	1	1	94
137	120	0.74	1.55	93.2	103.7	98.5	1	1	1	98
138	120	0.74	1.80	84.4	96.7	90.6	1	1	1	91
139	120	0.74	1.66	114.2	122.9	118.6	1	1	1	119
140	120	0.74	1.66	79.1	84.3	81.7	1	1	1	82
141	48.928	0.10	0.20	223	253	238	1	1	1	238
142	48.928	0.10	0.20	250	254	252	1	1	1	252
143	48.928	0.10	0.20	203	289	246	1	1	1	246
144	48.928	0.10	0.20	281	291	286	1	1	1	286
145	48.928	0.10	0.18	331	357	344	1	1	1	344
146	48.928	0.10	0.16	370	430	400	1	1	1	400
147	243.9	0.33	0.7	312	318	315	1	1	1	315
148	243.9	0.33	0.7	177.2	190	183.6	1	1	1	184
149	0.0	0.00	0	240.4	241	240.7	1	1	1	241
150	0.0	0.00	0	224.6	230	227.3	1	1	1	227

Wall #	AXIAL STRESS			EXPERIMENTAL SHEAR STRENGTH						
	P [kN]	**σ_{gross} [MPa]**	**σ_{net} [MPa]**	**V_{min} [kN]**	**V_{max} [kN]**	**V_{avg} [kN]**	**k_{avg}**	**k_{mono}**	**k_{rate}**	**V_{exp} [kN]**
151	0	0	0	-	-	208.2	1	1	1	208
152	0	0	0	-	-	201.1	1	1	1	201
153	0	0	0	-	-	325.6	1	1	1	326
154	0	0	0	-	-	249.1	1	1	1	249
155	0	0	0	-	-	266.0	1	1	1	266
156	0	0	0	-	-	348.3	1	1	1	348
157	0	0	0	-	-	431.0	1	1	1	431
158	0	0	0	-	-	405.7	1	1	1	406
159	49.286	0.10	0.20	211	234	221.8	1	1	1	222
160	49.286	0.10	0.20	227	230	227.7	1	1	1	228
161	49.286	0.10	0.20	193	215	202.9	1	1	1	203
162	49.286	0.10	0.18	258	262	260.0	1	1	1	260
163	49.286	0.10	0.17	290	302	295.0	1	1	1	295
164	416	1.37	2.02	-	297.0		0.9443	0.814	1	228
165	416	1.37	2.02	-	278.1		0.9443	0.814	1	214
166	416	1.37	2.02	-	275.9		0.9443	0.814	1	212
167	416	1.37	2.02	-	270.1		0.9443	0.814	1	208
168	416	1.37	2.02	-	261.1		0.9443	0.814	1	201
169	416	1.37	2.02	-	272.2		0.9443	0.814	1	209
170	416	1.37	2.02	-	257.4		0.9443	0.814	1	198
171	416	1.37	2.02	-	265.9		0.9443	0.814	1	204
172	416	1.37	2.02	-	259.4		0.9443	0.814	1	199
173	416	1.37	2.02	-	275.1		0.9443	0.814	1	211
174	416	1.37	2.02	-	281.5		0.9443	0.814	1	216
175	416	1.37	2.02	-	278.4		0.9443	0.814	1	214

Wall #	AXIAL STRESS			EXPERIMENTAL SHEAR STRENGTH						
	P [kN]	**σ_{gross} [MPa]**	**σ_{net} [MPa]**	**V_{min} [kN]**	**V_{max} [kN]**	**V_{avg} [kN]**	**k_{avg}**	**k_{mono}**	**k_{rate}**	**V_{exp} [kN]**
176	416	1.37	2.02	-	278.7		0.9443	0.814	1	214
177	416	1.37	2.02	-	287.6		0.9443	0.814	1	221
178	416	1.37	2.02	-	278.9		0.9443	0.814	1	214
179	236	0.78	2.11	-	149.5		0.9443	0.814	1	115
180	236	0.78	2.11	-	146.9		0.9443	0.814	1	113
181	236	0.78	2.11	-	157.2		0.9443	0.814	1	121
182	628	2.07	3.05	-	384.4		0.9443	0.814	1	295
183	628	2.07	3.05	-	346.6		0.9443	0.814	1	266
184	628	2.07	3.05	-	419.6		0.9443	0.814	1	323
185	628	2.07	3.05	-	347.9		0.9443	0.814	1	267
186	628	2.07	3.05	-	337.1		0.9443	0.814	1	259
187	628	2.07	3.05	-	390.1		0.9443	0.814	1	300
188	628	2.07	3.05	-	384.2		0.9443	0.814	1	295
189	628	2.07	3.05	-	362.3		0.9443	0.814	1	278
190	628	2.07	3.05	-	325.0		0.9443	0.814	1	250
191	628	2.07	3.05	-	338.4		0.9443	0.814	1	260
192	628	2.07	3.05	-	356.0		0.9443	0.814	1	274
193	628	2.07	3.05	-	373.9		0.9443	0.814	1	287
194	628	2.07	3.05	-	360.4		0.9443	0.814	1	277
195	628	2.07	3.05	-	349.7		0.9443	0.814	1	269
196	628	2.07	3.05	-	377.8		0.9443	0.814	1	290
197	353	1.16	3.15	-	186.4		0.9443	0.814	1	143
198	353	1.16	3.15	-	199.8		0.9443	0.814	1	154
199	353	1.16	3.15	-	215.5		0.9443	0.814	1	166
200	839	2.76	4.08	-	459.5		0.9443	0.814	1	353

Wall #	AXIAL STRESS			EXPERIMENTAL SHEAR STRENGTH						
	P [kN]	σ_{gross} [MPa]	σ_{net} [MPa]	V_{min} [kN]	V_{max} [kN]	V_{avg} [kN]	k_{avg}	k_{mono}	k_{rate}	V_{exp} [kN]
201	839	2.76	4.08	-	403.5		0.9443	0.814	1	310
202	839	2.76	4.08	-	433.6		0.9443	0.814	1	333
203	839	2.76	4.08	-	414.6		0.9443	0.814	1	319
204	839	2.76	4.08	-	393.8		0.9443	0.814	1	303
205	839	2.76	4.08	-	402.0		0.9443	0.814	1	309
206	839	2.76	4.08	-	437.0		0.9443	0.814	1	336
207	839	2.76	4.08	-	393.3		0.9443	0.814	1	302
208	839	2.76	4.08	-	425.7		0.9443	0.814	1	327
209	839	2.76	4.08	-	423.6		0.9443	0.814	1	326
210	839	2.76	4.08	-	400.9		0.9443	0.814	1	308
211	839	2.76	4.08	-	405.9		0.9443	0.814	1	312
212	839	2.76	4.08	-	410.3		0.9443	0.814	1	315
213	839	2.76	4.08	-	436.8		0.9443	0.814	1	336
214	839	2.76	4.08	-	443.4		0.9443	0.814	1	341
215	471	1.55	4.21	-	231.1		0.9443	0.814	1	178
216	471	1.55	4.21	-	250.8		0.9443	0.814	1	193
217	471	1.55	4.21	-	237.2		0.9443	0.814	1	182
218	315	1.04	2.81	-	186.4		0.9443	0.814	1	143
219	315	1.04	2.81	-	217.3		0.9443	0.814	1	167
220	315	1.04	2.81	-	208.0		0.9443	0.814	1	160
221	315	1.04	2.81	-	210.1		0.9443	0.814	1	161
222	315	1.04	2.81	-	206.7		0.9443	0.814	1	159
223	315	1.04	2.81	-	212.0		0.9443	0.814	1	163
224	608	2.00	2.96	-	350.7		0.9443	0.814	1	270
225	608	2.00	2.96	-	323.1		0.9443	0.814	1	248

Wall #	AXIAL STRESS			EXPERIMENTAL SHEAR STRENGTH						
	P [kN]	**σ_{gross} [MPa]**	**σ_{net} [MPa]**	**V_{min} [kN]**	**V_{max} [kN]**	**V_{avg} [kN]**	**k_{avg}**	**k_{mono}**	**k_{rate}**	**V_{exp} [kN]**
226	608	2.00	2.96	-	339.2		0.9443	0.814	1	261
227	608	2.00	2.96	-	320.4		0.9443	0.814	1	246
228	608	2.00	2.96	-	334.6		0.9443	0.814	1	257
229	608	2.00	2.96	-	333.2		0.9443	0.814	1	256
230	410.1	1.20	2.06	189.0	229.6	209.3	1	1	1	209
231	409	1.20	2.05	225.6	227.1	226.4	1	1	1	226
232	431.7	1.26	2.17	250.7	254.1	252.4	1	1	1	252
233	411.3	1.20	2.07	224.7	232.4	228.6	1	1	1	229
234	422.7	1.24	2.12	233.5	251.4	242.5	1	1	1	242
235	417.6	1.22	2.10	225.6	246.3	236.0	1	1	1	236
236	409	1.20	2.05	160.1	168.6	164.4	1	1	1	164
237	413.3	1.21	2.08	195.0	236.8	215.9	1	1	1	216
238	421.1	1.23	2.11	230.8	250.5	240.7	1	1	1	241
239	409	1.20	2.05	186.7	194.6	190.7	1	1	1	191
240	409	1.20	2.05	204.9	208.1	206.5	1	1	1	207
241	409	1.20	2.05	208.0	218.5	213.3	1	1	1	213
242	409	1.20	2.05	202.0	204.9	203.5	1	1	1	203
243	409	1.20	2.05	209.5	213.3	211.4	1	1	1	211
244	409	1.20	2.05	175.7	177.7	176.7	1	1	1	177
245	409	1.20	2.05	180.7	190.0	185.4	1	1	1	185
246	411.8	1.20	2.07	-	230.3		0.9443	0.814	1	177
247	416.7	1.22	2.09	-	235.8		0.9443	0.814	1	181
248	unknown	-	-	-	54.7		0.9443	0.814	1	42
249	86	0.77	1.69	-	51.6		0.9443	0.814	1	40
250	62	0.55	1.21	-	38.2		0.9443	0.814	1	29

Wall #	AXIAL STRESS			EXPERIMENTAL SHEAR STRENGTH						
	P [kN]	**σ_{gross} [MPa]**	**σ_{net} [MPa]**	**V_{min} [kN]**	**V_{max} [kN]**	**V_{avg} [kN]**	**k_{avg}**	**k_{mono}**	**k_{rate}**	**V_{exp} [kN]**
251	70	0.63	1.37	-	46.0		0.9443	0.814	1	35
252	78	0.70	1.53	-	42.68		0.9443	0.814	1	33
253	73	0.66	1.44	-	44.0		0.9443	0.814	1	34
254	181	0.84	1.94	-	108		0.9443	0.814	1	83
255	183	0.85	1.96	-	103		0.9443	0.814	1	79
256	190	0.88	2.03	-	105		0.9443	0.814	1	81
257	162	0.75	1.73	-	96		0.9443	0.814	1	74
258	189	0.88	2.02	-	95.52		0.9443	0.814	1	73
259	225	1.05	2.41	-	131		0.9443	0.814	1	101
260	320	1.49	3.23	-	197.3		0.9443	0.814	1	152
261	211	0.98	2.13	-	168.8		0.9443	0.814	1	130
262	226	1.05	2.29	-	184		0.9443	0.814	1	141
263	299	1.39	3.02	-	180		0.9443	0.814	1	138
264	298	1.38	3.01	-	185		0.9443	0.814	1	142
265	221	1.03	2.23	-	148		0.9443	0.814	1	114
266	39	0.50	1.01	-	25.1		0.9443	0.814	1	19
267	37	0.48	0.96	-	23.1		0.9443	0.814	1	18
268	47	0.60	1.20	-	30.6		0.9443	0.814	1	24
269	432	1.26	2.13	232	273	252.5	1	1	1	253
270	476	1.39	2.35	276	327	301.5	1	1	1	302
271	484	1.42	2.39	276	346	311	1	1	1	311
272	482	1.41	2.37	282	334	308	1	1	1	308
273	409	1.20	2.02	216	232	224	1	1	1	224
274	409	1.20	2.02	191	215	203	1	1	1	203
275	409	1.20	2.02	208	244	226	1	1	1	226

Wall #	AXIAL STRESS			EXPERIMENTAL SHEAR STRENGTH						
	P [kN]	**σ_{gross} [MPa]**	**σ_{net} [MPa]**	**V_{min} [kN]**	**V_{max} [kN]**	**V_{avg} [kN]**	**k_{avg}**	**k_{mono}**	**k_{rate}**	**V_{exp} [kN]**
276	409	1.20	2.02	217	223	220	1	1	1	220
277	409	1.20	2.02	214	226	220	1	1	1	220
278	409	1.20	2.02	184	213	198.5	1	1	1	199
279	409	1.20	2.02	180	211	195.5	1	1	1	196
280	409	1.20	2.02	206	209	207.5	1	1	1	208
281	409	1.20	2.02	175	215	195	1	1	1	195
282	409	1.20	2.02	206	230	218	1	1	1	218
283	156.0	0.56	0.78	211.7	221.1	216.4	1	1	1	216
284	156.0	0.56	0.78	196.3	220.9	208.6	1	1	1	209
285	156.0	0.56	0.78	283.6	303.1	293.4	1	1	1	293
286	156.0	0.56	0.78	291.6	308.3	299.9	1	1	1	300
287	203.1	0.56	0.79	290.1	316.4	303.2	1	1	1	303
288	203.1	0.56	0.79	330.4	342.4	336.4	1	1	1	336
289	0.0	0	0.00	199.9	221.8	210.8	1	1	1	211
290	77.6	0.56	0.69	99.2	100.3	99.8	1	1	1	100
291	77.6	0.56	0.69	116.5	141.7	129.1	1	1	1	129
292	0	0	0.00	98.4	99.9	99.2	1	1	1	99